

A LIFTING SURFACE SOLUTION FOR VORTEX  
INDUCED AIRLOADS AND ITS APPLICATION  
TO ROTARY WING AIRLOADS CALCULATIONS

by

WAYNE JOHNSON

S.B., S.M., Massachusetts Institute of Technology

(1968)

SUBMITTED IN PARTIAL FULFILLMENT  
OF THE REQUIREMENTS FOR THE  
DEGREE OF DOCTOR OF SCIENCE

at the

MASSACHUSETTS INSTITUTE OF TECHNOLOGY

June, 1970

Signature of Author\_

Department of Aeronautics  
and Astronautics, June 1970

Certified by\_\_\_\_\_

Thesis Supervisor

Accepted by\_\_\_\_\_

Chairman, Departmental  
Graduate Committee



11

A LIFTING SURFACE SOLUTION FOR VORTEX  
INDUCED AIRLOADS AND ITS APPLICATION  
TO ROTARY WING AIRLOADS CALCULATIONS

by

Wayne Johnson

Submitted to the Department of Aeronautics and  
Astronautics on May 14, 1970 in partial fulfillment  
of the requirements for the degree of Doctor of Science.

ABSTRACT

This report develops practical procedures for the use of lifting surface theory to calculate the airloading induced on a helicopter rotor blade by a nearby tip vortex. Planar lifting surface theory is applied to the model problem of an infinite aspect ratio wing and a straight, infinite vortex at an arbitrary angle with the wing, in a compressible free stream. The formulation of the solution requires the development of the general aerodynamic kernel for a lifting airfoil; this kernel includes as limits the Fourier transform of the three-dimensional, steady lifting surface kernel, and the kernel for two-dimensional, unsteady flow about an airfoil. The appropriate downwash for vortex induced airloads is a convected, one-dimensional downwash field, or equivalently a sinusoidal gust at an arbitrary angle with the wing, and the solution for the loads is in the form of an aerodynamic influence function, valid for all such downwash fields. Numerical solutions are obtained for





cases in the entire range of geometry and velocity of the model problem, and from these are constructed usable analytic approximations for the influence functions. These approximate expressions give the vortex induced loads in a form that may be practically used in rotary wing airloads calculations without the extensive calculations involved in usual lifting surface theory solutions. Procedures are developed for the application of the model problem to the rotary wing configuration. In order to evaluate the use of the lifting surface theory solution, it is compared with lifting line theory in the prediction of the airloads induced by a free vortex on a single-bladed rotor at high advance ratio. This comparison shows that the use of the lifting surface theory solution is necessary in order to obtain accurate loading prediction for cases involving vortices closer than a few chord lengths to the blade. The solution and procedures developed in this report remove one of the limitations of rotary wing airloads calculations. They allow the accurate prediction of loads due to a downwash distribution varying rapidly along the span of the blade, specifically the downwash due to a nearby tip vortex.

Thesis Supervisor: Norman D. Ham  
Title: Associate Professor of  
Aeronautics and Astronautics



To Professors Sheila Evans Widnall  
and Rene H. Miller, and in particular to  
Professor Norman D. Ham, I extend my  
appreciation for their counsel and support  
of the work in this report.

WG

This work was sponsored by the National  
Aeronautics and Space Administration, under  
Contract Number NGR 22-009-303.



TABLE OF CONTENTS

	PAGE
SECTION 1 Introduction	1
SECTION 2 A Lifting Surface Solution for Vortex Induced Airfoil Loading	9
2.1 Formation of the Model	9
2.1.1 The Vortex Induced Airloads Problem	9
2.1.2 The Model of the Problem	9
2.1.3 Details of the Model	12
2.1.4 The Nature of the Solution	15
2.2 Lifting Surface Solution of the Problem	18
2.2.1 Equations of Motion	18
2.2.2 Formulation of the Integral Equation	20
2.2.3 Representation of the Loading as a Series	27
2.2.4 The Results of the Solution	30
2.3 The Kernels	31
2.3.1 The Elliptic Kernel	31
2.3.2 The Hyperbolic Kernel	40
2.3.3 Similarity in the Kernels	52
2.3.4 The Incompressible Two-dimensional Kernel	53
2.3.5 The Transitional Kernel	59
2.3.6 The Linear Assumption	63
2.4 The Approximate Solution	65
2.4.1 Numerical Solution of the Integral Equation	65
2.4.2 The Approximate Influence Functions	71
2.4.3 Approximate Solutions for the Loading	97
SECTION 3 Application of the Lifting Surface Theory Solution to Rotary Wing Aerodynamics	114
3.1 The Calculation of Rotary Wing Airloads	114
3.1.1 The Rotor Wake	115
3.1.2 The Blade Airloading	116
3.1.3 The Blade Motion	117
3.1.4 The Wake Geometry	118
3.1.5 The Results	120
3.2 A Straight Infinite Vortex	120
3.2.1 Orthogonal Geometry	120
3.2.2 General Geometry	122
3.3 Rotary Wing Geometry for the Lifting Surface Solution	125
3.4 The Application of the Lifting Surface Solution	131

SECTION 4	Evaluation of the Use of the Lifting Surface Solution in the Calculation of Rotary Wing Airloads	PAGE 134
4.1	The Rotor Configuration	134
4.2	Comparison of Lifting Line and Lifting Surface Loading Calculations	136
4.3	Evaluation of the Use of the Lifting Surface Theory Solution	138
SECTION 5	Conclusions and Recommendations	141
REFERENCES		143
FIGURES		146

## LIST OF ILLUSTRATIONS

<u>Figure</u>	PAGE
2-1	146
2-2	147
2-3	148
2-4	149
2-5	150
2-6	151
2-7	152
2-8	153
2-9	154
2-10	155
2-11	156
2-12	157
2-13	158
2-14	159
2-15	160
2-16	161
2-17	162
2-18	163
2-19	164
2-20	165
2-21	166
2-22	167
2-23	168
2-24	169
2-25	170
2-26	171
2-27	172
2-28	173
2-29	174
2-30	175



LIST OF ILLUSTRATIONS (Concluded)

<u>Figure</u>	PAGE
2-31	176
2-32	177
2-33	178
2-34	179
2-35	180
2-36	181
2-37	182
2-38	183
2-39	184
3-1	185
3-2	186
3-3	187
3-4	188
3-5	189
3-6	190
4-1	191
4-2	192
4-3	193
4-4	194
4-5	195
4-6	196
4-7	197

## SECTION 1

### INTRODUCTION

The requirement to determine the airloads on a rotary wing of a helicopter or autogyro has occupied aerodynamicists for nearly half a century. Yet an entirely satisfactory prediction of these airloads is still not possible, and becomes even more difficult to obtain as the performance of new machines increases. This report presents the development of procedures to handle one of the problems involved in the calculation of rotary wing airloads.

The objective of rotary wing aerodynamics is to develop the most accurate, practical calculation method, in the context of the highly iterative calculation of helicopter airloads. Because of the geometry of the rotor wake, the interference of the rotary wing with its own wake and the wake of other blades is considerably more important than that of a fixed wing. This interference is manifested as a downwash at the blade which must be calculated in order to determine the loads on the blade and its subsequent motion. Thus the calculation of the airloads leads immediately to a consideration of the downwash field in which the rotor blade operates; accurate downwash information is essential in order to obtain accurate airloads. The downwash field is calculated from the vortex wake of the rotor, and this leads to the necessity for accurate wake geometry information. From the knowledge of the downwash field at the blade, aerodynamic theory must be used to obtain accurate loading. It is with this last problem that this report is concerned. Present rotary wing airloads calculations involve the determination of the downwash distribution along the blade, the aerodynamic loading along the blade, and the blade motion successively, following the blade around the azimuth of the rotor disk. In order to calculate the downwash due to the rotor wake -- which in forward flight is a distribution of trailed and shed vorticity over a

skewed, distorted helix -- the wake is represented by a net of line vortices (or more recently by rectangular vortex sheets) and the downwash at the blade is then the sum of the contributions from each element of the net. The geometry of the wake may be assumed, or it may be calculated by one of several methods of varying accuracy. The blade motion calculation is an aeroelastic problem; the equations of motion of the blade may be solved by numerical integration or harmonic analysis. An iterative solution, rather than a closed form solution, necessarily results unless the geometry of the wake is known or specified, and nonlinear aerodynamics associated with stall are neglected.

In the calculation of the aerodynamic loading on a rotary wing it has been customary to use lifting line theory. That is, it is assumed that the flow over the blade is locally two-dimensional, the influence of the rest of the blade and of the rotor wake being represented only by a uniform downwash at the blade section. Two-dimensional unsteady airfoil theory (or experimental or empirical section loads data) is then used to obtain the section lift and moment.

The calculation of the airloading on a rotary wing is deeply involved with the interaction of the blade with its vortex wake. The operating conditions of a rotary wing are such that its wake is not carried away by the free stream velocity as for a conventional wing, but rather spirals underneath the rotor disk. This wake may be considered sheets of shed and trailed vorticity. The outboard edge of the sheet quickly rolls up, the vorticity becoming highly concentrated about a line trailed from the tip of the rotor. Regions where the blade passes close to tip vortices, its own and those from other blades are numerous, and are quite important because of the strong downwash induced at the blade. Once the geometry of the vortex wake is known, it is necessary to have an accurate method for the calculation of the airloading induced on the blades by the tip vortices. The accuracy of the

airloads in current calculations is restricted by the use of lifting line theory. For the large variations of the downwash along the span associated with the nearby vortex, lifting line theory is not valid; moreover, this theoretical limitation is compounded by the practical difficulty of handling in sufficient detail the shed and trailed wake induced by this vortex. Therefore, it is necessary to turn to the more accurate lifting surface theory to obtain the vortex induced airloading.

The application of conventional lifting surface theories to the calculation of the vortex induced airloads is prohibited by the extensive calculations involved in these methods alone. What is required is a lifting surface solution that may be directly and simply applied in the highly iterative calculation of rotary wing airloads. The proper procedure is to construct a sufficiently general model for the vortex induced airloads problem, and to obtain the loads in this model using lifting surface theory. Then the solution for this model problem may be routinely applied in the calculation of rotary wing airloads. The development of this model, its solution, and its application is the subject of this report.

The use of lifting surface theory does not, of course, exactly solve the vortex induced airloads problem. There are first the limitations involved in using linear, planar lifting surface theory. Moreover, lifting surface theory is a solution for potential fluid flow, thus viscous aspects of the problem are completely neglected. The effects of viscosity in the vortex induced airloads problem will not be further considered in this report.

The problem which is the subject of this report has not before been approached directly; it is one of the steps that remains to be completed in the development of an accurate theory of rotary wing airloads. The aerodynamic bases of the problem are, however, well established. Miller (Refs. 1 and 2) and others have developed procedures for the calculation of rotary wing airloads using

nonuniform downwash. This work showed the importance of obtaining the loads from the actual downwash induced at the rotor disk by the vortex wake of the blades. While the use of nonuniform downwash allowed a significant improvement in the prediction of airloads, there are still features that should be treated more accurately. One of these is the wake geometry, and a major effort has been made to calculate the self-induced distortion of the geometry of the vortex wake, for example by Scully (Ref. 3) and by Landgrebe (Ref. 4). The basic features of the airloads calculation procedure using lifting line theory are sufficiently understood that it is now possible to direct attention to the construction of a practical method of using the more accurate lifting surface theory.

The kernel function formulation of planar lifting surface theory was constructed by Watkins, Runyan, and Woolston (Ref. 5) and others. Practical methods for solving the integral equation for the pressure on a wing, using assumed pressure modes to convert the integral equation into a set of linear algebraic equations, were developed by Watkins, Woolston, and Cunningham (Ref. 6). A survey of lifting surface results and methods, including multiple and nonplanar surfaces, was made by Ashley, Widnall, and Landahl (Ref. 7) and a more recent survey is that of Landahl and Stark (Ref. 8). The methods that have been developed for the solution for lifting surface pressures involve the conversion of the integral equation into a finite set of algebraic equations; in the more accurate method, using assumed pressure modes, the coefficients of the algebraic equations are integrals over the wing surface, which must be evaluated numerically. The amount of calculation involved in this method, however, prevents its direct application to rotary wing aerodynamics. The simpler method of representing the lifting surface by a lattice of vortex lines involves less calculation, but the accuracy is highly dependent on the skill with which the lattice elements are positioned. Using this method for a blade in the highly nonuniform downwash field

of a rotor disk, particularly for configurations where tip vortex induced loads are important, would be impossible to do with confidence. Not only is the downwash field complicated, it is also not known in advance, but must be calculated iteratively with the loading; moreover, the vortex wake as well as the blade must be correctly represented by a vortex lattice.

While the problem to be solved here is to obtain the pressure induced by a vortex on a lifting surface, it will be seen that the proper formulation will be more analogous to compressible, two-dimensional, thin airfoil theory. The kernel function formulation of two-dimensional airfoil theory was constructed by Possio (as in Ref. 9). This problem involves also an integral equation which must be inverted to obtain the pressure on the airfoil, and again the amount of calculation involved prevents the direct application of this problem to rotary wing aerodynamics. Among the many treatments of incompressible, two-dimensional, thin airfoil theory, that of von Karman and Sears (Ref. 10) will be most convenient here. These methods that have been developed for lifting surface theory and thin airfoil theory will be extended, and combined, here to obtain a solution for the vortex induced airloads problem. Of particular importance is the kernel function (integral equation) formulation, which is characteristic of lifting pressure distributions.

Some work has been done on the vortex induced airloads problem, although none in a form directly applicable to rotary wing aerodynamics. The loads induced on a finite wing in a uniform free stream by a vortex perpendicular to the span direction have been obtained using the vortex lattice method of lifting surface theory by Kfoury (Ref. 11), and using the assumed pressure modes method by Silver (Ref. 12). The difficulties encountered in choosing the proper lattice positions or the proper pressure modes, as well as the extent of the calculations involved in either of these methods, confirm their inapplicability to rotary wing airloads

calculations. Lifting surface theory (the vortex lattice method) has been used by Cummings and Kerwin (Ref. 13) to obtain the loads on a marine propeller; its use was necessary -- and possible -- because of the small aspect ratio of the blade rather than because of the importance of vortex induced loads, and again the calculations involved were extensive.

All of these applications of lifting surface theory illustrate the importance of developing a solution for a model problem that may then be used to calculate rotary wing airloads. Only if such a solution can be obtained without the computational difficulties of conventional methods, will the accuracy of lifting surface theory become available to rotary wing aerodynamics.

This report presents the development of a model problem for vortex induced airloads, its lifting surface theory solution, and its application to the calculation of rotary wing airloads. The model chosen is that of an infinite aspect ratio wing and a straight, infinite vortex at an arbitrary angle with the wing, in a compressible free stream (see Section 2.1.2). The problem is generalized to include any convected, one-dimensional (depending on only one variable) downwash field in the plane of the wing. Using the elementary doublet solution of the acceleration potential, the problem is formulated as a two-dimensional integral equation over the wing surface for the pressure. Utilizing the Fourier transform along the span of the blade, the problem is reduced to a one-dimensional integral equation for a universal (for all convected downwash fields) pressure influence function, with the span wave number as a parameter. After deriving the kernel function, this integral equation is solved numerically for cases in the entire range of geometry and velocity of the model problem. Approximate analytic expressions for the solution are obtained from the numerical solution; the Fourier integral then gives the actual loads on the wing from this approximate solution. The development of the approximate solution makes it possible to avoid in the

application of the model problem to rotary wing aerodynamics the extensive calculations involved in the usual lifting surface theory solutions.

Next the method of calculation of rotary wing airloads (using lifting line theory) is described in more detail. In applying the solution of the model problem to the calculation of rotary wing airloads, a tip vortex near a blade is represented by a straight infinite vortex of appropriate strength, position, and orientation. The downwash due to such a vortex is obtained, and the lifting surface solution of the model problem is formulated for such a downwash distribution. Since the lifting surface solution includes the vortex induced wake behind the blade, the wake of the rotor is divided into lifting surface and lifting line parts and procedures are developed to properly handle the effects of each. Finally, procedures are developed for the proper use of the combination of lifting surface and lifting line theories to calculate the loading on a rotary wing due to the tip vortices, the blade motion, and the rest of the vortex wake.

The application of the model problem to the calculation of rotary wing airloads is evaluated by comparing the loads induced by a free vortex on a one-bladed rotor at high advance ratio (see Section 4.1) as predicted by lifting surface and lifting line theories. This comparison shows that the use of lifting surface theory is necessary in order to accurately obtain the loads due to a vortex closer than a few chord lengths to the blade.

Thus the solution and procedures developed in this report remove one of the limitations of rotary wing airloads calculations. They allow the accurate prediction of loads due to a downwash distribution varying rapidly along the span of the blade, specifically the downwash due to a nearby tip vortex.

The development of the lifting surface solution for the model problem will be presented in Section 2. The development of



the application of this model to the calculation of rotary wing airloads will be presented in Section 3. A comparison of the results of using lifting line or lifting surface theory to calculate the airloads on a simplified rotary wing configuration will be presented in Section 4.

Two sets of quantities are used for nondimensionalization in this report. The density, wing semichord, and the free stream velocity ( $\rho$ ,  $b$ ,  $V$ ) are the appropriate quantities for lifting surface theory; they are used in Section 2, in the lifting surface solution of the model problem. The density, the rotor radius, and the rotor rotational speed ( $\rho$ ,  $R$ ,  $\Omega$ ) are the appropriate quantities for rotary wing aerodynamics, and are used in the remainder of this report. Nondimensional quantities are used exclusively throughout this work.

SECTION 2  
A LIFTING SURFACE SOLUTION FOR VORTEX  
INDUCED AIRFOIL LOADING

2.1 Formulation of the Model

2.1.1 The Vortex Induced Airloads Problem

It is necessary first to construct a model of the vortex induced airloads problem -- a model that can be solved by lifting surface theory and solved in a form that can be used to obtain vortex induced airloads for rotary wings.

The model to be solved here is the general three-dimensional problem of a planar lifting surface in a convected downwash field that depends on only one space coordinate. By general three dimensional is meant a combination of three variables out of the four possible (one time and three space variables). The solution is obtained using linear lifting surface theory. It involves the development of the general aerodynamic kernel which has as recognizable limits the three-dimensional steady lifting surface kernel (actually the Fourier transform of this) and the kernel for two-dimensional unsteady harmonic flow. Some singular behavior of the kernel may be expected as the first of the above limits is an elliptic problem, while the second is hyperbolic.

It is required that the solution give the airloading -- that is, the circulation, section lift, section moment, and pressure (in series form) -- due to an arbitrary distribution of downwash along the span of the blade. Furthermore, it is most important that the solution be of a form that is applicable in the highly iterative calculation of rotary wing airloads.

2.1.2 The Model of the Problem

The vortex induced airloads problem is first simplified to infinite straight geometry, as shown in Figure 2.1. The model

involves a swept, infinite aspect ratio, planar lifting surface in a subsonic free stream. A downwash distribution is induced in the plane of the airfoil ( $z=0$ ) by a skewed, infinite, straight free vortex also in an ( $x-y$ ) plane, and a distance  $h$  below the airfoil plane. As usual for a swept infinite wing, the problem will be subsonic in nature for

$$M \cos \Lambda < 1$$

where  $M \cos \Lambda$  is the Mach number of the free stream velocity normal to the span direction.

Because of the infinite geometry of the model, the problem is steady in a coordinate system with its origin traveling with the intersection of the blade centerline and the projection of the free vortex line on the ( $z=0$ ) plane. That is, in the ( $x',y'$ ) system defined by

$$x' = x - \frac{\cos \phi \sin \Lambda}{\sin(\phi + \Lambda)} t$$

$$y' = y - \frac{\cos \phi \cos \Lambda}{\sin(\phi + \Lambda)} t$$

the relative velocity is in the direction of the vortex, and this must be the direction of the trailed vorticity. In this coordinate system the vortex is stationary, so the problem is steady and there is no shed vorticity. A natural coordinate system for the problem is one with one coordinate ( $s'$ ) aligned in the direction of the free vortex. Making this transformation, obtain the geometry shown in Figure 2.2.

In Figure 2.2, the geometry has been nondimensionalized with the blade semichord  $b$ . It is seen that now the model depends on just two parameters: the normal Mach number  $M \cos \Lambda$ ; and the angle  $(\phi + \Lambda)$ .

The relative free stream Mach number in the (s',r') system is

$$M_R = \frac{M \cos \Lambda}{\sin(\phi + \Lambda)}$$

It can be seen that this Mach number is greater than 1 for  $M \cos \Lambda > \sin(\phi + \Lambda)$ ; in fact  $M_R \rightarrow \infty$  as  $(\phi + \Lambda) \rightarrow \pi$ . The fundamental influence of compressibility is, however, determined by the normal Mach number  $M \cos \Lambda$ , so the character of the problem remains subsonic. The relative Mach number  $M_R$  has more geometric than physical significance. This parameter reflects the change in the nature of the problem from elliptic to hyperbolic between the limits  $(\phi + \Lambda) = \frac{\pi}{2}$  and  $(\phi + \Lambda) = \pi$  (see Figure 2.3). In the first limit the original problem is the interaction of a blade and a vortex perpendicular to it; the problem is three dimensional and steady, and so elliptical. The second limit is the two-dimensional unsteady flow of a point vortex past an airfoil; the time dependence makes the problem hyperbolic. The transition between the elliptic and hyperbolic problems occurs at

$$\frac{M \cos \Lambda}{\sin(\phi + \Lambda)} = 1$$

with the regions as in Figure 2.4.

Now the model can be generalized to allow a more arbitrary distribution of the downwash along the blade. Consider an arbitrary distribution of downwash in the plane of the blade, which is dependent on only one variable; that is, a downwash distribution given by

$$\omega = \omega(r^*)$$

It can be seen that the downwash due to a free vortex can be put in this form, since the s' coordinate was parallel to the free

vortex direction. This form of the downwash distribution corresponds to a downwash in the original coordinate system (Figure 2.1) which depends on only one variable -- the perpendicular distance from the vortex line -- and which is being convected along by the free-stream velocity (as was the original vortex).

Thus, the model problem becomes an infinite aspect ratio lifting surface, with a convected, one-dimensional downwash field in the plane of the airfoil. The geometry is given in Figure 2.2 with the downwash given by

$$\omega = \omega(r^{\circ})$$

The problem is further dependent on the two parameters  $M \cos \Lambda$  and  $(\phi + \Lambda)$ . The limits  $(\phi + \Lambda) = \frac{\pi}{2}$  and  $(\phi + \Lambda) = \pi$  give, respectively, the problems of a symmetric, steady lifting surface, and a two-dimensional unsteady flow.

### 2.1.3 Details of the Model

The several coordinate systems which will be used are shown in Figure 2.5. The various transformations are given below.

$$x^{\circ} = x - \frac{\cos \phi \sin \Lambda}{\sin(\phi + \Lambda)} t$$

$$y^{\circ} = y - \frac{\cos \phi \cos \Lambda}{\sin(\phi + \Lambda)} t$$

$$s^{\nu} = x^{\nu} \sin \phi - y^{\nu} \cos \phi$$

$$r^{\nu} = x^{\nu} \cos \phi + y^{\nu} \sin \phi$$

$$s^{\nu} = s / \sin \Lambda - r \cos \Lambda$$

$$r^{\nu} = r \sin \Lambda$$

$$s = x^{\nu} \cos \Lambda - y^{\nu} \sin \Lambda$$

$$r = x^{\nu} \cos \phi / \sin \Lambda + y^{\nu} \sin \phi / \sin \Lambda$$

$$s^{\nu} = s^A \sin \Lambda - r^A \cos \Lambda$$

$$r^{\nu} = s^A \cos \Lambda + r^A \sin \Lambda$$

$$s^A = x^{\nu} \cos \Lambda - y^{\nu} \sin \Lambda$$

$$r^A = x^{\nu} \sin \Lambda + y^{\nu} \cos \Lambda$$

$$s = s^A$$

$$r = s^A / \tan \Lambda + r^A$$

with the convention, to be used in what follows, that sin, cos, or tan written alone imply the argument  $(\phi + \Lambda)$ .

The (x,y) system is the original absolute system.

The (x',y') system is the one in which the problem is steady.

The (s',r') system is the natural coordinate system for the convected velocity field, since the downwash then depends only on the coordinate r'.

The (s,r) system is the one in which the problem must be solved to obtain the circulation. One coordinate is along the span (so the Fourier transform may be used) and the other in the s' direction (along which must integrate to obtain the circulation). The s metric has been stretched so the blade leading and trailing edges are given by  $s = \pm 1$ .

The ( $s^A, r^A$ ) system is the one in which the problem must be solved to obtain the loads. One coordinate is along the span (so the Fourier transform may be used) and the other normal to the span direction (along which must integrate to obtain the section loads). The blade leading and trailing edges are given by  $s^A = \pm 1$ .

All the systems except (s,r) are orthogonal. All the origins lie on the blade centerline. The third space variable for all systems is the z coordinate, directed upwards.

The problem is nondimensionalized with ( $\rho, b, V$ ).

The downwash is positive directed in the negative z direction.

The range of the parameter ( $\phi + \Lambda$ ) can be restricted by symmetry considerations to

$$\frac{\pi}{2} < (\phi + \Lambda) < \pi$$

For the case  $0 < (\phi + \Lambda) < \frac{\pi}{2}$  the solution may be obtained by making the substitutions  $(\phi + \Lambda) \Rightarrow \pi - (\phi + \Lambda)$  and  $r^A \Rightarrow -r^A$ .

While the solution will be obtained for the general downwash  $w(r')$ , the free vortex case is useful as an indication of the form of the distributions to which the solution will be applied. The downwash due to a free vortex in the plane  $z = h$  is given by

$$\omega_{\Gamma}(r') = \frac{\Gamma}{2\pi bV} \frac{-r'}{r'^2 + h^2}$$

For later use, the Fourier transform is also required. The Fourier transform of  $w_{\Gamma}$  with respect to  $r'$  is then

$$\begin{aligned} \bar{\omega}_{\Gamma}(\lambda) &= \frac{1}{2\pi} \int_{-\infty}^{\infty} \omega_{\Gamma}(r') e^{-i\lambda r'} dr' \\ &= \frac{\Gamma}{2\pi bV} \frac{i}{2} \operatorname{sgn}(\lambda) e^{-|\lambda| h} \end{aligned}$$

The Fourier transform is used to obtain the lifting surface solution. The definitions of the Fourier integral and Fourier transform to be used here are

$$f(r) = \int_{-\infty}^{\infty} \bar{f}(\lambda) e^{i\lambda r} d\lambda$$

and

$$\bar{f}(\lambda) = \frac{1}{2\pi} \int_{-\infty}^{\infty} f(r) e^{-i\lambda r} dr$$

The following notation is convenient:

$$\bar{f}(\lambda) = \text{F.T. of } f(r') \text{ wrt } r$$

means

$$\bar{f}(\lambda) = \frac{1}{2\pi} \int_{-\infty}^{\infty} f(r') e^{-i\lambda r'} dr'$$

#### 2.1.4 The Nature of the Solution

The formulation of the model and obtaining the solution involves several steps in reducing the problem to a tractable form. Fundamental to the solution is the use of linear lifting surface



theory; that is, determine the loads on a planar lifting surface from the kernel function solution of the linearized equations of motion of the flow. Thus many effects, such as those due to thickness, to viscosity, or to vortex bursting are immediately ignored. Lifting surface theory allows the solution to be obtained for a wing with arbitrary planform and downwash distribution, including compressibility and unsteady flow effects. This is the general problem in four dimensions:  $(x, y, z, t)$ . However, the use in helicopter airloads calculations requires the solution in compact form for a general downwash distribution. The problem must be simplified further so the lifting surface solution may be obtained for as few parameters as possible, and then the solution may be routinely applied to airloads calculations.

An important step is the simplification of the planform to an infinite aspect ratio, constant chord airfoil.

Next, the type of downwash field is restricted by specifying that the downwash depends on only one variable, which must be linear in the spanwise variable. For application to vortex induced loading, the appropriate class of downwash fields is the convected field, which may be written  $w = w(r')$  so there is no variation with  $s'$ . The restriction to one-dimensional downwash fields, together with the infinite geometry of the wing, reduces the problem to three dimensions:  $(x, y \text{ and } t, z)$  or  $(s', r', z)$ .

Now linearization of the equations of motion of the flow and the boundary conditions allows the solution to be obtained, using the principle of superposition, as the solution of an integral equation. The kernel in the integral equation formulation is the general aerodynamic kernel function for a planar infinite aspect ratio wing, involving three of the possible four dimensions. The particular combination of the dimensions is specified by a geometric parameter,  $(\phi + \Lambda)$ .

Compressibility effects are essential to the problem, thus there is an additional parameter  $M \cos \Lambda$ . The integral equation is a two-dimensional integral, over the wing surface. Since the desired results are only the loads at  $z = 0$ , the problem reduces to two dimensions:  $(s^A, r^A)$ .

The two-dimensional integral equation still involves a solution for every specific downwash distribution, even though the problem has been already restricted to one-dimensional downwash fields. At this point, however, the infinite geometry of the wing allows the important step of the introduction of the Fourier transform along the span variable. This replaces the variable  $r^A$  by the wave number  $\gamma$ , which appears simply as a parameter. Thus, the problem is reduced to one dimension:  $(s^A)$ .

Now the problem has been formulated as a one-dimensional integral equation in the chordwise variable  $s^A$ . There are three quantities appearing as parameters in the integral equation:

Mach number	$M \cos \Lambda$
angle	$(\phi + \Lambda)$
and wave number	$\gamma$

There is an additional parameter implicit in the selection of the class of downwash fields. Here it is possible to restrict the problem to convected fields.

The reduction from a two-dimensional to a one-dimensional integral equation is primarily of calculational significance. The use of the Fourier transform has a more important result. Because the problem has been restricted to downwash fields dependent on only one variable, the application of the F.T. with respect to the span coordinate changes the downwash to a separable function of the wave number and the chordwise coordinate. The functional dependence on the chordwise coordinate will be known. The dependence on the wave number will remain arbitrary, but because the wave

number appears only as a parameter -- and because the integral equation is linear -- this function may be moved inside the integral equation. Thus, the solution of the problem involves the solution of a one-dimensional integral equation for a universal loading function which depends on the class of downwash fields chosen (here the convected field) but not on the particular downwash distribution from the class.

The reduction of the solution to a universal loading influence function for convected velocity fields is essential to producing a solution applicable to the calculation of rotary wing airloads. This formulation is accomplished by the use of the Fourier transform along the span, and depends on several features of the model: first, linearization of the equation of motion and boundary conditions; second, the infinite geometry of the wing; third, the restriction of type of downwash field to those dependent on only one variable.

Obtaining a numerical solution for the universal loading functions will not be sufficient, however. Numerical results may not be conveniently used to determine actual loadings, particularly with the results in terms of wave number. Thus, the exact numerical solutions must be used to produce approximate analytic solutions. These approximate influence functions, together with the Fourier transformation of the actual downwash distribution may be used to obtain the airloading by means of the Fourier integral.

## 2.2 Lifting Surface Solution of the Problem

### 2.2.1 Equations of Motion

The solution is most conveniently formulated in terms of the acceleration potential  $\psi$ . The linearized equation of motion is

$$\mathcal{L}[\psi] = \left[ \nabla^2 - M^2 \left( \frac{\partial}{\partial x} + \frac{\partial}{\partial t} \right)^2 \right] \psi = 0$$

where

$$\Psi = \frac{D}{Dt} \phi = \left( \frac{\partial}{\partial x} + \frac{\partial}{\partial t} \right) \phi = -P$$

Here  $\phi$  is the velocity potential. The boundary conditions are

$$\left. \frac{\partial \phi}{\partial z} \right|_{z=0} = \omega \quad \text{on the airfoil}$$

and with  $p =$  the perturbation pressure,

$$\Delta \Psi = -\Delta p = 0 \quad \text{off the airfoil}$$

Again, the problem has been nondimensionalized with  $(g, b, V)$ .

The natural coordinate system for the present problem is the  $(s', r')$  system, in which the problem is steady. In this system, the equation of motion becomes

$$\left[ \left( 1 - \left( \frac{M \cos \Lambda}{\sin(\phi + \Lambda)} \right)^2 \right) \frac{\partial^2}{\partial s'^2} + \frac{\partial^2}{\partial r'^2} + \frac{\partial^2}{\partial z^2} \right] \Psi = 0$$

where

$$\Psi = -P = \frac{\cos \Lambda}{\sin(\phi + \Lambda)} \frac{\partial}{\partial s'} \phi$$

The boundary conditions for the convected downwash field are

$$\left. \frac{\partial \phi}{\partial z} \right|_{z=0} = \omega(r') \quad \text{on the airfoil}$$

and

$$\Delta \Psi = -\Delta p = 0 \quad \text{off the airfoil}$$

It is seen that the relative Mach number

$$M_R = \frac{M \cos \Lambda}{\sin(\phi + \Lambda)}$$

does indeed determine whether the flow is basically elliptic or hyperbolic. For the elliptic case, the flow is like the three-dimensional steady flow problem; for the hyperbolic case, the flow is like the two-dimensional unsteady problem. The domains of the two types of flow were shown in Figure 2.4. In the actual derivation of the integral equations and their kernels, it will be necessary to treat the two cases separately, because of the fundamentally different nature of elliptic and hyperbolic elementary solutions. First, though, the general solution procedure will be developed.

The relation between  $\Psi$  and  $\phi$  will be integrated in the (s,r) system. In these coordinates

$$\Psi = \cos \Lambda \frac{\partial}{\partial s} \phi$$

which may be integrated to

$$\phi = \int_{-\infty}^s \Psi(s,r) \Big|_{s=\lambda} \frac{\partial \lambda}{\cos \Lambda}$$

which can be rewritten as

$$\phi = \int_0^{\infty} \Psi(s,r) \Big|_{\substack{s=s-\lambda \\ \text{OR} \\ s_0=s_0-\lambda}} \frac{\partial \lambda}{\cos \Lambda}$$

(where  $s_0 = s - \sigma$ )

which is more convenient because of the constant limits of integration.

### 2.2.2 Formulation of the Integral Equation

An integral equation for the airfoil loading will be obtained from the elementary solution of the equation of motion, using the principle of superposition. The integral equation will first be derived in the (s,r) system.

The elementary lifting solution for the acceleration potential is the dipole solution, denoted by  $\psi_d$ . Using superposition, the acceleration potential at an arbitrary point due to a lifting surface may be written

$$\psi(s, r, z) = \iint_{\text{airfoil}} A(\sigma, \xi) \psi_d(s_0^\sigma, r_0^\sigma, z) d\sigma d\xi$$

where

$$s_0^\sigma = s^\sigma - \sigma^\sigma, \quad r_0^\sigma = r^\sigma - \xi^\sigma$$

Evaluating this for a point on the airfoil, being careful of the limiting process, can identify (with the proper choice of the constant in  $\psi_d$ )

$$L(s, r) = -\Delta p = \Delta \psi = A(s, r)$$

where  $\Delta = \text{upper-lower}$  and  $L(s, r)$  is the airfoil loading. It is seen that taking the integral only over the airfoil surface automatically satisfies the boundary condition that

$$-\Delta p = \Delta \psi = 0 \quad \text{off the airfoil.}$$

This is the advantage of the acceleration potential formulation.

Now for the boundary condition on the airfoil. Recall from above that

$$\phi = \int_0^\infty \psi |_{s_0=s_0-\lambda} d\lambda / \cos \lambda$$

The boundary condition to be satisfied is

$$\frac{\partial \phi}{\partial z} \Big|_{z=0} = \omega(r^\sigma) \quad \text{on the airfoil}$$

Combining the two equations gives

$$\omega(r^\sigma) = \lim_{z \rightarrow 0} \frac{\partial}{\partial z} \int_0^\infty \psi |_{s_0=s_0-\lambda} d\lambda / \cos \lambda$$

Now introducing the result for  $\psi$  in terms of the loading  $L(s, r)$ , and for convenience normalizing the loading, gives the required

integral equation:

$$\omega(r^2) = \int_{-\infty}^{\infty} \int_{-1}^1 \frac{L(s, r) / g V^2}{2\pi \frac{\cos \lambda}{\alpha}} \left\{ \lim_{z \rightarrow 0} \frac{\partial}{\partial z} \int_0^{\infty} \psi_d \Big|_{s_0 = s_0 - \lambda} \partial \lambda \frac{2\pi}{\alpha} \right\} \partial \tau \partial s$$

where  $\alpha^2 = 1 - (M \cos \lambda)^2$

Now writing the pressure  $L(s, r)$  as a Fourier integral

$$L(s, r) = \int_{-\infty}^{\infty} \bar{L}(s, \tau) e^{i\tau r} \partial \tau$$

and taking the Fourier transform of both sides of the integral equation with respect to  $r$ , obtain

$$\int_{-1}^1 \bar{G}(s, \tau / \sin) K(s_0, \tau / \sin) \partial \tau = -1$$

where the kernel is

$$K(s_0, \tau / \sin) = \left[ \int_{-\infty}^{\infty} -e^{-i\tau r_0} \lim_{z \rightarrow 0} \frac{\partial}{\partial z} \int_0^{\infty} \psi_d \Big|_{s_0 = s_0 - \lambda} \partial \lambda \frac{2\pi}{\alpha} \partial r_0 \right]$$

and

$$\bar{G}(s, \tau / \sin) = \frac{\bar{L}(s, \tau / \sin) / g V^2}{2\pi \frac{\cos \lambda}{\alpha} \frac{1}{\sin} \bar{\omega}(\tau / \sin)}$$

is the universal loading influence function.

Here  $\bar{\omega}(\lambda) = \text{F.T. of } \omega(r^o) \text{ wrt } r^o$

so  $\frac{1}{\sin} \bar{\omega}(\lambda/\sin) = \text{F.T. of } \omega(r^o) \text{ wrt } r$

The integral equation in the orthogonal airfoil coordinates  $(s^A, r^A)$  is obtained in a similar manner. Writing  $\Psi$  in terms of the airfoil loading

$$L^A(s^A, r^A) = -\Delta p = \Delta \Psi$$

have

$$\Psi(s^A, r^A, z) = \iint_{\text{airfoil}} L^A(s^A, r^A) \Psi_d(s_o^o, r_o^o, z) \partial s^A \partial r^A$$

Then satisfying the boundary condition on the airfoil gives the integral equation

$$\omega(r^o) = \int_{-\infty}^{\infty} \int_{r^A}^1 \frac{L^A(s^A, r^A) / R^2}{2\pi \cos \lambda} \left\{ \lim_{z \rightarrow 0} \frac{\partial}{\partial z} \int_0^{\infty} \Psi_d \Big|_{s_o = s_o - \lambda} \partial \lambda \frac{z\pi}{\alpha} \right\} \partial s^A \partial r^A$$

Note that the integral over the wake ( $\lambda$ ) must still be in the free stream direction, that is, along the  $s$  coordinate.

Now writing  $L^A(s^A, r^A)$  as a Fourier integral

$$L^A(s^A, r^A) = \int_{-\infty}^{\infty} \bar{L}^A(s^A, \lambda) e^{i\lambda r^A} \partial \lambda$$

and taking the Fourier transform of the integral equation gives

$$\int_{-1}^1 \bar{G}^A(s^A, \lambda/\sin) K^A(s_o^o, \lambda/\sin) \partial s^A = -e^{i\lambda \sin s^A \cos}$$

where the kernel is

$$K^A(s_o^o, \lambda/\sin) = \left[ \int_{r_o^A}^b -e^{-i\lambda r_o^A} \lim_{z \rightarrow 0} \frac{\partial}{\partial z} \int_0^b \Psi_d \Big|_{s_o = s_o - \lambda} \partial \lambda \frac{z\pi}{\alpha} \partial r_o^A \right]$$



and

$$\bar{G}^A(s^A, \gamma/\sin) = \frac{\bar{L}^A(s^A, \gamma/\sin) / \gamma^2}{2\pi \frac{\cos \lambda}{\alpha} \frac{1}{\sin} \bar{\omega}(\gamma/\sin)}$$

is the universal influence function.

Here  $\bar{\omega}(\gamma) = \text{F.T. of } \omega(r^p) \text{ wrt } r^p$

so  $\frac{1}{\sin} \bar{\omega}(\gamma/\sin) e^{i\gamma/\sin s^A \cos} = \text{F.T. of } \omega(r^p) \text{ wrt } r^A$

and so  $\frac{1}{\sin} \bar{\omega}(\gamma/\sin) = \text{F.T. of } \omega(r^p) \text{ wrt } r^A, \text{ at } s^A=0$

In these results, the wave number has been written in the form

$$\gamma/\sin \quad (\sin = \sin(\phi + \lambda))$$

That this is indeed the significant wave number is shown by the detailed derivation of the kernels. It will be seen that it has the limits

$$\langle \phi + \lambda \rangle = \frac{\pi}{2}, \quad \gamma/\sin = \gamma = \text{span wave number}$$

$$\langle \phi + \lambda \rangle = \pi, \quad \gamma/\sin = \gamma_e = \text{reduced frequency}$$

This is a reflection of the fact that the natural coordinate system is the  $(s', r')$  system. Recalling

$$r^p = r \sin = r^A \sin + s^A \cos$$

then the properties of Fourier transforms imply that  $\gamma/\sin$  is the natural wave number.

The derivation of the kernels will also show that

$$K^A(s_0^A, \gamma/\sin) = e^{i\gamma/\sin s_0^A \cos} K(s_0 = s_0^A, \gamma/\sin)$$

Recalling the coordinate transform between the  $(s, r)$  and  $(s^A, r^A)$  systems:

$$\begin{aligned} s_0 &= s_0^A \\ r_0 &= r_0^A + s_0^A \cos/\sin \end{aligned}$$

and that the kernels are themselves Fourier transforms ( $K$  wrt  $r_0$  and  $K^A$  wrt  $r_0^A$ ), the above result follows simply from the properties of Fourier transforms.

The integral equation obtained is of the form

$$\int_{-1}^1 \bar{G}^A K^A \Delta r^A = -RHS$$

The kernel  $K^A$  (or  $K$ ) is the general aerodynamic kernel for the three-dimensional, planar lifting surface problem. Besides the explicit parameters  $s_0^A$  (or  $s_0$ ) and  $\gamma/\sin$ , it depends on the two parameters  $(\phi + \Lambda)$  and  $M \cos \Lambda$ . The kernel depends on the airfoil configuration alone, not on the downwash distribution or any assumptions made about it.

The RHS of the integral equation represents the downwash distribution. The quantity

$$\frac{1}{\sin} \bar{w}(\gamma/\sin) (RHS) = \text{F.T. of } w(r^A) \text{ wrt } r^A \text{ (or } r)$$

and if the assumption that the downwash  $w$  depends only on one variable (so that the F.T. is separable) was not made, this would still be the proper formulation of the lifting surface integral equation, to be solved for the particular downwash distribution. The quantity RHS may be interpreted as the downwash variation in the  $s^A$  (or  $s$ ) direction of the component of the downwash with  $r^A$  (or  $r$ ) wave number  $\gamma$ . For the limit  $(\phi + \Lambda) = \pi$  it is the downwash distribution of the component with harmonic time dependence, at reduced frequency  $k$ . Note that the  $s^A$  direction is the chordwise direction,

and the  $s$  direction is the relative free stream (in the  $(s', r')$  system) direction.

The function  $\bar{G}^A$  (or  $\bar{G}$ ) is the universal loading influence function. For a nonseparable downwash Fourier transform, it would be replaced by just the F.T. of the loading,  $\bar{L}^A$  (or  $\bar{L}$ ). Because the F.T. of the downwash is separable, and the integral equation is linear, it is possible to obtain the solution for an entire class of downwash fields (convected fields here) in terms of a single universal function. As a solution of the integral equation, it depends on the kernel, and thus on the wing parameters  $M \cos \Lambda$  and  $(\phi + \Lambda)$ ; further, it depends on the RHS and thus on the class of downwash fields chosen. Given the influence function  $\bar{G}^A$  (or  $\bar{G}$ ), the F.T. of the loading  $\bar{L}^A$  (or  $\bar{L}$ ) is obtained by multiplication by  $\frac{1}{\sin} \bar{w}(\gamma/\sin)$ , and the actual loading from that as a Fourier integral.

The negative sign before the RHS of the integral equation is due to the convention that the downwash  $w$  is positive directed downward (in the negative  $z$  direction). It reflects the fact that a positive downwash gives a negative angle of attack and so negative loading.

The integral equation must be solved for each value of the parameters

$$M \cos \Lambda \quad \text{and} \quad (\phi + \Lambda)$$

and for a given Mach number and angle must be solved for all wave numbers

$$\gamma/\sin \cdot$$

The integral equation must be solved for  $\bar{G}^A$  (or  $\bar{G}$ ) as a function of  $\sigma^A$  (or  $\sigma$ ) for a given  $\gamma/\sin$ . The coordinate  $s^A$  (or  $s$ ) remains a free parameter; the integral equation must be satisfied for every value of  $s^A$  (or  $s$ ) in the range  $-1$  to  $1$ . This provides the infinite data necessary to determine  $\bar{G}^A$  (or  $\bar{G}$ ) uniquely for

every  $\sigma^A$  (or  $\sigma$ ) in the range -1 to 1.

### 2.2.3 Representation of the Loading as a Series

The airfoil loading is now represented as a Glauert series of the form:

$$-\Delta p = L^A(s^A, r^A) = \sum_{n=0}^{\infty} \lambda_n^A(r^A) f_n(s^A)$$

where

$$f_n(s^A) = \begin{cases} \tan \theta/2 & n=0 \\ \sin n\theta & n \geq 1 \end{cases} \quad s^A = \cos \theta$$

and with similar forms for  $L(s, r)$ ,  $\bar{L}^A(s^A, \gamma/\sin)$ ,  $L(s, \gamma/\sin)$ ,  $\bar{G}^A(s^A, \gamma/\sin)$ , and  $\bar{G}(s, \gamma/\sin)$ .

Substituting these forms for  $\bar{G}^A$  and  $\bar{G}$  into the integral equations gives:

$$\sum_{n=0}^{\infty} \bar{g}_n^A(\gamma/\sin) \int_{-1}^1 f_n(r^A) K^A(s_0^A, \gamma/\sin) \mathcal{D}\sigma^A = -e^{i\gamma/\sin s^A \cos}$$

and

$$\sum_{n=0}^{\infty} \bar{g}_n(\gamma/\sin) \int_{-1}^1 f_n(r) K(s_0, \gamma/\sin) \mathcal{D}\sigma = -1$$

Truncating the sum and choosing a number of collocation points equal to (or greater than) the number of retained terms, the integral equation becomes a set of simultaneous linear algebraic equations, which may be solved (in a least squares sense) for the  $\bar{g}_n^A$  or  $\bar{g}_n$  at a given  $\gamma/\sin$ .

The pressure on the airfoil  $L^A(s^A, r^A)$  has been represented as a Glauert series. Now it is necessary to obtain the circulation, section lift, and section moment in terms of the coefficients of the series. These are required as a function of  $r^A$ .

The circulation about the blade is obtained from the expression given above for the velocity potential:

$$\phi = \int_{-\infty}^s \Psi(s, r, z) \Big|_{s=\lambda} \partial \lambda / \cos \Lambda$$

from which, at  $z = 0$ , have

$$\begin{aligned} \Delta \phi &= \int_{-\infty}^s \Delta \Psi \Big|_{\substack{s=\lambda \\ z=0}} \partial \lambda / \cos \Lambda \\ &= \int_{-1}^s L(s, r) \Big|_{s=\lambda} \partial \lambda / \cos \Lambda \end{aligned}$$

Thus, the circulation is

$$\Gamma = \Delta \phi_{TE} = \int_{-1}^1 L(s, r) \Big|_{s=\lambda} \partial \lambda / \cos \Lambda$$

Substituting for  $L(s, r)$  and integrating

$$\Gamma(r) = \frac{\pi}{\cos \Lambda} \left[ \varrho_0(r) + \frac{1}{2} \varrho_1(r) \right]$$

This is put in terms of  $r^A$  by noting that  $\Gamma$  is  $\Delta \phi$  at the blade trailing edge,  $s^A = 1$ , where

$$r = r^A + \cos / \sin$$

Thus,

$$\Gamma(r^A) = \frac{\pi}{\cos \Lambda} \left[ \varrho_0(r) + \frac{1}{2} \varrho_1(r) \right] \Big|_{r=r^A + \cos / \sin}$$

Now it is evident why the solution for the loads in the  $(s, r)$  system is required. The circulation is obtained from the integral of the velocity potential around the blade. The velocity potential is obtained from the acceleration potential, that is from the perturbation pressure, by integrating in the direction of the relative free stream, the  $s$  direction. The  $r$  coordinate, of course, must be directed along the span.

The section lift and moment are obtained by directly integrating the pressures. The lift and moment on sections normal to the span direction are required, so the loading in the  $(s^A, r^A)$  system is needed.

The section lift, positive nose upward is

$$L(r^A) = \int_{-1}^1 (-\Delta p) \partial s^A = \int_{-1}^1 L^A(s^A, r^A) \partial s^A$$

Substituting the Glauert series gives

$$L(r^A) = \pi \left[ \varrho_0^A(r^A) + \frac{1}{2} \varrho_1^A(r^A) \right]$$

The section moment, positive nose upward, about an axis at  $s^A = a$ , is

$$\begin{aligned} M(r^A) &= \int_{-1}^1 (-\Delta p) (a - s^A) \partial s^A \\ &= \int_{-1}^1 L^A(s^A, r^A) (a - s^A) \partial s^A \end{aligned}$$

Substituting the Glauert series gives

$$\begin{aligned} M(r^A) &= \left(\frac{1}{2} + a\right) L(r^A) + M_{QC}(r^A) \\ M_{QC}(r^A) &= -\frac{\pi}{4} \left[ \varrho_1^A(r^A) + \varrho_2^A(r^A) \right] \end{aligned}$$

where  $M_{QC}$  is the moment about the quarter chord at  $s^A = -1/2$ .

It is now possible to obtain the F.T. wrt  $r^A$  of the loads as:

$$\begin{aligned} \overline{L}(r/\sin) &= e^{i r/\sin \cos} \frac{\pi}{\cos \lambda} \left[ \overline{\varrho}_0(r/\sin) + \frac{1}{2} \overline{\varrho}_1(r/\sin) \right] \\ \overline{M}(r/\sin) &= \pi \left[ \overline{\varrho}_0^A(r/\sin) + \frac{1}{2} \overline{\varrho}_1^A(r/\sin) \right] \end{aligned}$$

and

$$\overline{M}_{QC}(r/\sin) = -\frac{\pi}{4} \left[ \overline{\varrho}_1^A(r/\sin) + \overline{\varrho}_2^A(r/\sin) \right]$$

### 2.2.4 The Results of the Solution

The solution of the integral equations will be in the form

$$\frac{\bar{F}(\lambda/\sin)}{\text{const} + \frac{1}{\sin} \bar{w}(\lambda/\sin)} = \text{function}(\lambda/\sin; M \cos \lambda \pm \frac{1}{2}(\phi + \lambda))$$

for

$\bar{F}(\lambda/\sin)$	const	function
$\bar{x}_n(\lambda/\sin)/gV^2$	$\frac{2\pi}{\alpha} \cos \lambda$	$\bar{g}_n(\lambda/\sin)$
$\bar{x}_n^A(\lambda/\sin)/gV^2$	$\frac{2\pi}{\alpha} \cos \lambda$	$\bar{g}_n^A(\lambda/\sin)$
$\bar{L}(\lambda/\sin)/gV^2 b$	$\frac{2\pi}{\alpha} \cos \lambda$	$\bar{g}_L(\lambda/\sin) = \pi \left[ \bar{g}_0^A(\lambda/\sin) + \frac{1}{2} \bar{g}_2^A(\lambda/\sin) \right]$
$\bar{M}_{oc}(\lambda/\sin)/gV^2 b^2$	$\frac{2\pi}{\alpha} \cos \lambda$	$\bar{g}_M(\lambda/\sin) = -\frac{\pi}{4} \left[ \bar{g}_2^A(\lambda/\sin) + \bar{g}_2^A(\lambda/\sin) \right]$
$\bar{P}(\lambda/\sin)/Vb$	$\frac{2\pi}{\alpha}$	$\bar{g}_c(\lambda/\sin) = \pi \left[ \bar{g}_0(\lambda/\sin) + \frac{1}{2} \bar{g}_2(\lambda/\sin) \right] e^{i\lambda/\sin \cos}$

These are the loading influence functions. All are Fourier transforms with respect to  $r^A$ .

The factor  $2\pi$  is the two-dimensional lift curve slope.

The factor  $1/\alpha = 1/\sqrt{1-(M\cos\Lambda)^2}$  is the Prandtl-Glauert compressibility correction expected for a swept wing.

The factor  $\cos\Lambda$  appears because the loads and downwash were nondimensionalized with the actual velocity  $V$ , rather than with the physically relevant velocity ( $V \cos\Lambda$ ). That the  $\cos\Lambda$  appears in the loads but not in the circulation can be viewed as a reflection of the general result that the circulation depends on the induced velocity but the loads depend on the induced angle of attack.

The factor  $e^{i\gamma/\sin\Lambda}$  appearing in  $\bar{g}_C$  results from the fact that the circulation is determined by a quantity at the trailing edge, while the  $r^A$  axis lies at the blade centerline.

From the numerical solution of the integral equation, it is necessary to obtain approximate analytic forms for the influence functions. It is the inverse transforms of these approximations which will be applied to the calculation of rotary wing airloads. Results in terms of wave number are generally not too meaningful physically. The value of the influence functions lies in their being universal functions, independent of the particular downwash distribution, and it was to formulate the solution in this manner that the use of the Fourier transform was essential. Thus approximating the influence functions is indeed the proper means to obtain an approximate solution for the vortex induced airloading.

## 2.3 The Kernels

### 2.3.1 The Elliptic Kernel

The elliptic domain is given by  $M\cos\Lambda < \sin(\phi + \Lambda)$ . The equation of motion can be written as

$$\left[ \beta^2 \frac{\partial^2}{\partial s^2} + \frac{\partial^2}{\partial r^2} + \frac{\partial^2}{\partial z^2} \right] \psi = 0$$



where

$$\beta^2 = 1 - \left( \frac{M \cos \Lambda}{\sin(\phi + \Lambda)} \right)^2 > 0$$

and with the boundary conditions

$$\left. \frac{\partial \phi}{\partial z} \right|_{z=0} = \omega(r^*) \quad \text{on airfoil}$$

$$-\Delta p = \Delta \psi = 0 \quad \text{off airfoil}$$

The doublet solution of this equation is

$$\psi_d = \frac{\partial}{\partial z} \frac{1}{R}, \quad R^2 = s_0'^2 + \beta^2 r_0'^2 + \beta^2 z^2$$

where  $s_0' = s' - r'$ ,  $r_0' = r' - \xi'$

and the doublet is located in the  $z=0$  plane.

The integral equation will be obtained first in the  $(s,r)$  system. Recalling that although the  $(s,r)$  system is nonorthogonal, the  $s$  metric has been stretched so the Jacobian  $J = \frac{\partial(s',r')}{\partial(s,r)} = 1$ , and the blade leading and trailing edges are given by  $s = \pm 1$ , may write the superposition integral as

$$-p = \psi = \int_{\xi}^{\infty} \int_{-1}^1 A(\sigma, \xi) \frac{\partial}{\partial z} \frac{1}{R} d\sigma d\xi$$

Then being careful about the limiting processes, find at the airfoil

$$-\Delta p = \Delta \psi = -4\pi A(s,r)$$

$\Delta =$  upper-lower

so let

$$L(s,r) = -\Delta p = -4\pi A(s,r)$$

As before, the velocity potential is

$$\phi = \int_0^{\infty} \Psi |_{s_0=s_0-\lambda} \partial \lambda / \cos \Lambda$$

Thus

$$\left. \frac{\partial \phi}{\partial z} \right|_{z=0} = \int_{-\infty}^{\infty} \int_{-\infty}^{\infty} \int_{-1}^1 - \frac{L(\tau, \xi)}{4\pi \cos \Lambda} \lim_{z \rightarrow 0} \frac{\partial^2}{\partial z^2} \left. \frac{1}{R} \right|_{s_0=s_0-\lambda} \partial \tau \partial \xi \partial \lambda$$

Performing the operation  $\lim_{z \rightarrow 0} \frac{\partial^2}{\partial z^2}$ , the boundary condition then gives the integral equation

$$\omega(r') = \int_{-\infty}^{\infty} \int_{-1}^1 \frac{L(\tau, \xi)/r'^2}{2\pi \frac{\cos \Lambda}{\alpha}} \frac{\beta^2}{2\alpha} \int_0^{\infty} \frac{1}{[s_0^2 + \beta^2 r_0'^2]^{3/2}} \Big|_{s_0=s_0-\lambda} \partial \lambda \partial \tau \partial \xi$$

Now writing  $L(\tau, \xi)$  as a Fourier integral, the equation may be written

$$\omega(r') = \int_{-\infty}^{\infty} \left\{ \int_{-1}^1 - \frac{L(\tau, \xi) \sin \tau / r'^2}{2\pi \frac{\cos \Lambda}{\alpha}} \frac{\beta^2}{2\alpha} \int_0^{\infty} \int_{r_0}^{\infty} \frac{-e^{-i\tau r_0}}{[s_0^2 + \beta^2 r_0'^2]^{3/2}} \Big|_{s_0=s_0-\lambda} \partial r_0 \partial \lambda \partial \tau \right\} e^{i\tau r'} \partial \tau$$

This is recognized as a Fourier integral representation. The term in brackets is then the F.T. of  $w(r')$  wrt  $r$ . Thus obtain the integral equation

$$\int_{-1}^1 \overline{G}(\tau, \xi / \sin) K_{\beta}(s_0, \xi / \sin) \partial \tau = -1$$

where

$$\bar{G}(r, \nu/\sin) = \frac{L(r, \nu/\sin) / \rho Y^2}{2\pi \frac{\cos \nu}{\alpha} \frac{1}{\sin} \bar{w}(\nu/\sin)}$$

and the kernel is

$$K_{\beta}(s_0, \nu/\sin) = \left[ \frac{\beta^2}{2\alpha} \int_{\lambda}^{\infty} \int_{r_0}^{\infty} \frac{-e^{-i\nu r_0}}{[s_0^2 + \beta^2 r_0^2]^{3/2}} \Big|_{s_0=s_0-\lambda} \mathcal{D}r_0 \mathcal{D}\lambda \right]$$

To evaluate the kernel, it is helpful to first replace the  $\lim_{z \rightarrow 0}$  operator. Thus the kernel actually is

$$K_{\beta}(s_0, \nu/\sin) = \lim_{z \rightarrow 0} \left[ \frac{\beta^2}{2\alpha} \int_{\lambda}^{\infty} \int_{r_0}^{\infty} \frac{-e^{-i\nu r_0}}{[s_0^2 + \beta^2 r_0^2 + \beta^2 z^2]^{3/2}} \Big|_{s_0=s_0-\lambda} \mathcal{D}r_0 \mathcal{D}\lambda \right]$$

Now writing

$$[s_0^2 + \beta^2 r_0^2] \Big|_{s_0=s_0-\lambda} = [r_0 \alpha - (s_0 - \lambda) / (\alpha \tan)]^2 + [(s_0 - \lambda) \beta / \alpha]^2$$

one can perform the  $r_0$  integration to get

$$K_{\beta}(s_0, \nu/\sin) = -\frac{\nu \beta^2}{\alpha^4} \int_0^{\infty} e^{-i\nu/\sin (s_0 - \lambda) \cos/\alpha^2} \lim_{z \rightarrow 0} \frac{K_1(\nu \beta / \alpha^2 \sqrt{(s_0 - \lambda)^2 + \alpha^2 z^2})}{\nu \beta / \alpha^2 \sqrt{(s_0 - \lambda)^2 + \alpha^2 z^2}} \mathcal{D}\lambda$$

where  $K_1$  is the modified Bessel function of the second kind.

For  $z = 0$  this is a singular integral of Mangler's type, so some care is needed in evaluating it further. For this type of integral the result of integrating and taking the limit as  $z \rightarrow 0$  may be obtained by simply setting  $z = 0$  and ignoring the singularity. That this procedure is valid can be verified directly for the limit  $\nu/\sin = 0$ , for which obtain

$$K_{\beta}(s_0, 0) = \frac{1}{s_0}$$

The procedure for further evaluation of the kernel is suggested by similar steps in the derivation of the hyperbolic kernel, which is given in Section 2.3.2.

The kernel may be rewritten as

$$K_{\beta}(s_0, \gamma/\sin) = \frac{1}{\alpha^2} \int_0^{\infty} e^{-i\gamma/\sin(s_0-\lambda)\cos/\alpha^2} \lim_{z \rightarrow 0} \frac{\partial^2}{\partial z^2} K_0\left(\frac{\gamma\beta}{\alpha^2} \sqrt{(s_0-\lambda)^2 + \alpha^2 z^2}\right) d\lambda$$

Now  $K_0\left(\frac{\gamma\beta}{\alpha^2} \sqrt{(s_0-\lambda)^2 + \alpha^2 z^2}\right)$  satisfies the PDE

$$\alpha^2 \frac{\partial^2 K_0}{\partial \lambda^2} + \frac{\partial^2 K_0}{\partial z^2} - \frac{\gamma^2 \beta^2}{\alpha^2} K_0 = 0$$

Substituting for  $\frac{\partial^2}{\partial z^2} K_0$  gives

$$K_{\beta}(s_0, \gamma/\sin) = - \int_0^{\infty} e^{-i\gamma/\sin(s_0-\lambda)\cos/\alpha^2} \frac{\partial^2}{\partial \lambda^2} K_0\left(\frac{\gamma\beta}{\alpha^2} |s_0-\lambda|\right) d\lambda + \frac{\gamma^2 \beta^2}{\alpha^4} \int_0^{\infty} e^{-i\gamma/\sin(s_0-\lambda)\cos/\alpha^2} K_0\left(\frac{\gamma\beta}{\alpha^2} |s_0-\lambda|\right) d\lambda$$

where the limit  $z \rightarrow 0$  has also been taken. Integrating by parts twice, the first term gives

$$K_{\beta}(s_0, \gamma/\sin) = - e^{-i\gamma/\sin s_0 \cos/\alpha^2} \left[ \mp \frac{\gamma\beta}{\alpha^2} K_{\perp}\left(\frac{\gamma\beta}{\alpha^2} |s_0|\right) + i\gamma/\sin \cos/\alpha^2 K_0\left(\frac{\gamma\beta}{\alpha^2} |s_0|\right) \right] + \frac{(\gamma/\sin)^2}{\alpha^2} \int_0^{\infty} e^{-i\gamma/\sin(s_0-\lambda)\cos/\alpha^2} K_0\left(\frac{\gamma\beta}{\alpha^2} |s_0-\lambda|\right) d\lambda$$

Now writing

$$\begin{aligned}
& \int_0^{\infty} e^{-i\beta/\sin(s_0-\lambda) \cos/\alpha^2} K_0\left(\frac{\beta}{\alpha^2} |s_0-\lambda|\right) d\lambda \\
&= \int_{-s_0}^{s_0} e^{-i\beta/\sin \lambda \cos/\alpha^2} K_0\left(\frac{\beta}{\alpha^2} |\lambda|\right) d\lambda \\
&= -\frac{\alpha^2}{\beta/\sin \cos} \int_{-\infty}^{-\beta/\sin s_0 \cos/\alpha^2} e^{i\beta/\sin \cos |\lambda|} K_0\left(\frac{\beta}{\alpha^2} |\lambda|\right) d\lambda
\end{aligned}$$

and using

$$\int_{-\infty}^0 K_0(a|\lambda|) e^{i\beta/\sin \cos |\lambda|} d\lambda = \frac{\frac{\pi}{2} - i \ln \frac{1+\sqrt{1+a^2}}{a}}{\sqrt{1+a^2}}$$

(from Watson, Ref. 14) and simplifying the notation, the kernel is written as

$$\begin{aligned}
K_{\beta}(s_0, \beta/\sin) &= e^{ia\mu s_0} \left[ \pm a K_1(a|s_0|) \right. \\
&\quad \left. + ia\mu K_0(a|s_0|) \right] \\
&\quad - \frac{i}{2\alpha} \frac{\beta}{\sin} \left[ \pi i + \ln \frac{\alpha - \cos}{\alpha + \cos} \right] \\
&\quad \pm \frac{1}{\beta \sin} \left( \frac{\beta}{\sin} \right)^{\alpha|s_0|} \int_0^{\alpha|s_0|} e^{\pm i\mu \xi} K_0(\xi) d\xi
\end{aligned}$$

where

$$\begin{aligned}
\pm &= \text{sgn}(s_0) \\
a &= \frac{\beta}{\sin} \frac{\beta \sin}{\alpha^2} \\
\mu &= \frac{-\cos}{\beta \sin} \\
a\mu &= \frac{-\cos}{\alpha^2} \frac{\beta}{\sin} \\
\beta \sin &= \sqrt{\alpha^2 - \cos^2} \\
\alpha^2 &= 1 - (M \cos \mathcal{L})^2
\end{aligned}
\quad
\begin{aligned}
\sin &\equiv \sin(\phi + \mathcal{L}) \\
\cos &\equiv \cos(\phi + \mathcal{L}) \\
\frac{\pi}{2} &< (\phi + \mathcal{L}) < \pi
\end{aligned}$$

Now we will derive the kernel in the  $(s^A, r^A)$  coordinate system. Writing the pressure as

$$-\Delta p = L^A(s^A, r^A)$$

the boundary condition gives

$$\omega(r^A) = \int_{s_0^A}^{s_0^A} \int_{-1}^1 \frac{L^A(s^A, r^A) / \beta^2}{2\pi \frac{\cos \lambda}{\alpha}} \frac{\beta^2}{2\alpha} \int_0^{r_0^A} \frac{1}{[s_0^A{}^2 + \beta^2 r_0^A{}^2]^{3/2}} \Big|_{s_0^A = s_0^A - \lambda} d\lambda d s^A d r^A$$

Substituting for  $L^A(s^A, r^A)$  as a Fourier integral and taking the F.T. wrt  $r^A$  of the integral equation obtain

$$\int_{-1}^1 \bar{G}^A(s^A, \gamma/\sin) K_{\beta}^A(s_0^A, \gamma/\sin) d s^A = -e^{i\gamma/\sin s^A \cos}$$

where

$$\bar{G}^A(s^A, \gamma/\sin) = \frac{L^A(s^A, \gamma/\sin) / \beta^2}{2\pi \frac{\cos \lambda}{\alpha} \frac{1}{\sin} \bar{\omega}(\gamma/\sin)}$$

and the kernel is

$$K_{\beta}^A(s_0^A, \gamma/\sin) = \left[ \frac{\beta^2}{2\alpha} \int_{-\infty}^{r_0^A} \int_0^{r_0^A} \frac{-e^{-i\gamma r_0^A}}{[s_0^A{}^2 + \beta^2 r_0^A{}^2]^{3/2}} \Big|_{s_0^A = s_0^A - \lambda} d\lambda d r_0^A \right]$$

As before, replacing the  $\lim_{z \rightarrow 0}$  process and writing

$$[s_0^A{}^2 + \beta^2 r_0^A{}^2] \Big|_{s_0^A = s_0^A - \lambda} = \left[ r_0^A \alpha + s_0^A \alpha / \tan - (s_0^A - \lambda) / (\alpha \tan) \right]^2 + [(s_0^A - \lambda) \beta / \alpha]^2$$

one can perform the  $r^A$  integration to get

$$K_{\beta}^A(s_0^A, \gamma/\sin) = -\frac{\gamma^2 \beta^2}{\alpha^4} e^{i\gamma/\sin s_0^A \cos} \int_0^{r_0^A} e^{-i\gamma/\sin (s_0^A - \lambda) \cos / \alpha z} \lim_{z \rightarrow 0} \frac{K_1(\gamma \beta / \alpha z \sqrt{(s_0^A - \lambda)^2 + \alpha^2 z^2})}{\gamma \beta / \alpha z \sqrt{(s_0^A - \lambda)^2 + \alpha^2 z^2}} d\lambda$$

From this form recognize that

$$\begin{aligned}
 K_{\beta}^A(s_0^A, \gamma/\sin) &= e^{i\gamma/\sin s_0^A \cos} K_{\beta}(s_0=s_0^A, \gamma/\sin) \\
 &= e^{-i\gamma \mu \alpha^2 s_0^A} K_{\beta}(s_0=s_0^A, \gamma/\sin)
 \end{aligned}$$

Several limiting cases of the elliptic kernel are of interest. First consider the lifting line limit,  $\gamma/\sin \rightarrow 0$ . For  $\gamma/\sin = 0$  have

$$K_{\beta}(s_0^A, 0) = K_{\beta}^A(s_0^A, 0) = \frac{1}{s_0^A}$$

So the integral equation becomes

$$\int_{-1}^1 \bar{G}^A(\sigma^A, 0) \frac{d\sigma^A}{s_0^A} = -1$$

which inverts directly to

$$\bar{G}^A(s^A, 0) = \bar{G}(s^A, 0) = -\frac{1}{\pi} \sqrt{\frac{1-s^A}{1+s^A}}$$

or

$$\bar{g}_0^A(0) = \bar{g}_0(0) = -\frac{1}{\pi}$$

$$\bar{g}_n^A(0) = \bar{g}_n(0) = 0, \quad n \geq 1$$

That this result is the lifting line limit can be seen by recalling that

$$\gamma/\sin = b \text{ times } [\text{dimensional wave number}]$$

Thus as  $b \rightarrow 0$ ,  $\gamma/\sin \rightarrow 0$  for any finite dimensional wave number, and  $b \rightarrow 0$  is the lifting line limit. The integral equation is reduced to the two-dimensional steady integral equation. This is the usual result of lifting line theory that the inner problem is locally two-dimensional, the influence of the finite span entering only through an induced downwash at the airfoil section due to the trailed wake. Here, for a given downwash field, as  $b \rightarrow 0$  the

wake induced velocity also  $\rightarrow 0$ , so the two-dimensional problem involves only the convected velocity field.

In the limit  $(\phi + \lambda) = \frac{\pi}{2}$ , the vortex and blade are perpendicular, and the kernels reduce to

$$K_{\beta}^A(s_0^A, \gamma/\sin) = K_{\beta}(s_0^A, \gamma/\sin) = \pm \alpha k_1(\alpha |s_0^A|) + \alpha \frac{\pi}{2} \pm \alpha \int_0^{\alpha |s_0^A|} k_0(\frac{\gamma}{\alpha}) d\gamma$$

where  $\alpha = (\gamma/\sin) \frac{1}{\alpha}$ , and  $\sin = 1$ . The kernel is real, due to the symmetric wing geometry. The integral equations in  $(s, r)$  and  $(s^A, r^A)$  become identical, for these coordinate systems are identical; this means the solutions for the lift and the circulation are equal. The Mach number dependence is simply a weakly singular  $1/\alpha$  factor. In this limit  $\gamma/\sin$  becomes just the span wave number  $\gamma$ .

For  $(\phi + \lambda) = \frac{\pi}{2}$  the kernel may be put in an interesting form. Starting with the definition of the kernel, which becomes here

$$K_{\beta}^A(s_0^A, \gamma/\sin) = \left[ \int_0^{s_0^A} \int_{-\infty}^{\infty} \frac{-e^{-i\gamma r_0^A}}{[s_0^{A2} + (\beta^2 r_0^{A2})^{3/2}]^{3/2}} \right]_{s_0^A = s_0^A - \lambda} \frac{\beta^2}{2\alpha} dr_0^A d\lambda$$

since the three systems  $(s', r')$ ,  $(s, r)$ , and  $(s^A, r^A)$  become identical, and then performing the  $\lambda$  integration gives

$$K_{\beta}^A(s_0^A, \gamma/\sin) = -\frac{1}{2\alpha} \int_{-\infty}^{\infty} e^{-i\gamma r_0^A} \frac{1}{r_0^{A2}} \left[ 1 + \frac{s_0^A}{\sqrt{s_0^{A2} + \alpha^2 r_0^{A2}}} \right] dr_0^A$$

(using also that  $\beta = \alpha$ ).



This result can be recognized as the Fourier transform of the steady, three-dimensional lifting surface kernel, which is the expected result for the limit  $(\phi + \Lambda) = \frac{\pi}{2}$ .

### 2.3.2 The Hyperbolic Kernel

The hyperbolic domain is given by  $M \cos \Lambda > \sin(\phi + \Lambda)$ .

The equation of motion may be written

$$\left[ -B^2 \frac{\partial^2}{\partial r^2} + \frac{\partial^2}{\partial r^2} + \frac{\partial^2}{\partial z^2} \right] \psi = 0$$

where

$$B^2 = \left( \frac{M \cos \Lambda}{\sin(\phi + \Lambda)} \right)^2 - 1 > 0$$

with the boundary conditions

$$\frac{\partial \psi}{\partial z} \Big|_{z=0} = \omega(r^*) \quad \text{on airfoil}$$

$$-\Delta \psi = \Delta \psi = 0 \quad \text{off airfoil}$$

The derivation of the integral equation and kernel follows Possio's derivation of the two-dimensional unsteady kernel (as in Ref. 9). The solution is not as direct as for the elliptic case, because of the singular nature of the hyperbolic doublet solution. The source solution of the equation is

$$\kappa_s = \begin{cases} \frac{1}{R} > & R^2 = s_0^2 - B^2 r_0^2 - B^2 z^2 \\ & \text{for } R^2 > 0 \text{ and in the rearward} \\ & \text{range of influence.} \\ 0 & \text{Otherwise} \end{cases}$$

for source in the  $z=0$  plane.

The integral equation will first be obtained in the  $(s,r)$  system. Using superposition, the potential due to a distribution of sources on the airfoil surface is

$$\psi_s = \iint_{\mathcal{R}} \frac{A(\sigma, \vartheta) d\vartheta d\sigma}{\sqrt{s_0^2 - B^2 r_0^2 - B^2 z^2}}$$

The integration is over the domain of dependence of the point  $(s', r', z)$ , which is the intersection of the airfoil surface (on which the sources lie) and the forward characteristic cone from the point  $(s', r', z)$ . This intersection area is bounded by a hyperbola which has characteristic coordinates,  $(s^*, r^*)$ , as asymptotes. See Figure 2.6. The boundary is the hyperbola given by

$$R^2 = s_0'^2 - B^2(r_0'^2 + z^2) = 0$$

This gives the limit of the integration as

$$\vartheta = \vartheta_b = \tau - s_0 / \alpha^2 \tan - \frac{B^2}{\alpha^2} \sqrt{s_0'^2 + \alpha^2 z^2}$$

Next, writing  $A(\sigma, \vartheta)$  as a Fourier integral, the potential may be written as

$$\psi_s = \int_{-\infty}^{\infty} \int_{\sigma_1}^{\sigma_2} \bar{A}(\sigma, \nu) \left[ \int_{\vartheta}^{\vartheta_b} \frac{e^{i\nu\vartheta}}{R} d\vartheta \right] d\sigma d\nu$$

Then writing

$$\begin{aligned} R^2 &= s_0'^2 - B^2(r_0'^2 + z^2) \\ &= [r_0 \alpha - s_0 / \alpha \tan]^2 - [s_0 B / \alpha]^2 - B^2 z^2 \end{aligned}$$

The  $\vartheta$  integration may be performed to give

$$\begin{aligned} \psi_s &= -\frac{\pi i}{2\alpha} \int_{\sigma_1}^{\sigma_2} e^{i\nu\tau} \int_{\nu_1}^{\nu_2} \bar{A}(\sigma, \nu) e^{-i\nu / \sin s_0 / \alpha^2 \cos} \\ &\quad H_0^{(2)} \left( \frac{B}{\alpha^2} \sqrt{s_0'^2 + \alpha^2 z^2} \right) d\sigma d\nu \end{aligned}$$

where  $H_0^{(2)} = J_0 - iY_0$  is the Hankel function of the second kind.

Now the doublet solution may be obtained by differentiation with respect to  $z$ :

$$\Psi = \frac{\partial}{\partial z} \Psi_s(s', r', z)$$

Thus obtain

$$\Psi = \frac{\pi i B^2 \gamma^2 z}{2 \alpha^3} \int_0^\infty e^{i\gamma r} \int_{-1}^1 \bar{A}(\gamma, \nu) e^{-i\gamma \sin s_0 / \alpha z \cos} \frac{H_1^{(2)}(\gamma B / \alpha z \sqrt{s_0^2 + \alpha^2 z^2})}{\gamma B / \alpha z \sqrt{s_0^2 + \alpha^2 z^2}} d\tau d\nu$$

This form is used to evaluate  $A(s, r)$ . By letting  $(s', r', z)$  approach the airfoil surface, with some care about the limiting process, obtain

$$-\Delta p = \Delta \Psi = -2\pi A(s, r)$$

$\Delta =$  upper-lower

Thus let

$$L(s, r) = -\Delta p = -2\pi A(s, r)$$

Then substituting for  $\bar{A}(s, \nu)$  and going back a step, before the operation  $\partial/\partial z$  was performed, have

$$\Psi = \frac{\pi i}{2\alpha} \int_0^\infty e^{i\gamma r} \int_{-1}^1 \frac{L(\tau, \nu / \sin)}{2\pi} e^{-i\gamma \sin s_0 / \alpha z \cos} \frac{\partial}{\partial z} H_0^{(2)}(\gamma B / \alpha z \sqrt{s_0^2 + \alpha^2 z^2}) d\tau d\nu$$

As before the boundary condition and the equation for  $\phi$  may be combined to give

$$\omega(r^\nu) = \int_0^\infty \lim_{z \rightarrow 0} \frac{\partial}{\partial z} \Psi(s, r) \Big|_{s_0 = s_0 - \lambda} \delta\lambda / \cos \lambda$$

Thus obtain the integral equation

$$\omega(r^\nu) = \frac{\pi i}{2\alpha^2} \int_0^\infty \int_\lambda^\infty e^{i\nu r} \int_{-1}^1 \frac{\Gamma(\nu, \nu/\sin)}{2\pi \frac{\cos \lambda}{\alpha}} e^{-i\nu/\sin(s_0 - \lambda)/\alpha z \cos} \lim_{z \rightarrow 0} \frac{\partial^2}{\partial z^2} H_0^{(2)} \left( \sqrt{\beta}/\alpha z \sqrt{s_0^2 + \alpha^2 z^2} \right) \Big|_{s_0 = s_0 - \lambda} \delta\lambda$$

Then by taking the F.T. wrt r of this equation, obtain

$$\int_{-1}^1 \overline{G}(\nu, \nu/\sin) K_B(s_0, \nu/\sin) \delta\lambda = -1$$

where

$$\overline{G}(s, \nu/\sin) = \frac{\Gamma(s, \nu/\sin) / \beta^{\nu^2}}{2\pi \frac{\cos \lambda}{\alpha} \frac{1}{\sin} \overline{\omega}(\nu/\sin)}$$

and the kernel is

$$\begin{aligned} K_B(s_0, \nu/\sin) &= -\frac{\pi i}{2\alpha^2} \int_0^\infty e^{-i\nu/\sin(s_0 - \lambda)/\alpha z \cos} \lim_{z \rightarrow 0} \frac{\partial^2}{\partial z^2} H_0^{(2)} \left( \sqrt{\beta}/\alpha z \sqrt{(s_0 - \lambda)^2 + \alpha^2 z^2} \right) \delta\lambda \\ &= \frac{\pi i}{2} \frac{\beta^2}{\alpha^4} \int_0^\infty e^{-i\nu/\sin(s_0 - \lambda)/\alpha z \cos} \frac{H_1^{(2)} \left( \sqrt{\beta}/\alpha z (s_0 - \lambda) \right)}{\sqrt{\beta}/\alpha z (s_0 - \lambda)} \delta\lambda \end{aligned}$$

The kernel may be evaluated by noting that  $H_0^{(2)} \left( \sqrt{\beta}/\alpha z \sqrt{(s_0 - \lambda)^2 + \alpha^2 z^2} \right)$  satisfies the PDE

$$\alpha^2 \frac{\partial^2 H_0^{(2)}}{\partial \lambda^2} + \frac{\partial^2 H_0^{(2)}}{\partial z^2} + \frac{\sqrt{B}^2}{\alpha^2} H_0^{(2)} = 0$$

Then substituting for  $\partial^2 H_0^{(2)} / \partial z^2$  gives

$$K_B(s_0, \sqrt{s}) = \frac{\pi i}{2} \int_0^\infty e^{-i\sqrt{s} \sin(s_0 - \lambda) / \alpha^2 \cos} \lim_{z \rightarrow 0} \frac{\partial^2}{\partial \lambda^2} H_0^{(2)} \left( \frac{\sqrt{B}}{\alpha^2} \sqrt{(s_0 - \lambda)^2 + \alpha^2 z^2} \right) d\lambda$$

$$+ \frac{\pi i}{2} \frac{\sqrt{B}^2}{\alpha^4} \int_0^\infty e^{-i\sqrt{s} \sin(s_0 - \lambda) / \alpha^2 \cos} \lim_{z \rightarrow 0} H_0^{(2)} \left( \frac{\sqrt{B}}{\alpha^2} \sqrt{(s_0 - \lambda)^2 + \alpha^2 z^2} \right) d\lambda$$

Integrating the first term by parts twice and taking obtain

$$K_B(s_0, \sqrt{s}) = \frac{\pi i}{2} e^{-i\sqrt{s} \sin s_0 / \alpha^2 \cos} \left[ \mp \frac{\sqrt{B}}{\alpha^2} H_1^{(2)} \left( \frac{\sqrt{B}}{\alpha^2} |s_0| \right) + i \frac{\sqrt{s}}{\sin} \frac{\cos s}{\alpha^2} H_0^{(2)} \left( \frac{\sqrt{B}}{\alpha^2} |s_0| \right) \right]$$

$$- \frac{\pi i}{2} \frac{(\sqrt{s})^2}{\alpha^2} \int_0^\infty e^{-i\sqrt{s} \sin(s_0 - \lambda) / \alpha^2 \cos} H_0^{(2)} \left( \frac{\sqrt{B}}{\alpha^2} |s_0 - \lambda| \right) d\lambda$$

Now writing

$$\int_0^\infty e^{-i\sqrt{s} \sin(s_0 - \lambda) / \alpha^2 \cos} H_0^{(2)} \left( \frac{\sqrt{B}}{\alpha^2} |s_0 - \lambda| \right) d\lambda$$

$$= \int_{-\infty}^{s_0} e^{-i\sqrt{s} \sin \lambda / \alpha^2 \cos} H_0^{(2)} \left( \frac{\sqrt{B}}{\alpha^2} |\lambda| \right) d\lambda$$

$$= -\frac{\alpha^2}{\sqrt{s} \cos} \int_{-\infty}^{-\sqrt{s} \sin s_0 / \alpha^2 \cos} e^{i\sqrt{s}} H_0^{(2)} \left( -\frac{\sqrt{B} \sin / \cos}{\sqrt{s}} |\lambda| \right) d\lambda$$

and using

$$\int_{-1}^0 H_0^{(2)}(a|\xi|) e^{i\frac{1}{2}\pi} d\xi = \frac{2}{\pi\sqrt{1-a^2}} \ln \frac{1+\sqrt{1-a^2}}{a}$$

(from Watson, Ref. 14) and simplifying the notation, the kernel is written as

$$K_B(s_0, \beta/\sin) = \frac{\pi i}{2} e^{i\alpha\mu s_0} \left[ \mp a H_1^{(2)}(a|\sin|) \right. \\ \left. -i\alpha\mu H_0^{(2)}(a|\sin|) \right] \\ - \frac{i}{2\alpha} \frac{\beta}{\sin} \ln \frac{-\cos + \alpha}{-\cos - \alpha} \\ \mp \frac{\pi i}{2} \frac{1}{\beta \sin} \frac{\beta}{\sin} \int_0^{a|\sin|} e^{\pm i\mu\xi} H_0^{(2)}(\xi) d\xi$$

where

$$\begin{aligned} \pm &= \text{sgn}(s_0) \\ a &= \frac{\beta}{\sin} \frac{\beta \sin}{\alpha^2} \\ \mu &= \frac{-\cos}{\beta \sin} \\ \alpha\mu &= \frac{-\cos}{\alpha^2} \frac{\beta}{\sin} \\ \beta \sin &= \sqrt{\cos^2 - \alpha^2} \\ \alpha^2 &= 1 - (M \cos \Lambda)^2 \end{aligned} \quad \begin{aligned} \sin &\equiv \sin(\phi + \Lambda) \\ \cos &\equiv \cos(\phi + \Lambda) \\ \frac{\pi}{2} &< (\phi + \Lambda) < \pi \end{aligned}$$

Now the kernel in the  $(s^A, r^A)$  system will be derived. The source potential is

$$\psi_s = \int_{-1}^1 \int_{g^A}^{g_b^A} \frac{A(r^A, g^A) \delta g^A \delta r^A}{\sqrt{s_0^2 - B^2(r_0^2 + z^2)}}$$

where  $g_b^A$  is obtained from  $R^2 = s_0^2 - B^2(r_0^2 + z^2) = 0$  as

$$g_b^A = r^A - s_0^A / \alpha^2 \tan + s_0^A / \tan - \frac{B}{\alpha^2} \sqrt{s_0^2 + \alpha^2 z^2}$$

Then writing  $A(s^A, r^A)$  as a Fourier integral wrt  $r^A$ , have

$$\psi_s = \int_{-\infty}^{\infty} \int_{-1}^1 \bar{A}(r^A, \gamma) \left[ \int_{g^A}^{g_b^A} \frac{e^{i\gamma g^A}}{R} \delta g^A \right] \delta r^A \delta \gamma$$

writing

$$\begin{aligned} R^2 &= s_0^2 - B^2(r_0^2 + z^2) \\ &= \left[ r_0^A \alpha + s_0^A \alpha / \tan - s_0^A / \alpha \tan \right]^2 - \frac{B^2}{\alpha^4} [s_0^2 + \alpha^2 z^2] \end{aligned}$$

the  $g^A$  integration may be performed to give

$$\psi_s = -\frac{\pi i}{2\alpha} \int_{-\infty}^{\infty} e^{i\gamma r^A} \int_{-1}^1 \bar{A}(r^A, \gamma) e^{-i\gamma / \sin s_0^A / \alpha^2 \cos + i\gamma / \sin s_0^A \cos} H_0^{(2)} \left( \frac{\gamma B}{\alpha^2} \sqrt{s_0^2 + \alpha^2 z^2} \right) \delta r^A \delta \gamma$$

Again the doublet solution is

$$\psi = \frac{\partial}{\partial z} \psi_s$$

and may identify as before

$$-\Delta p = \Delta \psi = -2\pi A(s^A, r^A)$$

So letting

$$L^A(s^A, r^A) = -\Delta p = -2\pi A(s^A, r^A)$$

obtain

$$\Psi = \frac{\pi i}{2\alpha} \int_{-\infty}^{\infty} e^{i\lambda r^A} \int_{r^A-1}^1 \frac{L^A(r^A, \lambda/\sin)}{2\pi} e^{-i\lambda/\sin s_0^A/\alpha z \cos + i\lambda/\sin s_0^A \cos} \frac{\partial}{\partial z^2} H_0^{(2)}\left(\frac{\lambda B}{\alpha^2} \sqrt{s_0^A{}^2 + \alpha^2 z^2}\right) \delta(r^A) \delta\lambda$$

The boundary condition is

$$\omega(r^A) = \int_0^{\infty} \lim_{z \rightarrow 0} \frac{\partial}{\partial z} \Psi \Big|_{\substack{s_0 = s_0 - \lambda \\ \text{or } s = s - \lambda}} \delta\lambda / \cos \lambda$$

Substituting for  $\Psi$  obtain

$$\omega(r^A) = \frac{\pi i}{2\alpha^2} \int_0^{\infty} \int_{-\infty}^{\infty} \left\{ e^{i\lambda r^A} \int_{r^A-1}^1 \frac{L^A(r^A, \lambda/\sin)}{2\pi \frac{\cos \lambda}{\alpha}} e^{i\lambda/\sin s_0^A \cos} e^{-i\lambda/\sin s_0^A/\alpha^2 \cos} \lim_{z \rightarrow 0} \frac{\partial^2}{\partial z^2} H_0^{(2)}\left(\frac{\lambda B}{\alpha^2} \sqrt{s_0^A{}^2 + \alpha^2 z^2}\right) \right\} \delta(r^A) \delta\lambda \Big|_{s = s - \lambda}$$

Recalling the transformation

$$s^A = s$$

$$r^A = r - s/\tan$$

the substitution  $s = s - \lambda$  may be made, to give

$$\omega(r^A) = \frac{\pi i}{2\alpha^2} \int_0^{\infty} \int_{-\infty}^{\infty} e^{i\lambda r^A} \int_{-1}^1 \frac{L^A(r^A, \lambda/\sin)}{2\pi \frac{\cos \lambda}{\alpha}} e^{i\lambda/\sin s_0^A \cos} e^{-i\lambda/\sin (s_0^A - \lambda)/\alpha^2 \cos} \lim_{z \rightarrow 0} \frac{\partial^2}{\partial z^2} H_0^{(2)}\left(\frac{\lambda B}{\alpha^2} \sqrt{(s_0^A - \lambda)^2 + \alpha^2 z^2}\right) \delta(r^A) \delta\lambda$$



Then taking the F.T. wrt  $r^A$  of this equation obtain

$$\int_{-1}^1 \bar{G}^A(r^A, \gamma/\sin) K_B^A(s_0^A, \gamma/\sin) \delta r^A = -e^{i\gamma/\sin s^A \cos}$$

where

$$\bar{G}^A(s^A, \gamma/\sin) = \frac{\Gamma^A(s^A, \gamma/\sin) / gV^2}{2\pi \frac{\cos \lambda}{\alpha} \frac{1}{\sin} \bar{\omega}(\gamma/\sin)}$$

and the kernel is

$$K_B^A(s_0^A, \gamma/\sin) = -\frac{\pi i}{2\alpha^2} e^{i\gamma/\sin s_0^A \cos} \int_0^\infty e^{-i\gamma/\sin (s_0^A - \lambda) / \alpha z \cos} \lim_{z \rightarrow 0} \frac{\partial^2}{\partial z^2} H_0^{(2)}\left(\frac{\gamma/\sin}{\alpha z} \sqrt{(s_0^A - \lambda)^2 + \alpha^2 z^2}\right) \delta \lambda$$

From which recognize that

$$\begin{aligned} K_B^A(s_0^A, \gamma/\sin) &= e^{i\gamma/\sin s_0^A \cos} K_B(s_0 = s_0^A, \gamma/\sin) \\ &= e^{-i\alpha \mu \alpha^2 s_0^A} K_B(s_0 = s_0^A, \gamma/\sin) \end{aligned}$$

Certain limiting cases of the hyperbolic kernel are of interest.

The steady state limit is  $\gamma/\sin \rightarrow 0$ . For  $\gamma/\sin = 0$  the kernel becomes

$$K_B^A(s_0^A, 0) = K_B(s_0^A, 0) = \frac{1}{s_0^A}$$

So the integral equation becomes

$$\int_{-1}^1 \bar{G}^A(r^A, 0) \frac{\delta r^A}{s_0^A} = -1$$

which inverts directly to

$$\bar{G}^A(s^A, 0) = \bar{G}(s^A, 0) = -\frac{1}{\pi} \sqrt{\frac{1-s^A}{1+s^A}}$$

$$\text{or } \bar{g}_0^A(0) = \bar{g}_0(0) = -\frac{1}{\pi}$$

$$\bar{g}_n^A(0) = \bar{g}_n(0) = 0, \quad n \geq 1$$

This is recognized as the steady solution for an airfoil in uniform downwash. That this corresponds to the limit  $\gamma/\sin \rightarrow 0$  follows from the fact that for the hyperbolic domain the proper interpretation of  $\gamma/\sin$  is as a reduced frequency.

The case  $(\phi + \lambda) = \pi$  should be investigated since it involves  $\sin(\phi + \lambda) = 0$  which introduces some apparent singularities in the problem formulation and the kernel. This is entirely due to the formulation of the geometry in a way that emphasizes the three-dimensional rather than the unsteady flow aspects of the problem.

This case may be studied by first rewriting the problem statement in terms of the  $(s^A, r^A)$  system and taking the limit  $(\phi + \lambda) \rightarrow \pi$ . Then in terms of the velocity potential, have

$$\text{PDE: } \left[ \frac{\partial^2}{\partial s^A \partial z} - (M \cos \lambda)^2 \left( \frac{\partial}{\partial s^A} + \frac{\partial}{\partial r^A \sin} \right)^2 + \frac{\partial^2}{\partial z^2} \right] \phi = 0$$

$$\text{Pressure: } -\rho = \cos \lambda \left[ \frac{\partial}{\partial s^A} + \frac{\partial}{\partial r^A \sin} \right] \phi$$

$$\text{b.c.: } \left. \frac{\partial \phi}{\partial z} \right|_{z=0} = \omega(r^A) = \omega(r^A \sin - s^A)$$

on the airfoil

Now compare this with the usual formulation of the two-dimensional unsteady thin airfoil problem. With the geometry as shown in Figure 2.7, one may state the problem as

PDE: 
$$\left[ \frac{\partial^2}{\partial x^2} - (M \cos \Lambda)^2 \left( \frac{\partial}{\partial x} + \frac{\partial}{\partial t} \right)^2 + \frac{\partial^2}{\partial z^2} \right] \phi = 0$$

pressure: 
$$-p = \cos \Lambda \frac{\partial}{\partial t} \phi = \cos \Lambda \left( \frac{\partial}{\partial x} + \frac{\partial}{\partial t} \right) \phi$$

b.c.: 
$$\frac{\partial \phi}{\partial z} \Big|_{z=0} = \omega(t-x) \quad \text{on the airfoil}$$

As expected, it is seen that the limit  $(\phi + \Lambda) \rightarrow \pi$  corresponds exactly with the two-dimensional unsteady flow problem, with the following interpretation of the variables:

$$\begin{aligned} r^A \sin &= t \\ s^A &= x \end{aligned}$$

Since  $r^A \sin$  is the proper nonsingular span variable, it is seen that indeed the proper wave number is:

$$\sqrt{1/\sin} = k = \text{reduced frequency}$$

It is in terms of this wave number that the integral equation is properly formulated for all angles  $(\phi + \Lambda)$ .

The interpretation of the F.T. of the downwash is

$$\frac{1}{\sin} \bar{\omega}(\sqrt{1/\sin}) = \bar{\omega}(k) = \text{F.T. of } \omega(t-x) \text{ wrt } t, \text{ at } x=0$$

With the above interpretation of the variables, the integral equation may be rewritten in terms of the usual two-dimensional notation as

$$\int_{-1}^1 \bar{G}^A(\sigma^A, k) K_z^A(s^A, k) d\sigma^A = -e^{-ik s^A}$$

where

$$K_2^A(s_0^A, k) = \lim_{(\phi+l) \rightarrow \pi} K_B^A(s_0^A, \nu \sin)$$

$$\bar{G}^A(r^A, k) = \frac{\Gamma^A(r^A, k) / \rho^2}{2\pi \frac{\cos k}{\alpha} \bar{\omega}(k)}$$

For the limit of  $K_B^A$  find as  $(\phi+l) \rightarrow \pi$

$$a \rightarrow k \frac{M \cos k}{\alpha^2}$$

$$\mu \rightarrow \frac{1}{M \cos k}$$

$$a\mu \rightarrow \frac{k}{\alpha^2}$$

$$B_{\sin} \rightarrow M \cos k$$

$$\alpha^2 = 1 - (M \cos k)^2$$

with these limits the kernel may be evaluated as

$$K_2^A(s_0^A, k) = \frac{\pi i}{2} e^{i k (M \cos k)^2 s_0^A / \alpha^2} \left[ \begin{aligned} &+ \frac{k M \cos k}{\alpha^2} H_1^{(2)} \left( \frac{k M \cos k}{\alpha^2} |s_0^A| \right) \\ &- \frac{i k}{\alpha^2} H_0^{(2)} \left( \frac{k M \cos k}{\alpha^2} |s_0^A| \right) \end{aligned} \right]$$

$$- \frac{i k}{\alpha} e^{-i k s_0^A} k \frac{1 + \alpha}{M \cos k}$$

$$- \frac{\pi i}{2} k e^{-i k s_0^A} \int_0^{|s_0^A|/\alpha^2} e^{i \frac{k}{2} H_0^{(2)}(M \cos k | \frac{1}{2} |)} d \frac{1}{2}$$

which can be identified as

$$K_2^A(s_0^A, \lambda) = \left(-\frac{2\pi}{\alpha} \lambda\right) K(M = M \cos \lambda; \lambda s_0^A)$$

where  $K(M; ks_0^A)$  is Possio's form of the kernel for unsteady two-dimensional flow (as in Ref. 9). The factor  $\left(-\frac{2\pi}{\alpha} \lambda\right)$  comes simply from the normalization chosen for the universal loading function.

### 2.3.3 Similarity in the Kernels

A number of points may be made about the forms derived for the elliptic and hyperbolic kernels.

The Hankel function  $H_0^{(2)}$ ,  $H_1^{(2)}$  is the Green's function for the wave equation in two space dimensions, with harmonic time dependence (Helmholtz's equation). Thus its occurrence in the hyperbolic kernel. Similarly, the modified Bessel function  $K_0, K_1$  is the Green's function for Laplace's equation in three dimensions, with one space variable (spanwise) replaced by the wave number; that is, with the equation operated on by the F.T. wrt  $r^A$ . Thus its occurrence in the elliptic kernel. The Hankel function has the characteristic wave behavior of solutions of hyperbolic equations, and the modified Bessel functions have the characteristic exponential decay behavior of solutions of elliptic equations.

The two kernels are actually complete duals. Using the relations

$$K_1(x) = -\frac{\pi}{2} H_1^{(2)}(-ix)$$

$$K_0(x) = -i \frac{\pi}{2} H_0^{(2)}(-ix)$$

and noting that

$$\beta^2 = -B^2$$

can show that

$$K_B = K_{\beta = iB}$$

and

$$K_{\beta} = K_{B = -i\beta}$$

The derivation of the integral equations and kernels was quite parallel, with the exception that the initial steps for the elliptic case are more direct. This difference is due to the singular nature of elementary dipole solutions of a hyperbolic equation; for the elliptic equation the characteristic exponential decay of disturbances results in all order elementary solutions being non-singular.

The limit  $\sqrt{1/\sin} \rightarrow 0$  has been given two interpretations: as the lifting line limit for the elliptic equation; and as the steady state limit for the hyperbolic equation. It is equivalent to removing the spanwise variable from the elliptic problem or the time variable from the hyperbolic problem. In both cases there remains a two-dimensional problem, and the solution is that for a two-dimensional thin airfoil in a uniform downwash. These interpretations should strictly be applied only to the cases  $(\phi + \lambda) = \frac{\pi}{2}$ , and  $(\phi + \lambda) = \pi$ , respectively. They are applicable to the general geometry in the sense that in the elliptic problem it is the spanwise space variable that is dominant while in the hyperbolic problem it is the time variable that is dominant. In fact, this interpretation of the significance of the elliptic and hyperbolic domains is more important than the exact meaning of the limit  $\sqrt{1/\sin} \rightarrow 0$ .

#### 2.3.4 The Incompressible Two-Dimensional Kernel

The double limit  $M \cos \lambda \rightarrow 0$  and  $(\phi + \lambda) \rightarrow \pi$  is rather special. Both the elliptic and the hyperbolic kernels as formulated are singular in this limit. Examination of Figure 2.4 shows that this limit is the coalescence of the elliptic case, the hyperbolic case, and the case  $\beta = B = 0$  (yet to be discussed). This

exceptional behavior arises because this limit is the problem of a two-dimensional thin airfoil in an incompressible flow. For  $M \cos \Lambda = 0$  and  $(\phi + \Lambda) \rightarrow \pi$ , the problem is elliptic, and three-dimensional for all  $(\phi + \Lambda) \neq \pi$ ; for exactly  $(\phi + \Lambda) = \pi$  there are no span effects and the problem is two-dimensional. For  $(\phi + \Lambda) = \pi$  and  $M \cos \Lambda \rightarrow 0$ , the problem is hyperbolic, and unsteady two-dimensional for all  $M \cos \Lambda \neq 0$ ; for exactly  $M \cos \Lambda = 0$ , there are no unsteady effects in the equation of motion (only in the boundary conditions, that is due to the wake) and the problem is two-dimensional. In both cases, the result of the limiting processes is the two-dimensional Laplace's equation. Actually, it is evident that this case does not properly belong to either the elliptic or hyperbolic domain, rather it is a special case of the transitional case  $\beta = B = 0$  (treated in Section 2.3.5). However, while the case is singular when viewed as a limit of either the elliptic or hyperbolic case, as a two-dimensional problem it is expected to take a much simpler form, as will be evident in the kernel. Indeed, for this case and this one alone, the solution is obtainable in closed form by classical techniques.

The two-dimensional incompressible kernel may be obtained from the present development by going back to the definition of either the elliptic or hyperbolic kernel. Choosing the hyperbolic kernel

$$K_B(s_0, \gamma/\sin) = \frac{\pi i}{2} \frac{\sqrt{2B^2}}{\alpha^4} \int_0^{\infty} e^{-i\gamma/\sin(s_0-\lambda)/\alpha^2 \cos} \frac{H_{\frac{1}{2}}^{(2)}(\sqrt{B}/\alpha^2(\lambda-s_0))}{\sqrt{B}/\alpha^2(\lambda-s_0)} d\lambda$$

In this form the limit  $M \cos \Lambda = 0$  and  $(\phi + \Lambda) = \pi$  gives

$$\begin{aligned}
K_0(s_0, \sqrt{s}) &= \lim_{\substack{(\phi+\lambda) \rightarrow \pi \\ \text{mesh} \rightarrow 0}} K_B(s_0, \sqrt{s}) \\
&= - \int_0^{\infty} e^{i\sqrt{s} \sin(s_0 - \lambda)} \frac{\partial \lambda}{(\lambda - s_0)^2} \\
&= - \int_{-s_0}^{\infty} e^{-i\sqrt{s} \lambda} \frac{\partial \lambda}{\lambda^2}
\end{aligned}$$

The appearance of the wave number in the proper form  $\sqrt{s}$  is familiar now. This integral is a singular one of Mangler's type. It is evaluated (taking some care with the singularity) to give

$$\begin{aligned}
K_0(s_0, \sqrt{s}) &= \frac{e^{i\sqrt{s} s_0}}{s_0} - i\sqrt{s} \sin \left[ \gamma + \frac{i\pi}{2} + \ln(\sqrt{s} |s_0|) \right] \\
&\quad - i\sqrt{s} \int_0^{\sqrt{s} |s_0|} \frac{e^{\pm it} - 1}{t} dt
\end{aligned}$$

where  $\pm = \text{sgn}(s_0)$  as usual and  $\gamma$  is Euler's number. The integral that appears here is the nonsingular part of the Sine and Cosine integrals which appear in the usual formulation of this kernel (see, for example, Ref. 9).

The kernel in the  $(s^A, r^A)$  system is then

$$\begin{aligned}
K_0^A(s_0^A, \sqrt{s}) &= e^{-i\sqrt{s} s_0^A} K_0(s_0 = s_0^A, \sqrt{s}) \\
&= \frac{1}{s_0^A} - i\sqrt{s} \sin e^{-i\sqrt{s} s_0^A} \left[ \gamma + \frac{i\pi}{2} + \ln(\sqrt{s} |s_0^A|) \right] \\
&\quad - i\sqrt{s} \sin e^{-i\sqrt{s} s_0^A} \int_0^{\sqrt{s} |s_0^A|} \frac{e^{\pm it} - 1}{t} dt
\end{aligned}$$

The solution for the loading on a two-dimensional thin airfoil in an incompressible flow has been obtained in closed form by many means. The most convenient method here is that of von Kármán



and Sears (Ref. 10), as formulated in Ref. 9.

Consider a convected downwash field given by

$$\omega_a(t-x)$$

Then writing

$$\gamma_a = \gamma_o + \gamma_{\perp} \quad \text{vorticity on airfoil}$$

$$\gamma_w = \gamma_w(x-t) \quad \text{vorticity in wake}$$

$$\Gamma = \Gamma_o + \Gamma_{\perp} \quad \text{circulation of the airfoil}$$

have these relations:

definition of circulation

$$\Gamma = \int_{-1}^1 \gamma_a(x,t) dx$$

conservation of vorticity

$$\Gamma + \int_{-1}^{\infty} \gamma_w(x,t) dx = 0$$

a solution of the PDE, satisfying the boundary condition at the airfoil

$$\gamma_o = \frac{2}{\pi} \sqrt{\frac{1-x}{1+x}} \int_{-1}^1 \sqrt{\frac{1+\xi}{1-\xi}} \frac{\omega_a(\xi,t)}{x-\xi} d\xi$$

Kutta condition

$$-\frac{2}{\pi} \int_{-1}^1 \sqrt{\frac{1+\xi}{1-\xi}} \omega_a(\xi,t) d\xi + \frac{1}{\pi} \int_{-1}^{\infty} \sqrt{\frac{\xi+1}{\xi-1}} \gamma_w(\xi,t) d\xi = 0$$

The geometry is as in Figure 2.7, with  $M \cos \Lambda = 0$  and a unity free stream velocity. The lift and moment are given by

$$L = \Gamma_o - \frac{\partial}{\partial t} \int_{-1}^1 \gamma_o \xi d\xi + \int_{-1}^{\infty} \frac{\gamma_w}{\sqrt{\xi^2-1}} d\xi$$

and

$$M_{QC} = -\int_{-1}^1 \chi_0 \left( \frac{1}{2} + \frac{1}{2} \right) \Delta \xi + \frac{1}{2} \frac{d}{d\xi} \int_{-1}^1 \chi_0 \left[ \xi^2 + \xi - \frac{1}{2} \right] \Delta \xi$$

By using the Fourier transform wrt  $t$  the solution may be obtained in terms of the reduced frequency. In the notation of the present problem, the solution is

$$\begin{aligned} \bar{g}_c(\nu/\sin) &= \pi \left[ \bar{g}_0(\nu/\sin) + \frac{1}{2} \bar{g}_1(\nu/\sin) \right] e^{-i\nu/\sin} \\ &= \bar{P}_0(\nu/\sin) \frac{2i/(\pi\nu/\sin)}{H_1^{(2)}(\nu/\sin) + iH_0^{(2)}(\nu/\sin)} e^{-i\nu/\sin} \end{aligned}$$

$$\begin{aligned} \bar{g}_L(\nu/\sin) &= \pi \left[ \bar{g}_0^A(\nu/\sin) + \frac{1}{2} \bar{g}_1^A(\nu/\sin) \right] \\ &= \bar{P}_0(\nu/\sin) C(\nu/\sin) - iJ_1(\nu/\sin) \end{aligned}$$

$$\begin{aligned} \bar{g}_M(\nu/\sin) &= -\frac{\pi}{4} \left[ \bar{g}_1^A(\nu/\sin) + \bar{g}_2^A(\nu/\sin) \right] \\ &\equiv 0 \end{aligned}$$

where

$$\bar{f}_0(\eta/\sin) = -J_0(\eta/\sin) + iJ_1(\eta/\sin)$$

$$C(\eta/\sin) = \frac{H_1^{(2)}(\eta/\sin)}{H_1^{(2)}(\eta/\sin) + iH_0^{(2)}(\eta/\sin)}$$

and  $J_0, J_1$  are Bessel functions. The singular term in the Glauert series representation of the pressure may also be determined as

$$\bar{g}_0^A(\eta/\sin) = \frac{1}{\pi} \left[ \bar{f}_0(\eta/\sin) C(\eta/\sin) - iJ_1(\eta/\sin) \right]$$

and it may be also shown, as by Garrick (Ref. 15), that

$$\bar{g}_n^A(\eta/\sin) \equiv 0, \quad n \geq 1$$

This is the solution for the loading due to a sinusoidal gust. That all terms in the Glauert series except the leading one are identically zero is another part of the exceptional nature of this case; it is not true for any other solution, even for the transitional case  $\beta = B = 0$ .

The behavior of the leading term of the series and the lift is characteristic of the solution found for all values of the parameters  $M \cos \Lambda$  and  $(\phi + \Lambda)$ . Thus the asymptotic behavior of the solution is of interest. Find for small  $\eta/\sin$

$$\bar{g}_L(\eta/\sin) \cong - \left[ 1 - \eta/\sin \left( \frac{\pi}{2} - \delta - \ln \frac{\eta/\sin}{2} \right) \right]$$

and for large  $\eta/\sin$

$$\bar{g}_L(\eta/\sin) \sim - \frac{1}{\sqrt{2\pi \eta/\sin}} e^{i(\eta/\sin - \pi/4)}$$

To be noted is the infinite derivative at  $\gamma/\sin = 0$  and the linear phase and decay like  $(\gamma/\sin)^{-1/2}$  as  $\gamma/\sin \rightarrow \infty$ .

### 2.3.5 The Transitional Kernel

The transitional case is given by  $M \cos \Lambda = (\phi + \Lambda)$ , or  $\beta = B = 0$ . For this case, the elliptic and hyperbolic kernels as formulated are singular, just as for the two-dimensional incompressible limit, which is in fact simply a special example of the present case. Indeed, here also the equation of motion is reduced to the two-dimensional Laplace's equation, namely

$$\left[ \frac{\partial^2}{\partial r^2} + \frac{\partial^2}{\partial z^2} \right] \psi = 0$$

However, while the two-dimensional incompressible case is a proper physical limit, in the general transitional case the singular limits of the kernels and the reduction of dimensions in the equation of motion are indications of a violation of one of the critical assumptions of the solution, namely the linear assumption.

To examine the nature of this case, it is necessary to return to the exact equation for the velocity potential in three-dimensional, unsteady, compressible flow (as in Ashley and Landahl, Ref. 16). The equation for the first order potential for

$$M \cos \Lambda = \sin(\phi + \Lambda)$$

may be obtained, and is of exactly the same form as the equation for the potential in three-dimensional steady transonic flow. Physically this is not a transonic flow, of course; there is no region where the flow has sonic velocity as long as  $M \cos \Lambda < 1$ . There is, however, a phenomenon that has sonic velocity; that is, the vector sum of the normal Mach number and the speed of convection along the blade of the intersection of the vortex line and the blade centerline, which is represented by the relative Mach number in the  $(s', r')$  system

$$M_R = \frac{M \cos \lambda}{\sin(\phi + \lambda)}$$

becomes sonic for the transitional case. It is this coincidence of the combination of the physical and geometric velocities at the sonic velocity acting as a disturbance reinforcement process that makes the linear assumption not valid.

The important feature of the equation for the velocity potential in the transitional case is its nonlinearity. Because of the nonlinearity, the use of the Fourier transform is not possible, and the methods used to obtain a solution for the elliptic and hyperbolic cases are not applicable. More generally, the nonlinearity implies that even if the transitional problem could be solved, the solution would not be in the form of a universal influence function, for the existence of such a function is the property of a linear problem. Thus the transitional solution would have to be obtained for every particular downwash distribution, and even if these solutions could be obtained, the result would not be practically applicable to the calculation of rotary wing airloads.

Some insight into the transitional case can be obtained from a study of the linear equation of motion in the  $(s^A, r^A)$  system. In these coordinates the equations are

$$\left[ \alpha^2 \frac{\partial^2}{\partial s^A \partial z} + (\sin^2 - (M \cos \lambda)^2 \cos^2) \frac{\partial^2}{\partial r^A \sin^2} \right. \\ \left. + (M \cos \lambda)^2 z \cos \frac{\partial^2}{\partial s^A \partial r^A \sin} + \frac{\partial^2}{\partial z^2} \right] \phi = 0$$

and

$$-\rho = \frac{\Delta}{\Delta t} \phi = \cos \lambda \left[ -\cos \frac{\partial}{\partial r^A \sin} + \frac{\partial}{\partial s^A} \right] \phi$$

For the transitional case, these become

$$\left[ \left( (M \cos \Lambda)^2 \frac{\partial}{\partial r^A \sin} - \alpha \frac{\partial}{\partial s^A} \right)^2 + \frac{\partial^2}{\partial z^2} \right] \phi = 0$$

and

$$-p = \frac{D}{Dt} \phi = \frac{\cos \Lambda}{\alpha} \left[ \frac{\partial}{\partial r^A \sin} - \left( (M \cos \Lambda)^2 \frac{\partial}{\partial r^A \sin} - \alpha \frac{\partial}{\partial s^A} \right) \right] \phi$$

Since in the transitional limit

$$\frac{\partial}{\partial r^A} = (M \cos \Lambda)^2 \frac{\partial}{\partial r^A \sin} - \alpha \frac{\partial}{\partial s^A}$$

this is the same equation given before for the potential. This equation for the potential shows the nature of the transitional limit. The coalescence of the  $s^A$  and  $r^A$  sin derivatives into a single total derivative corresponds to the exact coincidence of the sonic speed and the trace speed of the downwash distribution along the wing span. This coincidence gives the linearized problem a two-dimensional quality; disturbances produced by the downwash distribution remain exactly in step with it as both are convected along the blade. Of course, nonlinearities destroy the exact two-dimensional nature of the problem. However the two-dimensional problem does roughly represent the physical character of the transitional case, and as a linear problem it does have a solution of the form required here. Generally the nonlinearities of the transitional (transonic) equation are not very strong, and while the linear solution may be expected to overestimate the nonlinear loads, it will serve as a reasonable approximation. As it is the only way to obtain an influence function for the transitional case, the linear solution must be accepted. At least it will be a valid limit of the linear elliptic and hyperbolic results.

The linear transitional kernel is obtained, as the two-dimensional incompressible kernel was, from the definition of the elliptic or hyperbolic kernel. With

$$K_B(s_0, \gamma/\sin) = \frac{\pi i}{2} \frac{\gamma^2 B^2}{\alpha^4} \int_0^\infty e^{-i\gamma/\sin (s_0 - \lambda)/\alpha^2 \cos} \frac{1 - \frac{(2)}{2} \left( \frac{\gamma B}{\alpha^2 (s_0 - \lambda)} \right)}{\gamma B / \alpha^2 (s_0 - \lambda)} d\lambda$$

the transitional limit is

$$\begin{aligned} B &\rightarrow 0 \\ \mu \cos \lambda &\rightarrow \sin \\ \alpha &\rightarrow -\cos \end{aligned}$$

which gives

$$\begin{aligned} K_T(s_0, \gamma/\sin) &= \lim_{B \rightarrow 0} K_B(s_0, \gamma/\sin) \\ &= - \int_0^\infty e^{i\gamma/\sin (s_0 - \lambda)/\alpha} \frac{d\lambda}{(\lambda - s_0)^2} \\ &= - \int_{-s_0}^\infty e^{-i\gamma/\sin \frac{1}{\alpha} \lambda} \frac{d\lambda}{\lambda^2} \end{aligned}$$

It can be seen then, that

$$K_T(s_0, \gamma/\sin) = K_0(s_0, \gamma/\sin = \frac{1}{\alpha} \gamma/\sin)$$

The kernel in the  $(s^A, r^A)$  system is then

$$\begin{aligned}
K_T^A(s_0^A, \gamma/\sin) &= e^{-i\gamma/\sin s_0^A \alpha} K_T(s_0=s_0^A, \gamma/\sin) \\
&= e^{-i\gamma/\sin s_0^A \alpha} K_0(s_0=s_0^A, \gamma/\sin = \frac{1}{2} \gamma/\sin) \\
&= e^{i\gamma/\sin s_0^A \frac{1-\alpha^2}{\alpha}} K_0^A(s_0^A, \gamma/\sin = \frac{1}{\alpha} \gamma/\sin)
\end{aligned}$$

While  $K_T$  has been written here in terms of the more familiar  $K_0$ , the more proper view is that  $K_0$  is a special case of  $K_T$ .

### 2.3.6 The Linear Assumption

The restriction on the problem due to the linear assumption may now be examined.

First consider the linear assumption for the elliptic or hyperbolic domains. There the assumption as usual simply requires that the disturbance level be sufficiently small. An example of the disturbance is the downwash due to a free vortex. The maximum vortex induced downwash in the plane of the blade is

$$w_{\max} = \frac{\Gamma}{bV} \frac{1}{4\pi l/b} V$$

The linear assumption is then

$$w_{\max} \ll V$$

or

$$\frac{\Gamma}{bV} \ll 4\pi l/b$$

For a vortex from a generator of chord  $c$ , at an angle of attack  $\alpha_G$ , the circulation is

$$\Gamma = 2\pi \alpha_G V \frac{c}{2}$$



Thus, the linear assumption requires

$$\alpha_G \ll 2h/b \left( \frac{2b}{c} \right)$$

Typically, have  $\alpha_G \approx 0.1$  and  $2b/c \approx 1.0$  so the requirement becomes

$$h \gg 0.05 b$$

For vortices with a reasonable core size this requirement is not at all restrictive (the effective  $h$  is always greater than the core radius).

As has been pointed out by Miller (Ref. 17), however, a linear (small perturbation) assumption actually is no restriction at all on the application of an aerodynamic theory (lifting surface or lifting line) to the calculation of rotary wing airloads. The linearization assumption essentially requires that the airfoil be at small section angle of attack. For large angle of attack this assumption is not valid, but the airfoil will then be stalled and thus the linear theory will be replaced by an appropriate theory for nonattached flow for the calculation of the airloads.

Now consider the linear assumption near the transitional domain. That is, examine the requirement for the linearization of the equation of motion. From the exact equation for the velocity potential find that the requirement is

$$\left| 1 - \left( \frac{M \cos \lambda}{\sin(\phi + \lambda)} \right)^2 \right| \gg M(\gamma + 1) \frac{M \cos \lambda}{\sin(\phi + \lambda)} \phi^2$$

For small disturbances this will be satisfied except for where

$$\frac{M \cos \lambda}{\sin(\phi + \lambda)} \approx 1$$

which is, of course, the transitional limit. Now just considering the region near the transitional limit, the requirement may be written

or 
$$\frac{M \cos \lambda - \sin(\phi + \lambda)}{M \cos \lambda} \gg M \left( \frac{\delta + 1}{2} \right) \phi_{S^0}$$

$$\frac{\Delta(M \cos \lambda)}{M \cos \lambda} \gg M \left( \frac{\delta + 1}{2} \right) \phi_{S^0}$$

where  $\Delta(M \cos \lambda)$  is the separation from the transitional limit  $M \cos \lambda = \sin(\phi + \lambda)$  required for the linearization of the equation of motion to be valid. Typically, have  $M \approx 0.5$ , and  $\phi_{S^0} \approx \alpha \approx 0.1$ , so the boundary of the transitional region may be considered

$$\frac{\Delta(M \cos \lambda)}{M \cos \lambda} \approx 0.06$$

Thus it is seen that the nonlinearity near the transitional limit  $M \cos \lambda = \sin(\phi + \lambda)$  is not very great; the transitional region is rather narrow. Moreover, the width of the region is proportional to  $M \cos \lambda$ . As  $M \cos \lambda \rightarrow 0$  (and so  $(\phi + \lambda) \rightarrow \pi$ ) the width of the transitional region also goes to zero. Thus, the linearization of the equation of motion in the two-dimensional incompressible case is uniformly valid for all levels of disturbance (although linearization of the boundary conditions may not always be valid).

## 2.4 The Approximate Solution

### 2.4.1 Numerical Solution of the Integral Equation

The integral equations have been obtained in the form

$$\int_{-1}^1 \bar{G}^A(\sigma^A, \tau/\sin) K^A(s_0^A, \tau/\sin) d\sigma^A = -e^{i\tau/\sin} s^A \cos$$

and

$$\int_{-1}^1 \bar{G}(\sigma, \nu/\sin) K(s_0, \nu/\sin) d\sigma = -1$$

Substituting for the loading influence function as a Glauert series, that is

$$\bar{G}^A(s^A, \nu/\sin) = \sum_{n=0}^{\infty} \bar{g}_n^A(\nu/\sin) f_n(s^A)$$

where

$$f_n(s^A) = \begin{cases} \tan \theta/2 & n=0 \\ \sin n\theta & n \geq 1 \end{cases} \quad s^A = \cos \theta$$

obtain

$$\sum_{n=0}^{\infty} \bar{g}_n^A(\nu/\sin) \int_{-1}^1 f_n(\sigma^A) K^A(s_0^A, \nu/\sin) d\sigma^A = -e^{i\nu/\sin s^A \cos}$$

and

$$\sum_{n=0}^{\infty} \bar{g}_n(\nu/\sin) \int_{-1}^1 f_n(\sigma) K(s_0, \nu/\sin) d\sigma = -1$$

Since  $\nu/\sin$  appears in the integral equation only as a parameter, the substitution of a series of this form accomplishes the removal of the desired quantities,  $\bar{g}_n^A$  (or  $\bar{g}_n$ ), to outside the integral.

The integrals

$$\int_{-1}^1 f_n(\sigma^A) K^A(s_0^A, \nu/\sin) d\sigma^A$$

and

$$\int_{-1}^1 f_n(\sigma) K(s_0, \nu/\sin) d\sigma$$

now involve only known quantities, but must however be evaluated numerically. To do this, it is first necessary to identify the singularities of the kernels,  $K^A$  and  $K$ . These kernels may be written as

$$K^A(s_0^A, \nu/\sin) = \frac{1}{s_0^A} - i\alpha\mu \ln |s_0^A| + K^{A*}(s_0^A, \nu/\sin)$$

and

$$K(s_0, \gamma/\sin) = \frac{1}{s_0} - i\alpha\mu \ln|s_0| + K^*(s_0, \gamma/\sin)$$

where

$$\alpha\mu = \frac{-\cos}{\alpha^2} (\gamma/\sin)$$

These forms are valid for all values of the parameters  $m \cos \mu$  and  $(\phi + \mu)$ . The reduced kernels have the properties

$$K^{A*}(0, \gamma/\sin) = 0$$

and

$$K^*(0, \gamma/\sin) = 0$$

and possess no singularities in  $s_0^A$  (or  $s_0$ ) or in  $\gamma/\sin$ . The integrals now may be written

$$\begin{aligned} & \int_{-1}^1 f_n(\sigma^A) |K^A(s_0^A, \gamma/\sin)| d\sigma^A \\ &= \int_{-1}^1 f_n(\sigma^A) \frac{\partial \sigma^A}{s_0^A} - i\alpha\mu \int_{-1}^1 f_n(\sigma^A) \ln|s_0^A| d\sigma^A \\ &+ \int_{-1}^1 f_n(\sigma^A) |K^{A*}(s_0^A, \gamma/\sin)| d\sigma^A \end{aligned}$$

and similarly for the  $(s, r)$  system. The first two terms involve the singular parts of the kernel, but may be evaluated analytically as

$$\int_{-1}^1 f_n(\sigma^A) \frac{\partial \sigma^A}{s_0^A} = \pi \cos n\phi$$

$$\int_{-1}^1 f_n(\sigma^A) \ln|s_0^A| d\sigma^A =$$

$$\begin{cases} \pi \ln(s^A+1) + \pi s^A - \left[ \phi \ln \frac{1+s^A}{1-s^A} + \int_{-1}^1 \frac{\partial - \phi}{s^A - \sigma^A} d\sigma^A \right] & n=0 \\ \frac{\pi}{2} \ln(s^A+1) + \frac{\pi}{4} (2s^{A^2}-1) - \frac{1}{2} \left[ \phi \ln \frac{1+s^A}{1-s^A} + \int_{-1}^1 \frac{\partial - \phi}{s^A - \sigma^A} d\sigma^A \right] & n=1 \\ \frac{\pi}{2} \left[ \frac{\cos(n+1)\phi}{n+1} - \frac{\cos(n-1)\phi}{n-1} \right] & n \geq 2 \end{cases}$$

where  $\cos \theta = r^A$ ,  $\cos \phi = s^A$ .

The last term may now be integrated numerically since  $K^{A*}$  (or  $K^*$ ) has no singularities in  $s_0^A$  (or  $s_0$ ). Because of the square-root nature of the Glauert functions  $f_n(s^A)$ , this is properly accomplished by a Jacobi-Gauss quadrature (Refs. 18, 19, and 20) which gives

$$\int_{-1}^1 f_n(r^A) K^{A*}(s_0^A, r/\sin) \mathcal{D}r^A \\ \cong H \sum_{j=1}^J F_n(r_j^A) K^{A*}(s^A - r_j^A, r/\sin)$$

where

$$r_j^A = \cos \theta_j \quad j = 1 \dots J$$

$$\theta_j = \begin{cases} \frac{2\pi}{2J+1} j & n=0 \\ \frac{\pi}{J+1} j & n \geq 1 \end{cases}$$

$$H = \begin{cases} \frac{2\pi}{2J+1} & n=0 \\ \frac{\pi}{J+1} & n \geq 1 \end{cases}$$

and

$$F_0(r) = 1 - r$$

$$F_1(r) = 1 - r^2$$

$$F_2(r) = 2r(1 - r^2)$$

$$F_{n+1}(r) = 2rF_n(r) - F_{n-1}(r), \quad n \geq 2$$

While the reduced kernel  $K^{A*}$  (or  $K^*$ ) is not singular at  $s_0^A = 0$  (or  $s_0 = 0$ ), it does have an infinite derivative there. This may be seen by expanding the kernels further, obtaining the form for  $s_0^A \rightarrow 0$

$$K^A(s_0^A, \sqrt{s \sin}) = \frac{1}{s_0^A} - i \gamma \mu \ln |s_0^A| + C_1 + C_2 s_0^A \ln |s_0^A| + C_3 s_0^A + \dots$$

(similarly for  $K(s_0, \sqrt{s \sin})$ ); the term  $s_0^A \ln |s_0^A|$  has an infinite derivative at  $s_0^A = 0$ . This behavior of  $K^{A*}$  (or  $K^*$ ) introduces some error in the quadrature for very small values of the wave number ( $\sqrt{s \sin} \approx 0.1$ ). However, here the wave number of interest will be of the order  $\sqrt{s \sin} \approx 1.0$ . A further expansion of the kernel to remove the singularity in the derivative before performing the numerical quadrature introduces error for these larger wave numbers. Therefore, in the evaluation of the required integrals, the kernels were only expanded as above to remove the singularities, but not the infinite derivative at  $s_0^A = 0$ .

With the integrals evaluated, the integral equations still remain in the form of an infinite sum over  $\bar{g}_n^A$  (or  $\bar{g}_n$ ) to be satisfied at each of the infinity of points of  $s^A$  (or  $s$ ) in the interval  $-1$  to  $1$ . Since numerical procedures can only deal with finite data, the higher terms in the sum must be discarded, with correspondingly some loss of information. Thus truncating the sums, the integral equations take the form

$$\sum_{n=0}^{N/2} \bar{g}_n^A(\sqrt{s \sin}) \int_{-1}^1 f_n(\sigma^A) K^A(s_0^A, \sqrt{s \sin}) d\sigma^A = -2 i \sqrt{s \sin} s^A \cos$$

and

$$\sum_{n=0}^N \bar{g}_n(\gamma/\sin) \int_{-1}^1 f_n(r) K(s_0, \gamma/\sin) \delta r = -1$$

The collocation points in  $s^A$  (or  $s$ ) are chosen following the criterion of Hsu (Ref. 18). This again involves a Jacobi-Gauss quadrature, so obtain

$$s_j^A = \cos \phi_j \quad j=1 \dots M$$

$$\phi_j = \frac{2\pi}{2M+1} (j - \frac{1}{2})$$

With the sum truncated to  $N+1$  terms and choosing a finite number  $M$  of collocation points where the equation is to be satisfied, the integral equation has been transformed into a finite set of linear algebraic equations, for the quantities  $\bar{g}_n^A$  (or  $\bar{g}_n$ ) at a given  $\gamma/\sin$ . For  $M > N+1$ , these equations are solved in a least squares sense.

The integral equations were solved for  $\bar{g}_n^A$  and  $\bar{g}_n$  (and also  $\bar{g}_L$ ,  $\bar{g}_M$  and  $\bar{g}_C$ ) for values of  $\gamma/\sin$  in the range

$$0.0 < \gamma/\sin < 6.0$$

Six terms in the Glauert series were obtained; that is,

$$N = 5$$

satisfying the integral equation in a least squares sense at eleven collocation points,

$$M = 11$$

The integrals were evaluated by numerical quadrature using fifteen to twenty points, that is

$$J = 15 \text{ to } 20$$

The Hankel functions and modified Bessel functions occurring in the kernels were evaluated using polynomial approximations (Ref.20). The cosine and Sine integrals in the two-dimensional incompressible

(and transitional) kernels were evaluated using rational approximations, also from Ref. 20. The absolute error involved in these approximations was of the order  $\epsilon = 10^{-7}$ .

The accuracy of the numerical calculations was evaluated by comparison with the exact solution available for the two-dimensional incompressible case. The numerical calculations gave an absolute error of the order of  $\epsilon = 10^{-3}$ , which was sufficient for the range of  $\sqrt{s} \sin$  considered. This error did not depend on the number of terms in the Glauert series or the number of collocation points used (the error due to these was of the order  $\epsilon = 10^{-5}$ ). Rather it was due to the truncation and roundoff errors in the calculation procedure. The minimums obtainable for these were limited by the accuracy of the available approximations for the Hankel and Bessel functions. It was also expected and observed in the results that the calculations would be more accurate for the elliptic kernel than for the hyperbolic kernel. The exponential decay nature of the elliptic kernel resulted in more accurate numerical work.

The numerical calculations described above were carried out for the thirty-seven cases covering the range of the parameters

$$\frac{\pi}{2} \leq (\phi + \lambda) \leq \pi$$

$$0 \leq M \cos \lambda < 1$$

as shown in Figure 2.8.

#### 2.4.2 The Approximate Influence Functions

For routine application to the calculation of rotary wing airloads, numerical results are not very useful. Therefore it is necessary to use the numerical results to obtain approximate analytical expressions for the universal loading influence functions. Then these expressions may be used in an airloads calculation.

First, it is necessary to determine the range of  $\sqrt{s} \sin$  over



which the approximations should give valid information about the Fourier transform of the influence functions in order that accurate loadings may be obtained from the downwash. Generally, large and small wave numbers correspond to variations over small and large  $r$  distance (spanwise variable) respectively, so the limits in  $\mathcal{V}/s_{in}$  of the accuracy of the approximations correspond to limits in the allowable variations of the downwash along the span for which the loading results will be accurate. Specifically, very large and very small wave numbers are important for very close and very far free vortices.

Using the free vortex as an example, have

$$\bar{w}_r(\mathcal{V}/s_{in}) \propto e^{-|h\mathcal{V}/s_{in}|}$$

Thus, for  $h \cong 1/2$  (a reasonable lower limit for usual vortex core sizes) should need information in the influence function out to about

$$\mathcal{V}/s_{in} \cong 5.0$$

This criterion may be examined in more detail. The exponential form of  $\bar{w}_r$  corresponds to an actual downwash  $w$  with a pair of complex conjugate poles (since  $w$  must be real) with imaginary part equal to  $h$ . In terms of the downwash variation, this means a large variation of  $w$  occurs in a range of

$$\Delta r^p \cong 2h$$

An upper limit in  $\mathcal{V}/s_{in}$  on the required validity of the influence function approximation restricts the high wave number content of the downwash  $w$  that is allowed for an accurate loading prediction. In general, let  $h$  be a measure of the distance over which there is a large variation in the downwash. Then corresponding limits are a maximum wave number

$$\mathcal{V}/s_{in} \cong 5.0$$

and a minimum variation distance

$$b \approx \frac{1}{2}$$

(and the downwash  $w$  reasonably smooth). Again, for a free vortex, the minimum separation distance is itself a measure of the range of variation of the downwash. Furthermore, it may be shown that for a free vortex with a viscous core,

$$\left( \begin{array}{c} \text{minimum equivalent} \\ \text{separation distance} \end{array} \right) = \left( \begin{array}{c} \text{vortex} \\ \text{core} \\ \text{radius} \end{array} \right)$$

Then the restriction on maximum wave number simply becomes a restriction on minimum core size,

$$\left( \begin{array}{c} \text{minimum} \\ \text{core} \\ \text{radius} \end{array} \right) \approx \frac{1}{2} b$$

which is not a difficult criterion for usual applications.

To determine the requirements for small wave number, the free vortex example is again helpful

$$\bar{w}_r(\gamma/\sin) \propto e^{-|h\gamma/\sin|}$$

For the limit  $\gamma/\sin \rightarrow 0$ ,  $\bar{w}_r \rightarrow$  nonzero constant independent of  $h$ . Thus the behavior of the influence functions should be approximated closely for  $\gamma/\sin \rightarrow 0$ . The values at exactly  $\gamma/\sin = 0$  are easily matched. However, the expansions of the solutions for small  $\gamma/\sin$  frequently involve logarithmic terms, and the behavior of these near  $\gamma/\sin = 0$  is impossible to approximate with useful elementary functions (that is, functions with inverse Fourier transforms available in closed form). Thus, there will inevitably be inaccuracies in the approximate influence functions for very small wave number. These inaccuracies may be accepted, however, since very small wave numbers are important only for very distant vortices. For far vortices, the magnitude of the downwash  $w_r$  is decreasing like  $(h)^{-1}$ , so for very distant vortices the angle of

attack will be small and the loads negligible.

The behavior of the influence functions for small wave number may be obtained by expanding the kernels  $K^A$  (or  $K$ ) about  $\eta/\sin \lambda = 0$  and solving the integral equation successively for higher order terms in  $\bar{G}^A$  (or  $\bar{G}$ ). While this procedure may not practically be carried out, it does show that the solution must be of the form

$$\bar{G}^A(s^A, \eta/\sin \lambda) \cong a_0(s^A) + a_1(s^A) \eta/\sin \lambda + a_2(s^A) \eta/\sin \lambda \ln |\eta/\sin \lambda| + \dots$$

the term  $\eta/\sin \lambda \ln |\eta/\sin \lambda|$  means first that the influence functions will have an infinite derivative at  $\eta/\sin \lambda = 0$ , making an accurate approximation for very small  $\eta/\sin \lambda$  difficult to obtain. It also means that  $\bar{G}^A$  (or  $\bar{G}$ ) does not have a Taylor's series expansion in terms of the derivatives of the Fourier transform of the result for the limit  $\eta/\sin \lambda = 0$ . Recalling that this limit is the lifting line limit, this means the solution does not have an expansion about the lifting line limit. That is, the lifting surface influence is of a fundamentally different nature than the lifting line limit.

The behavior of the solutions for the influence functions may be shown by an examination of the two-dimensional incompressible result ( $M \cos \lambda = 0, \langle \phi + \lambda \rangle = 180^\circ$ ) which is available in closed form. While the result that all the terms in the Glauert series except the first are identically zero,

$$\bar{g}_n^A(\eta/\sin \lambda) \equiv 0, \quad n \geq 1$$

$$\bar{g}_m^A(\eta/\sin \lambda) \equiv 0$$

is exceptional for this case, the results for the lift and circulation are found to be typical of the solutions for the entire ranges of  $M \cos \lambda$  and  $\langle \phi + \lambda \rangle$ . The magnitude and phase of  $\bar{g}_L(\eta/\sin \lambda)$  are shown in Figure 2.9, and the real and imaginary

parts of  $\bar{g}_C(\gamma/\sin) e^{-i\gamma/\sin \cos}$  in Figure 2.10. The asymptotic behavior of the lift is shown to be

$$\bar{g}_L(\gamma/\sin) \sim -\frac{1}{\sqrt{2\pi\gamma/\sin}} e^{i(\gamma/\sin - \pi/4)}$$

While on inspection of Figures 2.9 and 2.10 the magnitudes appear to have exponential behavior, the decay is actually like  $(\gamma/\sin)^{-1/2}$ . Such behavior is not convenient in a Fourier transform however. It is found that the decay may be approximated out to sufficient wave number by a sum of exponential terms. While for large enough wave number any such approximation must underestimate the influence function, the behavior at very large wave number is unimportant because of the properties of  $\omega_F(\gamma/\sin)$  as above, and furthermore exponential terms are very convenient to work with as Fourier transforms.

The phase of  $\bar{g}_L$  is seen to be asymptotically linear in  $\gamma/\sin$ . This is characteristic of all the influence functions, as would be expected since the kernels also have this property. Typically, the asymptote is reached by  $\gamma/\sin \cong 2.0$ . The phase may be generally written

$$(b_1 \gamma/\sin - b_2)$$

where  $b_1 = b_2 = 0$  for  $(\phi + \lambda) = \pi$  (the vortex and blade perpendicular). It is found that  $b_2$  is typically linear in  $(\phi + \lambda)$  and  $b_1$  goes like  $\cos(\phi + \lambda)$ .

The behavior of the lift for small  $\gamma/\sin$  is

$$\bar{g}_L(\gamma/\sin) \cong -\left[1 - \gamma/\sin \left(\frac{\pi}{2} - \delta - \ln\left(\frac{\gamma/\sin}{2}\right)\right)\right]$$

Again the  $\gamma/\sin \ln \gamma/\sin$  term results in an infinite derivative at  $\gamma/\sin = 0$ . The effect on the phase of  $\bar{g}_L(\gamma/\sin)$  may be seen in Figure 2.9.

The solution for the influence functions for all  $M \cos \lambda$  and  $(\phi + \lambda)$  is known exactly for one wave number,  $\gamma/\sin = 0$ .

At  $r/\sin \theta = 0$  (the lifting line or steady-state solution), the solution is known to be

$$\bar{g}_L(0) = \bar{g}_c(0) = \pi \bar{g}_0^A(0) = -1$$

and

$$\bar{g}_M(0) = \bar{g}_n^A(0) = 0 \quad , \quad n \geq 1$$

These values will be matched exactly by the approximate expressions.

With the above background on the nature of the numerical solutions, the following expressions were adopted for the approximations to the influence functions:

$$\bar{g}_c(r/\sin \theta) = \left[ - \sum_{n=0}^{\infty} a_n (i r/\sin \theta)^{2n} e^{-c_n r/\sin \theta} + i \sin(b_0 r/\sin \theta) \sum_{n=0}^{\infty} a_n^r (i r/\sin \theta)^{2n} e^{-c_n^r r/\sin \theta} \right] e^{i r/\sin \theta \cos \theta}$$

$$\bar{g}_L(r/\sin \theta) \text{ OR } \bar{g}_0^A(r/\sin \theta) =$$

$$\left[ - a_0 e^{-c_0 r/\sin \theta} + i a_0^r \sin(b_0 r/\sin \theta) e^{-c_0^r r/\sin \theta} - e^{i(b_1 r/\sin \theta - b_2 r/\sin \theta)} \sum_{n=1}^{\infty} a_n (i r/\sin \theta)^{2n} e^{-c_n r/\sin \theta} \right]$$

$$\bar{g}_n(\nu/\sin) \text{ OR } -\bar{g}_1^A(\nu/\sin) =$$

$$\left[ -\sum_{n=1}^3 e^{i(b_1\nu/\sin - b_2\nu \frac{\nu/\sin}{|\nu/\sin|})} a_n (i\nu/\sin)^{2n} e^{-c_n|\nu/\sin|} \right]$$

$$\bar{g}_2^A(\nu/\sin) =$$

$$\left[ -\sum_{n=2}^3 e^{i(b_1\nu/\sin - b_2\nu \frac{\nu/\sin}{|\nu/\sin|})} a_n (i\nu/\sin)^{2n} e^{-c_n|\nu/\sin|} \right]$$

$$\bar{g}_3^A(\nu/\sin) =$$

$$\left[ e^{i(b_1\nu/\sin - b_2\nu \frac{\nu/\sin}{|\nu/\sin|})} a_3 (i\nu/\sin)^6 e^{-c_3|\nu/\sin|} \right]$$

$$\bar{g}_n^A(\nu/\sin) \equiv 0, \quad n \geq 4$$

The coefficients in the Glauert series for  $n \geq 4$  were considered negligible; typically, the values obtained for these coefficients were of the order of the error expected in the numerical calculations.

The constants that appear in these expressions must be determined from the numerical calculations. They depend on the parameters  $M \cos \Lambda$  and  $(\phi + \Lambda)$  and are of course different for each of the influence functions  $\bar{g}_C$ ,  $\bar{g}_L$ ,  $\bar{g}_M$ , and  $\bar{g}_n$ ,  $n=0,1,2,3$ .

The exponential terms of these expressions are similar to the form of the Fourier transform of the downwash due to a free vortex,  $\bar{w}_F(\sqrt{s} \sin)$ . This may be interpreted as indicative of the vortex nature of the induced trailed wake, which is an essential feature of the lifting surface formulation. Such an interpretation should not be carried too far however, since as shown above the exponential form of the influence functions is only approximate, the true behavior being like  $(\sqrt{s} \sin)^{-1/2}$  for large  $\sqrt{s} \sin$ . The influence functions could be approximated to any given accuracy by an infinite sum of exponential terms; but that simply implies the not very surprising result that the lifting surface solution can be formulated as an infinite sum of terms, each of a vortex nature.

The constants in the expressions for the approximate influence functions were determined from the numerical solutions for each of the cases shown in Figure 2.8. Then approximations for the behavior of the constants over the ranges of  $M \cos \Lambda$  and  $(\phi + \Lambda)$  were obtained. The procedure was as follows. First, the expressions for the phase constants (b) in terms of  $M \cos \Lambda$  and  $(\phi + \Lambda)$  were obtained. Then using these expressions for the phase constants, the remaining constants (a and c) were obtained for the individual cases by matching the magnitudes of the numerical and approximate solutions at selected points. From the values for these constants, expressions for the constants (a and c) for arbitrary  $M \cos \Lambda$  and  $(\phi + \Lambda)$  were constructed. The lift,

the circulation, and the zeroth Glauert coefficient were matched at

$$\gamma/\sin = 0.0, 0.4, 1.6, 2.6, 4.0, 5.0$$

All the functions have the correct value at  $\gamma/\sin = 0$ . The lift, the circulation, and the zeroth Glauert coefficient were matched out to  $\gamma/\sin \cong 6.0$ ; the moment and higher Glauert coefficients were matched out to  $\gamma/\sin \cong 4.0$ .

Generally, the magnitude of the approximations was matched to better accuracy than the phase. Since the phase in a Fourier transform corresponds to a linear shift in the argument (spanwise variable), the accuracy obtained was considered acceptable. Also, the asymptotic values of the phase were matched very accurately. The approximations for the lift, the circulation, and the zeroth Glauert coefficient were more accurate than those for the moment and higher Glauert series. This was acceptable since the former have a finite value, but the latter are identically zero at  $\gamma/\sin = 0$ . Thus the latter are usually smaller in the important range  $\gamma/\sin \cong 1$ , and correspondingly the actual moment and higher pressure coefficients will be small. The approximate expressions for the constants in the influence functions matched the behavior with  $(\phi + \lambda)$  better than that with  $M \cos \lambda$ ; this was consistent with the kernels for which the behavior with  $(\phi + \lambda)$  was more significant than that with  $(\phi + \lambda)$  (in a given domain). The approximations were considered sufficiently accurate out to  $M \cos \lambda = 0.9$ . The approximate expressions for the constants were more accurate for the elliptic domain than for the hyperbolic or transitional domains; this was consistent with the accuracy of the numerical solutions.

An example of the accuracy of the approximate expressions for the influence functions, using the approximate expressions for the constants, is shown in Figures 2.11, 2.12, and 2.13. These



show the circulation, lift, and moment, respectively, for the case  $M \cos \lambda = 0.0$  and  $(\phi + \lambda) = 135^\circ$ . The approximate results are compared with the numerical calculations. The accuracy shown is typical of most of the range of  $M \cos \lambda$  and  $(\phi + \lambda)$ . The scale of the magnitude of the moment should be noted.

Below are given the analytic expressions obtained for the constants appearing in the approximate influence functions. The following notation is used for the elliptic, transitional, and hyperbolic domains:

$$\begin{array}{ll} \text{ELP} & M \cos \lambda < \sin(\phi + \lambda) \\ \text{TRN} & M \cos \lambda = \sin(\phi + \lambda) \\ \text{HYP} & M \cos \lambda > \sin(\phi + \lambda) \end{array}$$

The behavior of the kernels, and consequently the influence functions and the constants, are significantly different in the three regions. The transitional domain (the actual nonlinear region, rather than the region where the linear kernel is valid) is not actually the line  $M \cos \lambda = \sin(\phi + \lambda)$  but rather a strip of width proportional to  $M \cos \lambda$ , as indicated in Section 2.3.6. Thus the behavior of the constants in the transitional domain may be taken as

$$f = f_{\text{TRN}} e^{-4\left(\frac{\Delta}{0.05}\right)^2} + f_{\text{HYP OR ELP}} \left(1 - e^{-4\left(\frac{\Delta}{0.05}\right)^2}\right)$$

where  $f$  is any of the constants (a,b,c) and  $f_{\text{TRN}}$  is based on the same  $M \cos \lambda$  as  $f_{\text{HYP}}$  or  $f_{\text{ELP}}$ . With

$$\Delta = \frac{M \cos \lambda - \sin(\phi + \lambda)}{\sin(\phi + \lambda)}$$

the transition region indeed has a width proportional to  $M \cos \lambda$ . It is also required then that  $f_{\text{HYP}}$ ,  $f_{\text{TRN}}$ , and  $f_{\text{ELP}}$  be equal at

the case  $M \cos \lambda = 0.0$  and  $(\phi + \lambda) = 180^\circ$ . Furthermore,

$$e^{-4 \left(\frac{\Delta}{0.05}\right)^2} \approx 0.02 \quad \text{at} \quad \Delta = \pm 0.05$$

which is a width consistent with the estimates from nonlinear theory. In what follows it should be noted that

$$\frac{\pi}{2} < \sin^{-1}(M \cos \lambda) < \pi$$

to be consistent with the range of  $(\phi + \lambda)$ .

Circulation:

$$\bar{g}_c(\eta/\sin) = \left[ - \sum_{n=0}^{\infty} a_n (i\eta/\sin)^{2n} e^{-cn|\eta/\sin|} + i \sin(\theta_0 \eta/\sin) \sum_{n=0}^{\infty} a_n' (i\eta/\sin)^{2n} e^{-c'n|\eta/\sin|} \right] e^{i\eta/\sin \cos}$$

$$\theta_0 = \frac{1.926}{\sqrt{\alpha^2 + 2.56 |(M \cos \lambda)^2 - (\sin)^2|}}$$

$$a_0 = 1$$

$$a_1 = \begin{cases} - \left[ 0.434 + 1.210 \left( \frac{2}{\pi} (\phi + \lambda) - 1 \right)^{2.25} + 0.143 (M \cos \lambda)^{1.9} \right] & \text{ELP} \\ - \left[ 1.644 - 0.624 (1 - e^{-10 M \cos \lambda}) \right] & \text{TRN} \\ - 1.644 (1 - 0.735 (M \cos \lambda)^{0.75}) (\theta_0 + \cos) & \text{HYP} \end{cases}$$

$$a_2 = \begin{cases} (0.0135 - 0.0051 \sin) (1 - 0.26 (M \cos \lambda)^2) & \text{ELP} \\ (0.0135 - 0.0051 M \cos \lambda) (1 - 0.26 (M \cos \lambda)^2) & \text{TRN} \\ 0.0010 + 0.0125 e^{-10 M \cos \lambda} & \text{HYP} \end{cases}$$

$$a_0^p = \begin{cases} \left[ \frac{(\phi+\lambda) - \frac{\pi}{2}}{\sin^{-1} M \cos \lambda - \frac{\pi}{2}} \right] (1.555 - 1.798 \alpha M \cos \lambda) & \text{ELP} \\ \quad \quad \quad - 0.899 \sin 2(\phi+\lambda) & \text{TRN} \\ 1.555 \left( \frac{\cos \alpha}{\alpha} \right)^2 & \text{HYP} \end{cases}$$

$$a_1^p = \begin{cases} - \left[ \frac{(\phi+\lambda) - \frac{\pi}{2}}{\sin^{-1} M \cos \lambda - \frac{\pi}{2}} \right] (0.9 (1 + 2.5 (M \cos \lambda)^3) - 2.3 \alpha M \cos \lambda) & \text{ELP} \\ \quad \quad \quad + 1.15 \sin 2(\phi+\lambda) & \text{TRN} \\ - 0.9 (1 + 2.5 (M \cos \lambda)^3) & \text{HYP} \\ - (0.9 - 0.57 M \cos \lambda + 3.3 (M \cos \lambda)^5) & \text{HYP} \end{cases}$$

$$c_0 = \left[ 1.683 + 0.563 \left( \frac{2}{\pi} (\phi+\lambda) - 1 \right)^{2.44} \right] (1 + 0.72 (M \cos \lambda)^{2.3})$$

$$c_1 = \begin{cases} \left[ 1.417 + 0.547 \left( \frac{2}{\pi} (\phi+\lambda) - 1 \right)^{2.13} \right] (1 + 0.26 (M \cos \lambda)^{2.2}) & \text{ELP} \\ 1.964 & \text{TRN} \\ 1.964 e^{-0.36 (M \cos \lambda - \sin)} & \text{HYP} \end{cases}$$

$$C_2 = \begin{cases} \left[ 0.910 + 0.108 \left( \frac{2}{\pi} (\phi + \lambda) - 1 \right)^{2.25} \right] (1 + 0.07 (M \cos \lambda)^{2.5}) & \text{ELP} \\ 1.018 & \text{TRN} \\ \left( 1.018 - 1.28 (M \cos \lambda) + 1.6 (M \cos \lambda)^{3.5} \right) (-\cos) & \text{HYP} \end{cases}$$

$$C_0^p = \frac{4.9}{\alpha} (1 + 0.15 (\sin - M \cos \lambda))$$

$$C_{\perp}^p = \begin{cases} \left( 4.15 + (-1.58 + 3.50 (M \cos \lambda)^{3.8}) e^{-7(\sin - M \cos \lambda)} \right) & \text{ELP} \\ & \text{or} \\ & \text{TRN} \\ \left( 2.10 + (0.47 + 3.5 (M \cos \lambda)^{3.8}) e^{-15(M \cos \lambda - \sin)} \right) & \text{HYP} \\ & \text{or} \\ & \text{TRN} \end{cases}$$

Lift:

$$\bar{g}_L(r/\sin) = \left[ -a_0 e^{-c_0 r/\sin} + i a_0^0 \sin(\theta_0 r/\sin) e^{-c_0 r/\sin} - e^{i(\theta_1 r/\sin - \theta_2 \frac{r/\sin}{17/\sin})} \sum_{n=1}^{\infty} a_n (i r/\sin)^{2n} e^{-c_n r/\sin} \right]$$

$$\theta_0 = \begin{cases} 5.12 + 1.88 \left[ \frac{(\phi + \lambda) - \sin^{-1} M \cos \lambda}{\frac{\pi}{2} - \sin^{-1} M \cos \lambda} \right] & \text{ELP} \\ 5.12 & \text{TEN} \\ 5.12 - 4.12 (M \cos \lambda)^2 & \text{HYP} \end{cases}$$

$$\theta_1 = \begin{cases} -\cos & \text{ELP} \\ (1 - 0.7 (M \cos \lambda)^3) & \text{TEN} \\ 1.0 e^{-10 M \cos \lambda} + 0.8 (1 - 0.1 \sin) (1 - e^{-10 M \cos \lambda}) & \text{HYP} \end{cases}$$

$$\theta_2 = \begin{cases} \frac{\alpha}{2} ((\phi + \lambda) - \frac{\pi}{2}) & \text{ELP} \\ \sqrt{\left[ \frac{\alpha}{2} ((\phi + \lambda) - \frac{\pi}{2}) \right]^2 + \left[ 0.2 M \cos \lambda + (M \cos \lambda)^2 - \sin^2 \right]} & \text{HYP} \\ & \text{\& TEN} \\ & \text{8 parts of ELP} \end{cases}$$

$$a_0 = 1$$

$$a_1 = \begin{cases} - \left[ 0.434 + 1.09 (1 - \sin)^{0.94} - 0.607 (1 - \sin)^{2.46} \right] (1 + 0.33 (M \cos \lambda)^{1.9}) & \text{ELP} \\ -0.917 (1 - 0.52 (M \cos \lambda)^{5.38}) & \text{HYP} \\ & \text{of TEN} \end{cases}$$

$$a_2 = \begin{cases} (0.0084 + 0.0069(-\cos)^{1.8}) (1 - 0.26(M\cos L)^2) & \text{ELP} \\ (0.0153 + 0.0188(M\cos L) - 0.0188(M\cos L)^2) & \text{HYP} \\ & \text{OR} \\ & \text{TRN} \end{cases}$$

$$a_0^* = \begin{cases} [0.554(-\cos) + 0.07\sin^2(\phi + \lambda)] (1 + 2.13(M\cos L)^{2.1}) & \text{ELP} \\ 0.554 (1 + 0.34(M\cos L)^{1.9}) & \text{TRN} \\ 0.554 (1 + 4.8(M\cos L)^{3.1}) & \text{HYP} \end{cases}$$

$$c_0 = \begin{cases} [1.683 + 0.27(1-\sin)^{0.9} - 0.154(1-\sin)^{2.9}] (1 + 0.72(M\cos L)^{2.3}) & \text{ELP} \\ 1.799 (1 + 0.6(M\cos L)^{2.6}) & \text{TRN} \\ 1.799 (1 + 1.84(M\cos L)^{3.46}) (-\cos)^{0.35} & \text{HYP} \end{cases}$$

$$c_1 = \begin{cases} [1.417 + 0.366(1-\sin)^{0.84} - 0.392(1-\sin)^{2.0}] (1 + 0.26(M\cos L)^{2.2}) & \text{ELP} \\ 1.391 (1 + 0.47(M\cos L)^{2.5}) & \text{TRN} \\ 1.391 (1 + 0.30(M\cos L)^{2.1}) (-\cos) & \text{HYP} \end{cases}$$

$$c_2 = \begin{cases} [0.91 + 0.93(1-\sin)^{1.0} - 1.025(1-\sin)^{1.45}] (1 + 0.07(M\cos L)^{2.5}) & \text{ELP} \\ 0.815 (1 + 0.28(M\cos L)^{0.9}) & \text{TRN} \\ 0.815 (1 + 0.55(M\cos L)^{0.5}) (-\cos)^{2.2} & \text{HYP} \end{cases}$$

$$c_0^* = 5.9 + 1.5(M\cos L)$$

Moment:

$$\bar{\sigma}_M(\lambda/\sin) = -\sum_{n=1}^3 e^{i(\delta_{1n}\lambda/\sin - \delta_{2n}\lambda/\sin)} a_n (i\lambda/\sin)^{2n} e^{-cn\lambda/\sin}$$

$$\delta_{13} = \begin{cases} (-\cos) (1 + 0.11 (M \cos \lambda)^{1.5}) & \text{ELP} \\ 1.0 & \text{TRN} \\ 0.65 + 0.35 e^{-10 M \cos \lambda} & \text{HYP} \end{cases}$$

$$\delta_{23} = \begin{cases} 0.75 \left( \frac{2}{\pi} (\phi + \lambda) - 1 \right) (1 + 1.4 (M \cos \lambda)^{1.5}) & \text{ELP} \\ \frac{3\pi}{4} - 1.6 e^{-10 M \cos \lambda} & \text{TRN} \\ \frac{3\pi}{4} \sqrt{1 + 4.1 (M \cos \lambda)^{0.3} \left[ 1 - \left( \frac{\pi - (\phi + \lambda)}{\pi - \sin^{-1} M \cos \lambda} \right)^2 \right]} - 1.6 e^{-10 M \cos \lambda} & \text{HYP} \end{cases}$$

$$\delta_{12} = \begin{cases} (-\cos) (1 + 0.11 (M \cos \lambda)^{1.5}) & \text{ELP} \\ 1.0 & \text{TRN} \\ 1.0 e^{-10 M \cos \lambda} & \text{HYP} \end{cases}$$

$$\delta_{22} = \begin{cases} 0.75 \left( \frac{2}{\pi} (\phi + \lambda) - 1 \right) (1 + 1.4 (M \cos \lambda)^{1.5}) & \text{ELP} \\ \frac{3\pi}{4} - 1.6 e^{-10 M \cos \lambda} & \text{TRN} \\ 2.68 (-\cos) + 2.5 (M \cos \lambda) - 0.89 - 1.04 e^{-10 M \cos \lambda} & \text{HYP} \end{cases}$$

$$b_{11} = \begin{cases} 3.35 (-\cos) (M \cos \lambda)^{0.8} & \text{ELP} \\ 0.0 & \text{TRN} \\ -4.3 (-\cos - 1) - 5.0 (M \cos \lambda)^4 & \text{HYP} \end{cases}$$

$$b_{21} = \begin{cases} 1.79 \left[ \frac{(\phi + \lambda) - \frac{\pi}{2}}{\sin^{-1}(M \cos \lambda) - \frac{\pi}{2}} \right] - \frac{0.69}{\ln(1 - M \cos \lambda)} & \text{ELP} \\ 1.79 & \text{TRN} \\ 2.55 - 0.76 \left[ \frac{\pi - (\phi + \lambda)}{\pi - \sin^{-1} M \cos \lambda} \right] & \text{HYP} \\ 0.0 & M \cos \lambda = 0.0 \end{cases}$$

$$a_1 = \begin{cases} -0.531 (\sin)^{1.95} (1 + 1.8 (M \cos \lambda)^{2.64}) & \text{ELP} \\ -4.08 (M \cos \lambda)^{2.53} & \text{TRN} \\ -(1.30 (M \cos \lambda)^{1.66} + 23.1 (M \cos \lambda)^{11.4}) (-\cos)^{1.4} & \text{HYP} \end{cases}$$

$$a_2 = \begin{cases} 1.145 (\sin)^{1.82} (1 + 0.84 (M \cos \lambda)^{2.48}) & \text{ELP} \\ 3.4 (M \cos \lambda)^{2.25} & \text{TRN} \\ (1.5 (M \cos \lambda)^{2.9} + 5.16 (M \cos \lambda)^{10.5}) (-\cos)^{1.4} & \text{HYP} \end{cases}$$

$$a_3 = \begin{cases} -0.0315 (\sin)^{1.4} (1 + 0.07 (M \cos \lambda)^{1.3}) & \text{ELP} \\ -0.065 (M \cos \lambda)^{2.2} & \text{TRN} \\ -0.047 (M \cos \lambda)^{3.5} (-\cos)^{2.4} & \text{HYP} \end{cases}$$



$$c_1 = \begin{cases} (4.414 - 0.8(1 - \sin)^{1.13})(1 + 0.11(M \cos \lambda)^{1.7}) & \text{ELP} \\ 3.61 + 2.10(1 - e^{-15M \cos \lambda}) & \text{TRN} \\ 3.61(1 + 0.47(M \cos \lambda)^2 + 2.55(M \cos \lambda)^8)(-\cos)^{0.9} & \text{HYP} \end{cases}$$

$$c_2 = \begin{cases} (3.579 - 0.68(1 - \sin)^{1.04})(1 + 0.13(M \cos \lambda)^{2.2}) & \text{ELP} \\ 2.9 + 0.6(1 - e^{-15M \cos \lambda})(1 + 1.4(M \cos \lambda)^{5.7}) & \text{TRN} \\ 2.9(1 - 1.04M \cos \lambda + 2.37(M \cos \lambda)^{3.1}) & \text{HYP} \end{cases}$$

$$c_3 = \begin{cases} (2.139 - 0.67(1 - \sin)^{1.43})(1 + 0.073(M \cos \lambda)^{2.1}) & \text{ELP} \\ 1.47 + 0.4(1 - e^{-15M \cos \lambda})(1 + 1.5(M \cos \lambda)^{2.7}) & \text{TRN} \\ 1.47(1 + 0.6(M \cos \lambda)^{3.3}) & \text{HYP} \end{cases}$$

Zeroth Glauert coefficient:

$$\bar{g}_0^A(r/\sin) = \left[ -a_0 e^{-c_0 r/\sin} + i a_0^v \sin(b_0 r/\sin) e^{-c_0 r/\sin} - e^{i(b_1 r/\sin - b_2 r/\sin)} \sum_{n=1}^{\infty} a_n (i r/\sin)^{2n} e^{-c_n r/\sin} \right]$$

$$b_0 = \begin{cases} 8.08 + (0.296 + (M \cos \lambda)^{2.5}) (2 - \frac{12}{\pi} (\phi + \lambda)) & \text{ELP} \\ 8.08 + (0.296 + (M \cos \lambda)^{2.5}) (2 - \frac{12}{\pi} \sin^{-1} M \cos \lambda) & \text{TRN} \\ 3.95 + 1.17 e^{-10 M \cos \lambda} - 2.29 (\pi - (\phi + \lambda))^3 & \text{HYP} \end{cases}$$

$$b_1 = -\cos$$

$$b_2 = \begin{cases} \frac{1}{2\alpha} ((\phi + \lambda) - \frac{\pi}{2}) & \text{ELP} \\ \frac{\pi}{4} & \text{TRN} \\ \frac{\pi}{4} & \text{HYP} \end{cases}$$

$$a_0 = \frac{1}{\pi}$$

$$a_1 = \begin{cases} -(0.204 + 0.234 (1 - \sin)^{0.9} - 0.144 (1 - \sin)^{2.4}) (1 + 0.25 (M \cos \lambda)^{1.7}) & \text{ELP} \\ -(0.294 - 0.016 e^{-10 M \cos \lambda}) & \text{TRN} \\ -0.294 (1 - 0.63 (M \cos \lambda)^2) & \text{HYP} \end{cases}$$

$$a_2 = \begin{cases} 0.005 (1 - 0.04 \sin) (1 - 0.115 (M \cos \lambda)^{1.4}) & \text{ELP} \\ 0.005 (1 - 0.04 M \cos \lambda) (1 - 0.115 (M \cos \lambda)^{1.4}) & \text{TRN} \\ 0.005 (1 - 0.5 (M \cos \lambda)^2) & \text{HYP} \end{cases}$$

$$\alpha_0^{\varphi} = \begin{cases} [0.175(-\cos) + 0.03 \sin 2(\phi + \lambda)] (1 + 4.25 (M \cos \lambda)^{2.5}) & \text{ELP} \\ 0.175 (1 + 4.1 (M \cos \lambda)^{3.2}) & \text{TRN} \\ 0.175 (1 + 2.5 (M \cos \lambda)^{1.57}) & \text{HYP} \end{cases}$$

$$c_0 = \begin{cases} [1.555 + 0.435(1 - \sin)^{0.9} - 0.188(1 - \sin)^{4.0}] (1 + 0.6 (M \cos \lambda)^{2.3}) & \text{ELP} \\ 1.802 (1 + 0.89 (M \cos \lambda)^{3.3}) & \text{TRN} \\ 1.802 (1 + 2.5 (M \cos \lambda)^{3.6}) (-\cos)^{0.9} & \text{HYP} \end{cases}$$

$$c_1 = \begin{cases} [1.297 + 0.285(1 - \sin)^{0.9} - 0.184(1 - \sin)^{1.6}] (1 + 0.2 (M \cos \lambda)^{2.3}) & \text{ELP} \\ 1.398 (1 + 0.17 (M \cos \lambda)^{3.5}) & \text{TRN} \\ 1.398 (1 + 0.16 (M \cos \lambda)^{1.2}) (-\cos)^{0.2} & \text{HYP} \end{cases}$$

$$c_2 = \begin{cases} [0.819 + 0.037(1 - \sin)^{0.84} - 0.031(1 - \sin)^{2.0}] (1 + 0.06 (M \cos \lambda)^{2.3}) & \text{ELP} \\ 0.825 (1 + 0.1 (M \cos \lambda)^{3.8}) & \text{TRN} \\ 0.825 (1 + 0.18 (M \cos \lambda)^3) (-\cos)^{0.3} & \text{HYP} \end{cases}$$

$$c_0^{\varphi} = 3.87 + \frac{2}{\pi}(\phi + \lambda) + 2.75 (M \cos \lambda)^2$$

First Glauert coefficient:

$$\frac{-A}{\sigma_1} \frac{1}{r \sin \mu} = \sum_{n=1}^{\infty} e^{i(\beta_{1n} r / \sin \mu - \beta_{2n} r / |\sin \mu|)} a_n (i)^n / \sin \mu^{2n} e^{-cn} r / \sin \mu$$

$$\beta_{13} = \begin{cases} (-\cos \mu) (1 + 0.11 (M \cos \mu)^{1.5}) & \text{ELP} \\ 1.0 - 0.68 (M \cos \mu)^3 & \text{TRN} \\ 0.77 + 0.23 e^{-10 M \cos \mu} & \text{HYP} \end{cases}$$

$$\beta_{23} = \begin{cases} \frac{1}{2} ((\phi + \mu) - \frac{\pi}{2}) (1 + 3.0 (M \cos \mu)^{2.5}) & \text{ELP} \\ \frac{3\pi}{4} (1 - \frac{2}{3} e^{-10 M \cos \mu}) & \text{TRN} \\ \frac{3\pi}{4} \sqrt{1 + 5.4 (M \cos \mu)^{0.67} \left[ 1 - \left( \frac{\pi - (\phi + \mu)}{\pi - \sin^2 \mu \cos \mu} \right)^2 \right]} - \frac{\pi}{2} e^{-10 M \cos \mu} & \text{HYP} \end{cases}$$

$$\beta_{12} = \begin{cases} (-\cos \mu) (1 + 0.11 (M \cos \mu)^{1.5}) & \text{ELP} \\ 1.0 - 0.68 (M \cos \mu)^3 & \text{TRN} \\ 1.0 e^{-10 M \cos \mu} & \text{HYP} \end{cases}$$

$$\beta_{22} = \begin{cases} \frac{1}{2} ((\phi + \mu) - \frac{\pi}{2}) (1 + 3.0 (M \cos \mu)^{2.5}) & \text{ELP} \\ \frac{3\pi}{4} (1 - \frac{2}{3} e^{-10 M \cos \mu}) & \text{TRN} \\ 2.68 (-\cos \mu) + 2.5 / (M \cos \mu) - 0.89 - 1.0 e^{-10 M \cos \mu} & \text{HYP} \end{cases}$$

$$b_{11} = \begin{cases} 3.35 (-\cos) (M \cos \lambda)^{0.8} & \text{ELP} \\ 0.0 & \text{TRN} \\ -5.7 (-\cos - 1) - 7.5 (M \cos \lambda)^4 & \text{HYP} \end{cases}$$

$$b_{21} = \begin{cases} 1.79 \left[ \frac{(\phi + \lambda) - \frac{\pi}{2}}{\sin^{-1} M \cos \lambda - \frac{\pi}{2}} \right]^{-\frac{0.69}{\ln(1 - M \cos \lambda)}} & \text{ELP} \\ 1.79 & \text{TRN} \\ 2.55 - 0.76 \left( \frac{\pi - (\phi + \lambda)}{\pi - \sin^{-1} M \cos \lambda} \right) & \text{HYP} \\ 0.0 & M \cos \lambda = 0.0 \end{cases}$$

$$a_1 = \begin{cases} -0.724 (\sin)^{1.7} (1 + 1.8 (M \cos \lambda)^{2.64}) & \text{ELP} \\ -4.08 (M \cos \lambda)^{2.22} & \text{TRN} \\ -[3.10 (M \cos \lambda)^{2.7} + 22.6 (M \cos \lambda)^{9.6}] (-\cos)^{2.4} & \text{HYP} \end{cases}$$

$$a_2 = \begin{cases} 1.552 (\sin)^{1.52} (1 + 0.84 (M \cos \lambda)^{2.48}) & \text{ELP} \\ 3.9 (M \cos \lambda)^{2.1} & \text{TRN} \\ [0.9 (M \cos \lambda)^{3.18} + 7.65 (M \cos \lambda)^{12}] (-\cos)^{2.4} & \text{HYP} \end{cases}$$

$$a_3 = \begin{cases} -0.0433 (\sin)^{1.1} (1 + 0.3 (M \cos \lambda)^{2.85}) & \text{ELP} \\ -0.135 (M \cos \lambda)^{2.6} & \text{TRN} \\ -0.033 (M \cos \lambda)^{2.32} (-\cos)^{2.4} & \text{HYP} \end{cases}$$

$$c_1 = \begin{cases} (4.277 - 0.63(1 - \sin)^{1.25}) (1 + 0.3(M \cos L)^{2.6}) & \text{ELP} \\ 3.65 + 2.10(1 - e^{-15 M \cos L}) & \text{TRN} \\ 3.65 [1 + 0.48(M \cos L)^2 + 4.0(M \cos L)^8] (-\cos)^{0.9} & \text{HYP} \end{cases}$$

$$c_2 = \begin{cases} (3.421 - 0.56(1 - \sin)^{1.07}) (1 + 0.14(M \cos L)^{2.6}) & \text{ELP} \\ 2.86 + 0.6(1 - e^{-15 M \cos L}) (1 + 1.4(M \cos L)^{5.7}) & \text{TRN} \\ 2.86(1 - 1.4(M \cos L) + 2.82(M \cos L)^{3.3}) & \text{HYP} \end{cases}$$

$$c_3 = \begin{cases} (1.992 - 0.22(1 - \sin)^{1.09}) (1 + 0.083(M \cos L)^{2.8}) & \text{ELP} \\ 1.77 + 0.1(1 - e^{-15 M \cos L}) (1 + 1.5(M \cos L)^{2.7}) & \text{TRN} \\ 1.77(1 + 0.32(M \cos L)^{6.8}) & \text{HYP} \end{cases}$$

Second Glauert coefficient:

$$\frac{-A}{g_2} (i/\sin) = - \sum_{n=2}^{\infty} e^{i(b_{1n} i/\sin - b_{2n} i/\sin)} a_n (i/\sin)^{2n} e^{-cn i/\sin}$$

$$g_{13} = \begin{cases} (-\cos) (1 + 0.17 (M \cos h)^{1.75}) & \text{ELP} \\ \alpha (1 + 0.17 (M \cos h)^{1.75}) & \text{TRN} \\ 0.0 & \text{HYP} \end{cases}$$

$$g_{23} = \begin{cases} 0.86 \left( \frac{2}{\pi} (\phi + h) - 1 \right) (1 + 5.0 (M \cos h)^{2.5}) & \text{ELP} \\ 0.86 \left( \frac{2}{\pi} \sin^{-1} M \cos h - 1 \right) (1 + 5.0 (M \cos h)^{2.5}) & \text{TRN} \\ 3.46 (-\cos - 1) + 0.82 (M \cos h) & \text{HYP} \end{cases}$$

$$g_{12} = \begin{cases} (-\cos) (1 + 0.17 (M \cos h)^{1.75}) & \text{ELP} \\ \alpha (1 + 0.17 (M \cos h)^{1.75}) & \text{TRN} \\ -10.0 [-\cos - 1 + 1.2 (M \cos h)^{4.6}] & \text{HYP} \end{cases}$$

$$g_{22} = \begin{cases} 0.86 \left( \frac{2}{\pi} (\phi + h) - 1 \right) (1 + 5.0 (M \cos h)^{2.5}) & \text{ELP} \\ 0.86 \left( \frac{2}{\pi} \sin^{-1} M \cos h - 1 \right) (1 + 5.0 (M \cos h)^{2.5}) & \text{TRN} \\ 2.65 + 1.25 (M \cos h) & \text{HYP} \end{cases}$$

$$a_2 = \begin{cases} 0.418 (\sin)^3 (1 + 1.65 (M \cos L)^{2.5}) & \text{ELP} \\ 0.418 (M \cos L)^3 (1 + 1.65 (M \cos L)^{2.5}) & \text{TRN} \\ 15.4 (M \cos L)^{10.4} (\alpha)^{-2} (-\cos)^{5.3} & \text{HYP} \end{cases}$$

$$a_3 = \begin{cases} -0.015 (\sin)^{2.5} (1 + 1.2 (M \cos L)^{3.5}) & \text{ELP} \\ -0.015 (M \cos L)^{2.5} (1 + 1.2 (M \cos L)^{3.5}) & \text{TRN} \\ -0.178 (M \cos L)^{6.8} (-\cos)^{9.4} & \text{HYP} \end{cases}$$

$$c_2 = \begin{cases} 3.67 (\sin)^{0.56} (1 + 0.09 (M \cos L)^{2.25}) & \text{ELP} \\ 3.67 (M \cos L)^{0.56} (1 + 0.09 (M \cos L)^{2.25}) & \text{TRN} \\ 5.20 (M \cos L)^2 (\alpha)^{-1} (-\cos)^{2.1} & \text{HYP} \end{cases}$$

$$c_3 = \begin{cases} 1.92 (\sin)^{0.36} (1 + 0.106 (M \cos L)^{2.4}) & \text{ELP} \\ 1.92 (M \cos L)^{0.36} (1 + 0.106 (M \cos L)^{2.4}) & \text{TRN} \\ 2.75 (M \cos L)^{0.84} (-\cos) & \text{HYP} \end{cases}$$



Third Glauert coefficient:

$$\bar{g}_3^A(\nu/\sin) = e^{i(b_1 \nu/\sin - b_2 \frac{\nu/\sin}{1/\sin})} a_3 (i\nu/\sin)^c e^{-c_3 \nu/\sin}$$

$$b_1 = \begin{cases} (-\cos) (1 + 0.5 (M \cos \mu)^3) & \text{ELP} \\ 0.0 & \text{TRN} \\ 0.0 & \text{HYP} \end{cases}$$

$$b_2 = \begin{cases} \frac{1}{2} ((\phi + \mu) - \frac{\pi}{2}) (1 + 8.0 (M \cos \mu)^{2.5}) & \text{ELP} \\ 0.0 & \text{TRN} \\ 0.0 & \text{HYP} \end{cases}$$

$$a_3 = \begin{cases} -0.0123 (\sin)^{3.8} (1 + 4.4 (M \cos \mu)^{2.6}) & \text{ELP} \\ 0.0 & \text{TRN} \\ 0.0 & \text{HYP} \end{cases}$$

$$c_3 = \begin{cases} 2.26 (\sin)^{0.4} (1 + 0.19 (M \cos \mu)^{2.5}) & \text{ELP} \\ 0.0 & \text{TRN} \\ 0.0 & \text{HYP} \end{cases}$$

### 2.4.3 Approximate Solutions for the Loading

The Fourier transforms of the loads, and from these by a Fourier integral the actual loads, may now be obtained from the downwash distribution and the approximate expressions for the universal loading influence functions. Thus one may write:

$$\frac{\bar{Q}_n^A(r/\sin\alpha)/qV^2}{2\pi \frac{\cos\alpha}{\alpha}} = \frac{1}{\sin\alpha} \bar{w}(r/\sin\alpha) \bar{g}_n^A(r/\sin\alpha)$$

$$\frac{\bar{L}(r/\sin\alpha)/qV^2b}{2\pi \frac{\cos\alpha}{\alpha}} = \frac{1}{\sin\alpha} \bar{w}(r/\sin\alpha) \bar{g}_L(r/\sin\alpha)$$

$$\frac{\bar{M}_{ac}(r/\sin\alpha)/qV^2b^2}{2\pi \frac{\cos\alpha}{\alpha}} = \frac{1}{\sin\alpha} \bar{w}(r/\sin\alpha) \bar{g}_M(r/\sin\alpha)$$

$$\frac{\bar{F}(r/\sin\alpha)/Vb}{2\pi \frac{1}{\alpha}} = \frac{1}{\sin\alpha} \bar{w}(r/\sin\alpha) \bar{g}_F(r/\sin\alpha)$$

The loads due to an arbitrary distribution of downwash along the span of the blade may be calculated by recognizing that the Fourier transforms of the loads appear as products of the downwash and influence function transforms. Then from the duality of product and convolution

$$\bar{Q}(r/\sin) = \frac{1}{\sin} \bar{w}(r/\sin) \bar{g}(r/\sin) \longleftrightarrow$$

$$Q(r/\sin) = \frac{1}{2\pi} \int_{-\infty}^{\infty} w(\rho/\sin) g(r/\sin - \rho/\sin) / \sin d\rho/\sin$$

where

$$g(r/\sin) / \sin = \int_{-\infty}^{\infty} \bar{g}(r/\sin) e^{i\rho/\sin r/\sin} d\rho/\sin$$

and everything is a F.T. wrt  $r^A$ , obtain

$$\left( \frac{Q_n^A(r/\sin) / \rho V^2}{2\pi \frac{\cos \lambda}{\alpha}} \right) = \frac{1}{2\pi} \int_{-b}^b w(\rho/\sin) g_n^A(r/\sin - \rho/\sin) / \sin d\rho/\sin$$

$$\left( \frac{L(r/\sin) / \rho V^2 b}{2\pi \frac{\cos \lambda}{\alpha}} \right) = \frac{1}{2\pi} \int_{-b}^b w(\rho/\sin) g_L(r/\sin - \rho/\sin) / \sin d\rho/\sin$$

$$\left( \frac{M_{oc}(r/\sin) / \rho V^2 b^2}{2\pi \frac{\cos \lambda}{\alpha}} \right) = \frac{1}{2\pi} \int_{-b}^b w(\rho/\sin) g_M(r/\sin - \rho/\sin) / \sin d\rho/\sin$$

$$\left( \frac{\Gamma(r/\sin) / V b}{2\pi \frac{1}{\alpha}} \right) = \frac{1}{2\pi} \int_{-b}^b w(\rho/\sin) g_c(r/\sin - \rho/\sin) / \sin d\rho/\sin$$

The approximate expressions for the influence functions are then:

$$g_c(rAsin)/sin = \left[ -\sum_{n=0}^{\infty} a_n \left( \frac{\partial}{\partial rAsin} \right)^{2n} \left[ \frac{2c_n}{(rAsin + cos)^2 + c_n^2} \right] \right. \\ \left. + \sum_{n=0}^{\infty} a_n^v \left( \frac{\partial}{\partial rAsin} \right)^{2n} \left[ \frac{-4b_0 c_n^v (rAsin + cos)}{[-(rAsin + cos)^2 + c_n^v{}^2 + b_0^2]^2 + 4(rAsin + cos)^2 c_n^v{}^2} \right] \right]$$

$$g_L(rAsin)/sin \text{ OR } g_0^A(rAsin)/sin =$$

$$\left[ -a_0 \left[ \frac{2c_0}{(rAsin)^2 + c_0^2} \right] \right. \\ \left. + a_0^v \left[ \frac{-4b_0 c_0^v (rAsin)}{[-(rAsin)^2 + c_0^v{}^2 + b_0^2]^2 + 4(rAsin)^2 c_0^v{}^2} \right] \right. \\ \left. - \sum_{n=1}^{\infty} a_n \left( \frac{\partial}{\partial rAsin} \right)^{2n} \left[ \frac{2(rAsin + b_1) \sin b_2 + 2c_n \cos b_2}{(rAsin + b_1)^2 + c_n^2} \right] \right]$$

$$g_n(rA \sin) / \sin \text{ OR } -g_n^A(rA \sin) / \sin =$$

$$\left[ -\sum_{n=1}^3 a_n \left( \frac{\partial}{\partial rA \sin} \right)^{2n} \left[ \frac{2(rA \sin + b_n) \sin b_n + 2c_n \cos b_n}{(rA \sin + b_n)^2 + c_n^2} \right] \right]$$

$$g_2^A(rA \sin) / \sin =$$

$$\left[ -\sum_{n=2}^3 a_n \left( \frac{\partial}{\partial rA \sin} \right)^{2n} \left[ \frac{2(rA \sin + b_n) \sin b_n + 2c_n \cos b_n}{(rA \sin + b_n)^2 + c_n^2} \right] \right]$$

$$g_3^A(rA \sin) / \sin =$$

$$\left[ a_3 \left( \frac{\partial}{\partial rA \sin} \right)^6 \left[ \frac{2(rA \sin + b_1) \sin b_2 + 2c_3 \cos b_2}{(rA \sin + b_1)^2 + c_3^2} \right] \right]$$

$$g_n^A(rA \sin) / \sin \equiv 0, \quad n \geq 4$$

With these loads known, the pressure is then given by

$$\left( \frac{-\Delta p / \rho V^2}{2\pi \frac{\cos \lambda}{\alpha}} \right) = \sum_{n=0}^3 \left( \frac{\rho_n^A (r^A \sin) / \rho V^2}{2\pi \frac{\cos \lambda}{\alpha}} \right) f_n(s^A)$$

where

$$f_n(s^A) = \begin{cases} \tan \Theta / 2 & n=0 \\ \sin n\Theta & n \geq 1 \end{cases} \quad s^A = \cos \Theta$$

The nose-up moment about an axis at  $s^A = a$  is

$$\left( \frac{M / \rho V^2 b^2}{2\pi \frac{\cos \lambda}{\alpha}} \right) = \left( \frac{M_{QC} / \rho V^2 b^2}{2\pi \frac{\cos \lambda}{\alpha}} \right) + \left( \frac{1}{2} + a \right) \left( \frac{L / \rho V^2 b}{2\pi \frac{\cos \lambda}{\alpha}} \right)$$

The center of pressure (referenced to the chord, with the origin at the leading edge) is located at

$$\frac{x_{c.p.}}{c} = \frac{1}{4} - \frac{1}{2} \frac{\left( \frac{M_{QC} / \rho V^2 b^2}{2\pi \frac{\cos \lambda}{\alpha}} \right)}{\left( \frac{L / \rho V^2 b}{2\pi \frac{\cos \lambda}{\alpha}} \right)}$$

The convolution form of the general solution is still not a form that may be conveniently used in a rotary wing airloads calculation. It is therefore necessary to consider now specific downwash distributions. The distribution that arises in the rotary wing airloads calculation is

$$\omega(r^A \sin) = \frac{\Gamma_{\infty} / V_b}{2\pi} \frac{-(r^A \sin) \rho_1 + h \rho_2}{(r^A \sin)^2 + h^2}$$

This arises as the downwash due to a straight, infinite vortex of strength  $\Gamma_{\infty}$ , at a minimum distance  $h$  from the blade centerline,

but not necessarily in a  $(s', r')$  plane. Such a vortex could be used to approximate the interaction of the blade with a tip vortex.

The Fourier transform wrt  $r^A$  of this distribution is then

$$\frac{1}{s \sin} \bar{w}(r/s \sin) = \frac{\Gamma_{b0}/Vb}{2\pi} \frac{1}{s \sin} \frac{1}{2} e^{-h|r/s \sin|} [\mathcal{D}_1 i \operatorname{sgn}(r/s \sin) + \mathcal{D}_2]$$

Now the Fourier transforms of the loads may be inverted directly

$$\bar{g}(r/s \sin) = \frac{1}{s \sin} \bar{w}(r/s \sin) \bar{q}(r/s \sin) \longleftrightarrow$$

$$g(rA \sin) = \int_{-\infty}^{\infty} \bar{w}(r/s \sin) \bar{q}(r/s \sin) e^{i r/s \sin rA \sin} \mathcal{D} r/s \sin$$

to give the loads:

$$\left( \frac{\Gamma(rA \sin)/Vb}{2\pi} \frac{1}{\alpha} \right) =$$

$$\frac{\Gamma_{b0}/Vb}{2\pi} \left[ - \sum_{n=0}^{\infty} a_n \left( \frac{\mathcal{D}}{\mathcal{D} rA \sin} \right)^{2n} \left[ \frac{-(rA \sin + \cos) \mathcal{D}_1 + \mathcal{D}_2 (h + c_n)}{(rA \sin + \cos)^2 + (h + c_n)^2} \right] \right.$$

$$\left. + \sum_{n=0}^{\infty} a_n^r \left( \frac{\mathcal{D}}{\mathcal{D} rA \sin} \right)^{2n} \left[ \frac{-b_0 [-(rA \sin + \cos)^2 + (h + c_n^r)^2 + b_0^2] \mathcal{D}_1}{[-(rA \sin + \cos)^2 + (h + c_n^r)^2 + b_0^2]^2} \right. \right.$$

$$\left. \left. - \frac{2b_0 (h + c_n^r) (rA \sin + \cos) \mathcal{D}_2}{+ 4 (rA \sin + \cos)^2 (h + c_n^r)^2} \right] \right]$$

$$\left( \frac{L (rA \sin) / \rho V^2 b}{2\pi \frac{\cos \lambda}{\alpha}} \right) \text{ OR } \left( \frac{Q_0^A (rA \sin) / \rho V^2}{2\pi \frac{\cos \lambda}{\alpha}} \right) =$$

$$\frac{\Gamma_{b0}/V_b}{2\pi} \left[ \begin{aligned} & -a_0 \left[ \frac{-(rA \sin) \partial_1 + (h+c_0) \partial_2}{(rA \sin)^2 + (h+c_0)^2} \right] \\ & + a_0^0 \left[ \frac{-b_0 [- (rA \sin)^2 + (h+c_0^0)^2 + b_0^2] \partial_1 - 2b_0 (h+c_0^0) (rA \sin) \partial_2}{[- (rA \sin)^2 + (h+c_0^0)^2 + b_0^2]^2 + 4 (rA \sin)^2 (h+c_0^0)^2} \right] \\ & - \sum_{n=1}^{\infty} a_n \left( \frac{\partial}{\partial rA \sin} \right)^{2n} \left[ \frac{-(rA \sin + b_n) (\partial_1 \cos b_{2n} - \partial_2 \sin b_{2n}) + (h+c_n) (\partial_1 \sin b_{2n} + \partial_2 \cos b_{2n})}{(rA \sin + b_n)^2 + (h+c_n)^2} \right] \end{aligned} \right]$$

$$\left( \frac{M_{QC} (rA \sin) / \rho V^2 b^2}{2\pi \frac{\cos \lambda}{\alpha}} \right) \text{ OR } - \left( \frac{Q_1^A (rA \sin) / \rho V^2}{2\pi \frac{\cos \lambda}{\alpha}} \right) =$$

$$\frac{\Gamma_{b0}/V_b}{2\pi} \left[ - \sum_{n=1}^{\infty} a_n \left( \frac{\partial}{\partial rA \sin} \right)^{2n} \left[ \frac{-(rA \sin + b_n) (\partial_1 \cos b_{2n} - \partial_2 \sin b_{2n}) + (h+c_n) (\partial_1 \sin b_{2n} + \partial_2 \cos b_{2n})}{(rA \sin + b_n)^2 + (h+c_n)^2} \right] \right]$$



$$\left( \frac{\rho_2^A (r^A \sin) / \rho V^2}{2\pi \frac{\cos \lambda}{\alpha}} \right) =$$

$$\frac{\Gamma_{\infty}/V_b}{2\pi} \left[ -\sum_{n=2}^3 a_n \left( \frac{\partial}{\partial r^A \sin} \right)^{2n} \frac{\left[ \begin{array}{l} -(r^A \sin + b_{1n})(\partial_1 \cos b_{2n} - \partial_2 \sin b_{2n}) \\ + (h + c_n)(\partial_1 \sin b_{2n} + \partial_2 \cos b_{2n}) \end{array} \right]}{(r^A \sin + b_{1n})^2 + (h + c_n)^2} \right]$$

$$\left( \frac{\rho_3^A (r^A \sin) / \rho V^2}{2\pi \frac{\cos \lambda}{\alpha}} \right) =$$

$$\frac{\Gamma_{\infty}/V_b}{2\pi} \left[ a_3 \left( \frac{\partial}{\partial r^A \sin} \right)^6 \frac{\left[ \begin{array}{l} -(r^A \sin + b_1)(\partial_1 \cos b_2 - \partial_2 \sin b_2) \\ + (h + c_3)(\partial_1 \sin b_2 + \partial_2 \cos b_2) \end{array} \right]}{(r^A \sin + b_1)^2 + (h + c_3)^2} \right]$$

$$\left( \frac{\rho_n^A (r^A \sin) / \rho V^2}{2\pi \frac{\cos \lambda}{\alpha}} \right) \equiv 0, \quad n \geq 4$$

To examine the nature of the lifting surface solution using the approximate expressions for the universal influence functions, return now to the original formulation of the problem -- the vortex induced airloads model -- as shown in Figure 2.1. The downwash is induced by a straight, infinite vortex of strength  $\Gamma_0$ , in an  $(s', r')$  plane at a distance  $z = h$  below the blade. The vortex projection on the blade plane ( $z=0$ ) makes an angle  $(\phi + \Lambda)$  with the infinite aspect ratio wing. The free stream Mach number normal to the blade is  $M \cos \Lambda$ ; the sweep angle  $\Lambda$  will be taken as zero since it is only a relative parameter for an infinite aspect ratio wing.

The downwash induced by such a vortex at the blade centerline ( $r^A$  axis) is given by:

$$\omega(r^A \sin) = \frac{\Gamma_0 / V b}{2\pi} \frac{-(r^A \sin)}{(r^A \sin)^2 + h^2}$$

(This is a special case of the vortex with more general geometry discussed above; the vortex in a  $(s', r')$  plane gives  $d_1 = 1$ ,  $d_2 = 0$ .)

The F.T. wrt  $r^A$  is then:

$$\frac{1}{\sin} \bar{\omega}(r/\sin) = \frac{\Gamma_0 / V b}{2\pi} \frac{1}{\sin} \frac{1}{2} i \operatorname{sgn}(r/\sin) e^{-|h| r/\sin}$$

The Fourier integral is then obtained to give the loads:

$$\left( \frac{\Gamma(r^A \sin)/\sqrt{b}}{2\pi \frac{1}{\alpha}} \right) =$$

$$\frac{\Gamma_{\infty}/\sqrt{b}}{2\pi} \left[ -\sum_{n=0}^{\infty} a_n \left( \frac{\partial}{\partial r^A \sin} \right)^{2n} \left[ \frac{-(r^A \sin + \cos)}{(r^A \sin + \cos)^2 + (h + c_n)^2} \right] \right.$$

$$\left. + \sum_{n=0}^{\infty} a_n^{\nabla} \left( \frac{\partial}{\partial r^A \sin} \right)^{2n} \left[ \frac{-b_0 [-(r^A \sin + \cos)^2 + (h + c_n^{\nabla})^2 + b_0^2]}{[-(r^A \sin + \cos)^2 + (h + c_n^{\nabla})^2 + b_0^2]^2 + 4(r^A \sin + \cos)^2 (h + c_n^{\nabla})^2} \right] \right]$$

$$\left( \frac{L(r^A \sin)/\sqrt{b}}{2\pi \frac{\cos k}{\alpha}} \right) \text{ OR } \left( \frac{\rho_0^A(r^A \sin)/\sqrt{b}}{2\pi \frac{\cos k}{\alpha}} \right) =$$

$$\frac{\Gamma_{\infty}/\sqrt{b}}{2\pi} \left[ -a_0 \left[ \frac{-(r^A \sin)}{(r^A \sin)^2 + (h + c_0)^2} \right] \right.$$

$$+ a_0^{\nabla} \left[ \frac{-b_0 [-(r^A \sin)^2 + (h + c_0^{\nabla})^2 + b_0^2]}{[-(r^A \sin)^2 + (h + c_0^{\nabla})^2 + b_0^2]^2 + 4(r^A \sin)^2 (h + c_0^{\nabla})^2} \right]$$

$$\left. - \sum_{n=1}^{\infty} a_n \left( \frac{\partial}{\partial r^A \sin} \right)^{2n} \left[ \frac{-(r^A \sin + b_1) \cos b_2 + (h + c_n) \sin b_2}{(r^A \sin + b_1)^2 + (h + c_n)^2} \right] \right]$$

$$\left( \frac{M_{QC}(rA \sin) / \rho V^2 b^2}{2\pi \frac{\cos \lambda}{\alpha}} \right) \text{ OR } - \left( \frac{\rho_1^A (rA \sin) / \rho V^2}{2\pi \frac{\cos \lambda}{\alpha}} \right) =$$

$$\frac{\Gamma_{\infty} / V_b}{2\pi} \left[ - \sum_{n=1}^3 a_n \left( \frac{\rho}{\rho_1 A \sin} \right)^{2n} \left[ \frac{-(rA \sin + b_{1n}) \cos b_{2n} + (h + c_n) \sin b_{2n}}{(rA \sin + b_{1n})^2 + (h + c_n)^2} \right] \right]$$

$$\left( \frac{\rho_2^A (rA \sin) / \rho V^2}{2\pi \frac{\cos \lambda}{\alpha}} \right) =$$

$$\frac{\Gamma_{\infty} / V_b}{2\pi} \left[ - \sum_{n=2}^3 a_n \left( \frac{\rho}{\rho_2 A \sin} \right)^{2n} \left[ \frac{-(rA \sin + b_{1n}) \cos b_{2n} + (h + c_n) \sin b_{2n}}{(rA \sin + b_{1n})^2 + (h + c_n)^2} \right] \right]$$

$$\left( \frac{\rho_3^A (rA \sin) / \rho V^2}{2\pi \frac{\cos \lambda}{\alpha}} \right) =$$

$$\frac{\Gamma_{\infty} / V_b}{2\pi} \left[ a_3 \left( \frac{\rho}{\rho_3 A \sin} \right)^6 \left[ \frac{-(rA \sin + b_1) \cos b_2 + (h + c_3) \sin b_2}{(rA \sin + b_1)^2 + (h + c_3)^2} \right] \right]$$

$$\left( \frac{\rho_n^A (rA \sin) / \rho V^2}{2\pi \frac{\cos \lambda}{\alpha}} \right) \equiv 0, \quad n \geq 4$$

Again the vortex nature of the approximations for the influence functions is apparent in these loads induced by a free vortex. The functional form of the downwash is preserved in the loading with what may be called an effective strength, an effective height, and some phase shift for each term. However, as before this interpretation should not be carried too far as the forms for the influence functions are only approximate and do not correctly represent the high wave number behavior. That the lifting surface solution has a vortex nature should not be unexpected.

The lift, moment, and circulation induced by a free vortex were calculated using these formulas. With the addition of the free vortex height, the loading depends now on three parameters:

$$M \cos \Lambda, (\phi + \Lambda), \text{ and } h/b$$

The height parameter is written in dimensional form to point out that it is measured in terms of the semichord  $b$ , as is also of course the spanwise coordinate  $r^A$ . The vortex strength  $\Gamma_\infty$  occurs only as a multiplicative factor, not as a parameter, as it should for a linear solution.

The values of the parameters for which the loads were calculated are given below, with the numbers of the figures which show the results.

$M \cos \Lambda$	$(\phi + \Lambda)$	$h/b$	Figures
0.0	$90^\circ$	variable	2.14-17
0.0	$180^\circ$	variable	2.18-21
0.0	variable	1.0	2.22-25
variable	$90^\circ$	1.0	2.26-28
variable	$180^\circ$	1.0	2.29-32
0.7	variable	1.0	2.33-35

The quantities of interest are: the peak values of the lift and circulation; the spanwise location of the lift and circulation

peaks; the lift and circulation as a function of  $r^A \sin$ ; and the location of the center of pressure as a function of  $r^A \sin$ .

The spanwise coordinate used here is the variable  $r^A \sin$ , which has the limits  $r^A \sin = r^A$  for the vortex and blade perpendicular, and  $r^A \sin = t$  for the vortex and blade parallel. Thus this is the proper coordinate; however, for comparing results with varying  $(\phi + \Lambda)$ , it should be remembered that the spanwise distance is being compressed by the use of this variable.

When the induced lift and circulation are unsymmetrical in  $r^A \sin$  (that is when  $(\phi + \Lambda) \neq \pi$ ) there will be both positive and negative peak values, occurring at positive and negative  $r^A \sin$  locations, respectively. The results for these will be indicated by the notation POS and NEG respectively.

Figures 2.14 through 2.17 are for the case  $M_{\infty} \Lambda = 0.0$ ,  $(\phi + \Lambda) = 90^\circ$ ; that is, the blade and vortex are perpendicular. The results are shown for  $h/b$  in the range 0.0 to 6.0. Figure 2.14 shows the variation of the peak value of the lift with  $h/b$ . For  $(\phi + \Lambda) = 90^\circ$ , the lift and circulation (nondimensionalized) are equal, and the geometry is symmetric in  $r^A \sin$ . Figure 2.14 also shows the results of other methods for calculating the vortex induced loading. Simons (Ref. 21) used a lifting line calculation for a wing of aspect ratio 20. Kfoury (Ref. 11) used a vortex lattice lifting surface calculation for a wing of aspect ratio 20. Silver (Ref. 12) used an assumed mode lifting surface calculation for a wing of aspect ratio 6. Silver's method is considered the most accurate, and for small vortex height ( $h/b = 0.5$ ) where the effects of the small aspect ratio may be expected to be small, the agreement with the present calculation method is quite good. Kfoury's results also agree well with the present method, showing that he set up the vortex lattice correctly. As would be expected, the lifting line results (Simons) are accurate only for large  $h/b$ . A comparison of the approximate and numerical solutions for the

influence function indicates that the use of the approximate expression introduces very little error into the calculation of the loading (for this case). The only limitation on the accuracy of the results shown for the present calculation is for very small  $h/b$ ; the effect of the last term in the approximate influence function indicates that the present calculation is accurate down to  $h/b = 0.1$ , which is quite sufficient. Figure 2.15 shows the variation of the location of the peak with  $h/b$ . Again, the lifting surface results show good agreement; for large  $h/b$  the lift curves become rather flat, so the comparison here is not as important as for the peak magnitudes. Figure 2.16 shows the lift as a function of  $r^A \sin = r^A$ . Figure 2.17 shows the center of pressure location as a function of  $r^A \sin = r^A$ ; the variation from the quarter chord value is small.

Figures 2.18 through 2.21 are for the case  $M \cos \Lambda = 0.0$ ,  $\langle \phi + \Lambda \rangle = 180^\circ$ ; that is the vortex and blade are parallel. The range of  $h/b$  is from 0.0 to 6.0. Figure 2.18 shows the variation of the peak lift and circulation with  $h/b$ ; for  $\langle \phi + \Lambda \rangle \neq 90^\circ$  there are unequal negative and positive peaks. Also shown are the results of a calculation by Inversin (Ref. 22). He used a rational approximation for Kussner's function to obtain the lift induced by a vortex starting eight chords upstream. Figure 2.19 shows the variation of the position of the peak with  $h/b$ . Figures 2.20 and 2.21 show the lift and circulation as a function of  $r^A \sin = t$ . For this case,  $M \cos \Lambda = 0.0$  and  $\langle \phi + \Lambda \rangle = 180^\circ$ , the moment (and all Glauert coefficients except the zeroth) is identically zero; thus the center of pressure is at the quarter chord for all  $h/b$  and  $r^A \sin = t$ .

Figures 2.22 through 2.25 are for  $M \cos \Lambda = 0.0$ ,  $h/b = 1.0$ , and  $\langle \phi + \Lambda \rangle$  varied from  $90^\circ$  to  $180^\circ$ . Figure 2.22 shows the variation of the peak magnitudes of the lift and of circulation with  $\langle \phi + \Lambda \rangle$ . The effect of changing  $\langle \phi + \Lambda \rangle$  from the perpendicular case  $\langle \phi + \Lambda \rangle = 90^\circ$  is to slightly decrease the positive peak, and

to greatly increase the negative peak magnitude. Figures 2.23 and 2.24 show the lift and circulation as a function of  $r^A \sin$ . The delay in the circulation as  $(\phi + \Lambda)$  increases from  $90^\circ$  to  $180^\circ$  in Figure 2.24 is a reflection of the fact that the circulation is a quantity ( $\Delta\phi$ ) measured at the trailing edge, not at the blade centerline. Figure 2.25 shows the center of pressure location. Again, the shift from the quarter chord is small; the center of pressure moving off the blade reflects not a large moment, but rather the lift going to zero with a finite moment.

Figures 2.26 through 2.28 are for  $(\phi + \Lambda) = 90^\circ$ ,  $h/b = 1.0$ , and  $M \cos \Lambda$  varied from 0.0 to 0.9. To examine the properties of the solution for varying  $M \cos \Lambda$ , the effect of the Prandtl-Glauert correction factor  $1/\alpha$  must be separated from other compressibility effects; the figures show the loads with and without the  $1/\alpha$  factor. Figure 2.26 shows the variation of the peak lift with  $M \cos \Lambda$ . It is seen that the compressibility effects in the influence functions are in the opposite direction from the Prandtl-Glauert factor; that is, they decrease the magnitude of the loads. Figure 2.27 shows the lift as a function of  $r^A \sin = t$ . Figure 2.28 shows the center of pressure location; the effect of  $M \cos \Lambda$  is small, and is greatest at the higher Mach numbers.

Figures 2.29 through 2.32 are for  $(\phi + \Lambda) = 180^\circ$ ,  $h/b = 1.0$ , and  $M \cos \Lambda$  varied from 0.0 to 0.9. Figure 2.29 shows the variation of the peak magnitudes of the lift and circulation with  $M \cos \Lambda$ . Again the effect of compressibility on the influence functions produces a decrease in the load magnitude with increasing  $M \cos \Lambda$  (except for the circulation at high Mach number). Here as for  $(\phi + \Lambda) = 90^\circ$  (Figure 2.26), the compressibility effects combine to make the peak magnitudes of the actual lift and moment rather insensitive to  $M \cos \Lambda$ ; for high enough Mach number, the Prandtl-Glauert factor becomes dominant however, and increases the load peaks. Figures 2.30 and 2.31 show the lift and circulation as a function of  $r^A \sin = t$ . It is seen that while the



peak magnitudes are not too sensitive to Mach number, the functional forms are quite dependent on  $M \cos \Lambda$ . Compressibility effects produce a significant flattening of the positive peak (after the vortex has passed). This effect was not seen for  $\langle \phi + \Lambda \rangle = 90^\circ$  (Figure 2.27). This difference is due to the fact that for  $\langle \phi + \Lambda \rangle = 180^\circ$  the coordinate  $r^A \sin = t$  is in the free stream direction, for which compressibility (signal propagation) effects will be greatest; for  $\langle \phi + \Lambda \rangle = 90^\circ$ , the coordinate  $r^A \sin = r^A$  is in the lateral direction, for which Mach number effects will be minimized. Figure 2.32 shows the center of pressure location. The deviations from the quarter chord are small still, but are here in the opposite direction to that which has been previously seen (Figures 2.17, 2.25, 2.28); this is a characteristic difference between the elliptic and hyperbolic domains.

Figures 2.33 through 2.35 are for  $M \cos \Lambda = 0.7$ ,  $h/b = 1.0$ , and  $\langle \phi + \Lambda \rangle$  varied from  $90^\circ$  to  $180^\circ$ . The boundary between the elliptic and hyperbolic domains,  $M \cos \Lambda = \sin \langle \phi + \Lambda \rangle$ , is crossed at  $\langle \phi + \Lambda \rangle \cong 135.56^\circ$ . Figure 2.33 shows the variation of the lift and circulation peaks with  $\langle \phi + \Lambda \rangle$ . Most significant is the increase in the peak lift near the transitional point. Figures 2.34 and 2.35 show the variation of the lift and circulation with  $r^A \sin$ . The phase shift in the circulation is again seen as for  $M \cos \Lambda = 0.0$  (Figure 2.24). The change in form of the lift and circulation as a function of  $r^A \sin$  between the elliptic and hyperbolic domains is again seen (as for the comparison between Figure 2.27 and Figures 2.30 and 2.31).

Considering Figure 2.33 again, it is possible that the behavior near the transitional domain is in the approximate solution but not actually in the true solution; that is, an error in the approximation not evident in a rough comparison of the two solutions (by which the approximate solution appears adequate). Figure 2.36 shows the magnitude of the lift influence function,

$|\bar{g}_L|$ , for  $M \cos \Lambda = 0.7$  and several  $(\phi + \Lambda)$  values; these results are from the original numerical solution. The behavior indicated in Figure 2.33 is indeed present here also. The Fourier transform of the downwash for  $h/b = 1.0$  is proportional to  $e^{-\nu/\sin}$ , recalling that

$$\frac{1}{\sin} \bar{w}(\nu/\sin) = \frac{\Gamma_{\infty}/Vb}{2\pi} \frac{1}{\sin} \frac{1}{2} i \operatorname{sgn}(\nu/\sin) e^{-|\nu/\sin|}$$

The maximum values observed for the moment coefficient are shown in Figures 2.37 and 2.38. Figure 2.37 is for  $h/b = 1.0$ ,  $(\phi + \Lambda) = 90^\circ$  and  $180^\circ$ , and  $M \cos \Lambda$  varied from 0.0 to 0.9. Figure 2.38 is for  $M \cos \Lambda = 0.0$ ,  $(\phi + \Lambda) = 90^\circ$ , and  $h/b$  varied. The factor  $\Gamma_{\infty}/Vb$  is generally of the order 1.0. It is seen that the peak moment coefficient is small even for high Mach number and very small  $h/b$ . For most of the blade, the moment will be very much smaller.

The results of the present calculation may be compared with a strip theory application of the two-dimensional limiting case ( $(\phi + \Lambda) = \pi$ ,  $M \cos \Lambda = 0.0$ ), for which the exact solution may be obtained by classical methods (as in Section 2.3.4). The two-dimensional results may be used to obtain the loads for cases with  $(\phi + \Lambda)$  near  $\pi$  by using an equivalent reduced frequency

$$(\nu/\sin)_{\text{equivalent}} = (\nu/\sin) / (-\cos)$$

in the two-dimensional influence function. Figure 2.39 shows a comparison of the lift influence function (the lift due to a sinusoidal gust) calculated by such a strip theory, with the exact results, for several values of reduced frequency. For small  $\nu/\sin$  and small  $(\phi + \Lambda) - \pi$  strip theory is reasonably accurate, but this is a result of neither the approximate nor the exact result changing much with  $(\phi + \Lambda)$  at low reduced frequency.

## SECTION 3

### APPLICATION OF THE LIFTING SURFACE THEORY SOLUTION TO ROTARY WING AERODYNAMICS

#### 3.1 The Calculation of Rotary Wing Airloads

The calculation procedure used to determine the airloads and blade motion of a helicopter rotor blade follows one blade, which will be called the reference blade, around the azimuth. At each azimuth station, the induced velocity due to the wake is calculated at several downwash stations along the span of the reference blade. Then the airloads are calculated at several load stations along the span of the reference blade. Next, the blade motion is calculated. Finally, the changes in the strength and geometry of the wake during the motion of the reference blade to the next azimuth station are calculated. These steps are shown in Figure 3.1. The use of a variable inflow calculated from the strength and geometry of a wake of trailed and shed vorticity precludes any closed form solution. The calculations are therefore performed iteratively, following the reference blade around the azimuth, until the results converge to the steady state solution. Further description of the steps in the calculation procedure is given below.

The development below will be presented in nondimensional form. The appropriate reference quantities for rotary wing aerodynamics are the density, the rotor radius, and the rotor rotational speed ( $\rho, R, \Omega$ ). This set of reference quantities will be used throughout the remainder of this report.

The airloading and blade motion are determined by the physical properties of the blade (semichord to span ratio  $b$ , Lock number L.N., and others) and by the collective pitch  $\Theta^o$ , the tip-path plane inclination angle  $i$  (positive for rearward tilt of the thrust vector), the advance ratio  $\mu$  (rotor forward speed divided by rotor rotational speed), and the advancing tip Mach number

$M_{1.0,90}$ . The rotary wing configuration is shown in Figure 3.2 (only the reference blade is shown). The polar coordinates for the rotor disk are  $r$  and  $\psi$ , measured from the hub and from the downstream blade position, respectively. The  $(\vec{i}', \vec{j}', \vec{k}')$  system is the tip-path plane coordinate system, with the origin at the rotor hub. The free stream velocity  $\vec{u}$  is in the  $\vec{i}'$ - $\vec{k}'$  plane and the tip-path plane is parallel to the  $\vec{i}'$ - $\vec{j}'$  plane.

### 3.1.1 The Rotor Wake

Because of the interference of the rotor blade with its own wake and the wake of other blades, the wake of a rotary wing is considerably more important than that of a fixed wing. This interference is manifested as a downwash at the blade, which must be calculated in order to determine the loads on the blade and its subsequent motion. This interference also effects the geometry of the wake itself. The necessity for calculating the distorted geometry depends on the flight conditions.

The wake of a helicopter rotor in forward flight consists of shed and trailed vorticity in a distorted, skewed helix behind each blade of the rotor. This vorticity is shed and trailed in sheets. The edges of these sheets roll up to form tip vortices, the vorticity becoming highly concentrated about a line trailed from the tip of the blade. The bound circulation of a rotary wing is highly concentrated at the tip, so the rolling up is accomplished within a short distance from the tip and the tip vortex formed is very strong. The bound circulation at the root of the blade goes to zero rather smoothly so the root vortex will be weak and slowly forming, and therefore the rolling up of the vorticity at the root may be neglected. The strong tip vortices however are most important in determining both the blade loading and the wake geometry.

The very complex geometry of the wake prohibits an exact calculation of the downwash due to the wake. Therefore an approximate representation of the wake is necessary. In order to calculate

the downwash at the reference blade, the wake behind each blade of the rotor is approximated by a net of finite strength, finite length, straight line vortices (see Figure 3.3). The azimuthal spacing in the vortex net is determined by the azimuth step in the calculation procedure, and the spanwise spacing (number and position of the wake trailers) may be arbitrarily predetermined.

The wake geometry is known at the beginning of the calculation procedure at an azimuth station. The geometry is given by the positions of the node points of the tip and root trailed vortices from each blade (see Figure 3.3). Linear interpolation between the positions of corresponding tip and root nodes gives the geometry of the wake. Also known is the distribution over the rotor disk of the bound circulation of the reference blade (as calculated in previous steps). The requirement of continuity of vortex lines is sufficient to determine the strength of each vortex line element from this distribution of bound vorticity. From its position and strength, the velocity induced by each line element may be calculated. Then the downwash at a station on the reference blade is the sum of the contributions from each element of the vortex net.

### 3.1.2 The Blade Airloading

The airloading on the reference blade is determined using the calculated downwash and blade motion. It has been customary in the calculation of rotary wing airloads to use lifting line theory. Thus it is assumed that the flow over the blade is locally two-dimensional, and the loading is obtained from two-dimensional unsteady airfoil theory (or experimental or empirical section loads data). The effect of the rotor wake and the rest of the blade are represented by the downwash at the blade section.

The two-dimensional aerodynamic theory used is essentially that of Theodorsen (as in Ref. 9), with the use of the lift deficiency function replaced by an independent calculation of the

downwash induced by the wake. Compressibility effects are included only through the use of the Prandtl-Glauert correction factor based on the Mach number of the flow normal to the span of the blade. Thus

$$\left( \begin{array}{c} \text{compressible} \\ \text{load} \end{array} \right) = \frac{1}{\sqrt{1-M_N^2}} \left( \begin{array}{c} \text{incompressible} \\ \text{load} \end{array} \right)$$

where

$$M_N = M_{1.0,90} \frac{|r + \mu \sin \psi|}{r_T + \mu}$$

$$M_{1.0,90} = \text{Mach number at the advancing tip } (r = r_T \text{ and } \psi = 90^\circ)$$

The basic assumptions of lifting line theory are linearity and a high aspect ratio blade. The linear assumption is not a restriction on the calculation of rotary wing airloads if an appropriate stall model is used when the section angle of attack is too large (Miller, Ref. 17). The assumption of high aspect ratio is that

$$b \ll 1$$

where  $b$  is the blade semichord to span ratio. Implicit in this assumption is the requirement that the variation of the downwash along the span of the blade be  $O(1)$ . For large variations of the downwash in distances  $O(b)$  lifting line theory is not valid. Such a case frequently occurs in the calculation of rotary wing airloads, when a tip vortex passes within several chord lengths of a blade. For such configurations, the accurate determination of airloads requires the use of lifting surface theory. The use of lifting surface theory to calculate the vortex induced airloads on a rotary wing is the subject of this report.

### 3.1.3 The Blade Motion

The aeroelastic equations of motion for a constant chord (uniform spanwise structural properties), coincident elastic axis

and inertial axis, articulated (no lag hinge, zero flapping hinge offset) blade are

$$\ddot{\beta} + \beta = \text{L.N.} \int_{r_R}^{r_T} r \frac{L}{4\pi b} dr$$

$$I(\ddot{\theta} + \theta + \omega_0^2(\theta - \theta^0)) = \text{L.N.} \int_{r_R}^{r_T} \frac{M}{4\pi b} dr$$

(Miller and Ellis, Ref. 23).

where

$\beta$  = rigid flapping angle

$\theta$  = rigid pitching angle

L.N. = Lock number =  $\frac{\rho a c R^4}{I_b}$

$$I_b = \int_0^{r_T} r^2 m dr$$

$$I = \frac{1}{I_b} \int_0^{r_T} I_{\theta} dr$$

$I_{\theta}$  = blade section moment of inertia about the feathering axis

$\omega_0$  = nonrotating natural pitch frequency

$\theta^0$  = collective pitch

$L$  = section lift, with lift curve slope  $2\pi$

$M$  = section nose-up moment

The equations of motion are solved for the blade motion by harmonic analysis of the integrated loads.

#### 3.1.4 The Wake Geometry

The change in the geometry of the wake as the reference blade moves to the next azimuth station is calculated on the basis that a point in the wake moves with the velocity of the fluid at that point, that velocity being composed of free stream and induced

components. There are several schemes for calculating the wake geometry, varying in the detail with which the induced velocity at a wake element is determined.

- a) Rigid Wake. For the purpose of computing wake geometry only, the induced downwash is taken as a constant over  $r$  and  $\Psi$ ; thus the wake is an undistorted, skewed helix.
- b) Semirigid Wake. Each point of the wake (each node of the vortex net) is assumed to travel downward always at a velocity equal to the downwash at the point on the disk where it was trailed or shed. This involves only slightly more complexity and calculation than the rigid wake model.
- c) Modified Semi-rigid Wake. A combination of the rigid and semirigid methods, which should be more accurate, is to use the semirigid geometry up to, and the rigid geometry after, the passage of the following blade over the vortex.
- d) Nonrigid Wake. The actual downwash is calculated at selected points of the wake -- at least for the points on the tip trailed vortices -- and is used to determine the change in the wake geometry during the azimuth increment. This involves considerably more calculation than the other methods.

Which geometry should be used depends primarily on how close the wake comes to the rotor blades; the closer it gets the more accuracy is required of the geometry in order to obtain accurate loads. The nonrigid geometry calculation is quite complex, but this report is concerned only with the aerodynamic theories and their application to rotary wing aerodynamics. For further information on the wake geometry problem, reference must be made to other work, for example that of Scully (Ref. 3) or Landgrebe (Ref. 4).



### 3.1.5 The Results

The calculation procedure is performed iteratively as the reference blade moves around the rotor disk, until a converged (steady state) solution is obtained. The solution then gives: the section lift and moment over the disk; the section angle of attack over the disk; the state of flow (stalled or attached) over the disk; the blade motion (flapping and pitching); and the rotor thrust,  $C_T/\sigma$ .

### 3.2 A Straight Infinite Vortex

A straight, infinite vortex will be used to approximate the effects of a tip vortex. Therefore it is necessary to develop the velocity induced along a blade feathering axis by such a vortex.

#### 3.2.1 Orthogonal Geometry

Consider first the case with the vortex and blade perpendicular to each other, the vortex at a distance  $h$  below the blade (see Figure 3.4). The  $(x,y,z)$  system is orthogonal, with  $\vec{j}$  in the direction of the blade and  $\vec{i}$  parallel to the vortex. The vortex has strength  $\Gamma$  and a core radius  $r_c$ . The induced velocity  $\vec{v}$  is required at a point  $P$  on the  $y$  axis (its  $x$  location is arbitrary because of the infinite extent of the vortex). The following expressions give the induced velocity increment due to a vortex element  $\vec{ds}$ :

$$\vec{dv} = \begin{cases} -\frac{\Gamma \vec{r} \times \vec{ds}}{4\pi r^3} & r > r_c \\ -\frac{\Gamma \vec{r} \times \vec{ds}}{4\pi r_c^3} & r < r_c \end{cases}$$

where

$$\vec{r} = -x\vec{i} + y\vec{j} + h\vec{k}, \quad r = |\vec{r}|$$

For  $r > r_c$  this is the usual Biot-Savart law, and for  $r < r_c$  it is a generalization of the solid body rotation in the core of a two-dimensional (point) vortex.

Integrating over the length of the vortex, obtain

$$\vec{v} = \begin{cases} \frac{\Gamma}{2\pi h} \frac{-\vec{j} + (y/h)\vec{k}}{1 + (y/h)^2} \left[ 1 - \left( \frac{r_c^2 - (y^2 + h^2)}{r_c^2} \right)^{\frac{3}{2}} \right] & \text{for } y^2 + h^2 < r_c^2 \\ \frac{\Gamma}{2\pi h} \frac{-\vec{j} + (y/h)\vec{k}}{1 + (y/h)^2} & \text{for } y^2 + h^2 > r_c^2 \end{cases}$$

The downwash  $w$  is the  $\vec{k}$  component of  $\vec{v}$ . There is a peak in the magnitude of  $w$ , which must occur either outside the core or at the core boundary:

$$|w_{\max}| = \begin{cases} \frac{\Gamma}{4\pi h} \quad \text{at } |y| = h & \text{for } \sqrt{2}h > r_c \\ \frac{\Gamma}{2\pi r_c} \sqrt{1 - (h/r_c)^2} \quad \text{at } |y| = \sqrt{r_c^2 - h^2} & \text{for } \sqrt{2}h < r_c \end{cases}$$

The form of  $w(y)$  changes little if the  $(x-y)$  plane does or does not intersect the core ( $\sqrt{2}h < r_c$  or  $\sqrt{2}h > r_c$ ). Thus it is reasonable when it does intersect the core to replace the free vortex by an equivalent vortex, of strength  $\Gamma_{\text{eq}}$  and at a distance  $h_{\text{eq}}$ , such that the simpler velocity form derived by just using the

Biot-Savart law will be uniformly valid. Requiring that the positions and magnitudes of the downwash peaks be the same, find

$$\Gamma_{eq} = 2\Gamma (1 - l^2/r_c^2)$$

and

$$h_{eq} = \sqrt{r_c^2 - l^2}$$

which are used if  $\sqrt{2}h < r_c$ . It is seen that the minimum separation of the blade and vortex that need be considered is the core radius:

$$(h_{eq})_{min} = r_c.$$

### 3.2.2 General Geometry

Now consider the more general geometry, shown in Figure 3.5. It is necessary to obtain the downwash along an arbitrary line (the blade feathering axis) due to a straight infinite vortex of arbitrary orientation. Following the above results, the vortex core need not be considered in the derivation. The orientation of the vortex is given by  $\vec{i}^*$ , and its location by  $\vec{r}_0$ . The position of the point at which the induced velocity is required is given by

$$\vec{r}_1 = \vec{y} + \vec{h} = y\vec{j}^* + h\vec{k}^*$$

where  $\vec{i}^*$ ,  $\vec{j}^*$ ,  $\vec{k}^*$  are unit vectors, here not necessarily orthogonal;  $h$  is a constant and  $y$  gives the position of the point along the line with orientation  $\vec{j}^*$ .

The Biot-Savart law gives the induced velocity

$$\vec{v} = \frac{\Gamma}{2\pi} \frac{-(\vec{r}_1 \times \vec{z}^*)}{(\vec{r}_1 \cdot \vec{r}_1) - (\vec{z}^* \cdot \vec{r}_1)^2}$$

or

$$\vec{v} = \frac{\Gamma}{2\pi} \frac{y(\vec{z}^* \times \vec{j}^*) + h(\vec{z}^* \times \vec{k}^*)}{ay^2 + by + c}$$

where

$$a = 1 - (\vec{j}^* \cdot \vec{z}^*)^2$$

$$b = h [(\vec{k}^* \cdot \vec{j}^*) - (\vec{j}^* \cdot \vec{z}^*)(\vec{k}^* \cdot \vec{z}^*)]$$

$$c = h^2 [1 - (\vec{k}^* \cdot \vec{z}^*)^2]$$

It is convenient now to transform the geometry so the vector  $\vec{h} = h \vec{k}^*$  is the minimum distance between the vortex and the blade line. It may be shown that the distance between the vortex and the blade line

$$r^2 = x^2 + y^2 - 2(\vec{j}^* \cdot \vec{z}^*)xy - 2h(\vec{k}^* \cdot \vec{z}^*)x + 2h(\vec{k}^* \cdot \vec{j}^*)y + h^2$$

is a minimum at

$$x = x_{\min} = \frac{h [ -(\vec{j}^* \cdot \vec{z}^*)(\vec{k}^* \cdot \vec{j}^*) + (\vec{k}^* \cdot \vec{z}^*) ]}{1 - (\vec{j}^* \cdot \vec{z}^*)^2}$$

and

$$y = y_{\min} = \frac{h [ (\vec{j}^* \cdot \vec{z}^*)(\vec{k}^* \cdot \vec{z}^*) - (\vec{k}^* \cdot \vec{j}^*) ]}{1 - (\vec{j}^* \cdot \vec{z}^*)^2}$$

It is seen that the minimum distance occurs when the vector  $\vec{k}^*$  is perpendicular to both  $\vec{i}^*$  and  $\vec{j}^*$ . The new (minimum distance)  $h$  and  $\vec{k}^*$  are given in terms of the old geometry by

$$(h\vec{k}^*)_{\text{new}} = (h\vec{k}^*)_{\text{old}} - x_{\text{min}}\vec{i}^* + y_{\text{min}}\vec{j}^*$$

and the origins of  $y$  and  $x$  are shifted so

$$(x)_{\text{new}} = (x)_{\text{old}} - x_{\text{min}}$$

$$(y)_{\text{new}} = (y)_{\text{old}} - y_{\text{min}}$$

At this point, the vortex core correction may be applied. If the point of minimum distance  $y_{\text{min}}$  lies within a core radius  $r_c$  of the blade, that is if

$$(\tau_{\text{root}} - r_c) < y_{\text{min}} < (\tau_{\text{tip}} + r_c)$$

then the minimum distance (new  $h$ ) is used in the criterion for using the equivalent vortex to account for vortex core effects. As in the case with orthogonal geometry, the vortex core correction is then:

If  $h^2 < \frac{1}{2} r_c^2$

Then use

$$\Gamma_{eq} = 2\Gamma (1 - h^2/r_c^2)$$

$$h_{eq}^2 = r_c^2 - h^2$$

With the new geometry ( $\vec{k}^*$  now perpendicular to  $\vec{i}^*$  and  $\vec{j}^*$ ) the result for the induced velocity simplifies to

$$\vec{v} = \frac{\Gamma}{2\pi} \frac{y(\vec{i}^* \times \vec{j}^*) + h(\vec{i}^* \times \vec{k}^*)}{[1 - (\vec{j}^* \cdot \vec{i}^*)^2]y^2 + h^2}$$

(new  $h, \vec{k}^*, y$ )

With the vector  $\vec{k}_n$  normal to the blade surface, the induced downwash is then

$$\omega = \vec{v} \cdot \vec{k}_n = \frac{\Gamma}{2\pi} \frac{y(\vec{i}^* \times \vec{j}^*) \cdot \vec{k}_n + h(\vec{i}^* \times \vec{k}^*) \cdot \vec{k}_n}{[1 - (\vec{j}^* \cdot \vec{i}^*)^2]y^2 + h^2}$$

### 3.3 Rotary Wing Geometry for the Lifting Surface Solution

The lifting surface theory solution was developed for the loads on an infinite aspect ratio wing in a convected downwash

field. Procedures must be developed to apply the model problem for vortex induced loads to rotary wing geometry. The restriction of the lifting surface solution to convected downwash fields introduces a limitation in the application of the theory; the model problem is steady in a frame of reference traveling with the downwash field (that is, with the vortex), while there is no such frame of reference for the rotary wing -- the downwash is only locally a convected field. Moreover, the theory was developed for an airfoil in a uniform free stream rather than for a rotary wing. These differences between the model problem and the rotary wing configuration place limitations on the application of the lifting surface theory solution. Thus lifting surface theory should only be used where necessary, for vortex induced loads for which lifting line theory is no longer valid. Lifting line theory should still be used to obtain the other loads.

The tip vortex near a rotor blade will be approximated by a straight, infinite line vortex of appropriate strength, position, and orientation. The induced velocity along the span of the blade due to such a vortex is available in analytic form. In order to apply the lifting surface solution, it is necessary to obtain the parameters  $M \cos \Lambda$  and  $(\phi + \Lambda)$  which determine that solution. For each blade section the geometry of the blade and vortex configuration is locally like the model problem, and it is in a local sense that the lifting surface theory parameters are determined.

With a rotary wing, the relative velocity normal to the blade varies along the span. The local value of  $M \cos \Lambda$  will be used at each span station; that is,  $M \cos \Lambda$  is the Mach number of the flow normal to the span:

$$M \cos \Lambda = M_N = M_{1,0,90} \frac{|\Gamma + \mu \sin \Psi|}{\Gamma + \mu}$$

The angle  $(\phi + \Lambda)$  is determined from the orientation of

the straight, infinite vortex relative to the blade. It is the angle between the span direction,  $\vec{j}^*$ , and the direction of the convected vortex,  $\vec{i}^*$  (see Figure 3.6). The orientation of the vortex gives  $\vec{i}^*$ , and the blade direction is

$$\vec{j}^* = \frac{[\cos \psi \vec{z}^v - \sin \psi \vec{j}^v - \beta_0 \vec{k}^v]}{\sqrt{1 + \beta_0^2}}$$

where  $\beta_0$  = rotor coning angle, and the only blade motion included is the rigid flapping ( $\vec{i}^v - \vec{j}^v$  is the tip-path plane). Then recalling that the lifting surface solution is set up for  $\frac{\pi}{2} < (\phi + \Lambda) < \pi$  (the remainder of the angle range is handled by symmetry), may obtain

$$\sin(\phi + \Lambda) = \sqrt{1 - (\vec{j}^* \cdot \vec{z}^*)^2}$$

$$\cos(\phi + \Lambda) = -|\langle \vec{j}^* \cdot \vec{z}^* \rangle|$$

and

$$\langle \phi + \Lambda \rangle = \pi - \sin^{-1} \sqrt{1 - (\vec{j}^* \cdot \vec{z}^*)^2}$$

In the rotary wing configuration, the relative free stream velocity seen by the blade varies both with  $r$  and  $\psi$ . There are variations in both the geometry and the free stream ( $\langle \phi + \Lambda \rangle$  and  $M \cos \Lambda$ ), and on a scale of the order of the rotor radius the model problem is not applicable to the rotor geometry. However the lifting surface theory solution was developed to handle variation of the downwash over distances of the order of  $b$ , and on that scale the model problem will be a good representation for vortex induced airloads. The lifting surface solution will give accurate loading due to a nearby vortex, but lifting line theory should still be used to obtain the remainder of the loads (due to



blade motion and most of the vortex wake).

The application of the lifting surface theory further requires the variable  $r^A$ . The direction of this coordinate depends on the orientation of the vortex, and on whether the blade is in the reverse flow region. Examination of the geometry (Figure 3.6) gives (recalling  $r^A$  is nondimensionalized with  $b$ )

$$r^A = y/b \operatorname{sgn}(r + \mu \sin \psi) \operatorname{sgn} \left( \frac{\vec{z}^* \cdot \hat{r}}{\vec{z}^* \cdot \hat{x}} \right)$$

where  $\hat{x}$ ,  $\hat{r}$  are the unit vectors

$$\begin{aligned} \hat{r} &= \cos \psi \vec{i}^\circ - \sin \psi \vec{j}^\circ \\ \hat{x} &= \sin \psi \vec{i}^\circ + \cos \psi \vec{j}^\circ \end{aligned}$$

and recall that  $y$  is the  $r$  coordinate with the origin at the minimum distance to the vortex:

$$y = r - (r)_{\text{minimum vortex distance}}$$

Now the induced downwash may be written in a convenient form. The vector normal to the blade surface (considering only rigid flapping again) is

$$\vec{k}_n = \frac{[\vec{k}^\circ + \beta_0 \hat{r}]}{\sqrt{1 + \beta_0^2}}$$

Thus

$$\begin{aligned} (\vec{z}^* \times \vec{j}^*) \cdot \vec{k}_n &= (\vec{j}^* \times \vec{k}_n) \cdot \vec{z}^* \\ &= -\hat{x} \cdot \vec{z}^* \end{aligned}$$

and since

$$|(\vec{i}^* \times \vec{j}^*)| = \sqrt{1 - (\vec{i}^* \cdot \vec{j}^*)^2} = \sin(\phi + \Lambda)$$

the quantity  $(\hat{x} \cdot \vec{i}^*) / \sin(\phi + \Lambda)$  is identically unity if  $\vec{i}^*$  lies in the tip-path plane, and is finite for all  $\sin(\phi + \Lambda)$ . Also note that the quantity  $(\vec{i}^* \times \vec{k}^*) \cdot \vec{k}_n$  is identically zero for  $\vec{i}^*$  in the tip-path plane.

Then the downwash may be written as

$$\omega = \frac{\Gamma}{2\pi} \frac{-(y \sin(\phi + \Lambda)) \mathcal{D}_1 + h \mathcal{D}_2}{(y \sin(\phi + \Lambda))^2 + h^2}$$

where

$$\begin{aligned} \mathcal{D}_1 &= (\hat{x} \cdot \vec{i}^*) / \sin(\phi + \Lambda) \\ \mathcal{D}_2 &= (\vec{i}^* \times \vec{k}^*) \cdot \vec{k}_n \end{aligned}$$

or as

$$\omega = \frac{\Gamma}{2\pi b} \frac{-(\pm r^A \sin(\phi + \Lambda)) \mathcal{D}_1 + (h/b) \mathcal{D}_2}{(r^A \sin(\phi + \Lambda))^2 + (h/b)^2}$$

where the sign of  $r^A$  is determined as above. Here  $w$  and  $\Gamma$  are still based on  $\Omega$  and  $R$ . This is the form of the downwash distribution for which the lifting surface solution was obtained.

The lifting surface loads are nondimensionalized with  $b$  and  $V$ ; they must be converted to loads based on  $R$  and  $\Omega$  for use in rotary wing aerodynamics. Considering also the sign conventions for the loads, obtain:

$$\frac{L}{4\pi b} = \frac{|u_T| \frac{1}{2}}{\sqrt{1-M_N^2}} \left( \frac{L/\rho V^2 b}{2\pi \frac{\cos\Lambda}{\alpha}} \right)$$

$$\frac{M}{4\pi b} = \frac{u_T b \frac{1}{2}}{\sqrt{1-M_N^2}} \left( \frac{M/\rho V^2 b^2}{2\pi \frac{\cos\Lambda}{\alpha}} \right)$$

$$\Gamma = \frac{\pm 2\pi b}{\sqrt{1-M_N^2}} \left( \frac{\Gamma/Vb}{2\pi \frac{1}{\alpha}} \right)$$

$$-\Delta p = \frac{2\pi |u_T|}{\sqrt{1-M_N^2}} \left( \frac{-\Delta p/\rho V^2}{2\pi \frac{\cos\Lambda}{\alpha}} \right)$$

where

$$u_T = \Gamma + \mu \sin\psi$$

$$\pm = \text{sgn}(u_T)$$

Here the lifting surface results are used with the downwash  $w$  based on  $\Omega R$ ; that is, since  $w$  is the downwash due to a vortex, the vortex strength  $\Gamma_\infty$  is based on the velocity  $\Omega R$ . A length is also involved in the nondimensionalization of the vortex strength, and of the distances that appear in the lifting surface formulas; that length is the blade semichord  $b$ .

### 3.4 The Application of the Lifting Surface Solution

The lifting surface solution has now been put into a form suitable for rotary wing aerodynamics. In order to use the lifting surface theory correctly, some care must be taken with the division of the wake, downwash, and loads between it and lifting line theory.

Lifting surface theory includes the vortex induced trailed wake behind the reference blade. (It is only a trailed wake in the steady coordinate system of the model problem; in the blade coordinate system there will be shed vorticity as well.) This trailed vorticity is assumed in the model problem to extend straight back from the blade to infinity. Since it is included in the lifting surface solution, this induced wake vorticity is not used in calculating the downwash due to the nearby part of the wake of the reference blade -- nearby meaning for  $\Delta\psi$  of the order of 60 to 90 degrees. Thus the bound circulation due to the lifting surface theory is not used in the calculation of the strength of the nearby part of the wake of the reference blade.

The wake is now divided into two parts: the tip vortices from all of the blades; and the rest of the wake, except for the lifting surface part of the nearby wake of the reference blade.

The downwash induced by the tip vortices will be handled using lifting surface theory. At the downwash calculation stations of the reference blade, the downwash due to the tip vortices is calculated as the sum of the induced velocities of all the straight line segments that make up the tip vortices (the tip vortices are the outer edge trailed segments of the vortex net). Simultaneously the points of nearest approach of the tip vortices to the reference blade are calculated. These points are a local minimum in the distances from each short line segment to the blade. Next, the tip vortex at each of these points of nearest approach to the reference blade is approximated by a straight infinite

vortex, with strength, position, and orientation the same as the tip vortex at the point of nearest approach. It is to this field of straight infinite vortices, approximating the tip vortices of the rotor, that the lifting surface theory solution may be applied.

The downwash due to this field of straight infinite vortices is calculated at the downwash stations of the reference blade, and the difference is obtained between this calculation and the earlier calculation of the actual downwash due to the tip vortices. This difference is added to the downwash of the rest of the wake (see below) so that the combination of lifting surface and lifting line theories models the correct angle of attack of the blade section.

The downwash induced by the rest of the wake (as defined above) will be handled using lifting line theory. At the downwash calculation stations of the reference blade, the downwash due to the rest of the wake is calculated as the sum of the induced velocities of all the elements of the vortex net (except the outer trailed segments, and the lifting surface nearby wake). To this calculated downwash is added: first, the difference between the actual and approximate downwash induced by the tip vortices (as above); second, the inflow due to the tip-path plane inclination ( $-\mu \tan \lambda$ ); and third, the inflow due to the no-feathering plane inclination ( $-\mu \beta_{1c}$ ). The result is the total downwash (except for the induced velocity of the field of straight infinite vortices representing the tip vortices) at the downwash calculation station.

The downwash is obtained at the loading calculation stations, which will in general not be the same as the downwash calculation stations, by Lagrange (polynomial) interpolation between the downwash stations.

The angle of attack is calculated at each loading station of the reference blade, using as the downwash the sum of the

induced velocity of the field of straight infinite vortices, the interpolated downwash of the rest of the wake, and the downwash due to the nearby part of the lifting surface wake (which is not used in the loading calculation since it is already included in the lifting surface theory solution). If the angle of attack is too large, an appropriate stall model is used to obtain the loads (see Johnson, Ref. 24).

If the blade section is not stalled, the aerodynamic loads are calculated at the loading calculation station using the combination of lifting surface and lifting line theories. The lifting surface theory solution is used to obtain the vortex induced loads of nearby tip vortices; that is, it is used with any vortices in the field of straight infinite vortices, which come closer to the reference blade than a distance of the order of five chord lengths or so. Lifting line theory is then used to obtain the remaining loads: the loads due to the blade motion, the rest of the wake, and the far vortices in the field of straight infinite vortices.

The procedure developed here to calculate rotary wing airloads emphasizes the importance of careful handling of the wake and downwash, which have always been the outstanding features of rotary wing aerodynamics. In order to obtain accurate airloads two features of the calculation procedure have been stressed: first, it is necessary to obtain as accurate information as practical about the downwash distribution; second, accurate loads calculations require the use of lifting surface theory to obtain vortex induced loading.

## SECTION 4

### EVALUATION OF THE USE OF THE LIFTING SURFACE SOLUTION IN THE CALCULATION OF ROTARY WING AIRLOADS

#### 4.1 The Rotor Configuration

In order to evaluate the use of the lifting surface theory solution to replace lifting line theory in the calculation of vortex induced airloads on a rotary wing, the rotor geometry was simplified to a single-bladed rotor at high advance ratio encountering a free vortex from a fixed upstream airfoil (see Figure 4.1). The rotor is at zero tip-path plane incidence, so the free vortex lies in a plane parallel to the tip-path plane; it lies in the free stream direction, at a lateral distance  $y_G$  from the rotor hub, and at a distance  $h$  below the tip-path plane; that is, the tip of the vortex generator in the tip-path plane reference system is located at

$$\vec{r}_G = x_G \vec{i}' + y_G \vec{j}' + h \vec{k}'$$

(Figure 4.1).

The parameters describing the blade, the vortex, and the calculation procedure are as follows (recall that all lengths are nondimensionalized using  $R$ , the rotor radius).

a) Blade semichord:  $b = 0.025$

The blade aspect ratio was large, so lifting line theory was valid for loads due to blade motion, and the effect of the tip on the loading was minimized.

b) Blade Lock number:  $L.N. = 0.0$

Then the only blade motion was first harmonic rigid flapping (no elastic flapping, rigid or elastic twisting, or other harmonics of rigid flapping) and the tip-path plane remained undistorted (also the coning angle was then zero).

- c) Advance ratio:  $\mu = 0.5$

The advance ratio was high so that the loading induced by the blade's own tip vortex was minimized.

- d) Tip-path plane inclination angle:  $i = 0$

Collective pitch:  $\theta^0 = 0$

Built-in twist:  $\theta_{tw}^0 = 0$

Thus the only airloading was that induced by the free vortex.

- e) Tip Mach number (at  $\psi = 90^\circ$ ):

$$M_{1.0,90} = 0.0 \text{ or } 0.5 \text{ or } 0.9$$

- f) Vortex generator location:

$$r_G = -4.0 \vec{i}' + y_G \vec{j}' + h \vec{k}'$$

$$y_G = -0.5 \text{ or } 0.0$$

$$h = (h/b) b$$

- g) Free vortex core radius:  $r_c = 0.001$

This was smaller than the minimum  $h$  used, so the core size did not enter the lifting surface theory evaluation (recall that for usual applications, the minimum effective  $h$  that will be encountered is the vortex core radius).

- h) Free vortex strength:  $\Gamma = 0.011$

This corresponds to a generator angle of attack  $\alpha_G = 8$  degrees, or a tip vortex of a rotor with  $C_T/r \cong 0.05$ .

- i) Azimuth increment in the calculation procedure:

$$\Delta\psi = 10 \text{ degrees}$$



- j) Number of trailers in vortex net = 4  
Number of downwash calculation points = 3  
Extent of blade wake:  $\Delta\phi = 220$  degrees  
Extent of nearby portion of lifting surface wake = 90 degrees  
(The nearby wake is that part which is considered as handled by lifting surface theory; it was varied from 60 to 180 degrees with negligible effect for this single-bladed rotor at high advance ratio.)

Because of the high advance ratio and the zero collective pitch, the loading induced by the blade's own tip vortex was negligible and occurred only in the fourth quadrant of the disk. Thus it was sufficiently accurate to use semirigid geometry for the rotor wake. (In semirigid geometry, each element of the wake is assumed to move downward at a speed equal to the downwash at the point on the rotor disk from which it was trailed.) Moreover, the blade tip vortex could be treated with the rest of the wake, using lifting line theory, and only the free vortex was treated using lifting surface theory.

Rigid geometry was used for the free vortex; that is, it was a straight line in the free stream direction parallel to the tip-path plane. Since with zero Lock number the blade tip-path plane was not distorted by rigid or elastic blade motion, the position of the blade relative to the free vortex was simply and exactly determined. Thus in these theoretical calculations the back influence of the blade loading on the geometry of the vortex was not included.

#### 4.2 Comparison of Lifting Line and Lifting Surface Loading Calculations

The blade loading on the rotor described above was calculated using both lifting line theory and the lifting surface theory solution. A comparison of the two predictions of the airloading allows an evaluation of the application of the lifting surface solution to the rotary wing airloads calculation.

The loading was calculated for several values of the vortex height,  $h/b$ , and of the advancing tip Mach number,  $M_{1.0,90}$ , with the vortex lateral position

$$y_G = - 0.5$$

(the vortex on the advancing side of the disk). Figures 4.2, 4.3, and 4.4 show the lift variation with azimuth at a blade radial station  $r = 0.6$ , for  $h/b = 2.0, 1.0,$  and  $0.5$  respectively, and  $M_{1.0,90} = 0.0$ . The scale changes of the ordinate should be noted. The difference between the lifting line and lifting surface loads is significant. Figure 4.2 also shows the lift calculated using lifting line theory with a wake net of ten trailers and with nine downwash calculation points. Little improvement is gained over the  $3 \times 4$  lifting line calculation.

Figure 4.5 shows the ratio of peak-to-peak lifting surface lift to peak-to-peak lifting line lift for  $h/b$  from 0.2 to 10.0. Figure 4.3 shows what is meant by peak-to-peak lift. The data in Figure 4.5 is for  $r = 0.6$  and includes results at an advancing tip Mach number of  $M_{1.0,90} = 0.0, 0.5,$  and  $0.9$ . The Mach number had little effect on the peak-to-peak ratios (unless the peak just happens to occur when the blade section is in the transition region of the lifting surface theory, the Mach number effects are small except for the Prandtl-Glauert factor, which is the same for both lifting line and lifting surface theories). It can be seen in Figure 4.5 that as  $h/b$  decreases from about 10.0 the lifting line results become increasingly inaccurate as compared with the lifting surface results.

The loading was calculated for several values of the vortex height,  $h/b$ , and of the advancing tip Mach number,  $M_{1.0,90}$ , with the vortex lateral position

$$y_G = 0.0$$

(the vortex below the centerline of the disk). Figure 4.6 shows

the lift variation with azimuth at  $r = 0.75$  and with  $h/b = 1.0$  and  $M_{1.0,90} = 0.0$ . This case is typical of the results for all values of  $h/b$  (0.2 to 10.0) and  $M_{1.0,90}$  (0.0 to 0.9) considered. Figure 4.7 shows the ratio of peak-to-peak lifts for  $h/b$  from 0.2 to 10.0. Typically in the lifting line results the peaks are 5 to 15 percent low and the entire lift distribution delayed by  $\Delta\psi = 3$  to 5 degrees as compared with the lifting surface results. However, from the downwash distribution it is known that the peaks must occur at a distance of about  $2(h/b)b$  apart, while the azimuth increment of  $\Delta\psi = 10$  degrees corresponds at  $r = 0.75$  to a distance of about  $5b$ . Thus it is probable that the peak values have not actually been defined by a calculation of the loading only at stations every ten degrees around the azimuth. Such a problem may be expected whenever a configuration is encountered with the vortex and the rotor blade nearly parallel, as may occur with tandem rotors. Generally, difficulties defining the peak loads may be expected whenever the component normal to the vortex direction of the distance between calculation points on the rotor disk (for a given blade section as  $\psi$  is incremented, or for a given azimuth as  $r$  is incremented) is less than the vortex-blade separation or so. Little would be added to the comparison of lifting surface and lifting line theories by the use of a smaller azimuth step, and the size necessary to define the peaks adequately ( $\Delta\psi < 2$  degrees) would not be at all typical of rotary wing airloads calculations. The proper handling of vortices nearly parallel to the blade is one of many procedural problems that remain to be solved in rotary wing aerodynamics.

#### 4.3 Evaluation of the Use of the Lifting Surface

##### Theory Solution

The above results show that there is a significant difference between the loadings calculated using the lifting line and the lifting surface theories. Simply on the basis that lifting

line theory is an approximation to lifting surface theory, resulting from the assumption of large (effective) aspect ratio, the lifting surface results must be accepted as more accurate (within the limitations of both theories). Therefore the lifting surface solution should replace lifting line theory in the calculation of vortex induced airloads. The above results also suggest the criterion that lifting surface theory be used for any vortex at a distance from the blade less than  $10b$  or so.

The lifting surface solution was developed to be as direct to apply as the lifting line theory, and it is that. The amount of calculation involved in a rotary wing airloads calculation is increased by the use of lifting surface theory rather than lifting line theory, but still the airloads calculation remains small compared with the downwash calculation.

What is involved in the use of lifting surface theory rather than lifting line theory may be made more explicit. An exact, although discrete element, representation of the vortex wake with the accuracy of the airloads limited by the rate of variation of the downwash along the span (that is, a vortex net wake plus lifting line theory airloads) is being traded for a distributed sheet, although only locally valid, representation of the wake with the accuracy of the loads limited by the accuracy of the approximation to the numerical solution of the model problem (that is, lifting surface theory airloads, including a trailed vortex wake).

The limitation on the lifting surface theory arises from the application of the model problem to rotary wing geometry. The model problem involves fixed geometry, with a constant free stream. The solution for this model is applied to a rotary wing, where there are variations of the free stream velocity with both  $\psi$  and  $r$ , and also changing relative geometry (between the blade and a vortex), by using local (in  $\psi$  and  $r$ ) values of the parameters  $M \cos \Lambda$  and  $(\phi + \Lambda)$  (the velocity and geometry). However, these changes

in the velocity and geometry occur over distances of  $O(R)$  while the vortex induced airloads vary over distances of  $O(b)$ . The lifting surface solution can handle variations in the downwash over distances of  $O(b)$  (while lifting line theory cannot) and on this scale the local geometry is well approximated by the model problem. The application of the lifting surface theory solution developed here requires that the geometry of the blade, vortex, and wake be locally like the model problem; and the use of lifting surface theory is necessary only for very close vortices. These two conditions are entirely consistent if the semichord to span ratio  $b$  is small. This is, in fact, the same assumption as in lifting line theory, arising here because of the geometry of the wake rather than the aerodynamics of the blade.

Thus with the application of the lifting surface solution to the rotary wing, the assumption about the rate of variation of the relative free stream velocity and of the geometry of the wake relative to the blade remains, but the restriction on the variation of the downwash along the span of the blade has been removed. The lifting surface theory solution of this particular model problem should not be used for the airloads due to the blade motion or the far wake, but should be used for the vortex induced airloads. Lifting line theory and the lifting surface solution respectively are appropriate for these two classes of airloads.

## SECTION 5

### CONCLUSIONS AND RECOMMENDATIONS

The following has been accomplished in this report:

- a) A lifting surface theory solution and a useable approximation to it have been obtained for a model problem appropriate for the calculation of vortex induced airloads.
- b) Procedures have been developed for the application of this solution of the model problem to the calculation of rotary wing airloads.
- c) The application of the lifting surface solution has been evaluated using a simplified rotary wing configuration.

The comparison between the use of lifting line theory and the use of the lifting surface solution in the calculation of vortex induced airloads on a rotary wing showed a significant difference between the results of the two methods. Thus it is recommended that the lifting surface solution developed here be applied to the calculation of airloads for the actual helicopter rotor; furthermore, this application should itself be subjected to extensive correlation with the results of experiments and other theories, in order to further the understanding of the rotary wing airloads problem and the application of the present method to that problem.

From the necessity of the use of lifting surface theory to obtain accurate vortex induced airloads, it follows that accurate wake geometry information is also required. Therefore, it is recommended that the present lifting surface solution be used with a nonrigid wake geometry calculation. Moreover, small scale vortex geometry distortions induced by the blade loading, which is itself due partly to the vortex, are possibly important in the airloads

calculations. If this proves to be so, procedures should be developed to handle such distortions.

Even with the completion of the application of lifting surface theory and nonrigid wake geometry to the calculation of rotary wing airloads (the development of these applications is currently in progress), what will undoubtedly be found is that entirely satisfactory airloads prediction is still not possible. There remain yet several important features of the problem that have not been correctly handled. The following appear most important at present:

- a) the viscous aspects of the mutual influence of the vortex and the rotor blade (the theory presented here involves only a potential flow solution);
- b) the general problem of vortex roll-up and formation, of vortex core development and size; specifically, information is needed about the growth and structure of the tip vortex of a rotary wing; also included in the problem is secondary vortex interaction (that is, the combination of a vortex with the trailed wake vorticity it induces on a blade and the influence of the combination on a following blade);
- c) and the loading at the blade tip, including the effects of an arbitrary sweep angle and angle of attack; this problem involves both vortex formation and induced airloads, and it is probable the even planar lifting surface theory will not be sufficient to obtain accurate loading.

These and other features will have to be handled before confident predictions of airloads can be made. The rotary wing airloads problem will only be solved by a continued effort to isolate, model, and resolve all of the aerodynamic, dynamic, and geometric factors that form the problem.

#### REFERENCES

1. Miller, R.H., "Unsteady Air Loads on Helicopter Rotor Blades," Journal of the Royal Aeronautical Society, 68, 640, April 1964.
2. Miller, R.H., "Rotor Blade Harmonic Air Loading," AIAA Journal, 2, 7, July 1964.
3. Scully, M.P., "A Method of Computing Helicopter Vortex Wake Distortion," Massachusetts Institute of Technology, Aeroelastic and Structures Research Laboratory, TR 138-1, June 1967.
4. Landgrebe, A.J., "An Analytic Method for Predicting Rotor Wake Geometry," Journal of the American Helicopter Society, 14, 4, October 1969.
5. Watkins, C.E., Runyan, H.C., and Woolston, D.S., "On the Kernel Function of the Integral Equation Relating the Lift and Downwash Distributions of Oscillating Finite Wings in Subsonic Flow," NACA TR 1234, 1955.
6. Watkins, C.E., Woolston, D.S., and Cunningham, H.J., "A Systematic Kernel Function Procedure for Determining Aerodynamic Forces on Oscillating or Steady Finite Wings at Subsonic Speeds," NASA TR R-48, 1959.
7. Ashley, H., Widnall, S.E., and Landahl, M.T. "New Directions in Lifting Surface Theory," AIAA Journal, 3, 1, January 1965.
8. Landahl, M.T., and Stark, V.J.E., "Numerical Lifting Surface Theory -- Problems and Progress," AIAA Journal, 6, 11, November 1968.
9. Bisplinghoff, R.L., Ashley, H., and Halfman, R.L., Aeroelasticity, Addison-Wesley, Reading, Massachusetts, 1955.
10. von Karman, Th., and Sears, W.R., "Airfoil Theory for Non-Uniform Motion," Journal of the Aeronautical Sciences, 5, 10, August 1938.



11. Kfoury, D.J., "A Routine Method for the Calculation of Aerodynamic Loads on a Wing in the Vicinity of Infinite Vortices," Massachusetts Institute of Technology, Aeroelastic and Structures Research Laboratory, TR 133-2, May 1966.
12. Silver, L.W., "An Investigation of the Interaction of a Trailing Vortex with a Lifting Surface," Massachusetts Institute of Technology, S.M. Thesis, June 1967.
13. Cummings, D.E., and Kerwin, J.E., "Propeller Wake Deformation Due to Instability of a Trailing Vortex Sheet," Proceedings of Third CAL/AVLABS Symposium, 18-20 June 1969.
14. Watson, G.N., A Treatise on the Theory of Bessel Functions, Second Edition, Cambridge University Press, London, 1944.
15. Garrick, I.E., "Nonsteady Wing Characteristics," Aerodynamic Components of Aircraft at High Speeds, A.F. Donovan and H.R. Lawrence, editors, Princeton University Press, Princeton, New Jersey, 1957.
16. Ashley, H., and Landahl, M.T., Aerodynamics of Wings and Bodies, Addison-Wesley, Reading, Massachusetts, 1965.
17. Miller, R.H., Massachusetts Institute of Technology, private communication, 1969.
18. Hsu, P.-T., "Some Recent Developments in the Flutter Analysis of Low Aspect Ratio Wings," Proceedings of the National Specialists Meeting on Dynamics and Aeroelasticity, 1958.
19. Hildebrand, F.B., Introduction to Numerical Analysis, McGraw-Hill Book Co. Inc., New York, 1956.
20. Abramowitz, M. and Stegun, I.A., editors, Handbook of Mathematical Functions, National Bureau of Standards, U.S.G.P.O., Washington, 1964.

21. Simons, I.A., "Blade-Vortex Interaction on Helicopter Rotors in Forward Flight," Symposium on the Noise and Loading Actions on Helicopter V/STOL Aircraft and Ground Effect Machines, August 30-September 3, 1965, Institute of Sound and Vibration Research, University of Southampton, Hampshire, England.
22. Inversin, A.R., "The Effect of Wing Leading and Trailing Edge Shed Vorticity on Tailplane Loading," Massachusetts Institute of Technology, S.M. Thesis, June 1968.
23. Miller, R.H., and Ellis, C.W., "Helicopter Blade Vibration and Flutter," Journal of the American Helicopter Society, 1, 3, July 1956.
24. Johnson, Wayne, "The Effect of Dynamic Stall on the Response and Airloading of Helicopter Rotor Blades," Journal of the American Helicopter Society, 14, 2, April 1969.

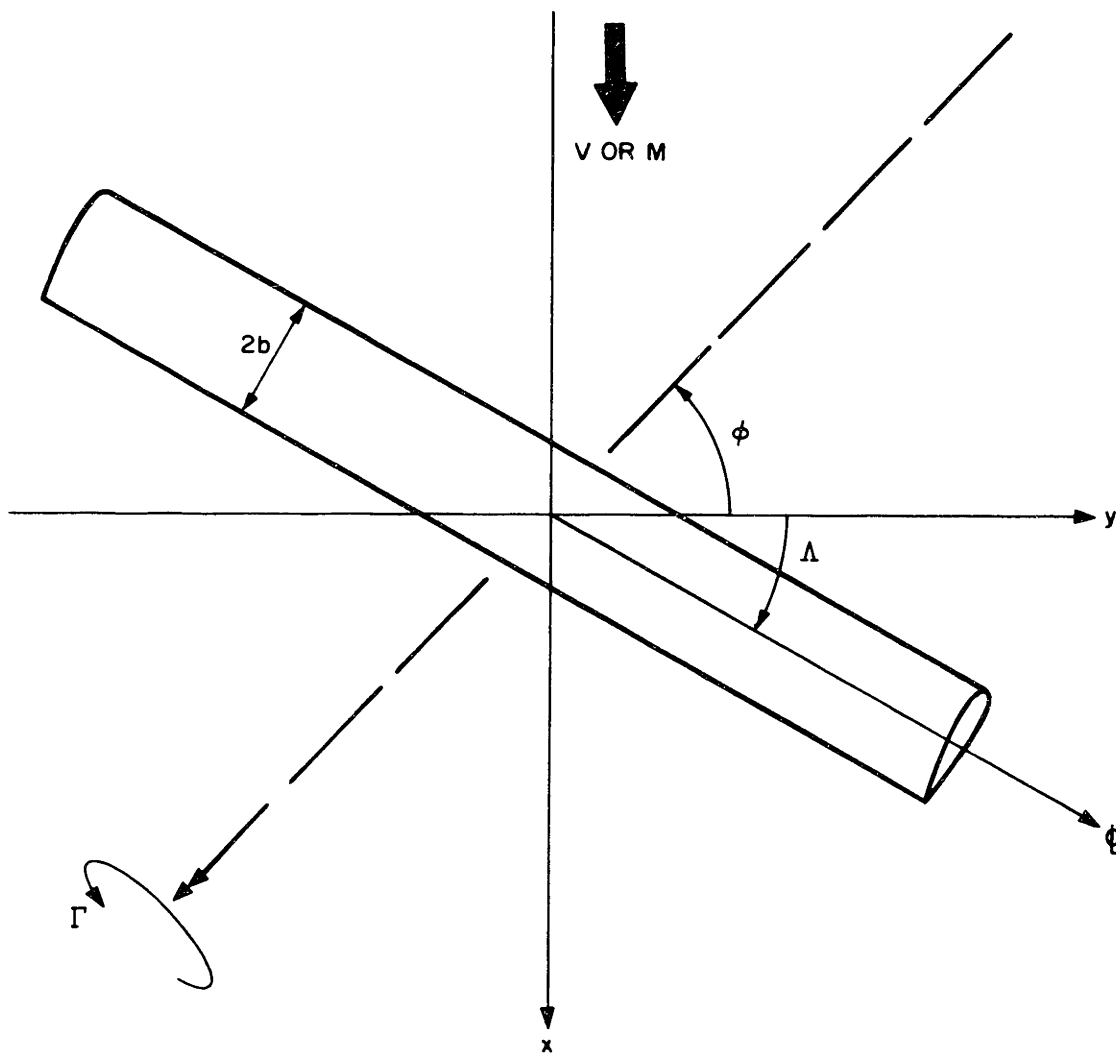


FIGURE 2-1 MODEL PROBLEM FOR VORTEX INDUCED AIRLOADS

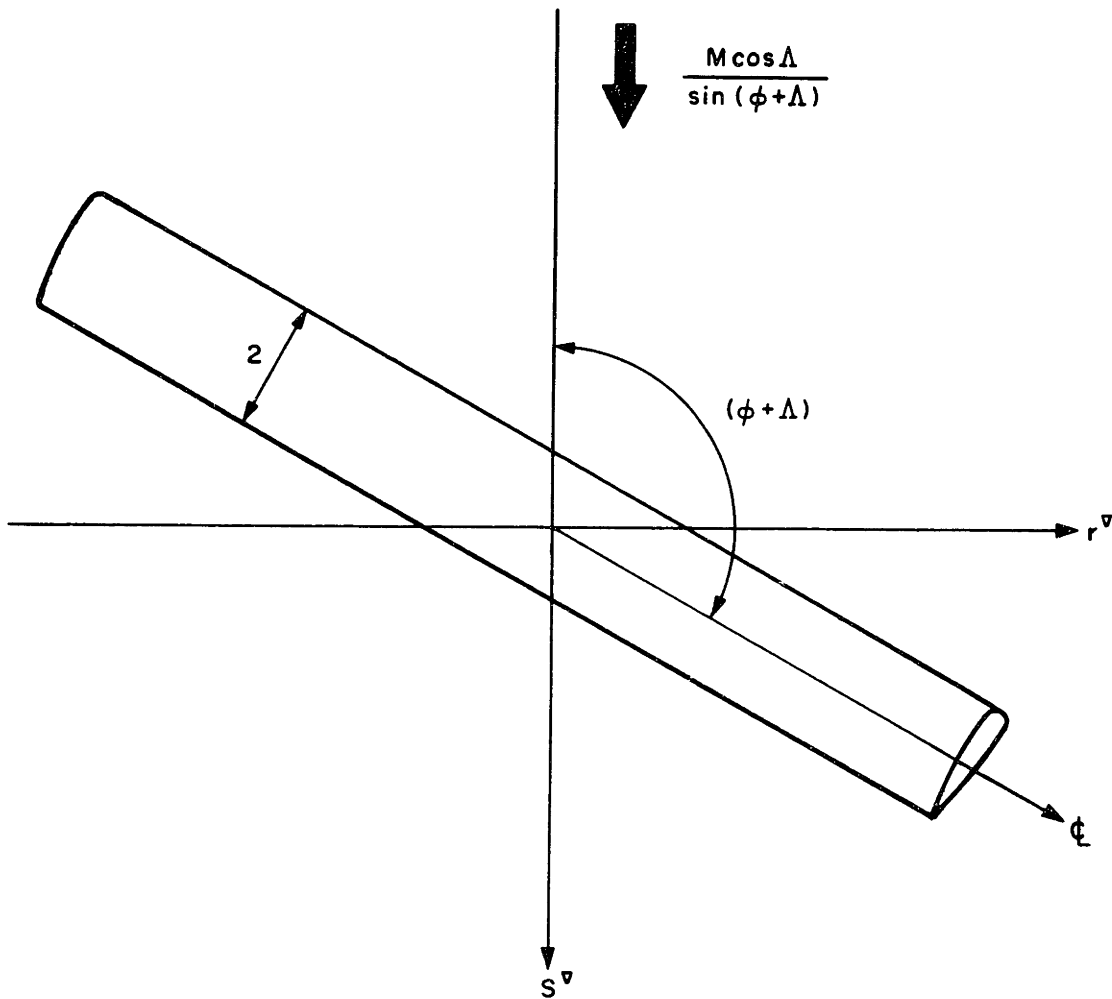


FIGURE 2-2 GEOMETRY OF THE MODEL PROBLEM IN THE STEADY COORDINATE SYSTEM

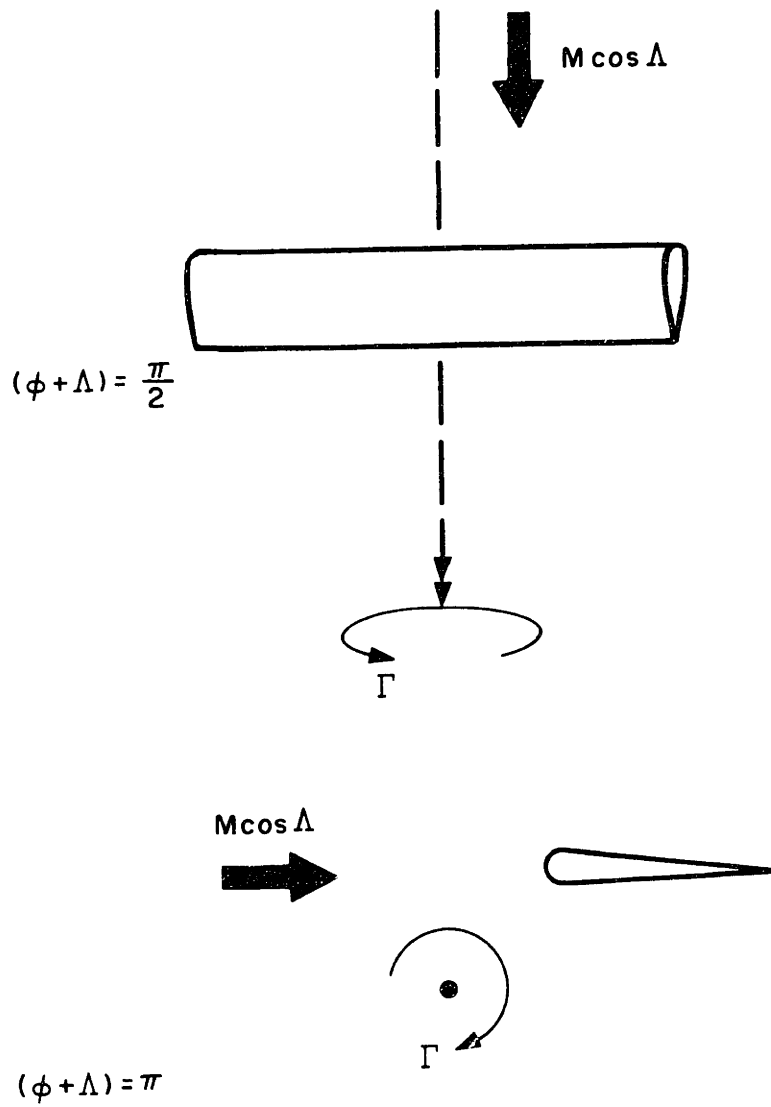


FIGURE 2-3 LIMITS OF THE MODEL PROBLEM :  
 THREE-DIMENSIONAL, STEADY CASE  
 AND TWO-DIMENSIONAL,  
 UNSTEADY CASE

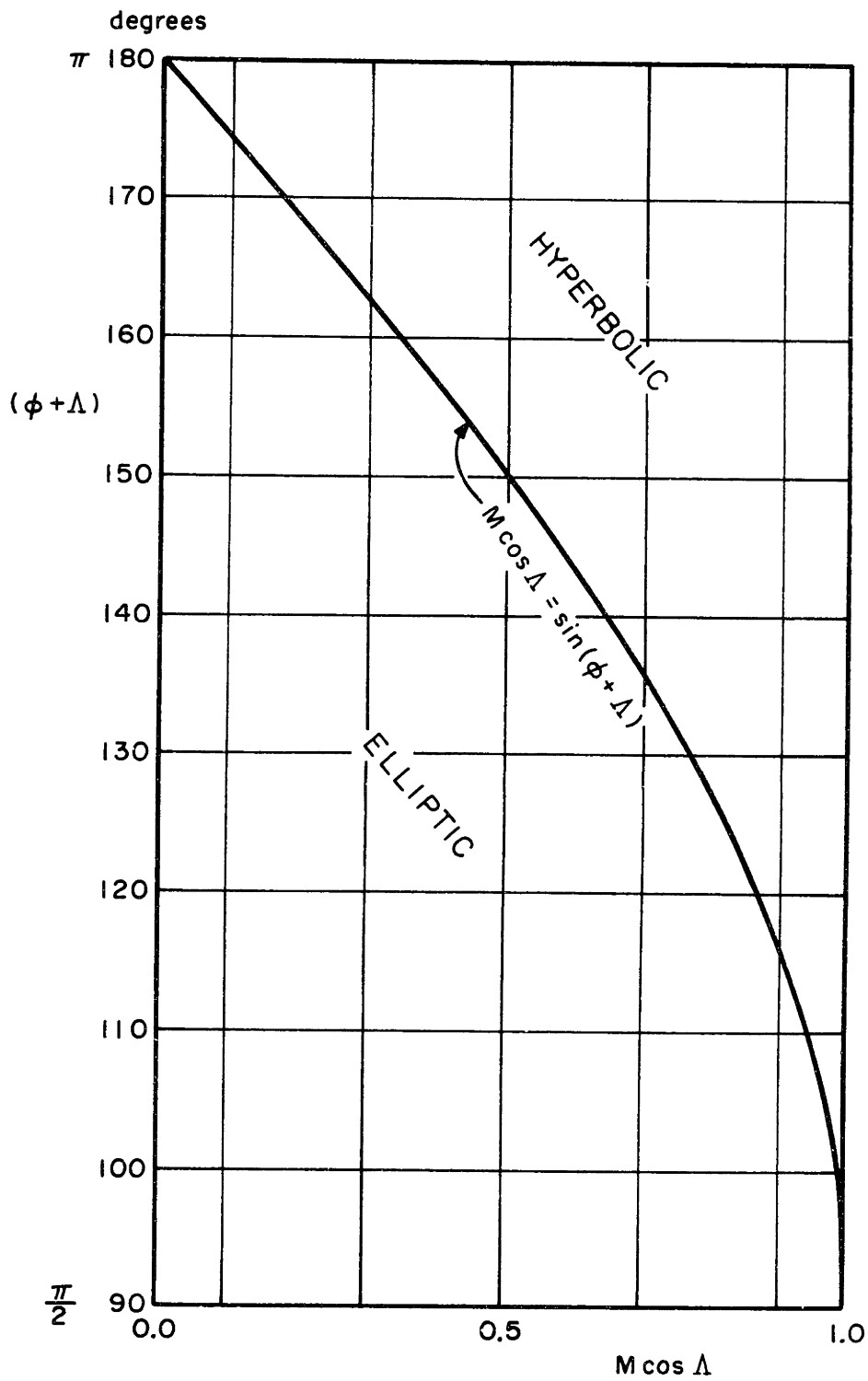


FIGURE 2-4 THE HYPERBOLIC AND ELLIPTIC DOMAINS

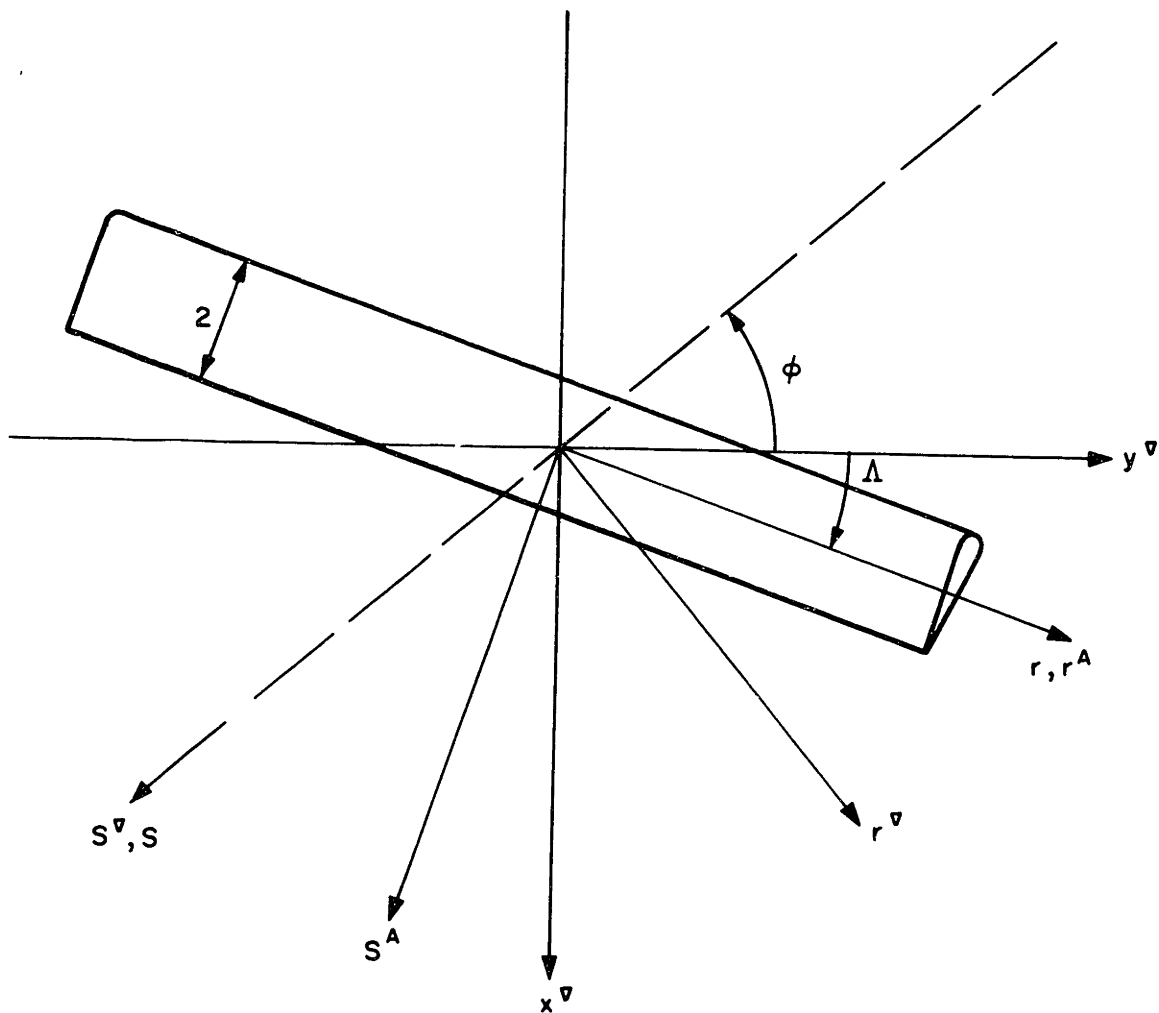


FIGURE 2-5 THE COORDINATE SYSTEMS USED  
(THE THIRD AXIS IS  $z$ ,  
DIRECTED UPWARDS)

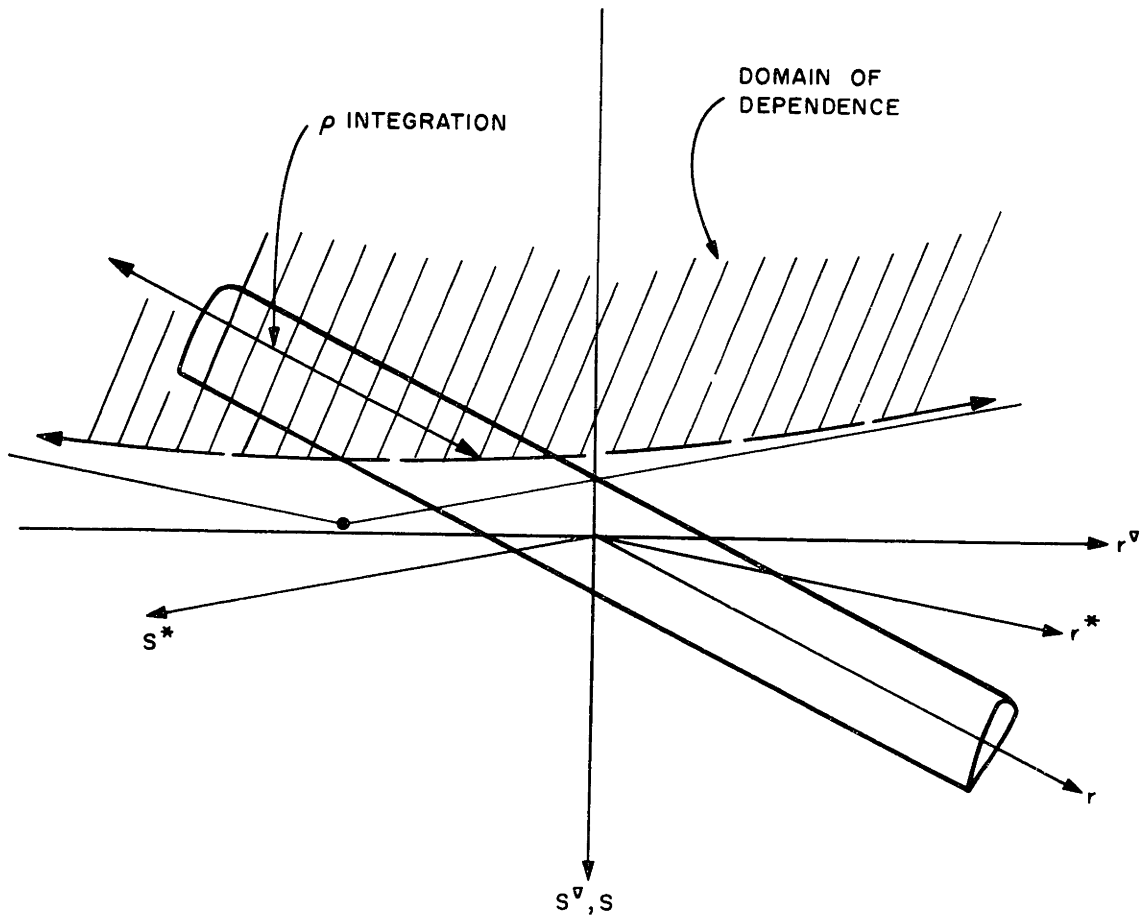


FIGURE 2-6 REGION OF INTEGRATION IN THE HYPERBOLIC KERNEL



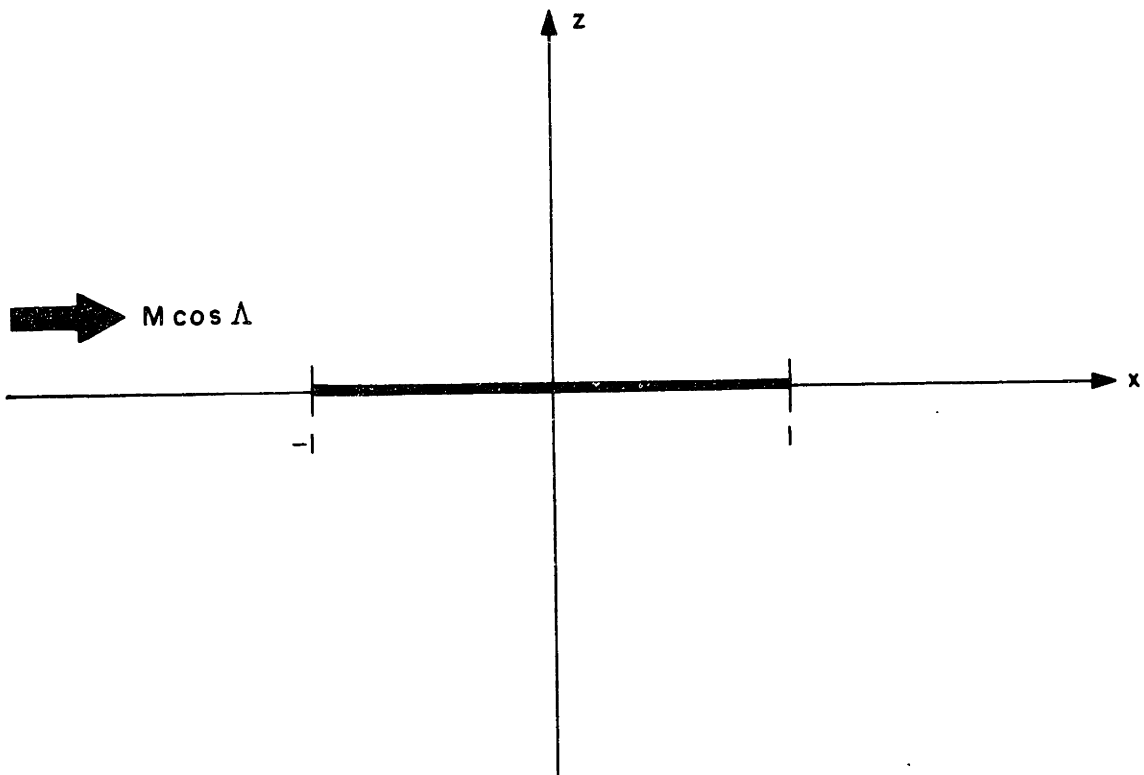


FIGURE 2-7 TWO-DIMENSION, THIN AIRFOIL GEOMETRY

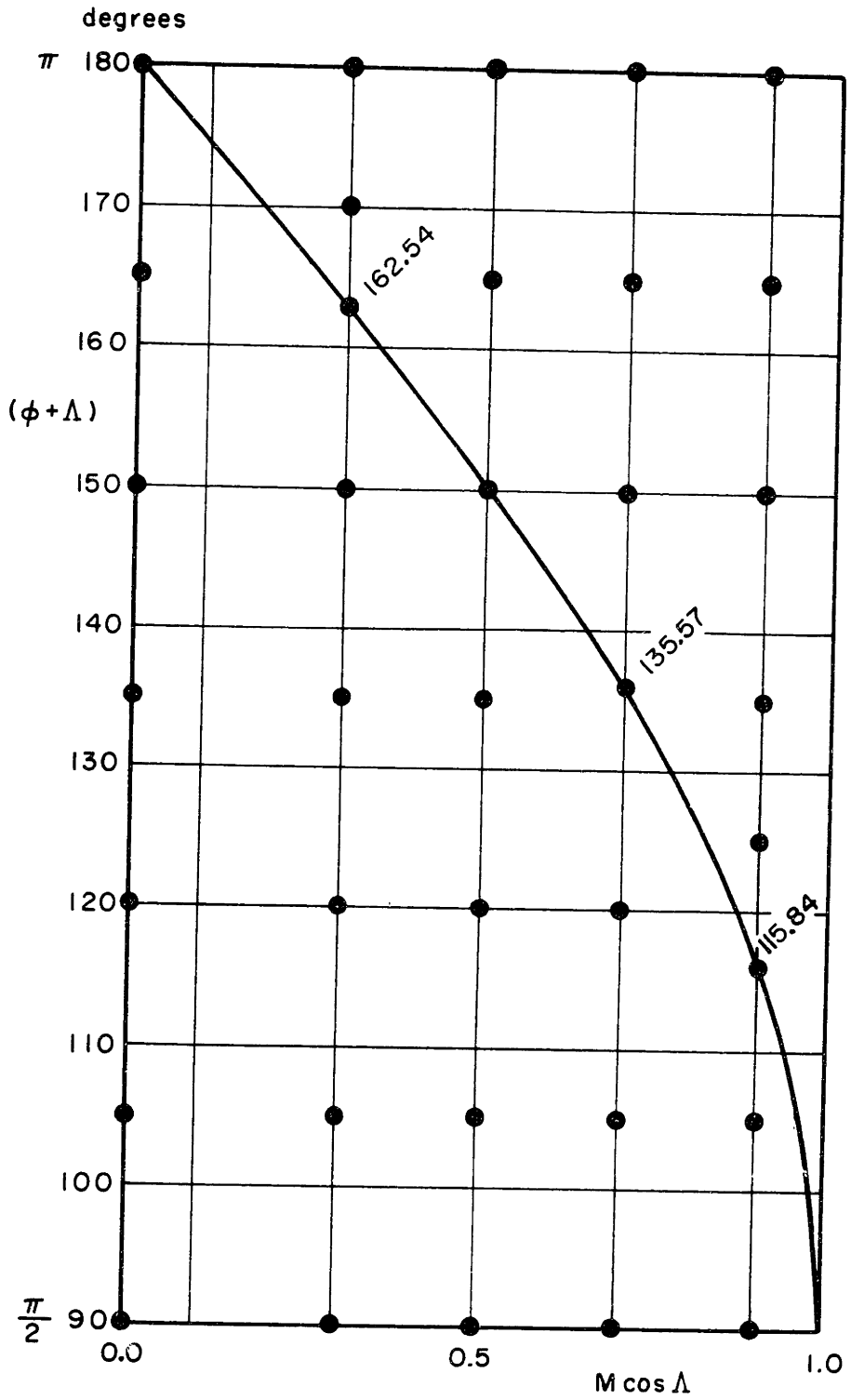


FIGURE 2-8 NUMERICAL CALCULATION CASES (INDICATED BY ●)

FIGURE 2-9

$$M \cos \Delta = 0.0$$
$$(\phi + \Delta) = 180^\circ$$

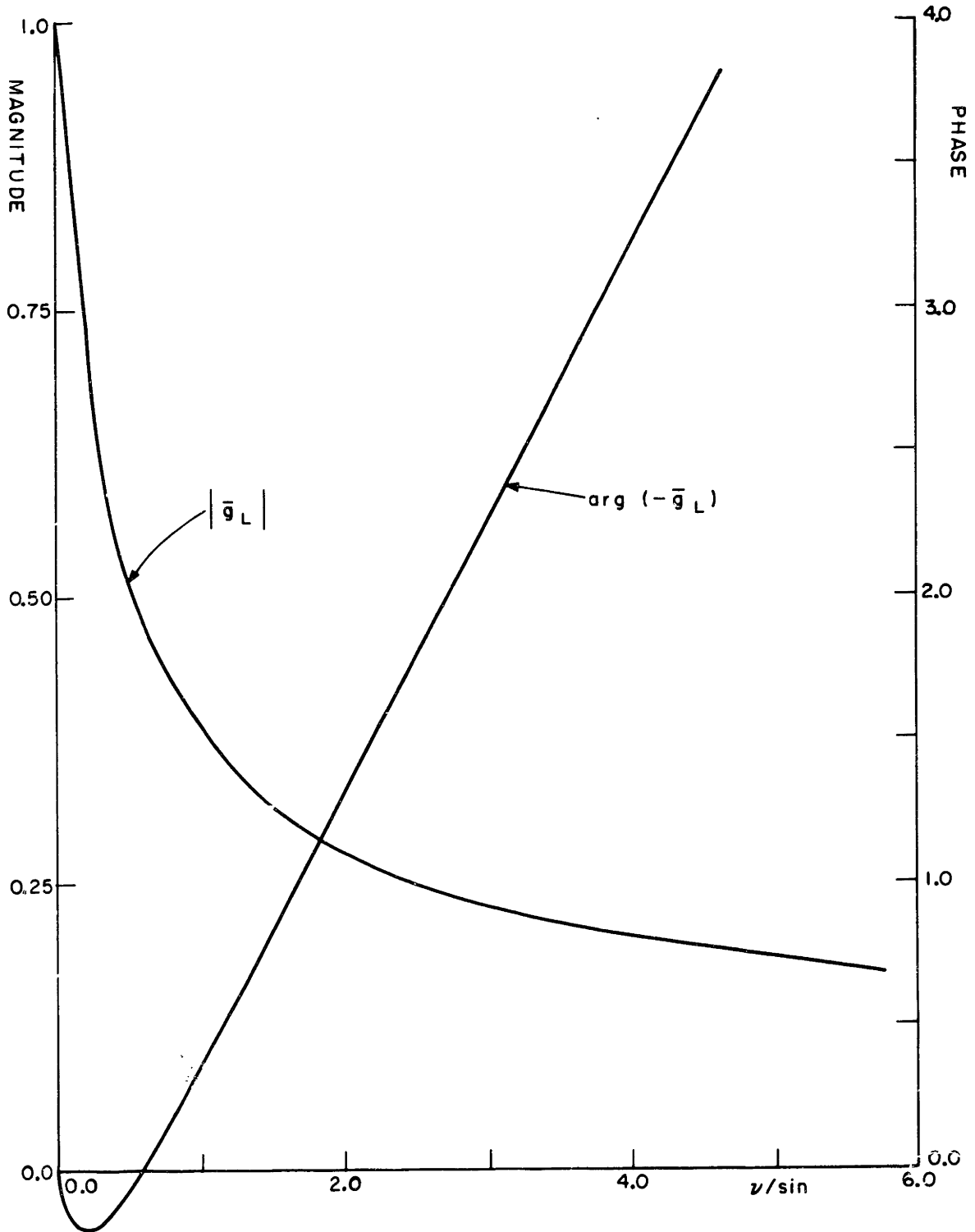


FIGURE 2-10

$M \cos \Delta = 0.0$   
 $(\phi + \Delta) = 180^\circ$

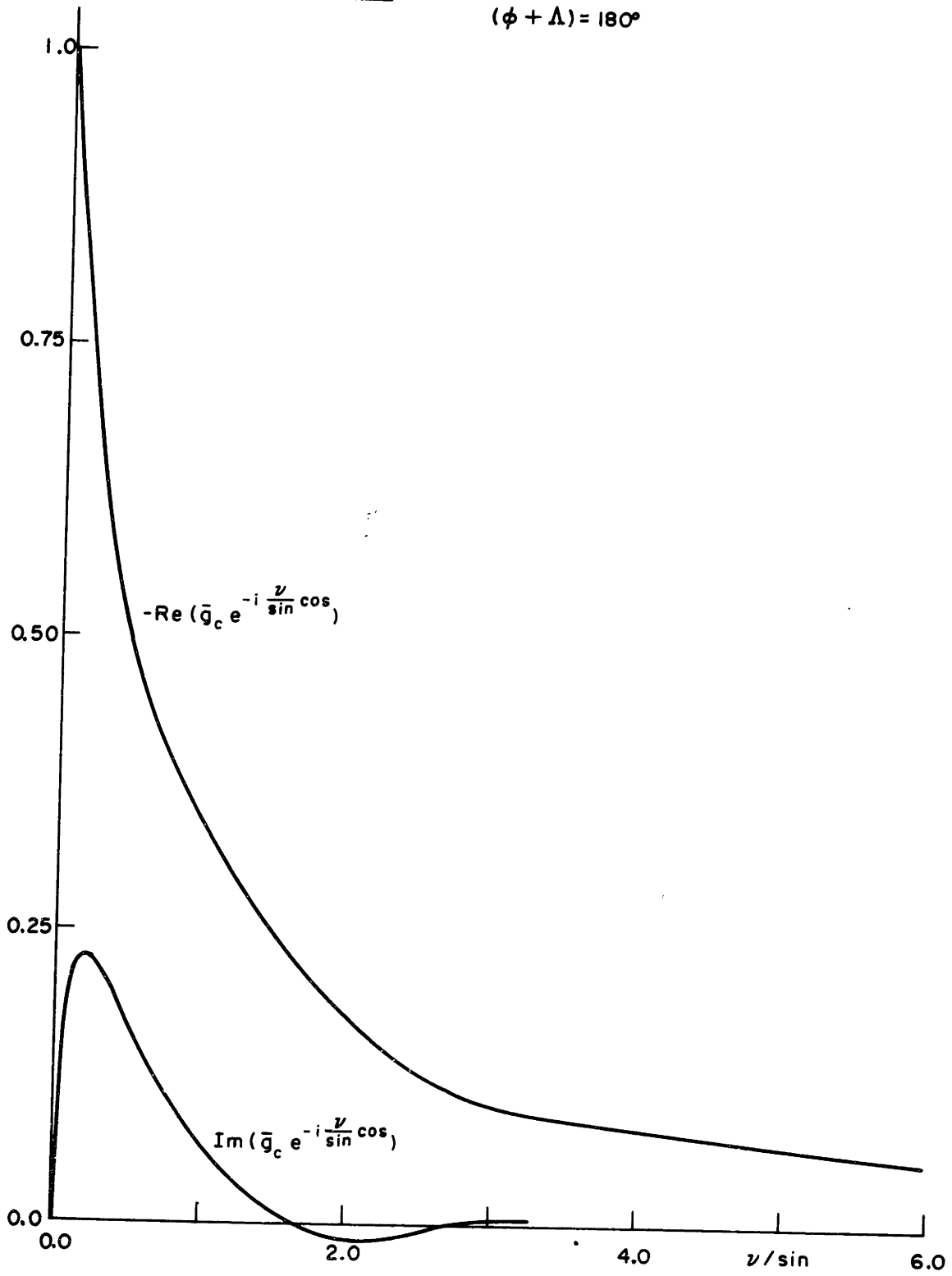


FIGURE 2-11

$M \cos \Lambda = 0.0$   
 $(\phi + \Lambda) = 135^\circ$

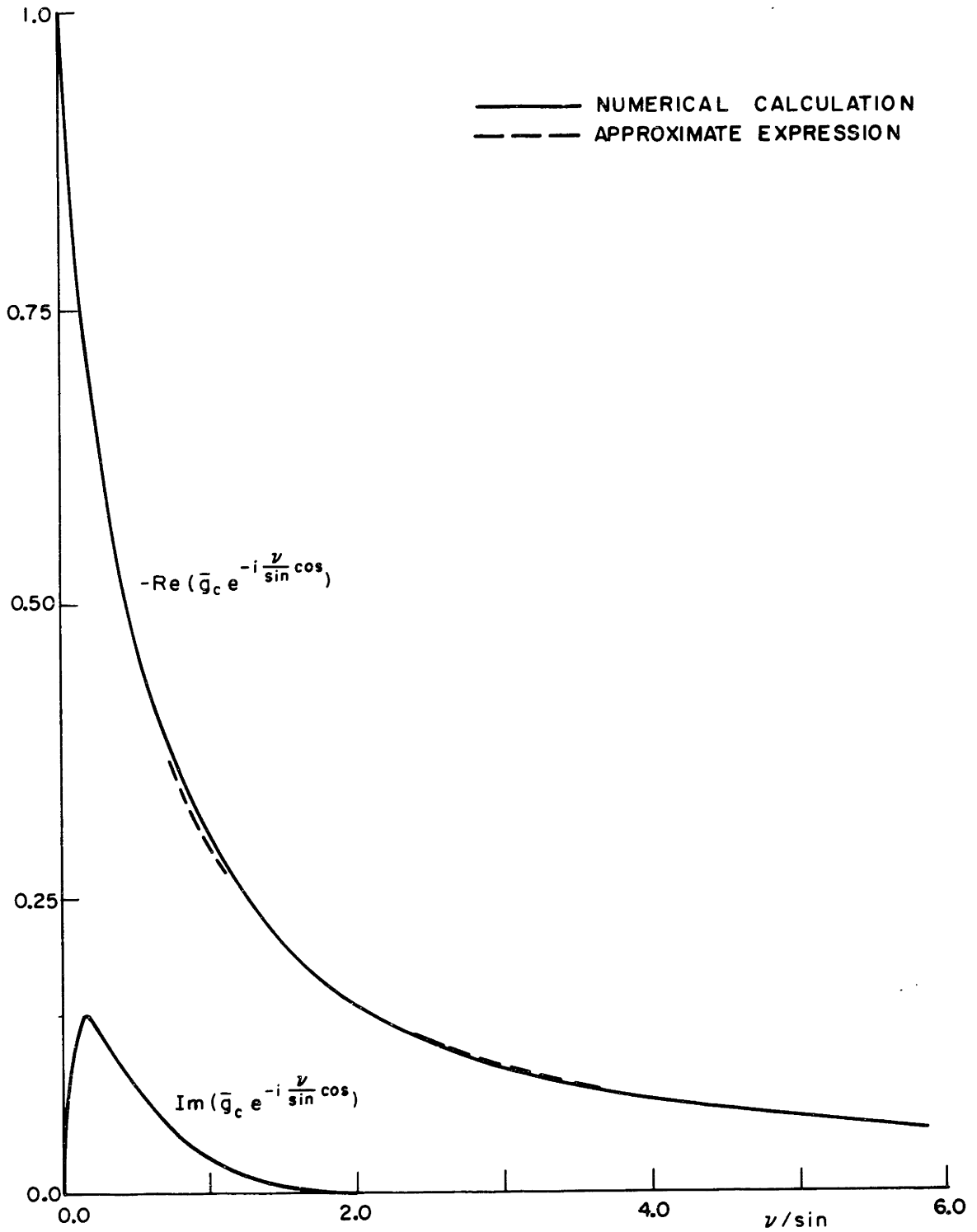


FIGURE 2-12

$M \cos \Lambda = 0.0$   
 $(\phi + \Lambda) = 135^\circ$

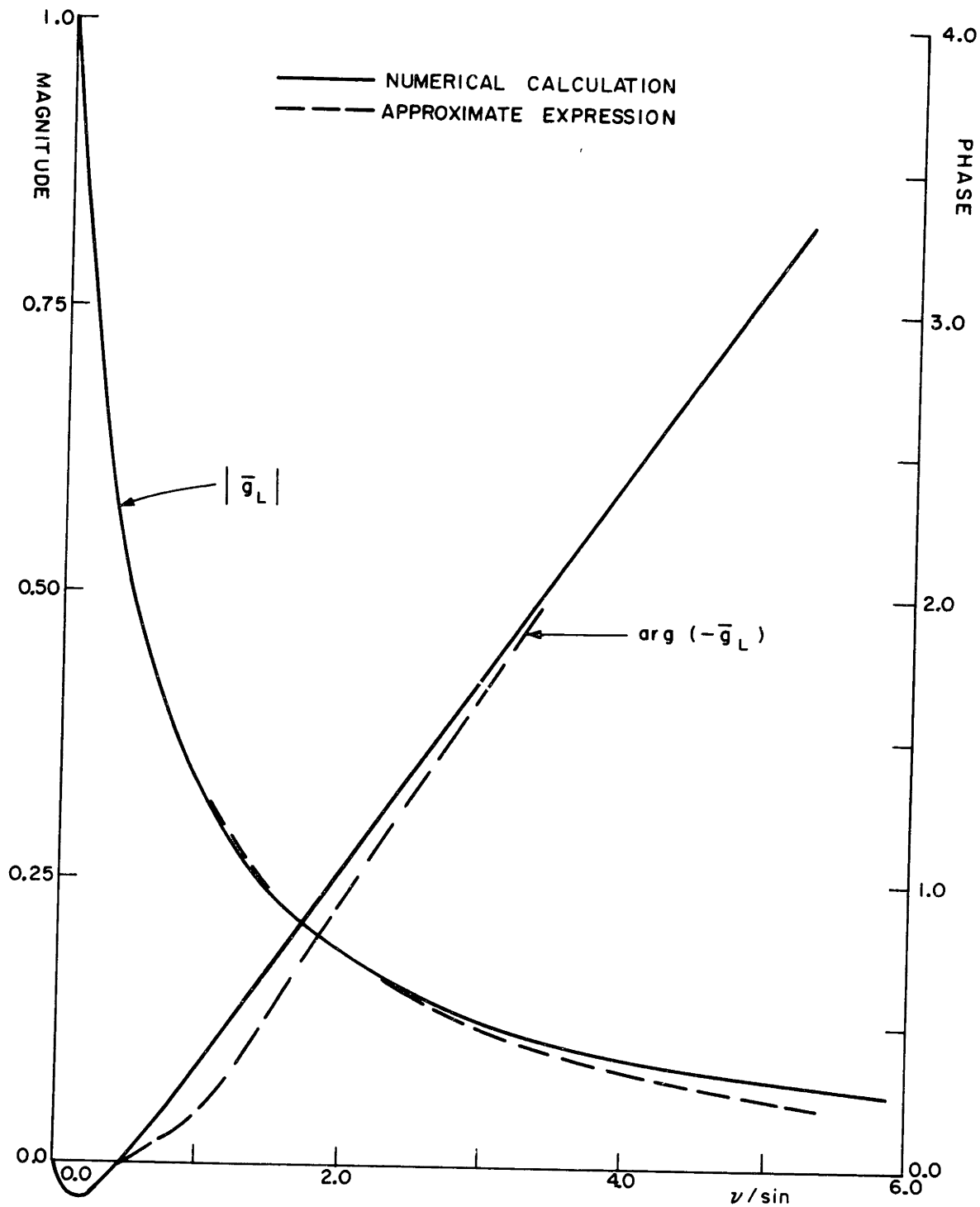


FIGURE 2-13

$M \cos \Delta = 0.0$   
 $(\phi + \Delta) = 135^\circ$

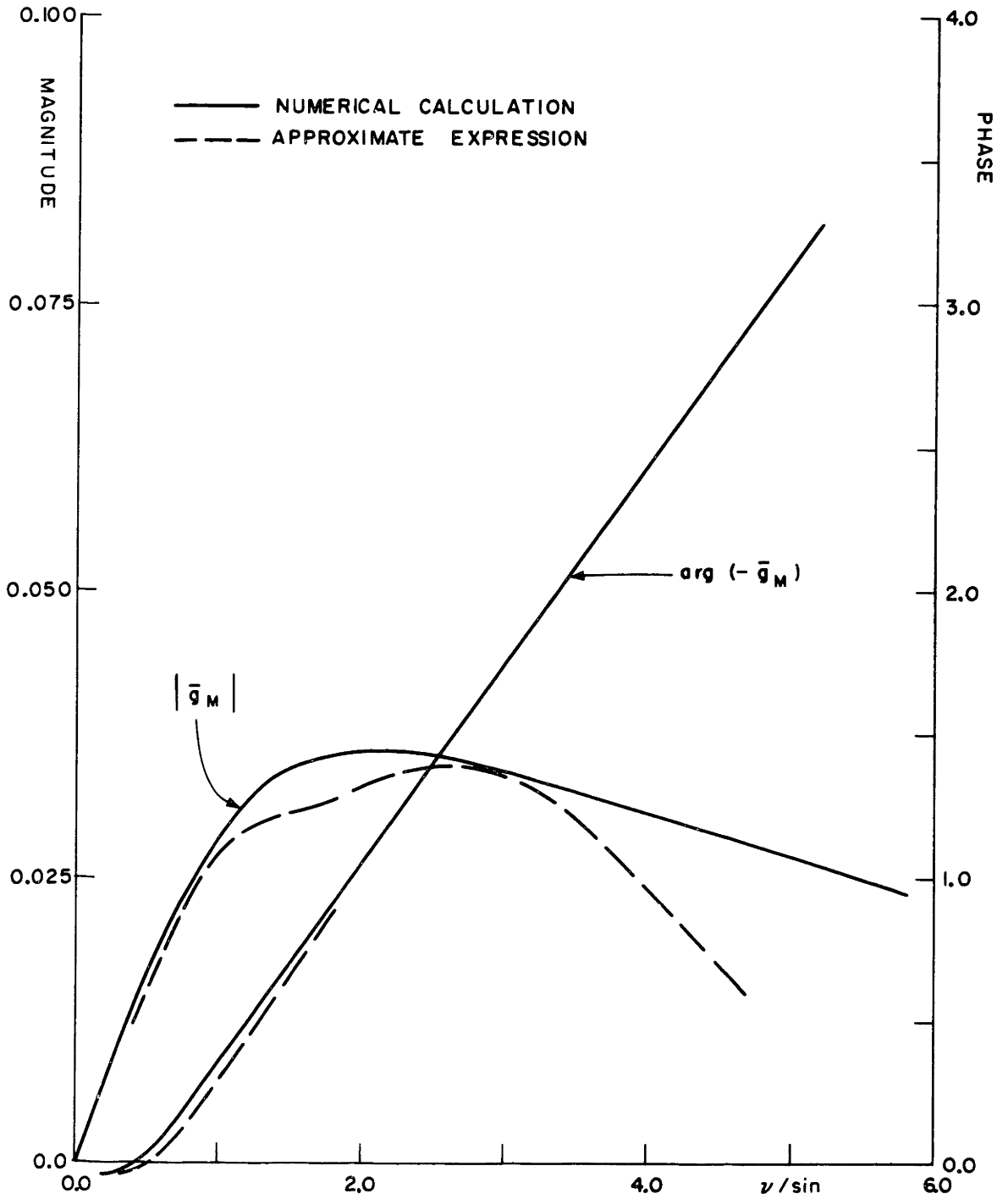


FIGURE 2-14

$M \cos \Delta = 0.0$   
 $(\phi + \Delta) = 90^\circ$

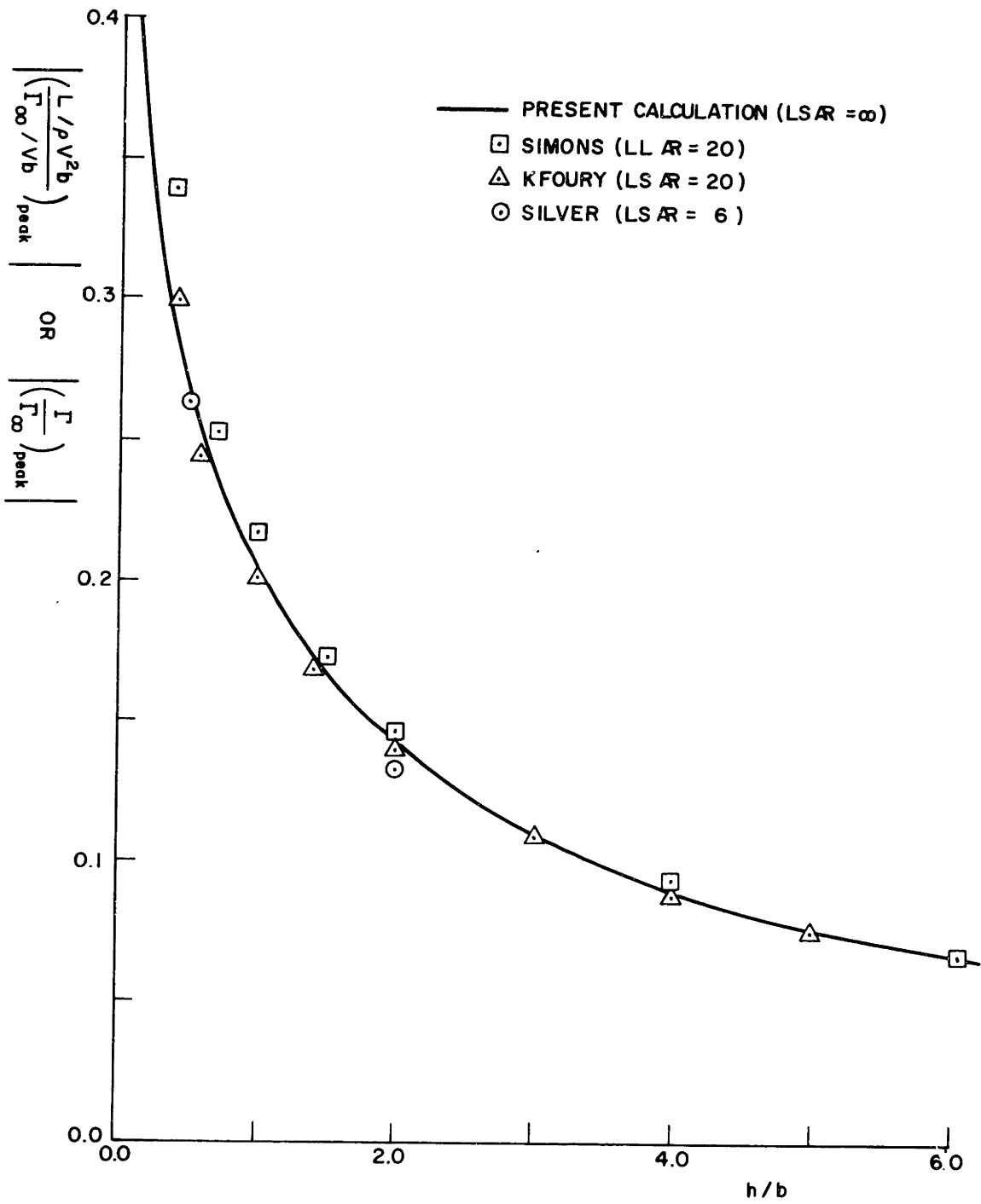




FIGURE 2-15

$M \cos \Delta = 0.0$   
 $(\phi + \Delta) = 90^\circ$

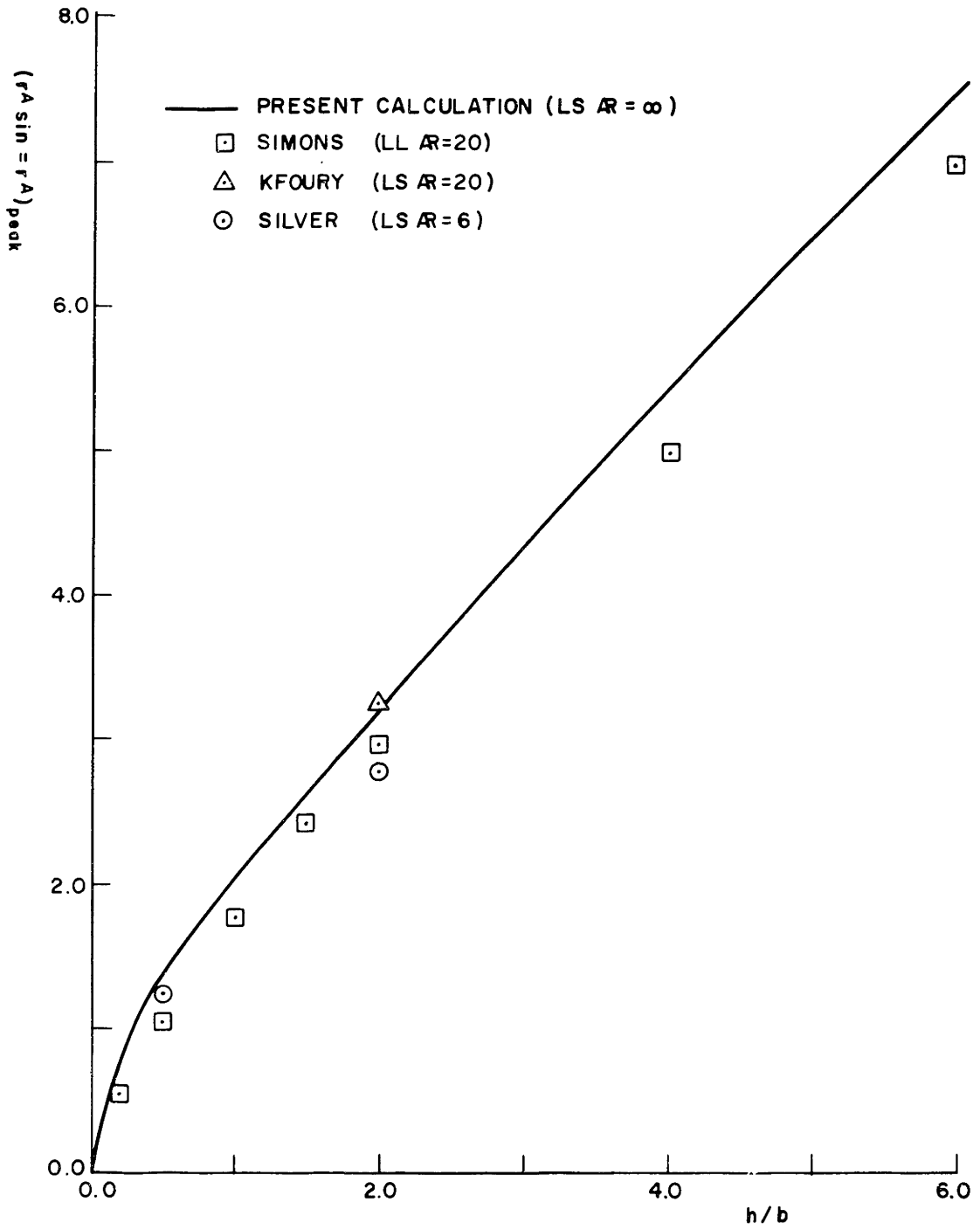
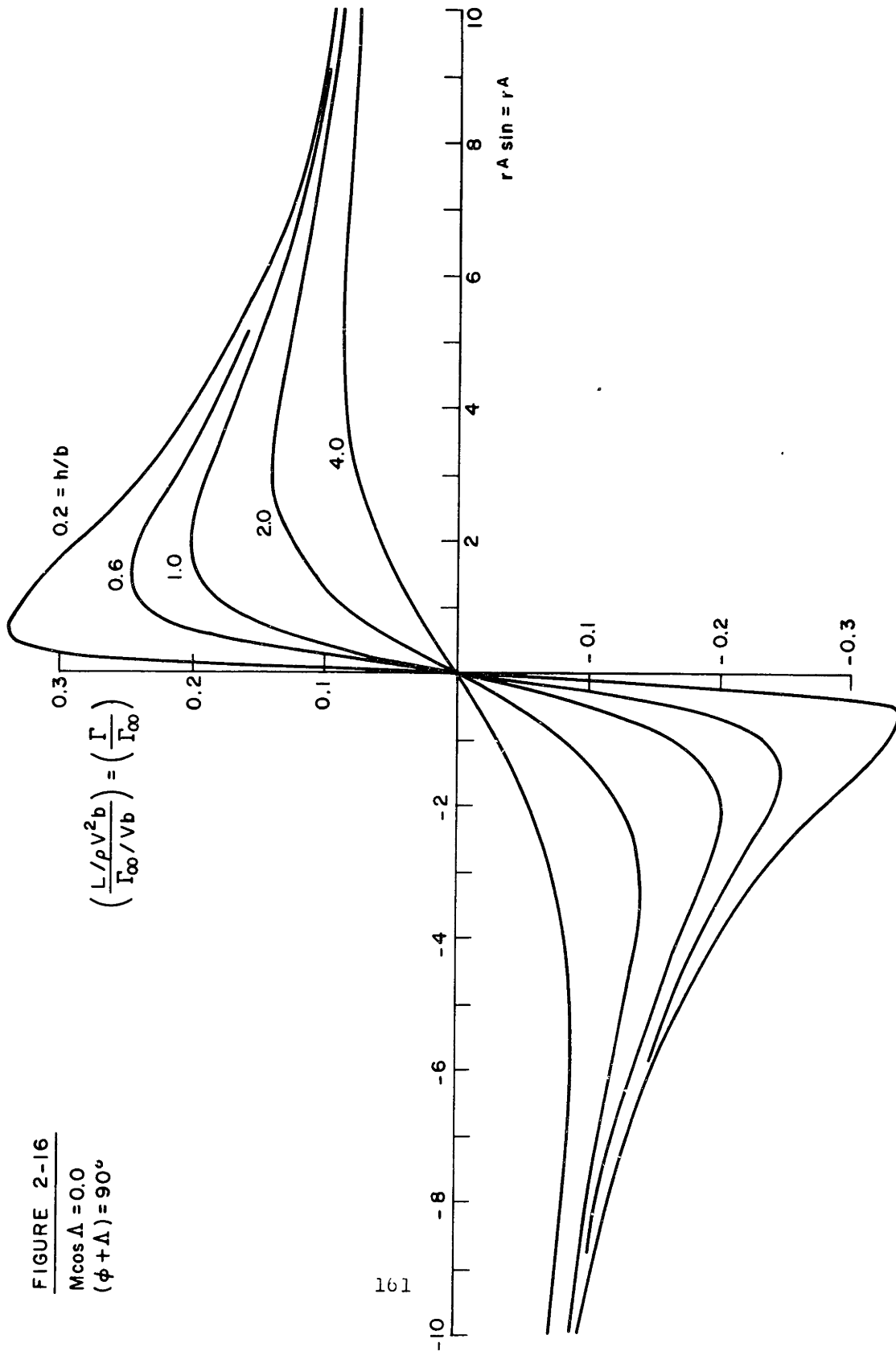


FIGURE 2-16

$M \cos \Lambda = 0.0$   
 $(\phi + \Lambda) = 90^\circ$



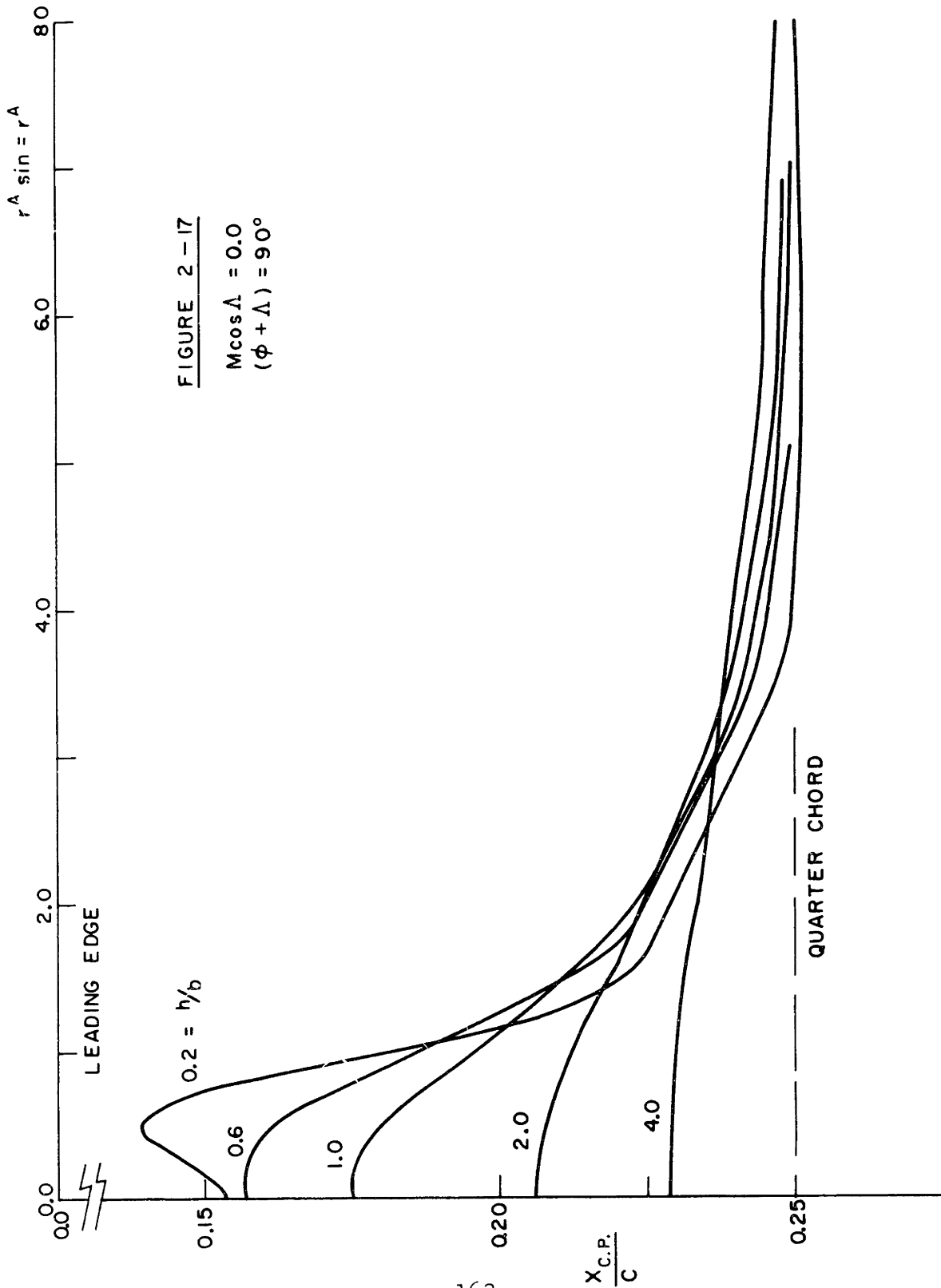


FIGURE 2-18

$M \cos \Delta = 0.0$   
 $(\phi + \Delta) = 180^\circ$

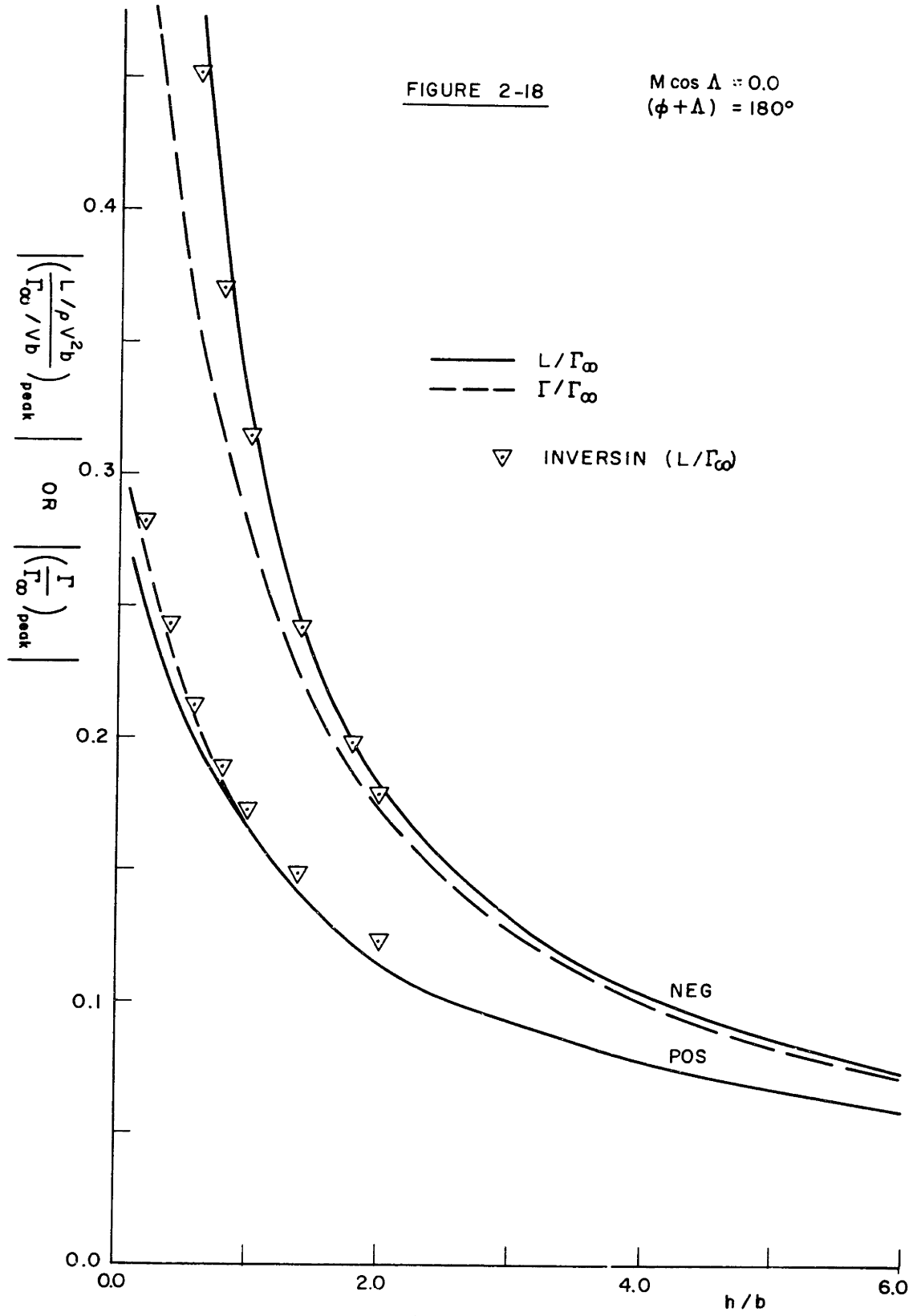


FIGURE 2-19

$M \cos \Delta = 0.0$   
 $(\phi + \Delta) = 180^\circ$

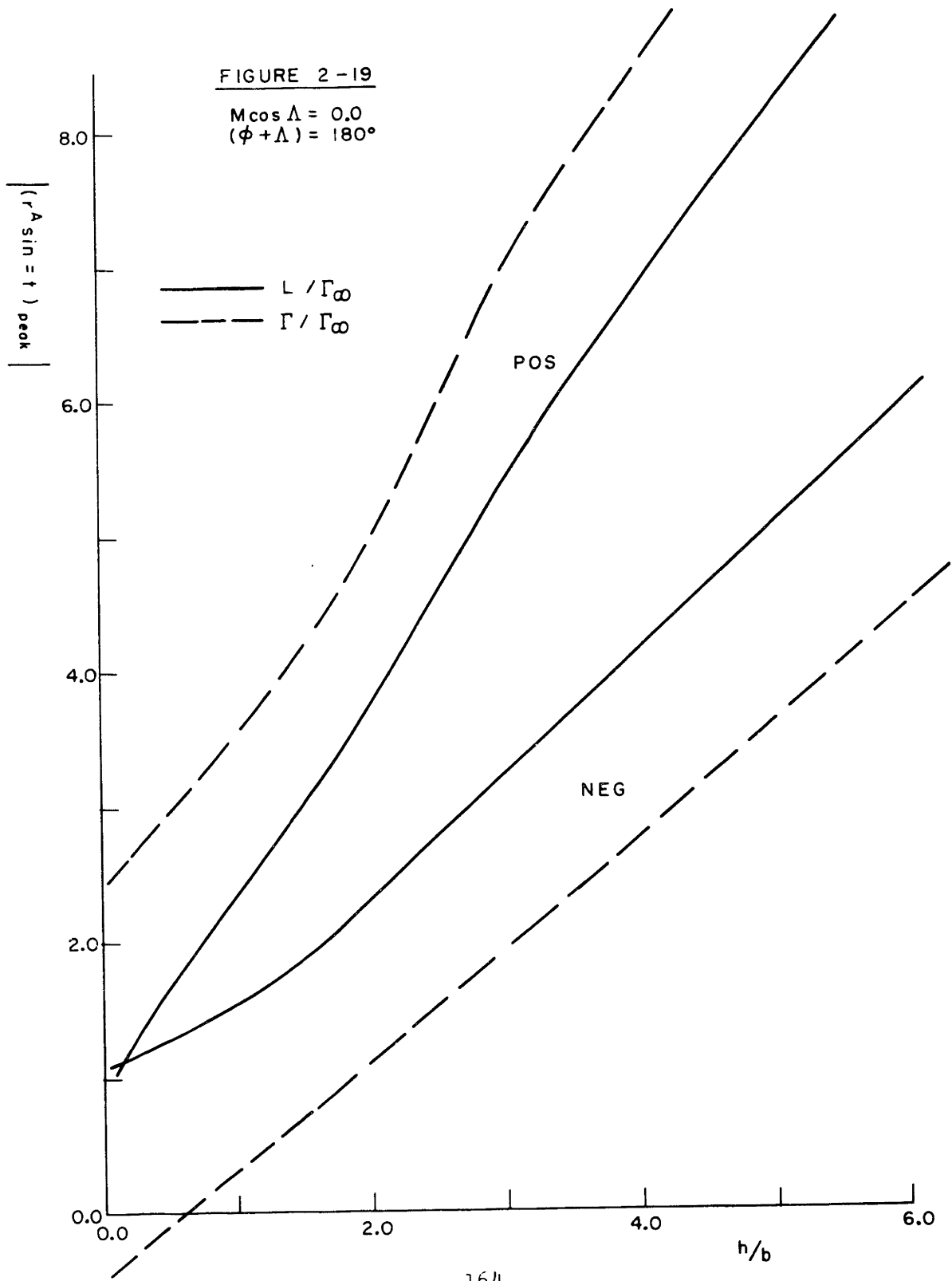


FIGURE 2-20

$M \cos \Delta = 0.0$   
 $(\phi + \Delta) = 180^\circ$

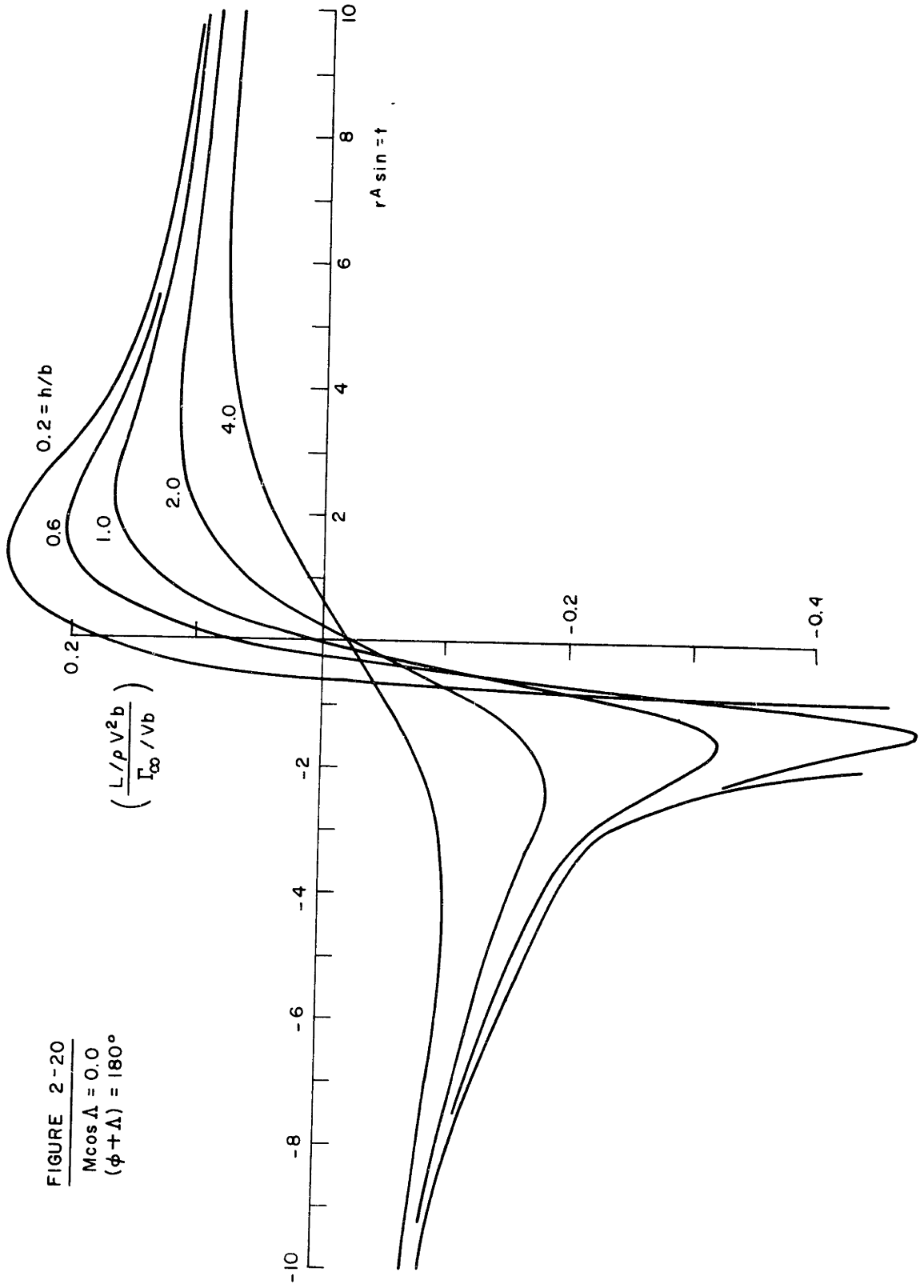


FIGURE 2-21  
 $M \cos \Delta = 0.0$   
 $(\phi + \Delta) = 180^\circ$

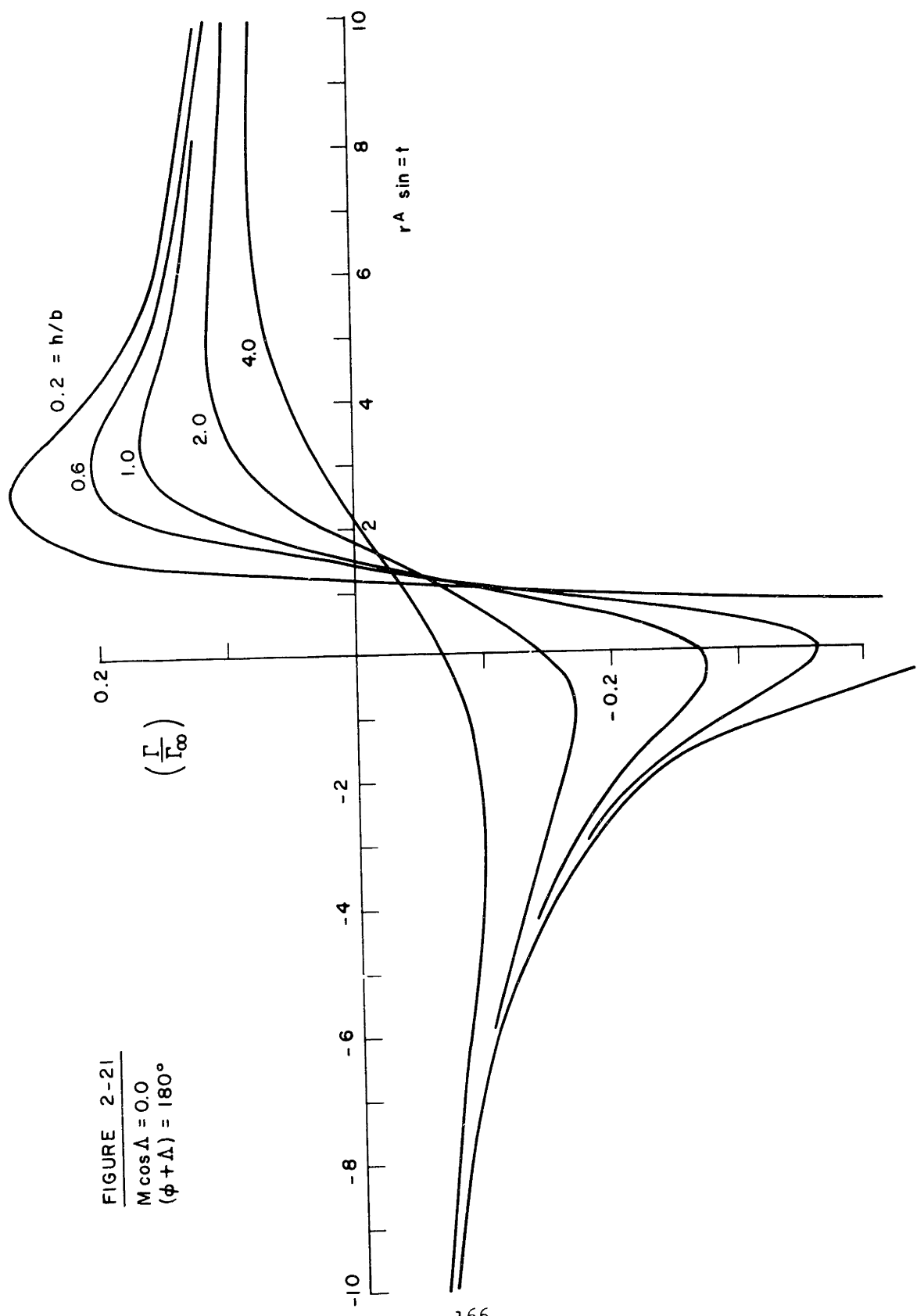


FIGURE 2-22

$$M \cos \Lambda = 0.0$$
$$h/b = 1.0$$

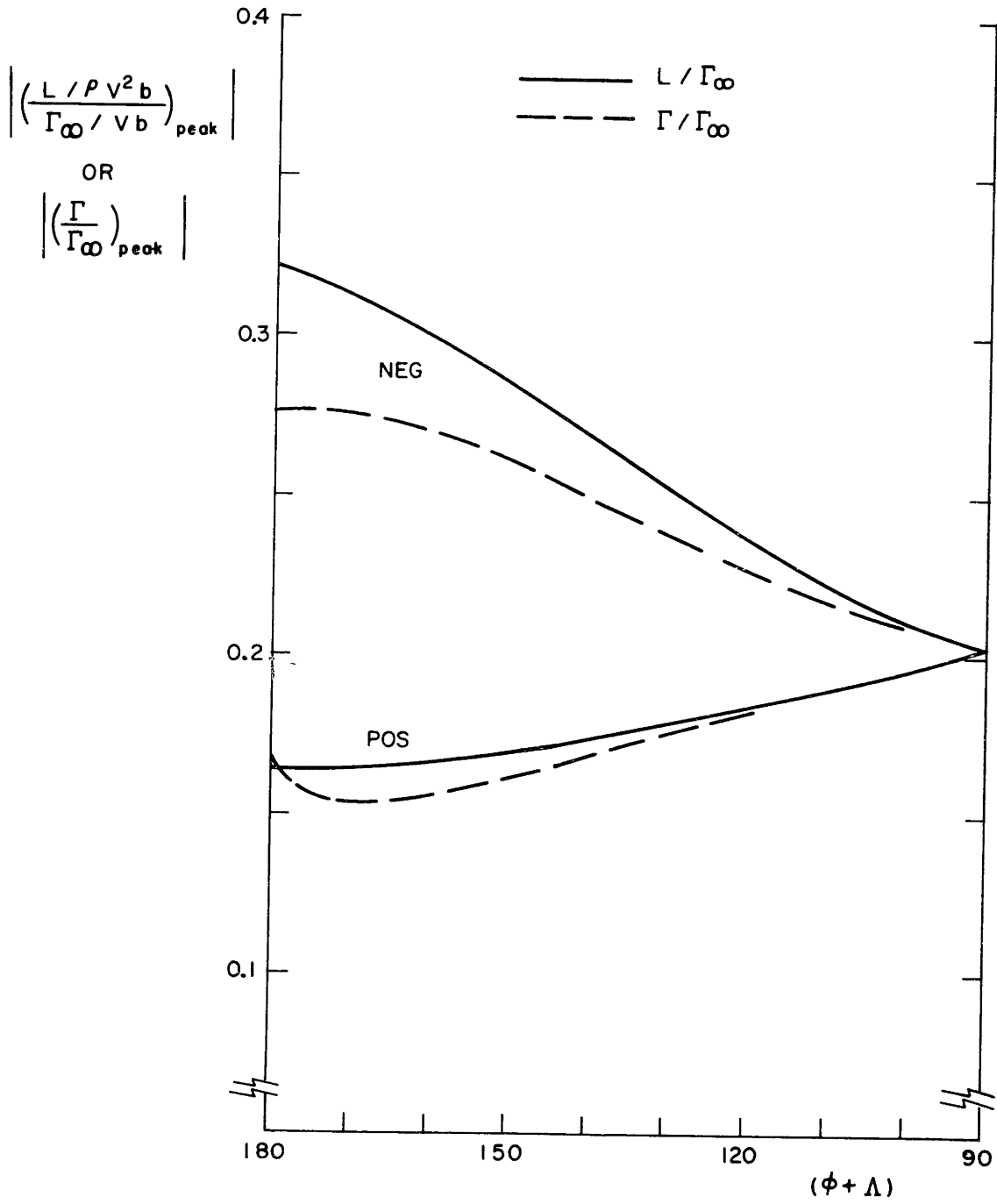




FIGURE 2-23

$M \cos \Delta = 0.0$   
 $h/b = 1.0$

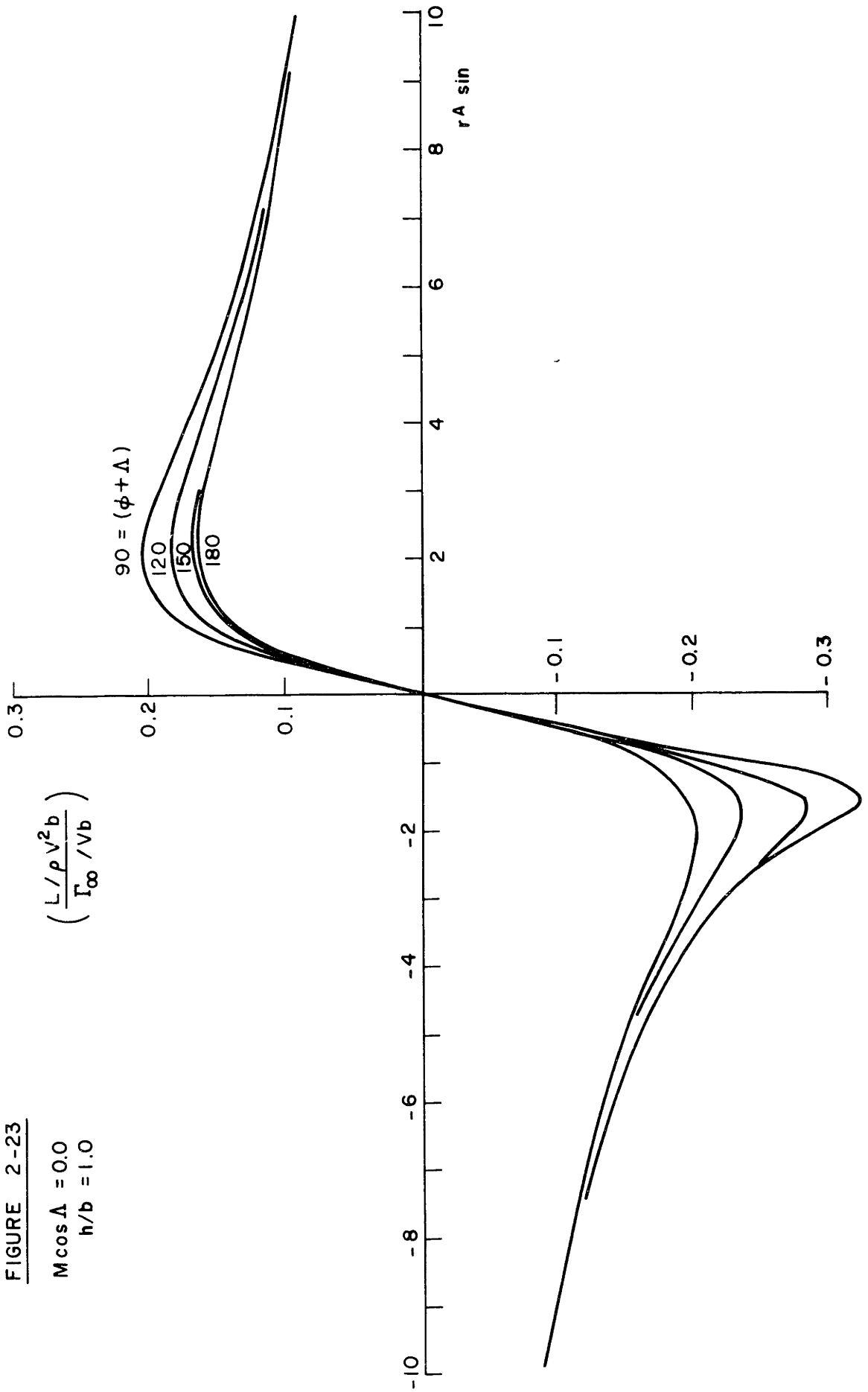
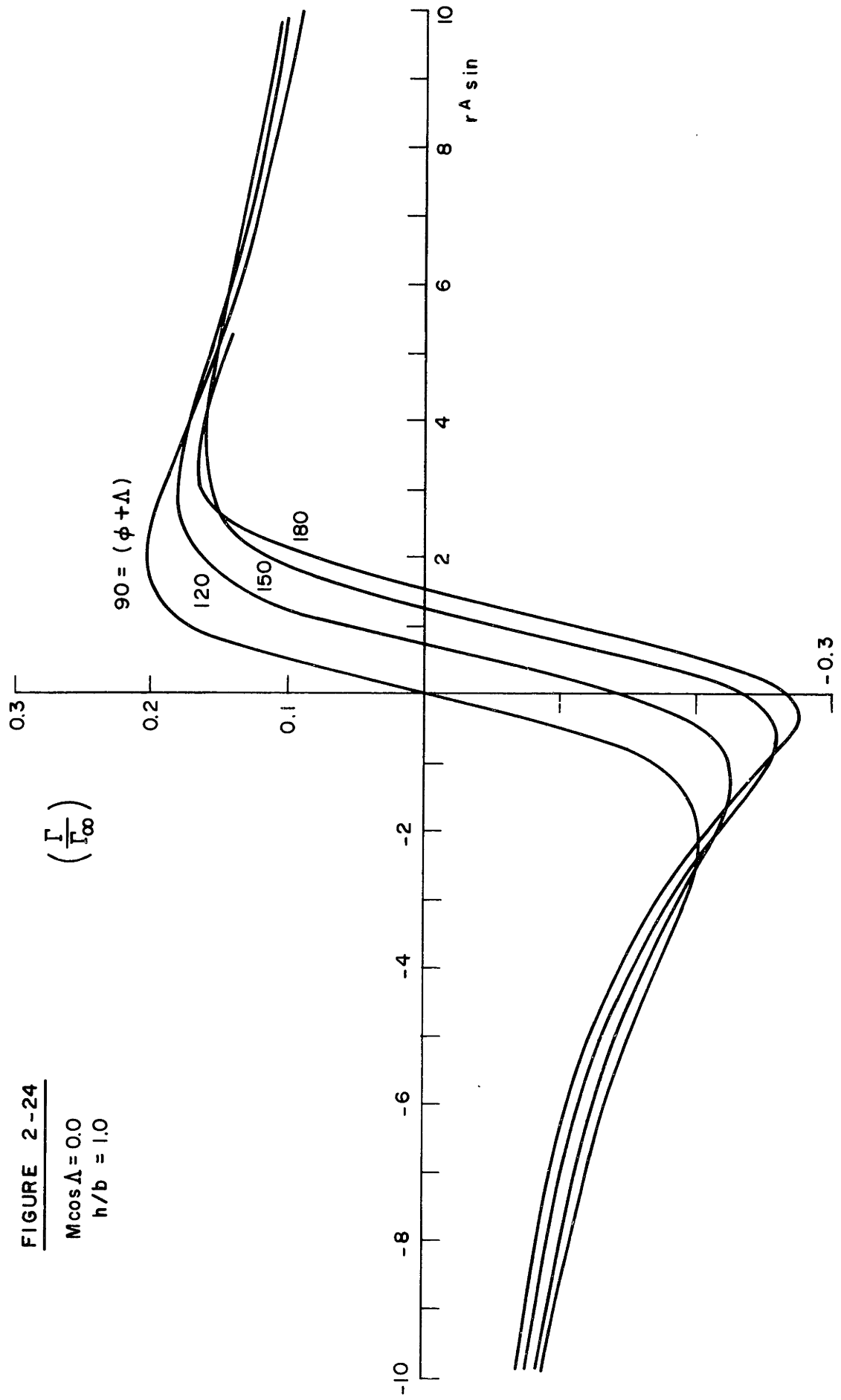


FIGURE 2-24

$M \cos \Delta = 0.0$   
 $h/b = 1.0$



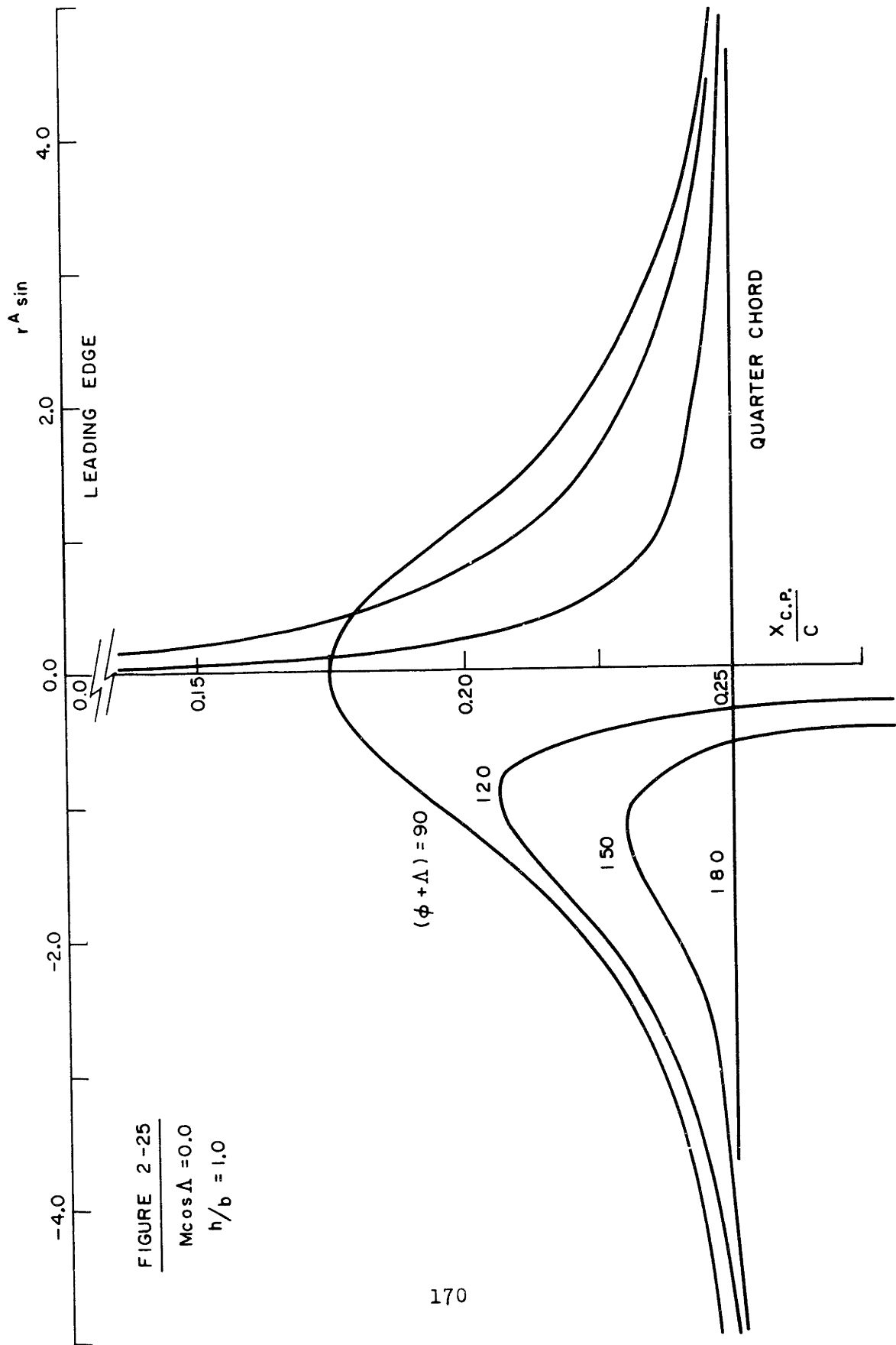


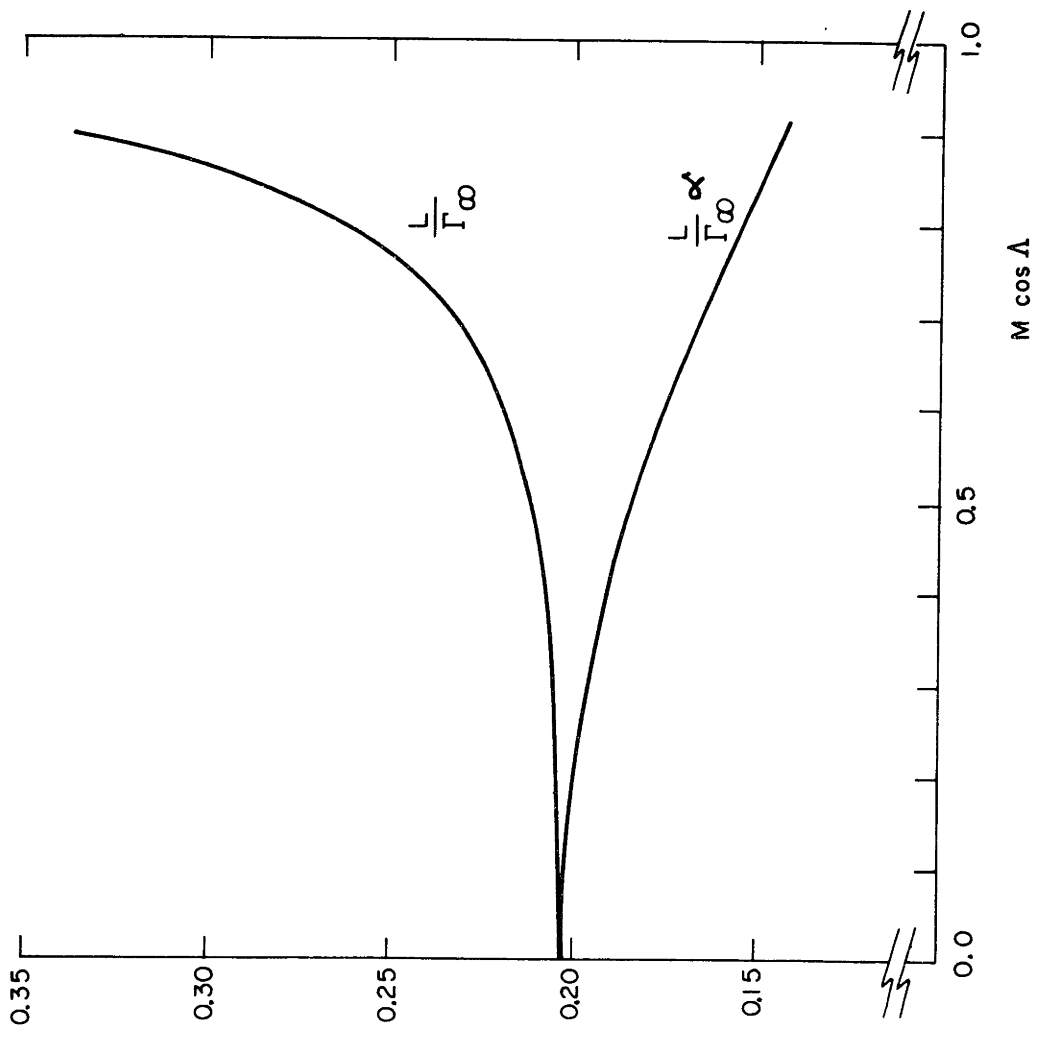
FIGURE 2-25

$M \cos \Delta = 0.0$

$h/b = 1.0$

FIGURE 2-26

$(\phi + \Delta) = 90^\circ$   
 $h/b = 1.0$



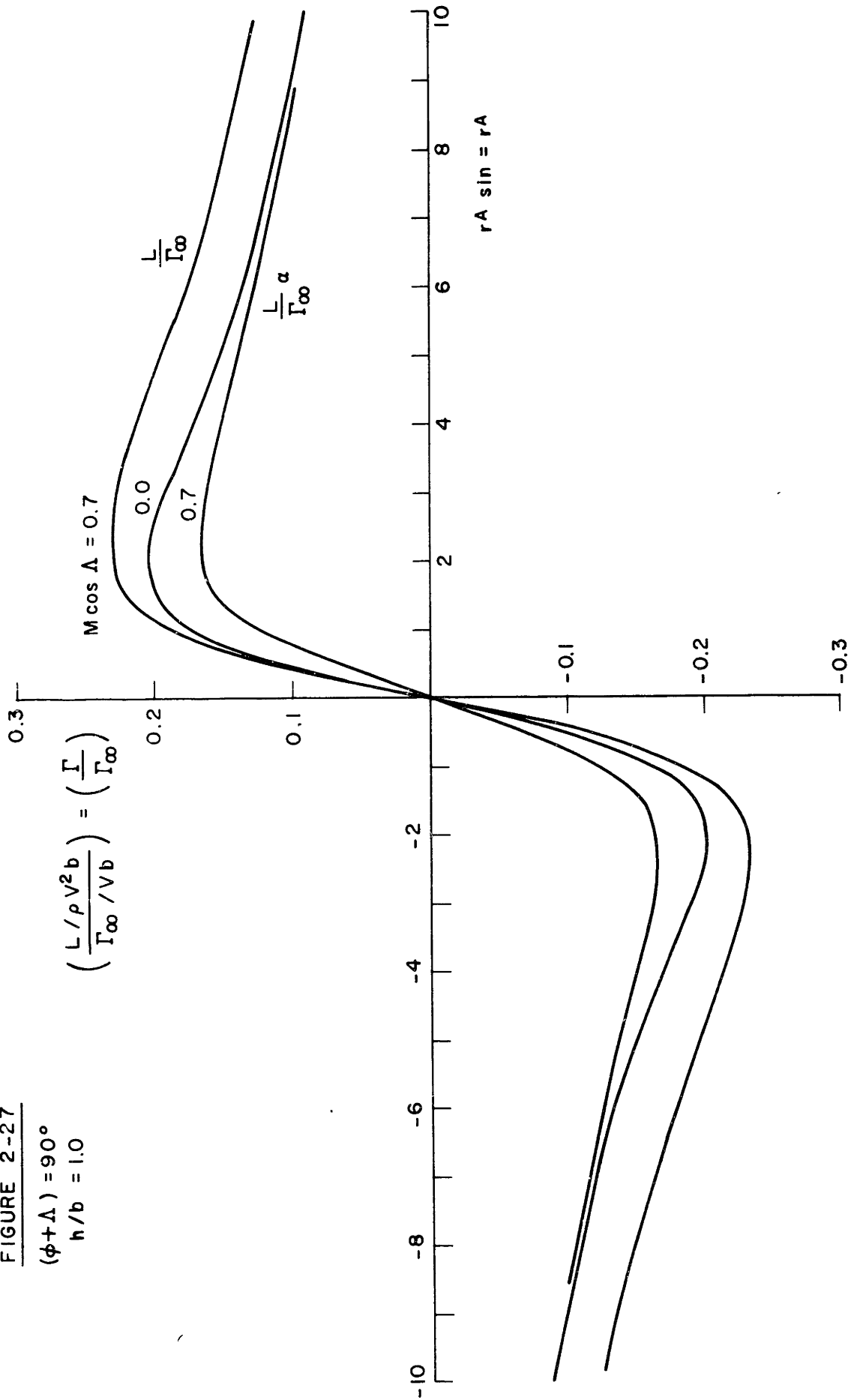
OR

$$\left( \frac{L/\rho V^2 b}{\Gamma_\infty/Vb} \right)_{\text{peak}} = \left( \frac{\Gamma}{\Gamma_\infty} \right)_{\text{peak}}$$

$$\left( \frac{L/\rho V^2 b}{\Gamma_\infty/Vb} \right)_{\text{peak}}^\alpha = \left( \frac{\Gamma}{\Gamma_\infty} \right)_{\text{peak}}^\alpha$$

FIGURE 2-27

$(\phi + \Delta) = 90^\circ$   
 $h/b = 1.0$



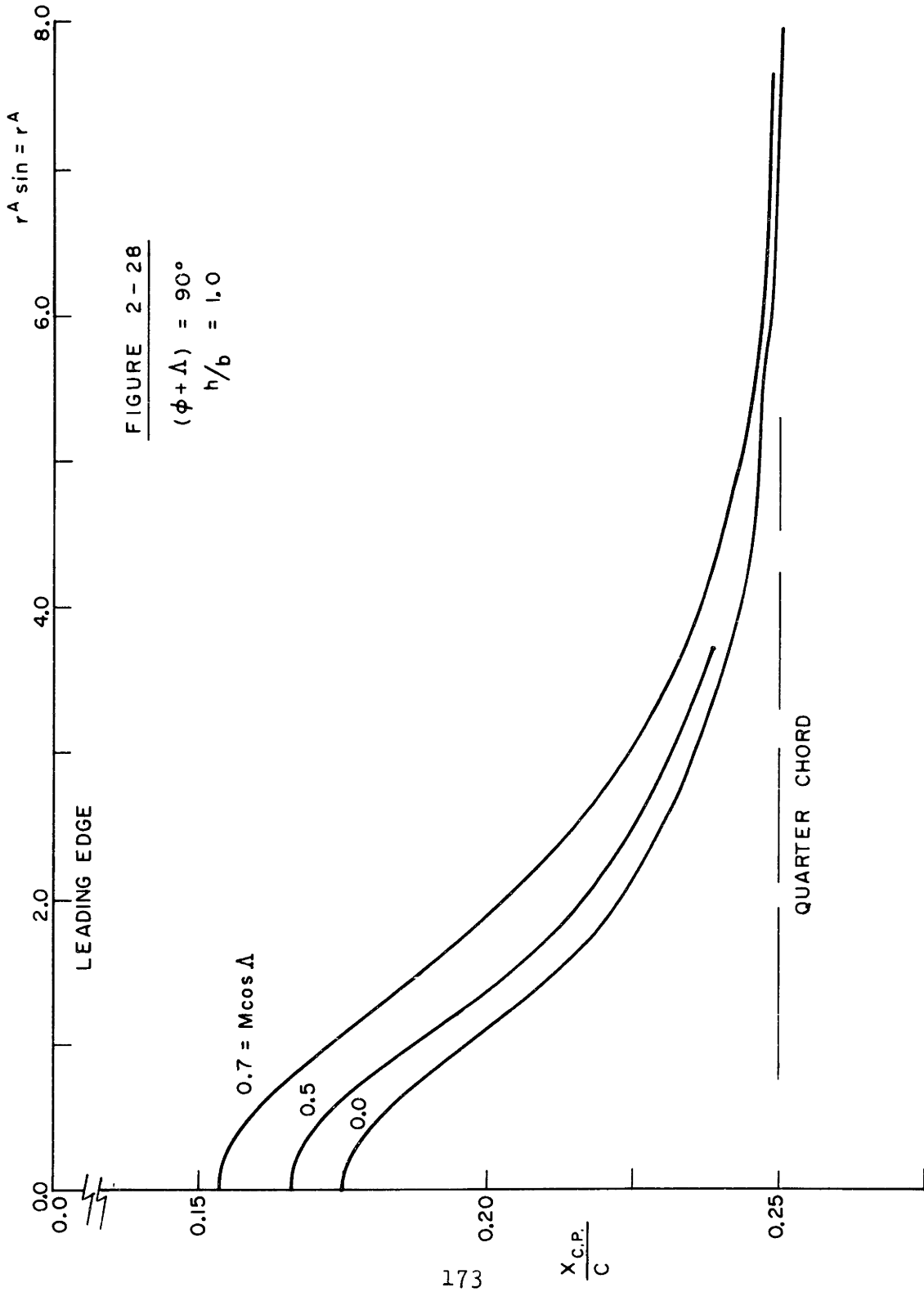


FIGURE 2 - 28

$(\phi + \Delta) = 90^\circ$   
 $h/b = 1.0$

FIGURE 2-29

$(\phi + \Lambda) = 180^\circ$   
 $h/b = 1.0$

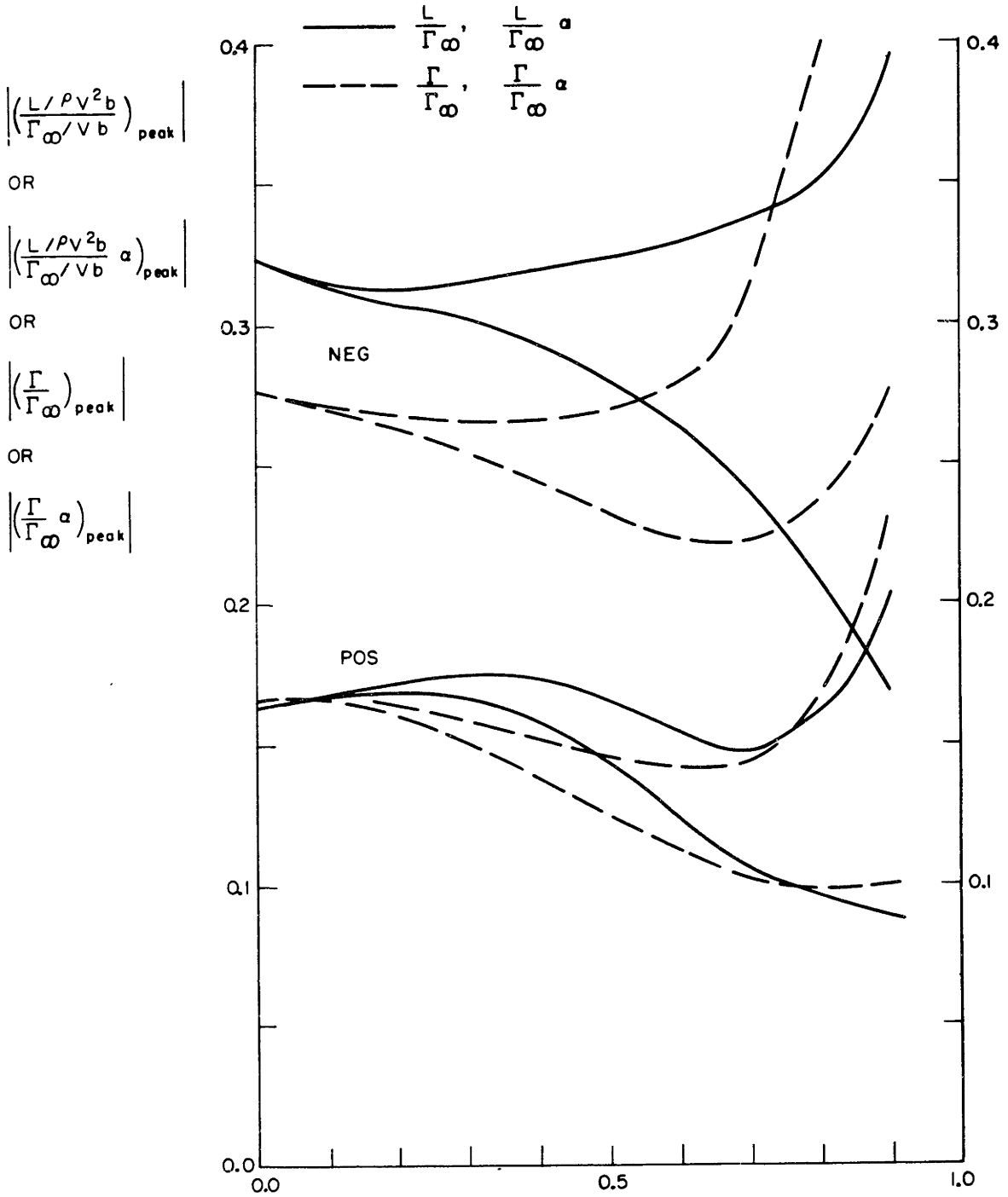


FIGURE 2-30

$(\phi + \Delta) = 180^\circ$   
 $h/b = 1.0$

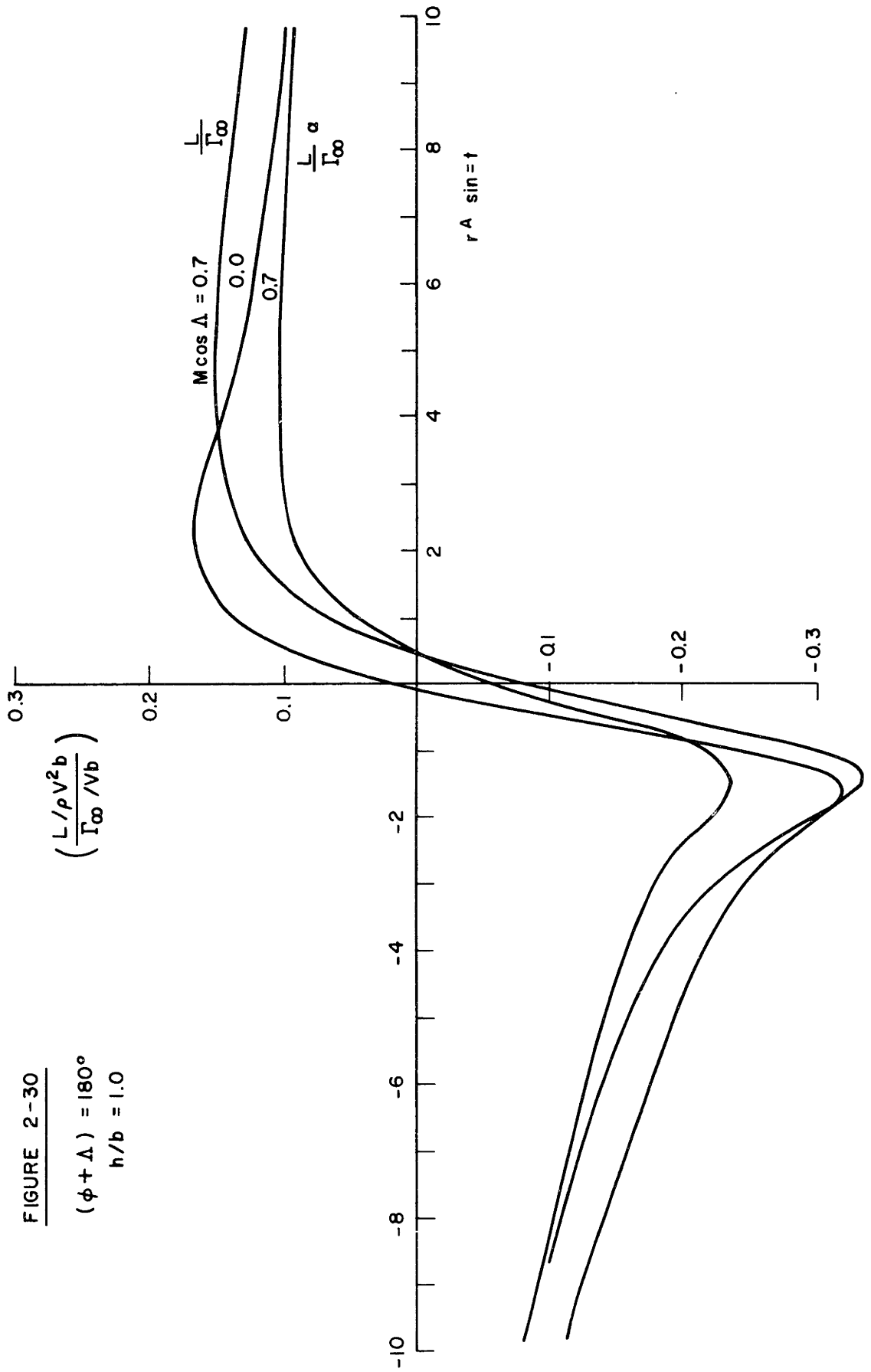
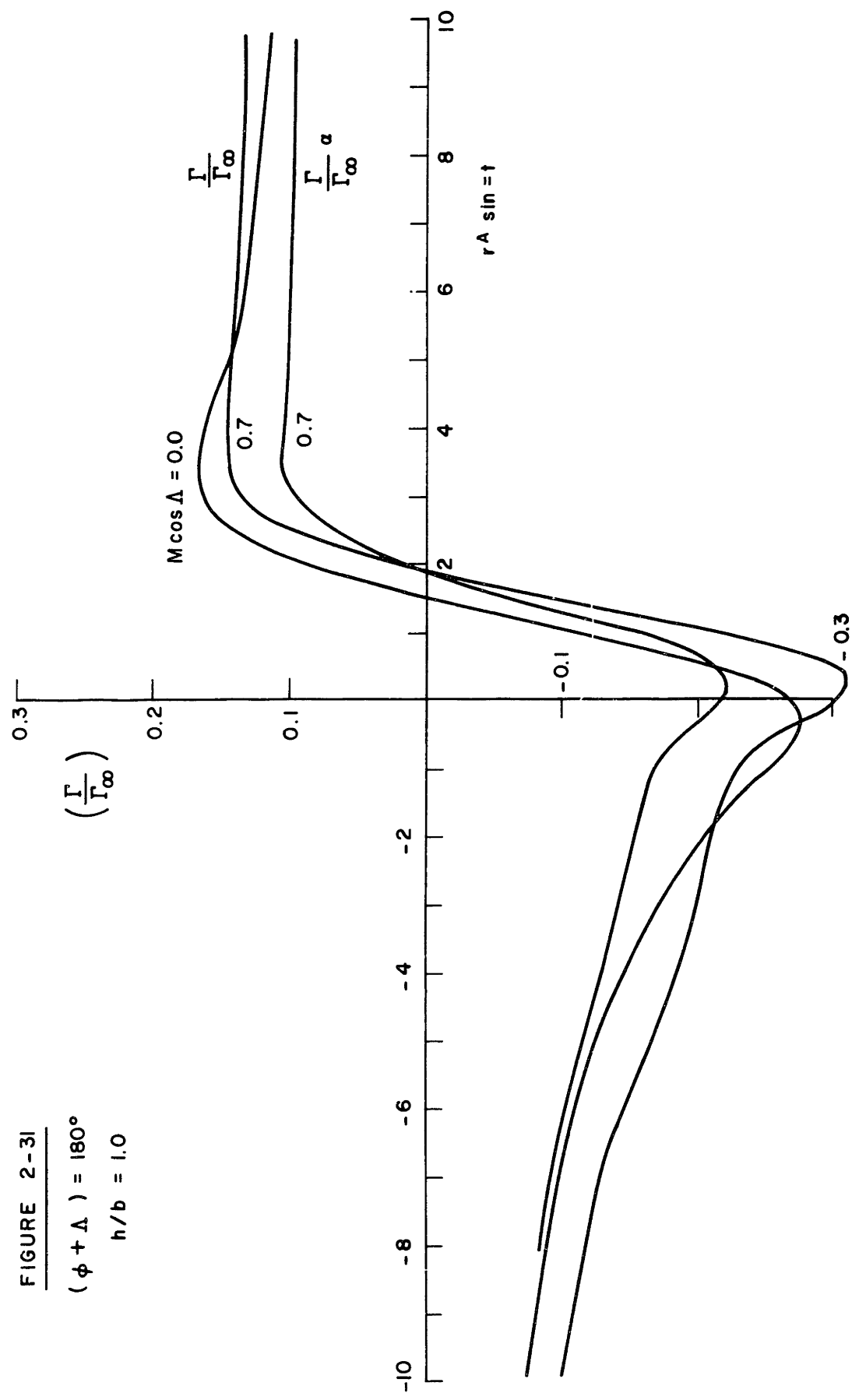




FIGURE 2-31  
 $(\phi + \Delta) = 180^\circ$   
 $h/b = 1.0$



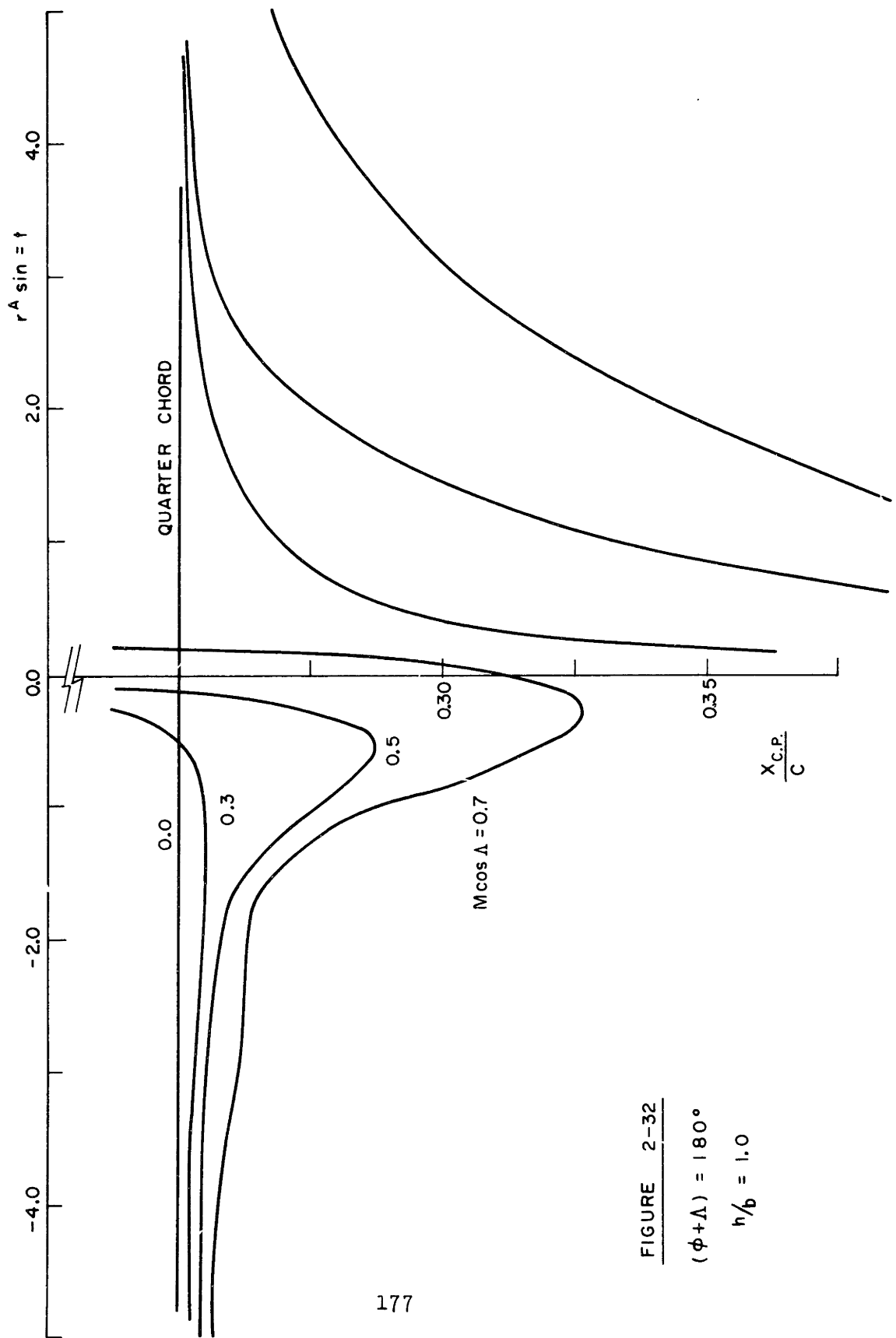


FIGURE 2-32

$(\phi + \Delta) = 180^\circ$

$h/b = 1.0$

FIGURE 2-33

$M \cos \Delta = 0.7$   
 $h/b = 1.0$

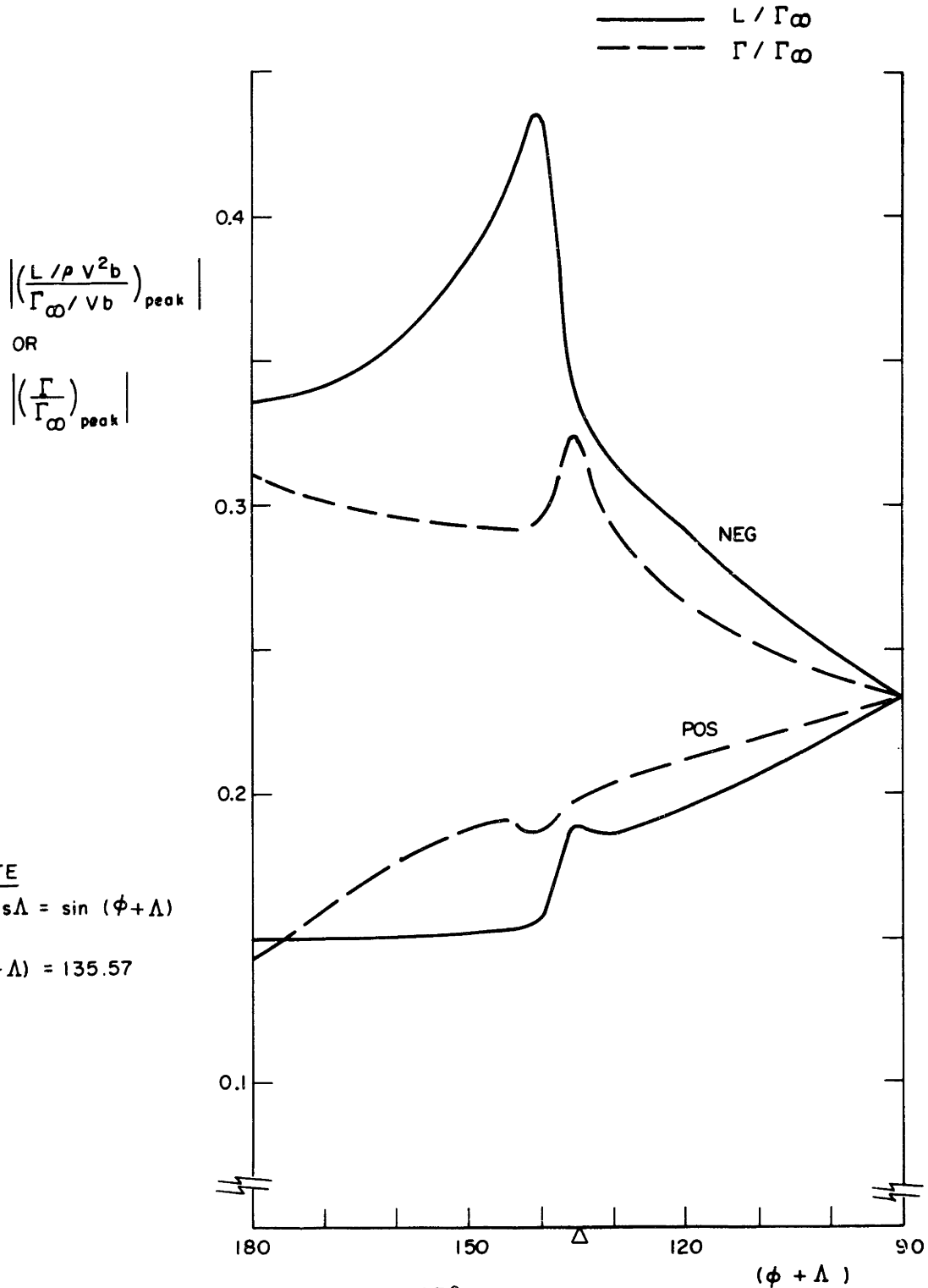


FIGURE 2-34

$M \cos \Delta = 0.7$   
 $h/b = 1.0$

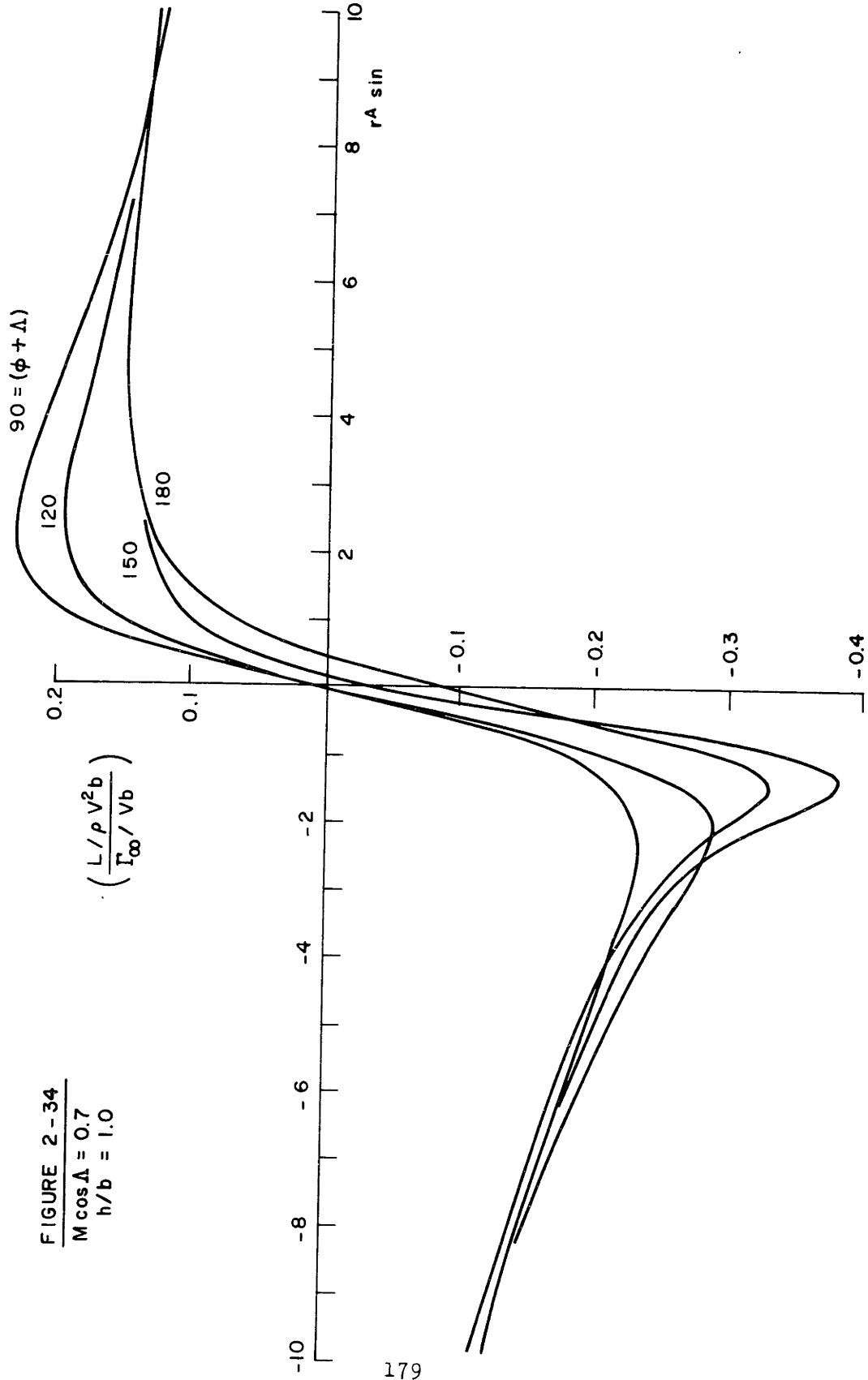


FIGURE 2 -35

$M \cos \Lambda = 0.7$   
 $h/b = 1.0$

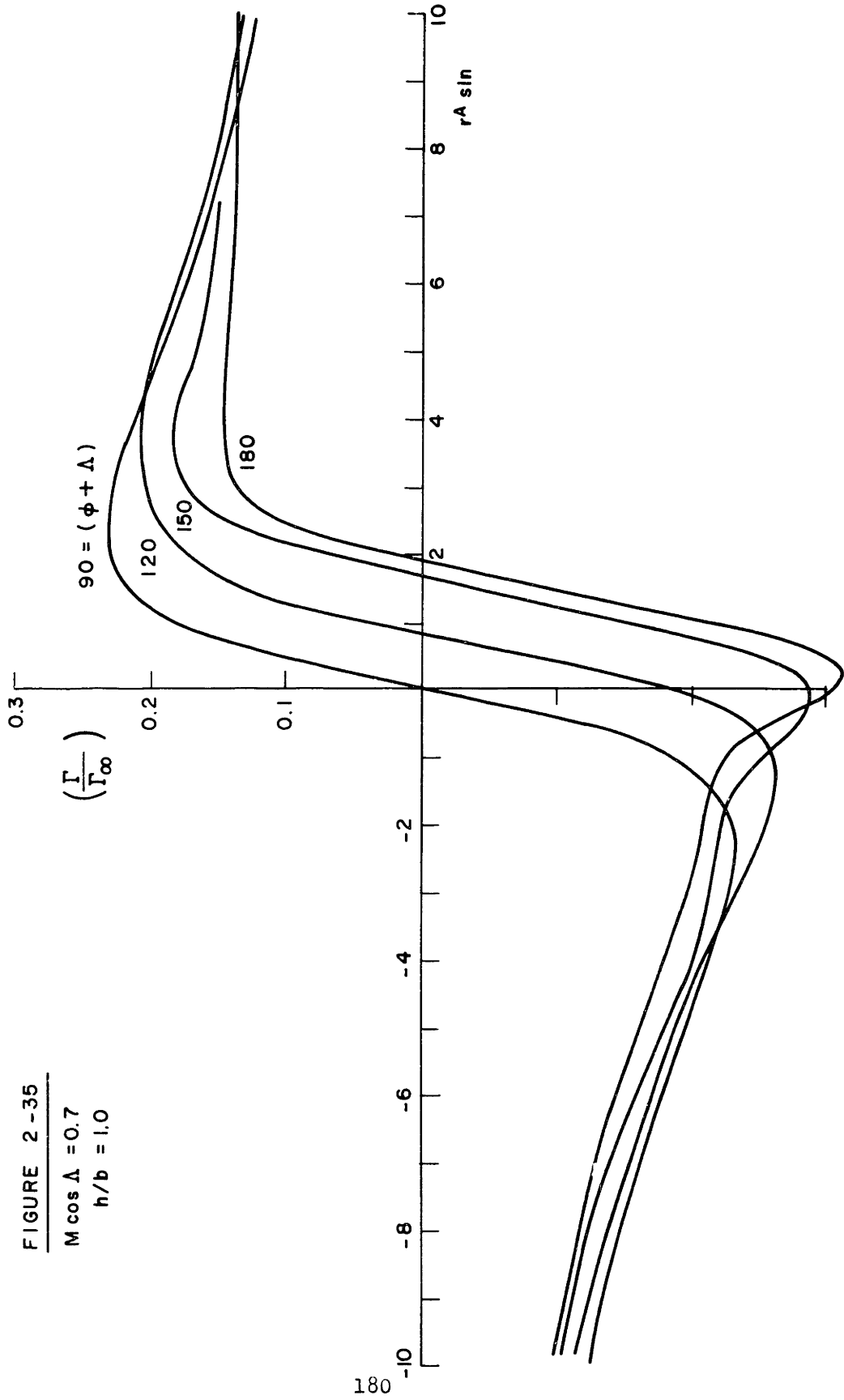


FIGURE 2-36

$M \cos \Lambda = 0.7$

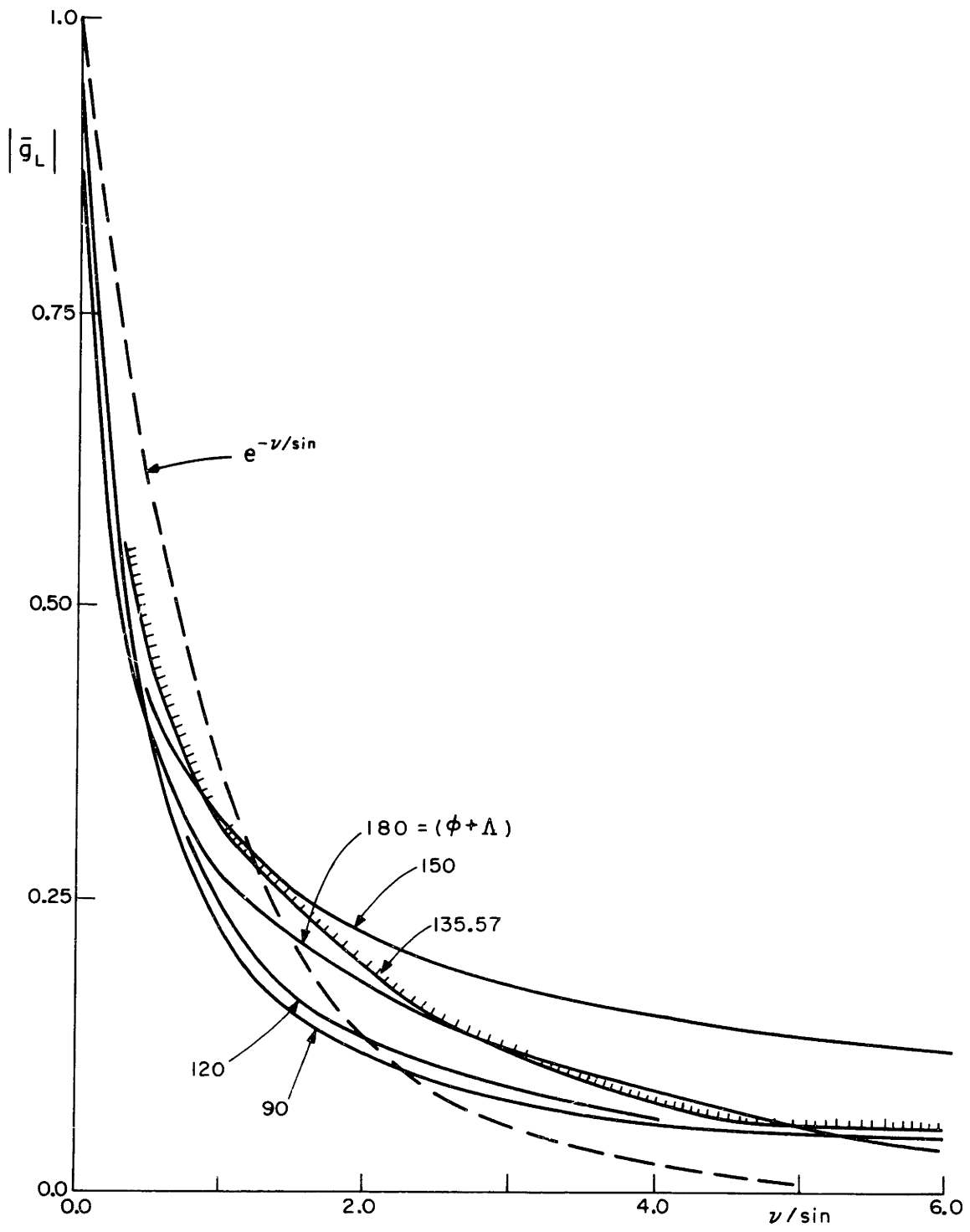


FIGURE 2-37

$h/b = 1.0$

—  $(\phi + \Lambda) = 90^\circ$   
 - - -  $(\phi + \Lambda) = 180^\circ$

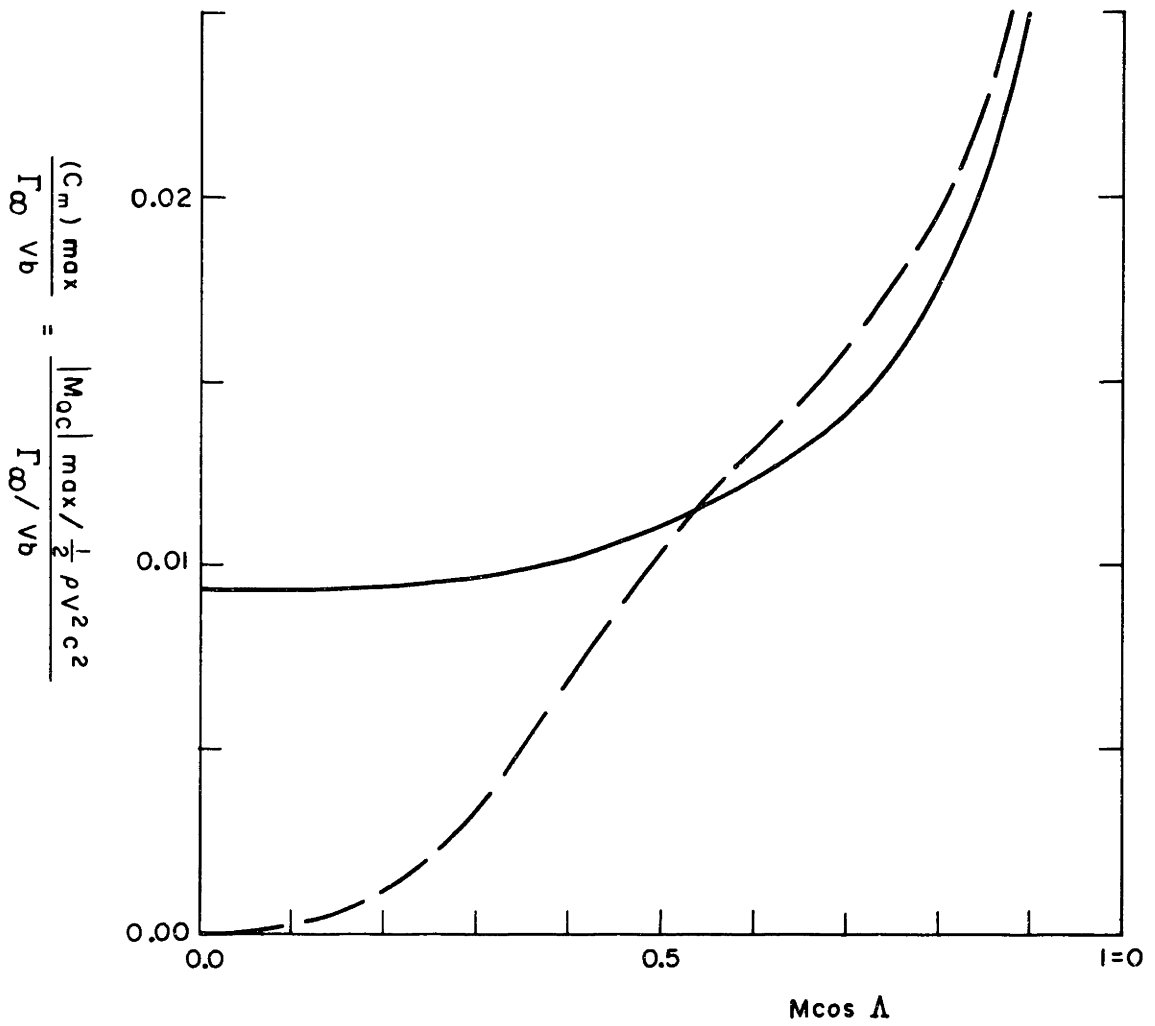


FIGURE 2 - 38

$M \cos \Lambda = 0.0$   
 $(\phi + \Lambda) = 90^\circ$

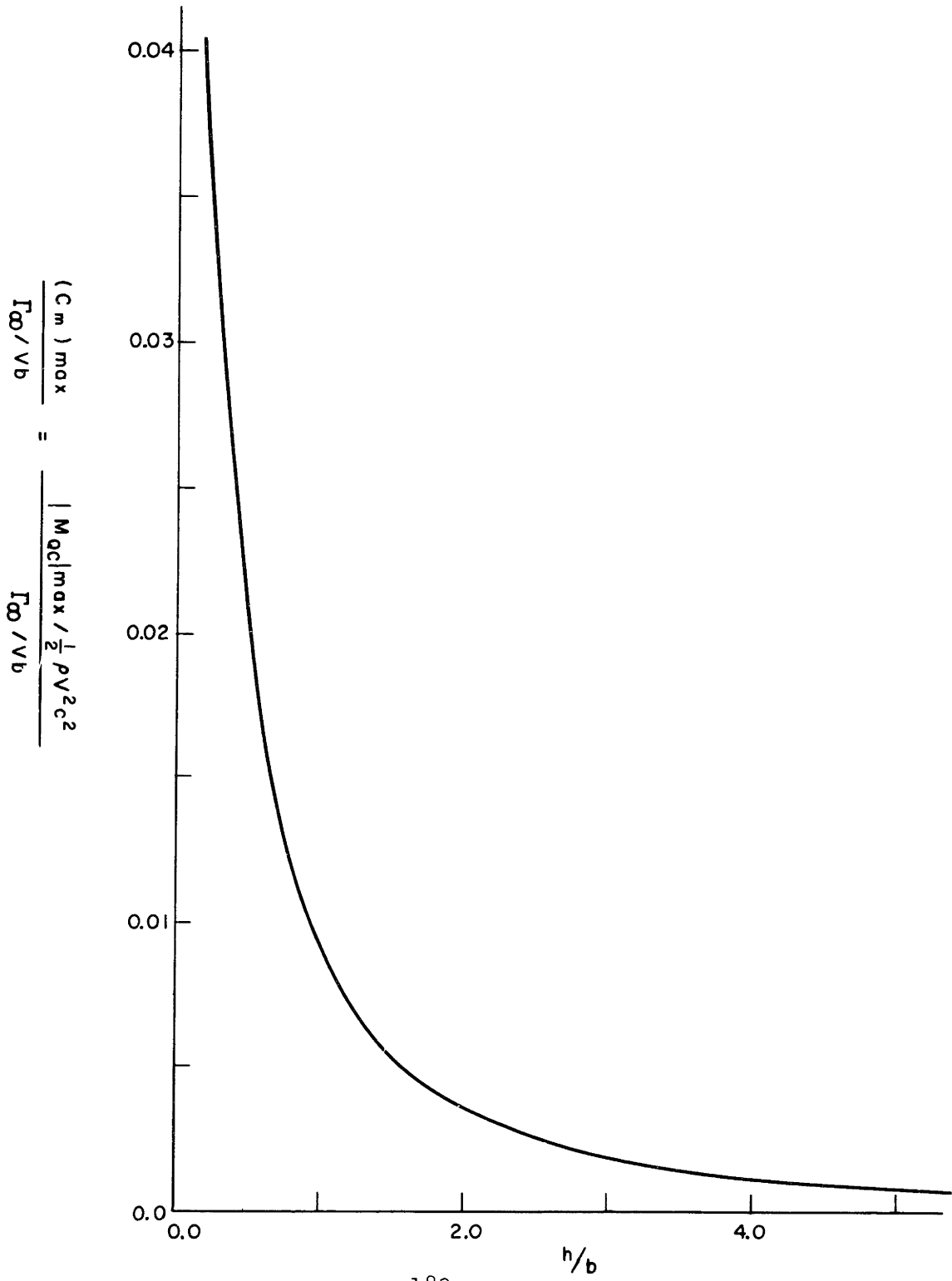
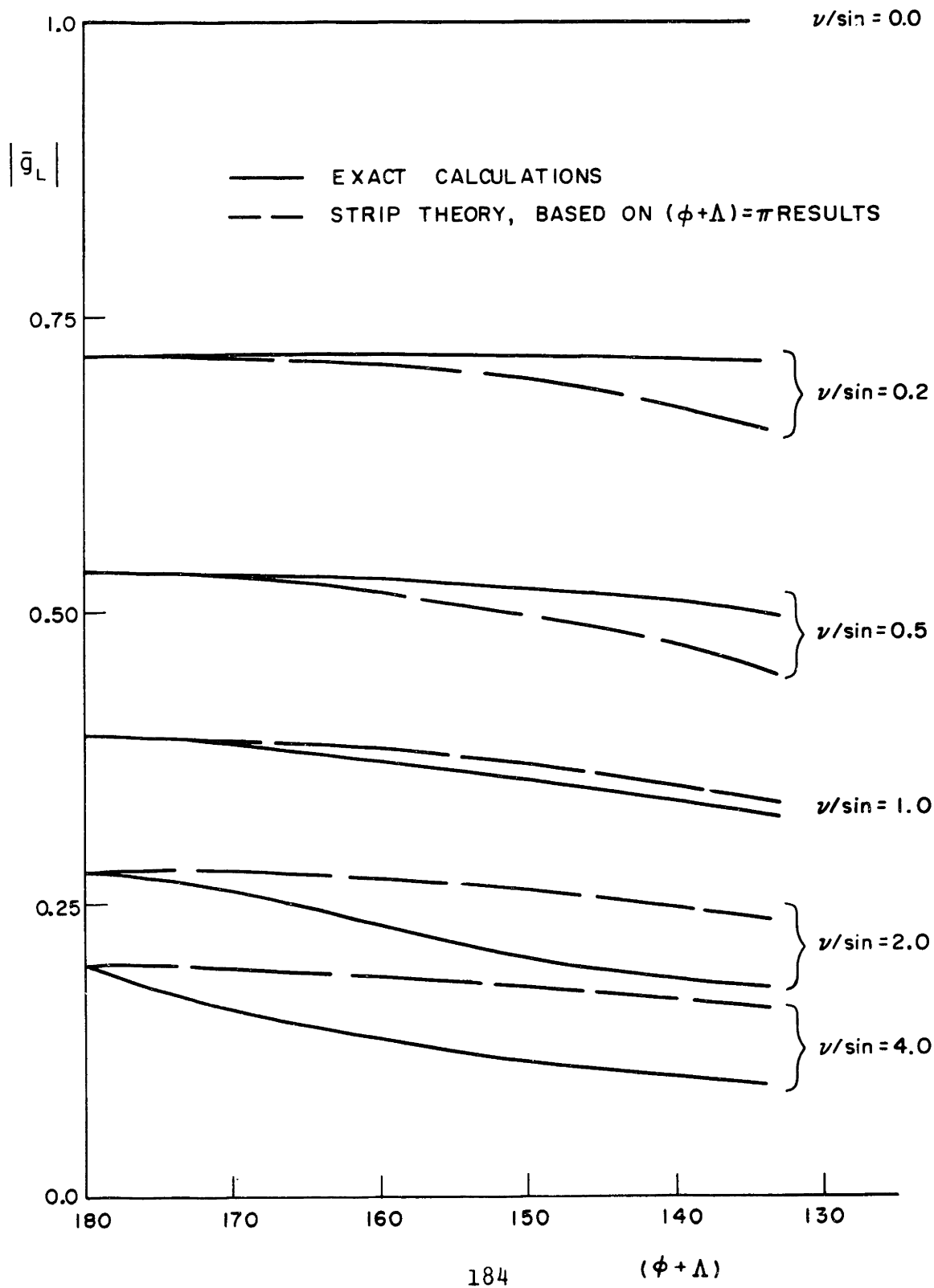




FIGURE 2-39

$M \cos \Delta = 0.0$



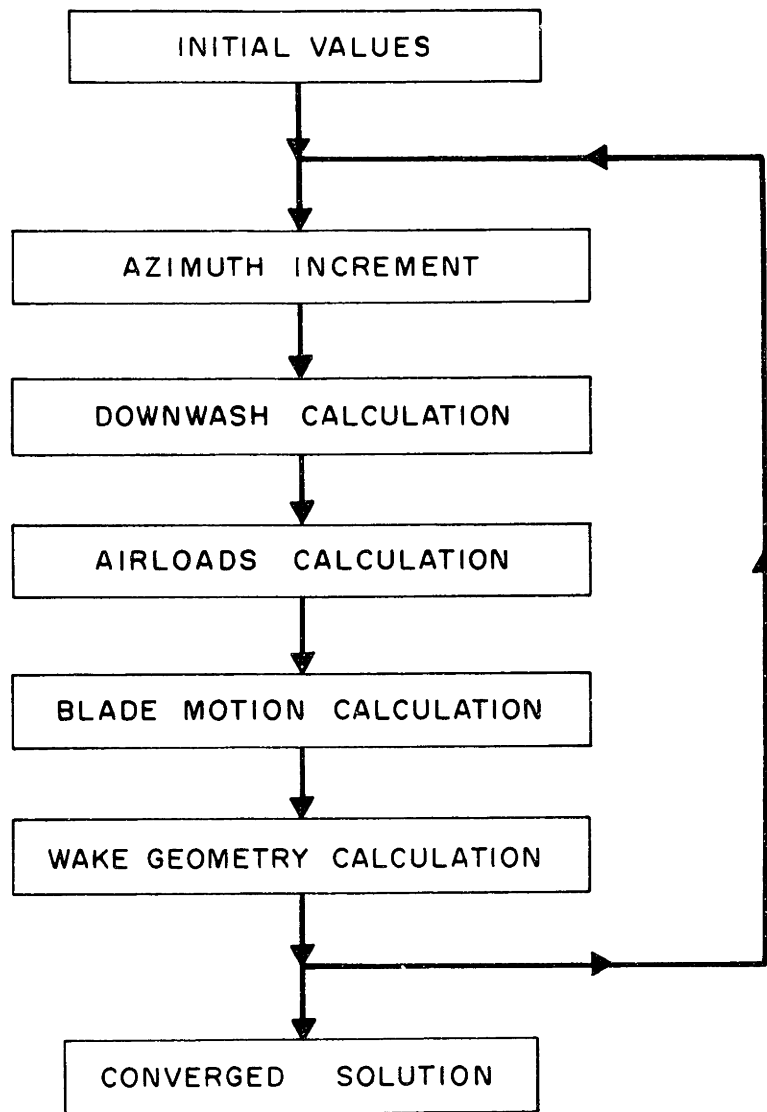


FIGURE 3-1 PROCEDURE FOR CALCULATION OF ROTARY WING AIRLOADS

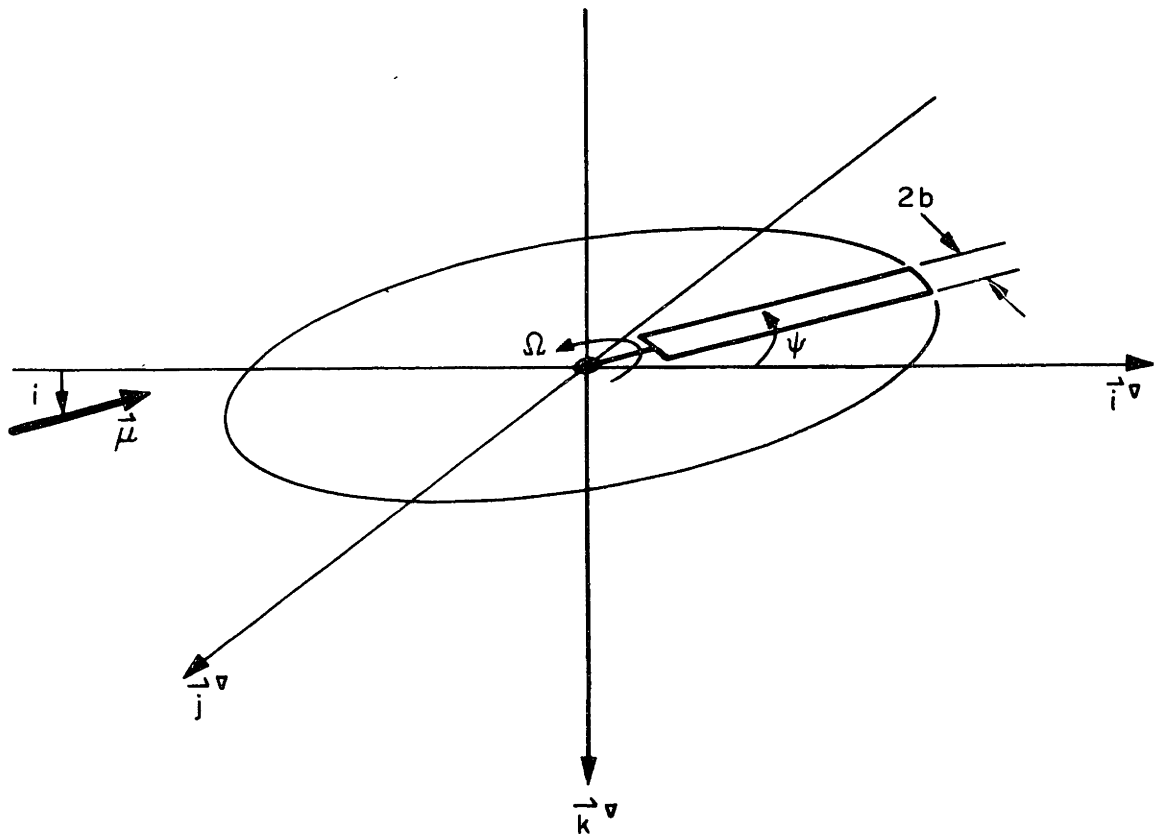


FIGURE 3-2 ROTARY WING GEOMETRY

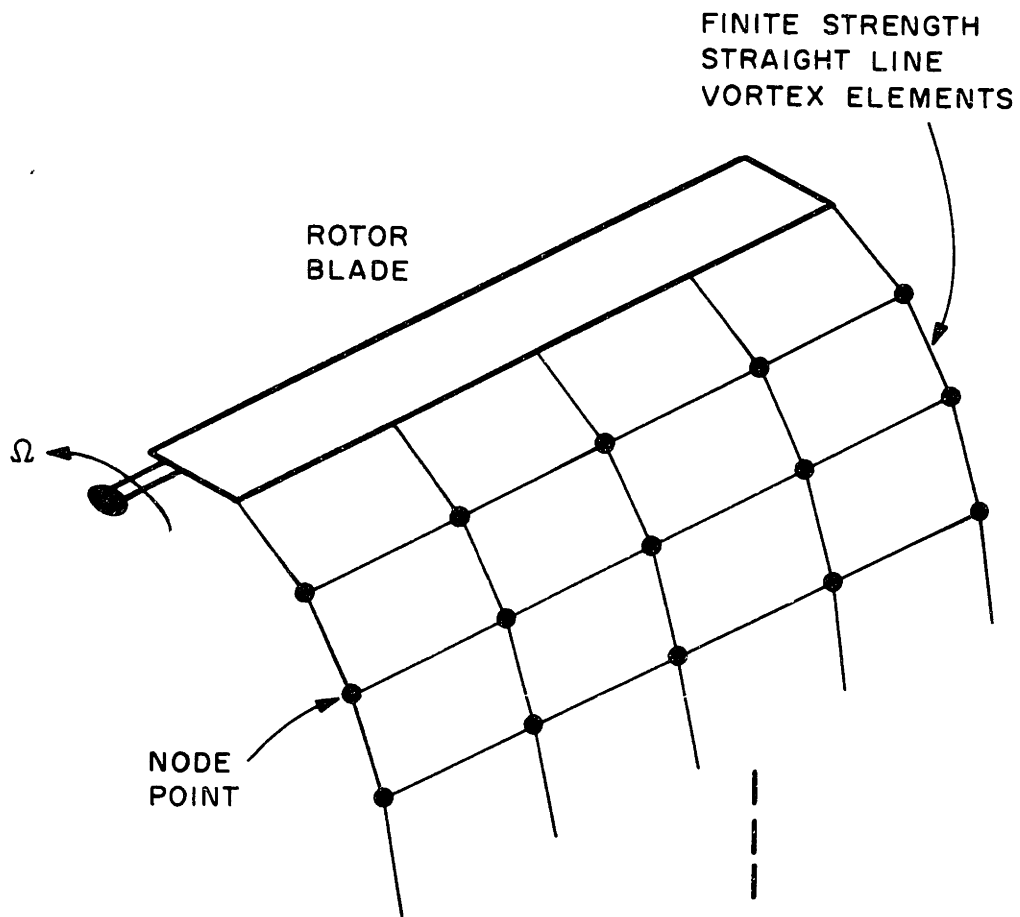


FIGURE 3-3 VORTEX NET REPRESENTATION  
 OF THE ROTOR WAKE

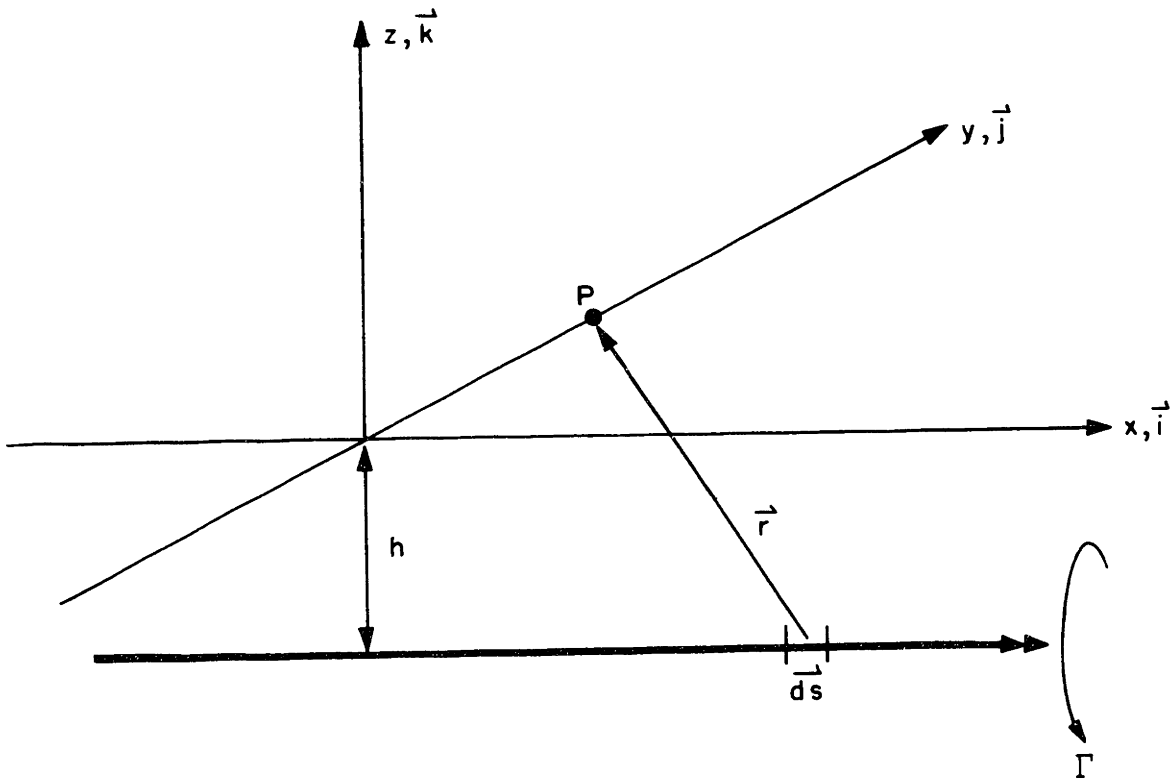


FIGURE 3-4 STRAIGHT, INFINITE VORTEX WITH ORTHOGONAL GEOMETRY

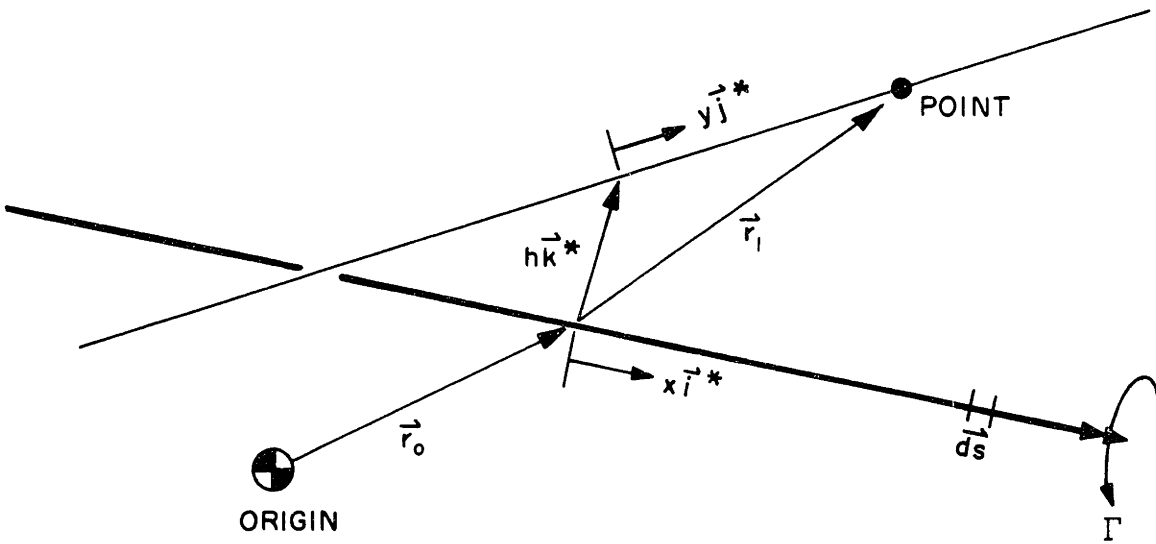


FIGURE 3-5 STRAIGHT, INFINITE VORTEX WITH GENERAL GEOMETRY

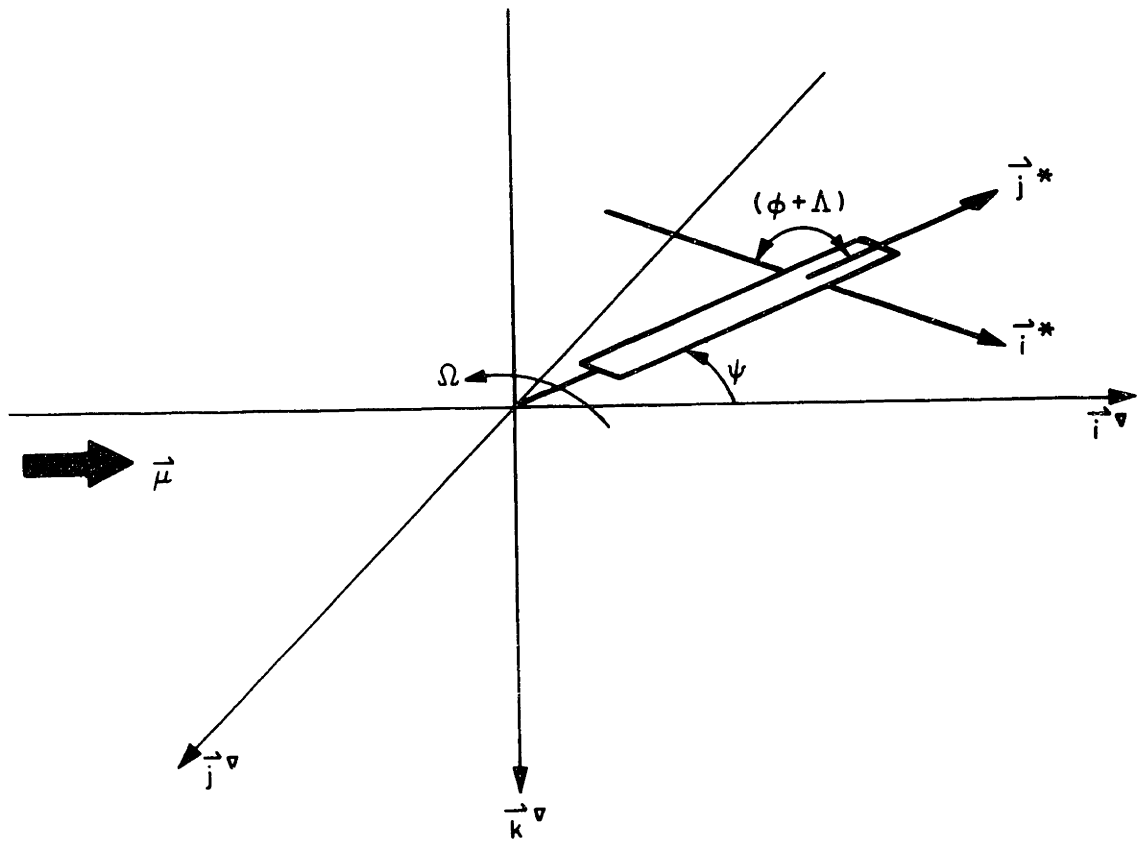


FIGURE 3-6 VORTEX AND BLADE GEOMETRY IN THE ROTARY WING CONFIGURATION

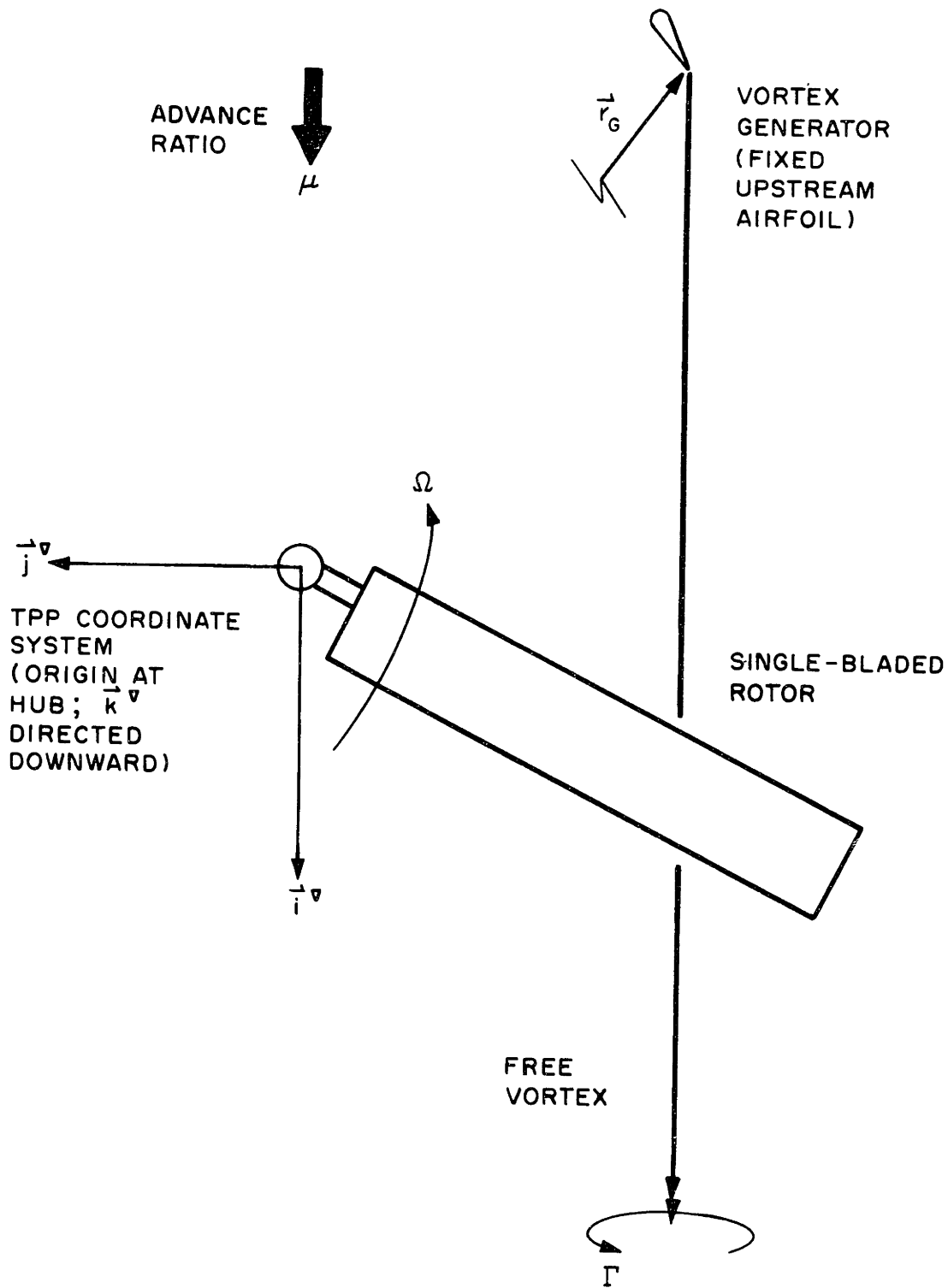


FIGURE 4-1 ROTARY WING CONFIGURATION FOR EVALUATION OF LIFTING SURFACE THEORY SOLUTION



FIGURE 4-2

$M_{1,0,90} = 0.0$        $h/b = 2.0$   
 $\gamma_G = 0.5$           $r = 0.6$

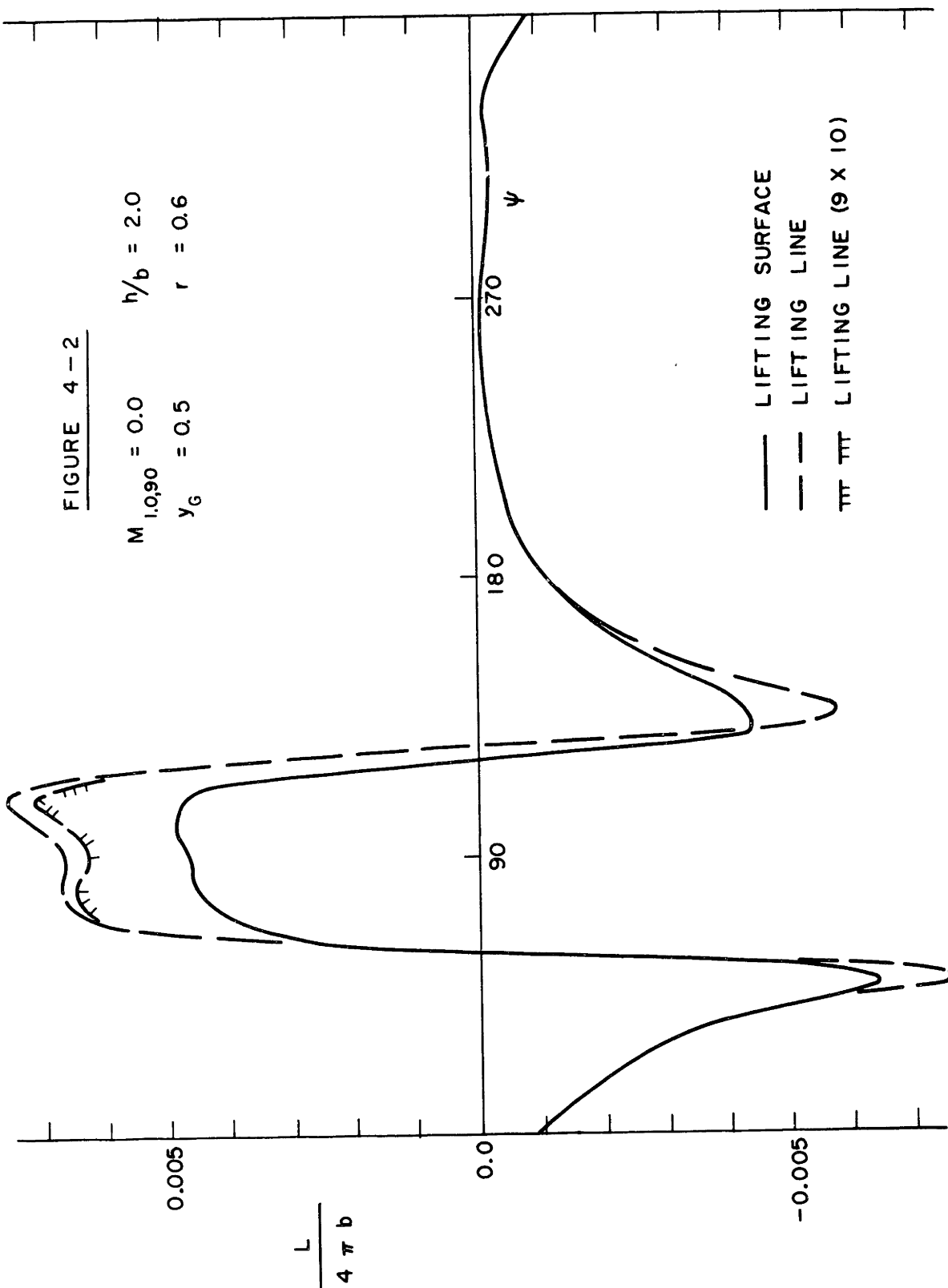


FIGURE 4-3

$M_{1,0,90} = 0.0$        $h/b = 1.0$   
 $\gamma_G = 0.5$            $r = 0.6$

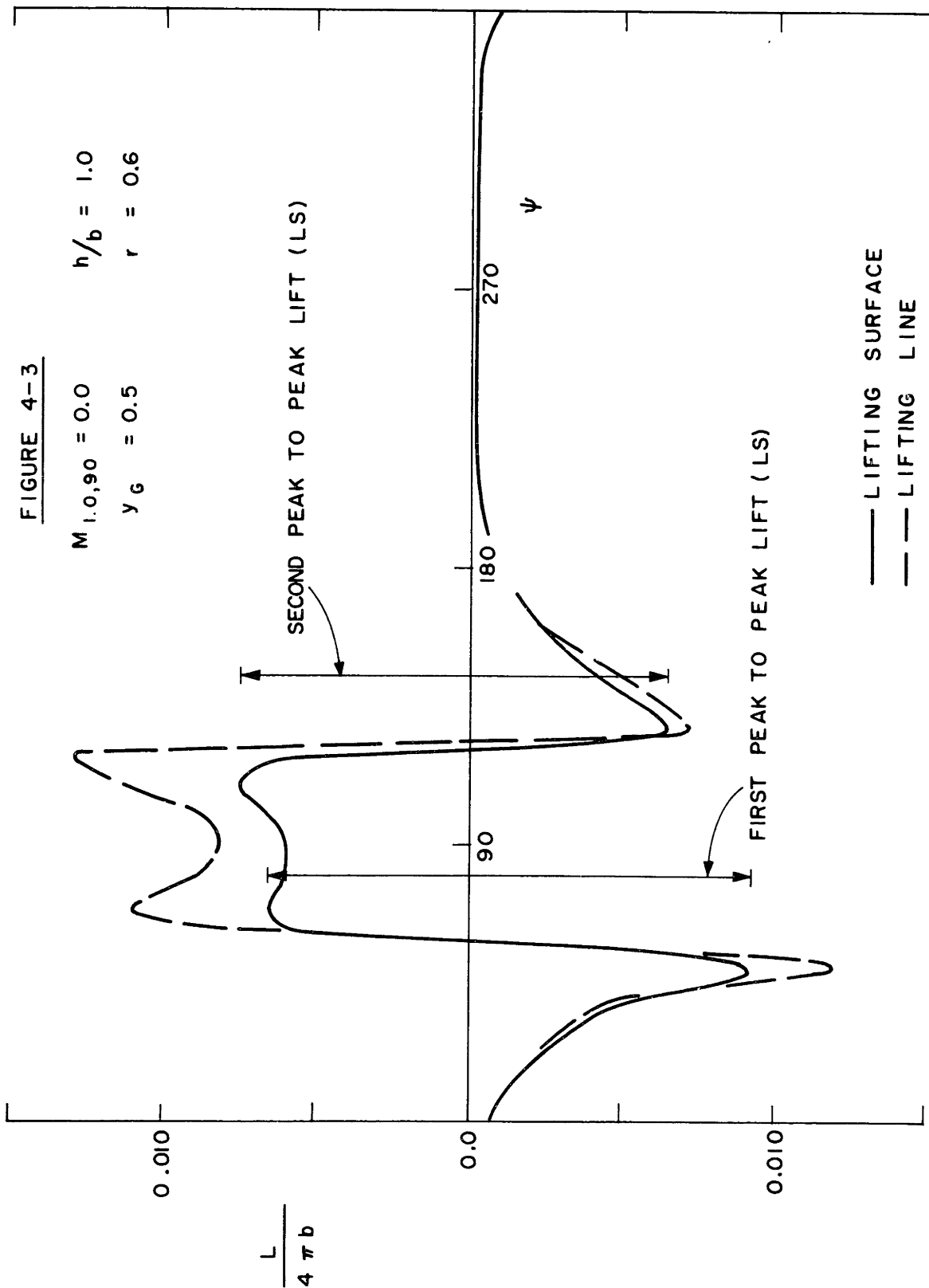


FIGURE 4-4

$M_{1.0, 90} = 0.0$        $h/b = 0.5$   
 $\gamma_G = 0.5$              $r = 0.6$

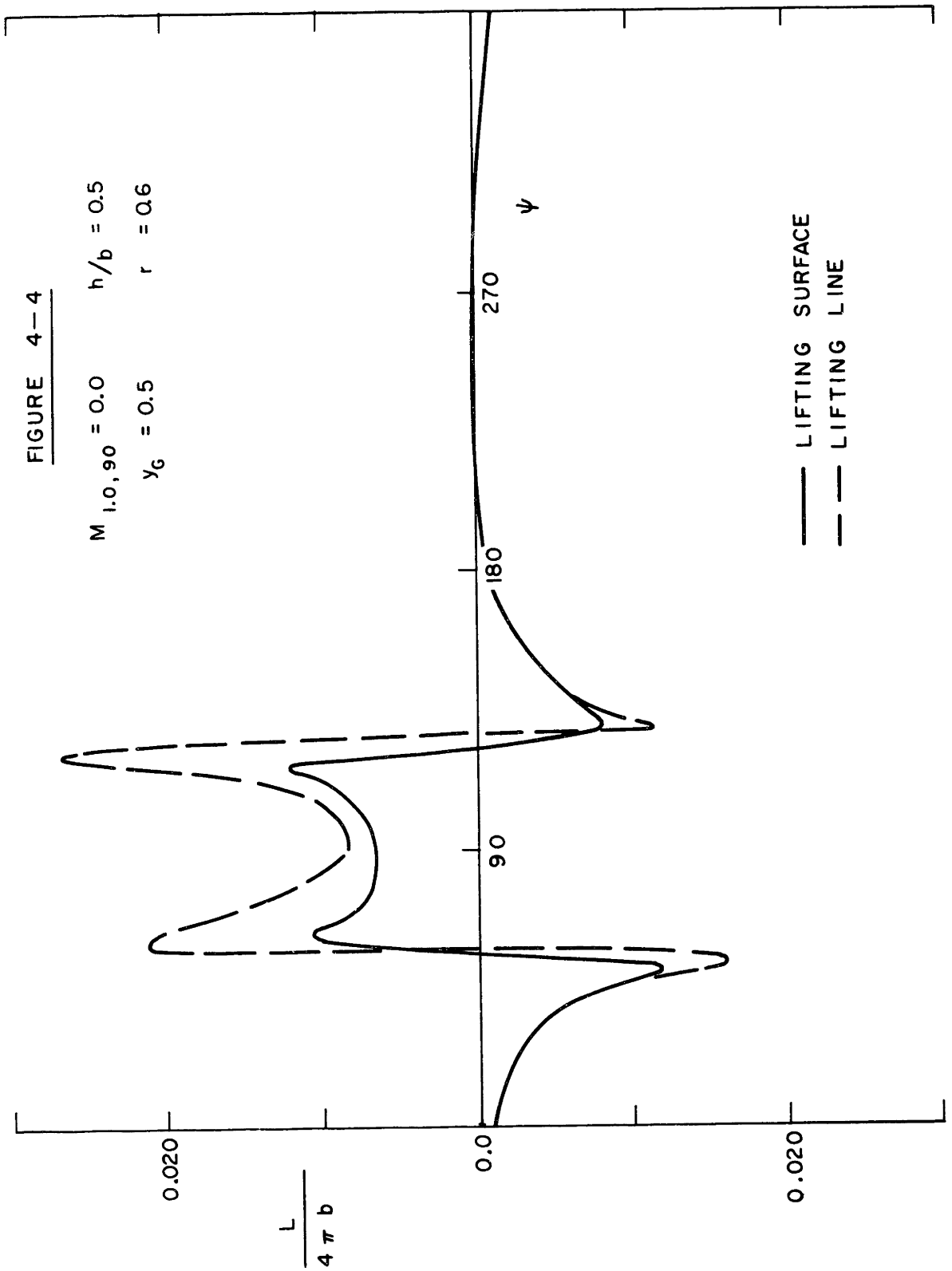


FIGURE 4-5

$y_G = 0.5$

$r = 0.6$

$M_{1.0,90} = 0.0, 0.5, 0.9$

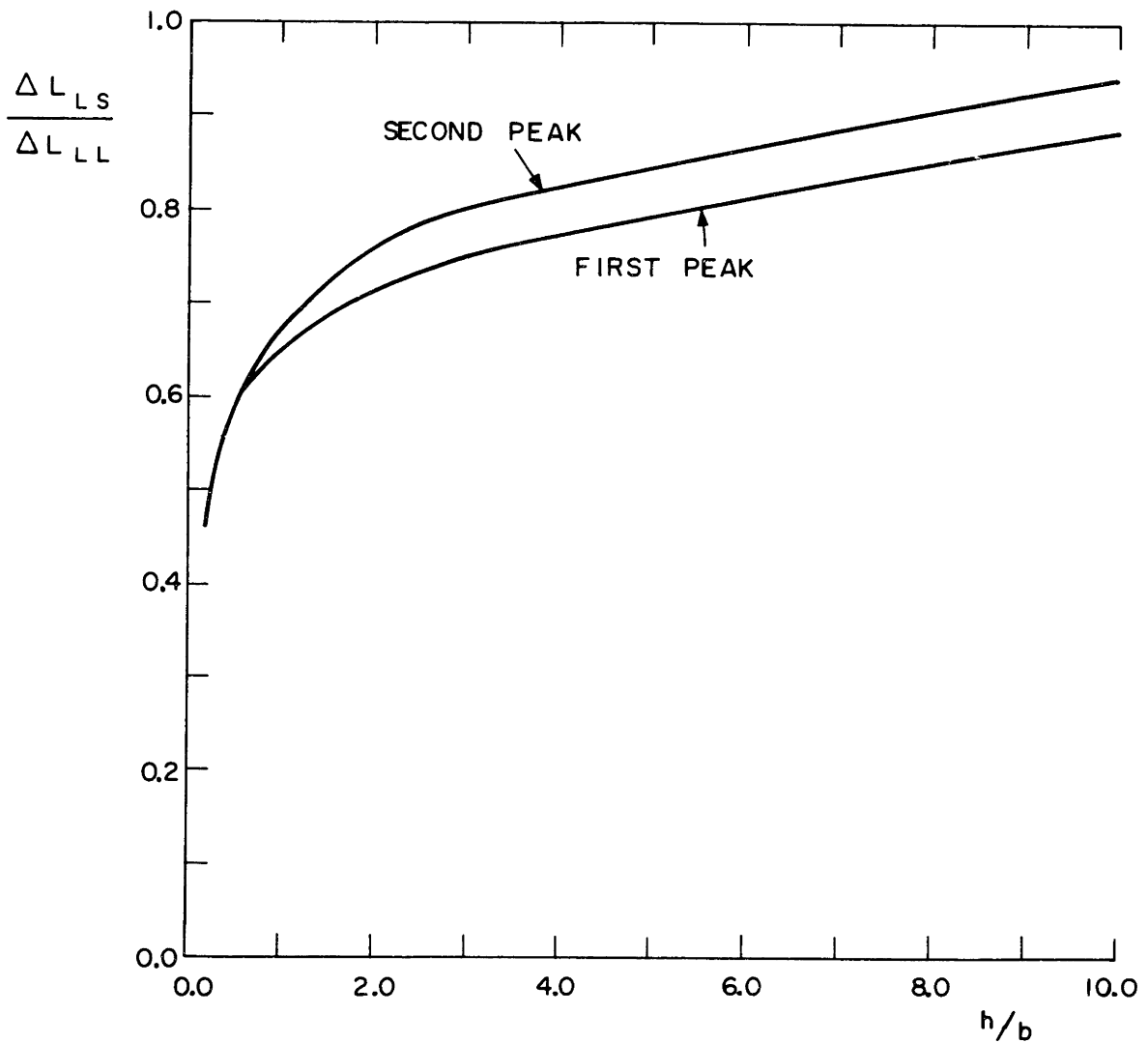


FIGURE 4-6

$M_{1.0, 90} = 0.0$        $h/b = 1.0$   
 $\gamma_G = 0.0$              $r = 0.75$

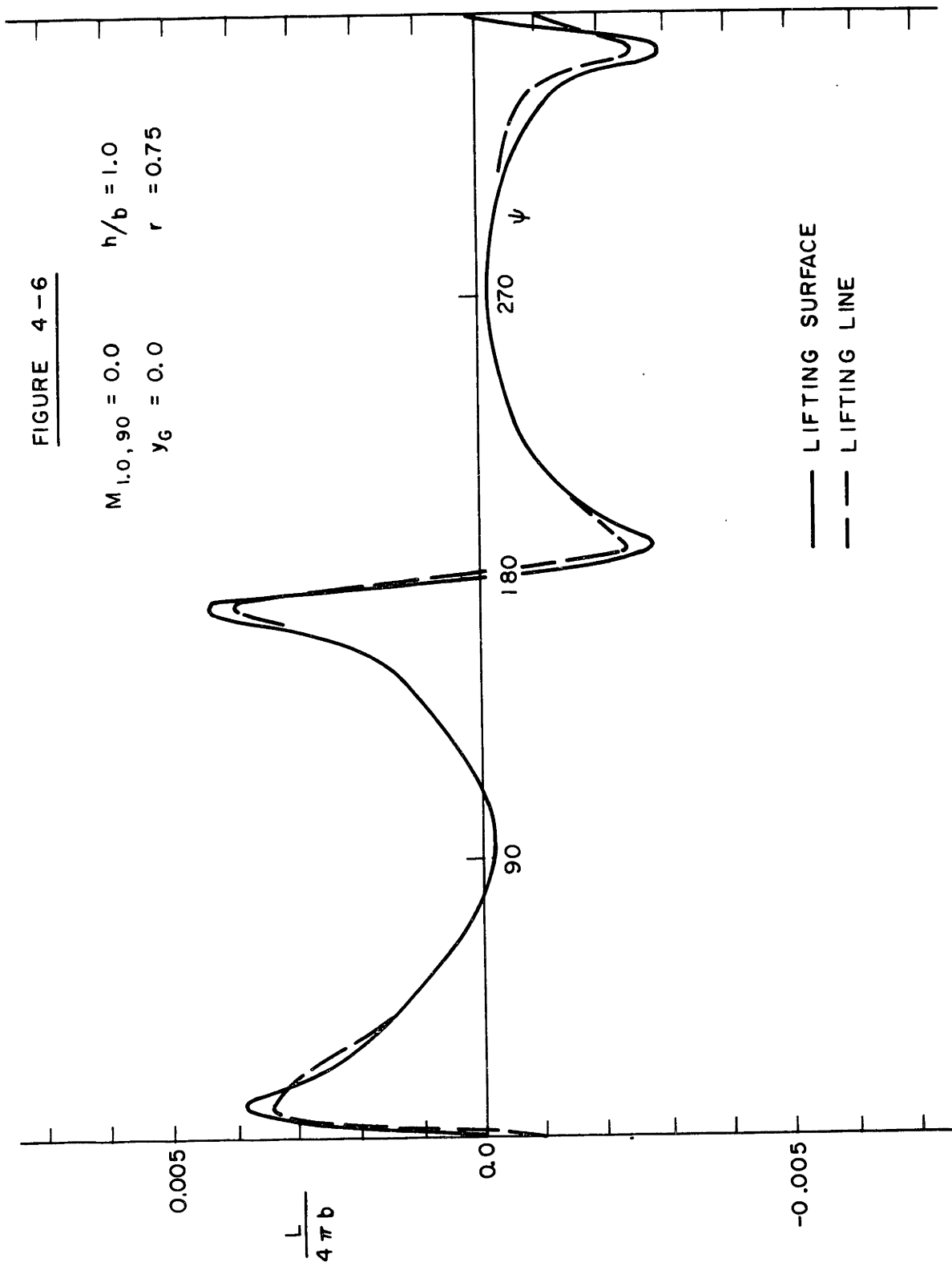
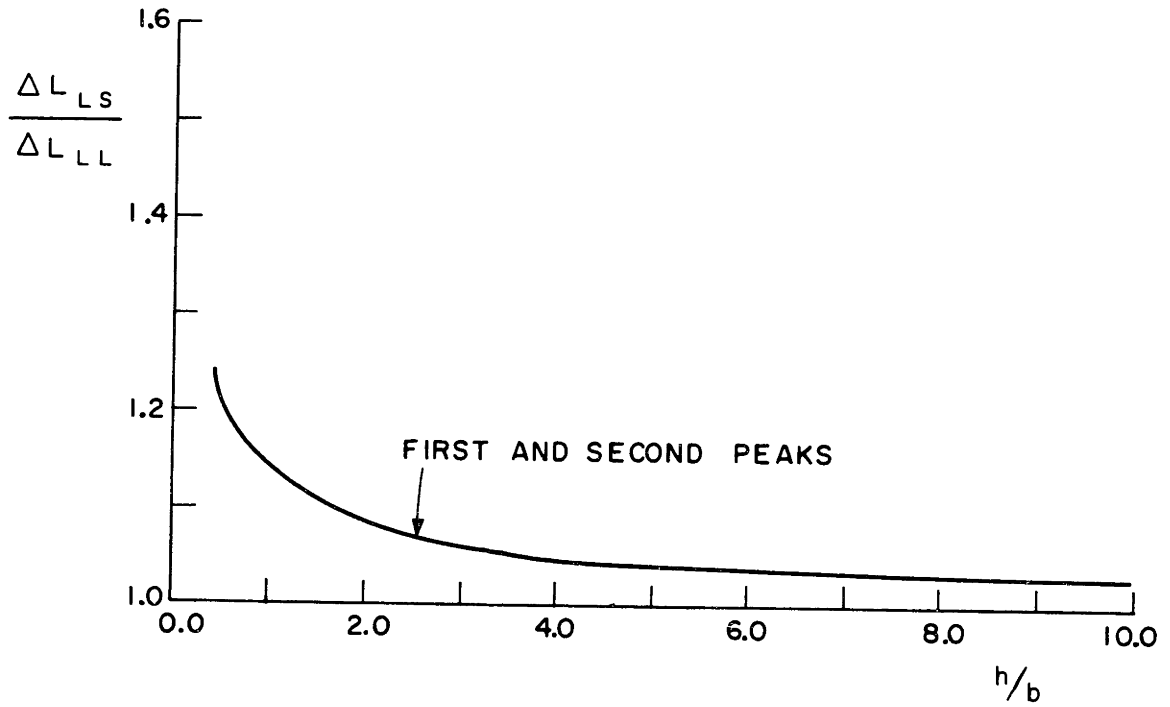
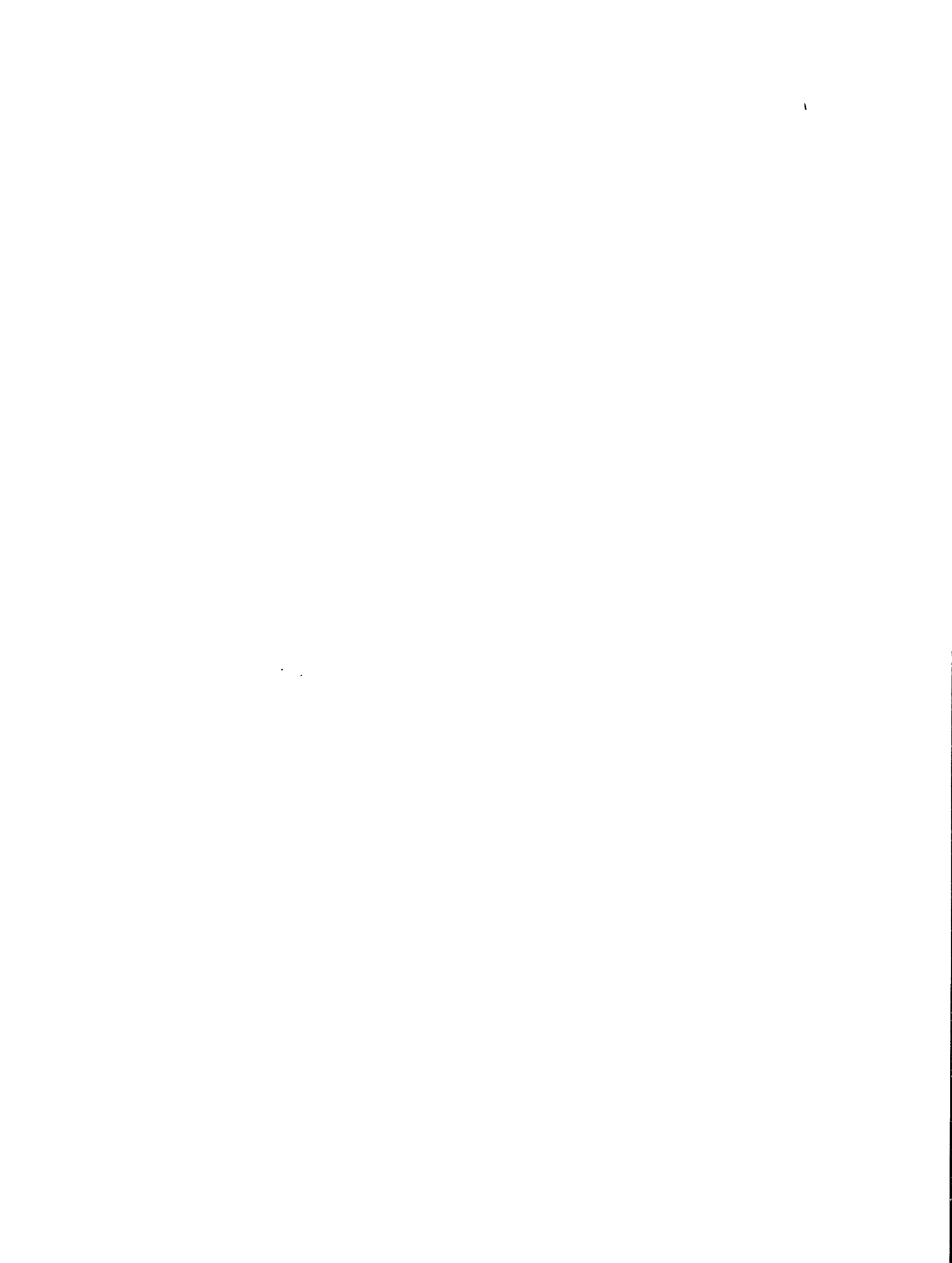


FIGURE 4-7

$y_G = 0.0$        $r = 0.75$        $M_{1.0,90} = 0.0, 0.5, 0.9$





## BIOGRAPHY

Wayne Johnson was born on January 23, 1946 in Waterloo, Iowa. He entered the Massachusetts Institute of Technology in September of 1964, and received from that institution on June 7, 1968 the degrees of Bachelor of Science and Master of Science in aeronautics and astronautics. He was the recipient of the de Florez Award and the Salisbury Award from the Department of Aeronautics and Astronautics. He has published work on the subject of rotary wing airloads individually and with Professor Norman D. Ham.